UNIVERSITY OF LONDON THESIS

Degree PhD Year 2006 Name of Author TERESA FERRARO

Cellular localisation and function of neuronal SK potassium channels

Thesis submitted at the University College of London for the degree of Doctor of Philosophy by

Teresa Ferraro

Department of Pharmacology
Laboratory for Molecular Pharmacology
University College London

ProQuest LLC
789 East Eisenhower Parkway
P.O. Box 1346
Ann Arbor, MI 48106-1346

Abstract

In the central nervous system, small conductance calcium-activated potassium channels (SK) are important for the generation of the afterhyperpolarisation that follows single or trains of action potentials. Three SK channels have been cloned (SK1, SK2 and SK3), which are selectively blocked by the venom toxin apamin and present distinct pharmacological properties. The principal aim of this work is to investigate the subcellular distribution of SK2 and SK3 channels in neurones. For this purpose, antibodies directed against specific regions of SK2 and SK3 subunits were raised, purified and characterised. Immunohistochemistry on rat brain sections showed that the SK2 protein is localised in somatic and dendritic structures in various brain regions. SK3 immunoreactivity is mainly associated with fibers, but also with neuronal somata and dendrites. Intense SK3 expression was detected in the substantia nigra pars compacta, the locus coeruleus and the dorsal raphe. In these brain regions, the distribution of the channel was analysed in relation to monoamine-containing neurones, at two different developmental stages. In this work, I also report the characterization of a new SK2 variant, SK2-860, which differs from the SK2 subunit by having an extended amino terminus. Heterologous expression of this variant in primary neurones indicates that the majority of the protein is located in clusters distributed throughout the cytoplasm. Western blot analysis with the SK2 antibody and with a specific antibody for the new variant showed that SK2-860 subunit is expressed in the rat central nervous system. The distribution pattern of the SK2-860 in the rat brain largely overlaps the one observed for SK2.

Finally, in the last part of this work, the molecular determinants responsible for the difference in apamin sensitivity among the different members of the SK channel family were investigated. The study showed that the extracellular loop that connects transmembrane segments S3 and S4 of SK channel α subunits significantly contributes to apamin sensitivity of SK2 channels.

Declaration

I, Teresa Ferraro, confirm that the work presented in this thesis is my own. Where information has been derived from others sources, I confirm that this has been indicated in the thesis.

Acknowledgments

I would like to thank the Wellcome Trust for the three-year Wellcome Prize Studentship. I'm very grateful to my supervisor, Dr. Martin Stocker, for giving me the opportunity to do my PhD at UCL. I would also like to thank him for his guidance and for being always present for help and advice. I am grateful to my second supervisor, Dr. Paola Pedarzani, for her generous help with the neuroanatomy and for showing continuous interest in the progress of my work.

I am very grateful to all the past and present members of the lab, Dieter, Manuel, Klaus, Andreas, Florian and Hannah. Thanks to all of them for teaching me so much, for being always there for help and discussions, and for making pleasant the long hours in the lab.

I would like to thank all the friends that I met in London. In particular, the biggest thanks goes to Fede for her great friendship, continuous support and for making me feel at home in London. I'm also grateful to all the Italian friends that did not forget about me during these years. In particular, thanks to Rossella, Marica and especially to Nico for following every single step of my PhD.

Un ringraziamento particolare va ai miei genitori e a mio fratello per essermi stati sempre così vicini, per i preziosi consigli e il continuo supporto.

Infine, grazie a Frà per essere stato una presenza forte e paziente durante tutti questi anni e, soprattutto, per non aver mai smesso di incoraggiarmi a superare le difficoltà.

Table of contents

List of figures

List of tables

CHAPTER 1

Introduction

1.1 Ion channels

Electrical signalling plays an essential role for many biological processes and is made possible by the activity of ion transporters and pumps that create and maintain ion gradients across the cell membranes of animal cells. Pumps and transporters establish the precise concentration of several important ions inside and outside the cell: Na^+, Ca^{2+} and Cl^- are actively extruded to the extracellular space, whereas K^+ is actively concentrated in the cytoplasm. These gradients represent the energy source for the passive movement of ions through specialised ionic pores, the ion channels (Hille, 1992).

Ion channels are integral membrane proteins (Jan and Jan, 2004). They are present nearly in all cell types, where they are important components of cell function. In excitable cells, such as the muscle, the heart and the brain, they are responsible for setting the resting membrane potential, and for the generation and transmission of electrical stimuli (Jan and Jan, 2004; Ashcroft, 2000; Hille, 1992). Ion channels open or close in response to different signals. Some channels are sensitive to changes of the membrane voltage, others open upon binding of specific ligands, such as Ca^{2+} and neurotransmitter, or in response to post-translational modifications including, for example, phosphorylation (Jan and Jan, 2004; Hille, 1992).

Ion channels are grouped in several families depending on their ion selectivity. The main families of ion channels are: Na^+ channels, Ca^{2+} channels, Cl^- channels, K^+ channels and non selective cation channels (Alexander and Peters, 2004).

1.2 Potassium channels

K^+ channels represent the largest and most diverse ion channel family (Coetzee et al., 1999). They conduct K^+ across the cell membrane down the electrochemical gradient. Opening of these channels generates efflux of K^+ ions, reducing the number of positive charges inside the cell and, as a consequence, terminating or limiting excitation (Hille, 1992). In neuronal cells, K^+ channels underlie different cellular functions, including the duration and the frequency of action potentials, the duration of interspike intervals during repetitive firing, the termination of periods of intense activity and neurotransmitters release from nerve terminals (Hille, 1992) .

1.2.1 Potassium channel families

K^+ channels are multimeric membrane proteins made of principal, pore-forming α subunits that are often associated with auxiliary β subunits (Deutsch, 2002). Every K^+ channel principal subunit contains a basic structure consisting of two transmembrane domains (TM) and a loop (P loop) between them. Four of these structural elements are grouped together to form the ion-permeation pore across the cell membrane (MacKinnon, 1991).

Based on the predicted membrane topology of the α subunits, K^+ channels can be divided in four classes: 2 TM, 6 TM, 7 TM and 4 TM/2P (Wei et al., 1996). 2 TM proteins represent the inward-rectifying K^+ channels (Kir) (Bichet et al., 2003). These subunits are composed of two transmembrane segments separated by a loop, and have the amino- and carboxy-terminal domains located intracellulary (Fig. 1.1 A). A functional Kir channel consists of tetramers of 2 TM subunits. 6 TM α subunits (Fig. 1.1 B) contain six transmenbrane domains, with the P-loop located between the S5 and S6 transmembrane regions. This family comprises the voltage-gated Kv subfamily (Tempel et al., 1987; Stuhmer et al., 1989; Pongs, 1992; Gutman et al., 2005), the Ca^{2+}-activated small and intermediate conductance, SK (Kohler et al., 1996) and IK (Ishii et al., 1997a; Joiner et al., 1997; Logsdon et al., 1997) subfamilies. 6TM subunits associate in a tetramer to form a functional channel (MacKinnon, 1991; Liman et al., 1992). 7 TM α subunits are represented by the Ca^{2+} and voltage-sensitive, large conductance K^+ channel (BK) (Atkinson et al., 1991; Adelman et al., 1992; Butler et al., 1993). The BK principal subunit contains seven membrane spanning domains. Unlike all the other K^+ channels, the amino terminus of the BK α subunits is placed on the extracellular side of the membrane (Meera et al.,1997). Functional BK channels are tetrameric complexes of 7 TM subunits. The last group of K^+ channels principal subunits is the 4TM/2P, that most likely evolved by gene duplication from the 2 TM proteins coding genes. These proteins are components of the leak K^+ channels. The 4TM/2P subunits are thought to dimerise to form functional channels, thereby maintaining the fourfold symmetry around the pore (Lesage et al., 1996; Goldstein et al, 1998) . This family comprises a number of subfamilies including TASK, TREK, TRAAK, TWIK, THIK and TALK (Goldstein et al., 2005).

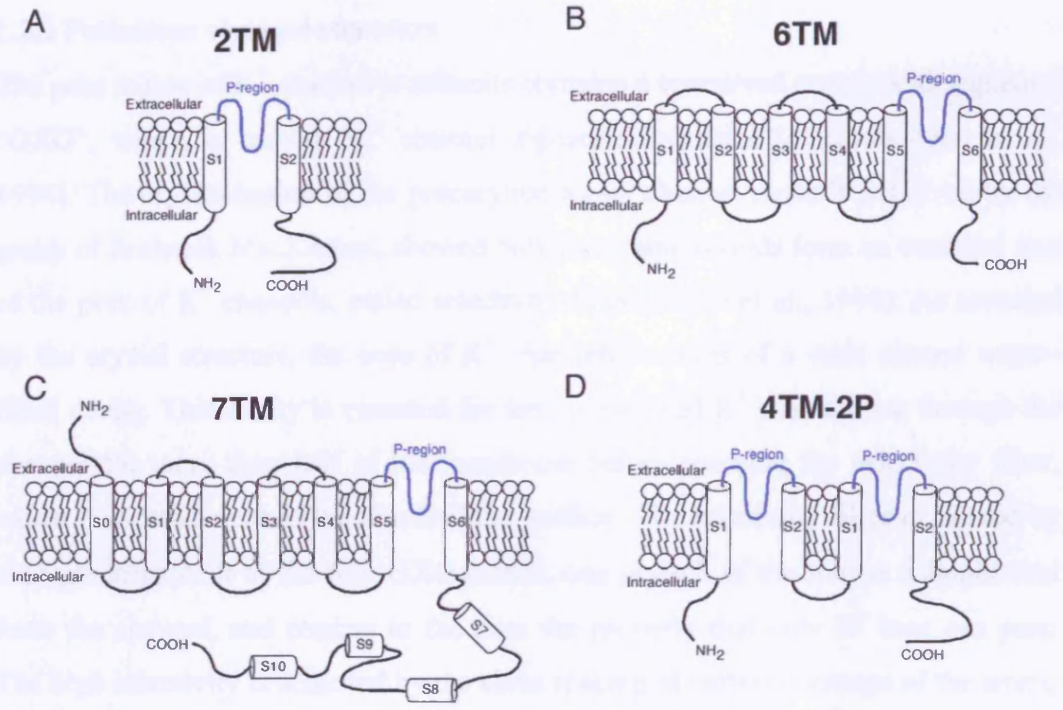

FIGURE 1.1: Membrane topology of K^+ channel α subunits. The pore region (P-region) is represented in blue and the transmembrane segments are named S1-S6. **A:** 2 transmembrane α subunit. **B:** 6 transmembrane α subunit. **C**: 7 transmembrane α subunit, having the extracellular amino-terminal domain, and 6 hydrophobic segments (S7-S10) in the carboxy-terminal region. **D**: 4 transmembrane and two pores α subunit.

Several K^+ channel α subunits form heteromeric complexes with auxiliary β subunits, which can be cytosolic or integral membrane proteins. The association of β subunits modulates the channel properties. β subunits can influence the voltage dependence properties of the channel (Castellino et al., 1995; McManus et al., 1995), can affect the sensitivity of the principal subunit to toxins and drugs (Kaczorowski et al., 1996; Meera et al. 2000) or, in some cases, enable or increase the channel inactivation (Rettig et al., 1994; Morales et al., 1995). Moreover, some β subunits have been shown to have a chaperone-like effect by promoting and stabilising the cell surface expression of the channel complex (Fink et al., 1996; Shi et al., 1996; Trimmer, 1998)

1.2.2 Potassium channel structure

The pore region of K^+ channel α subunits contains a conserved amino acid sequence, "GXG", which is named "K^+ channel signature sequence" (Heginbotham et al., 1994). The crystallisation of the procaryotic KcsA channel recently achieved by the group of Roderick MacKinnon, showed how these amino acids form an essential part of the pore of K^+ channels, called selectivity filter (Doyle et al., 1998). As revealed by the crystal structure, the pore of K^+ channels consists of a wide central water–filled cavity. This cavity is essential for letting hydrated K^+ ions diffuse through the channel for more than half of the membrane before reaching the selectivity filter, which is located close to the extracellular surface. The selectivity filter is formed by the tight alignment of the four GXG motifs, one in each of the four α subunits that form the channel, and confers to the pore the property that only K^+ ions can pass. The high selectivity is achieved by the close spacing of carboxyl groups of the amino acid backbone around the pore axis that forms a cavity perfectly fitting the size of a dehydrated K^+ ion. The interactions between these carboxyls and the K^+ ions mimic the interactions between the K^+ ions and water (Doyle et al., 1998). The selectivity filter contains four adjacent binding sites for the dehydrated K^+ ions transiting through the channel (Fig. 1.2). The repulsion between the K^+ ions occupying adjacent positions overcomes the affinity that each ion has for its binding site and allows permeation (Morais-Cabral et al., 2001; Miller, 2001).

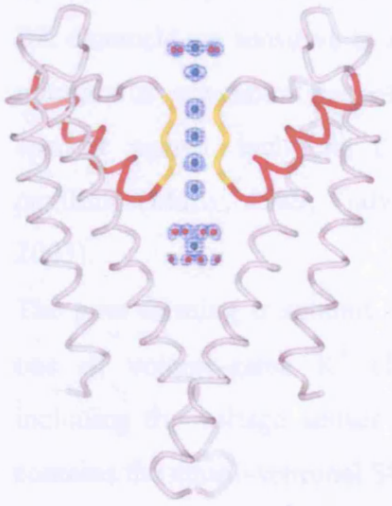

FIGURE 1.2 Ion conductance pore of the 2TM potassium channel KcsA. Ribbon representation illustrating two of the four α subunits of the KcsA. The extracellular side of the channel is at the top. Each subunit is composed of: an outer helix; an inner helix close to the pore; a pore helix, which is represented in red; and the selectivity filter, which is represented in yellow. The dehydrated K^+ ions inside the selectivity filter are represented in green. Inside the central cavity and outside the channel, K^+ ions are surrounded by water molecules (red). (From MacKinnon, 2003).

1.3 The calcium activated potassium channel family

Ca^{2+}-activated K^+ channels integrate changes in intracellular Ca^{2+} concentration with changes in the membrane potential in many different cell types. These channels are involved in numerous physiological functions, such as smooth muscle tone, secretion, control of neuronal firing properties and transmitter release (Vergara et al., 1998). Ca^{2+}-activated K^+ channels have been subdivided into three main families, which are different in their physiological, molecular and pharmacological properties. These are the large conductance (BK), intermediate conductance (IK) and small conductance (SK) channels (Vergara et al., 1998).

1.3.1 BK channels

BK channels are widely distributed Ca^{2+}- and voltage-sensitive K^+ channels. They have single channel conductance between 100 and 220 pS (Marty, 1989; Latorre et al., 1989; Reinhart et al., 1989), and are activated by the simultaneous increase in intracellular Ca^{2+} and depolarization. The Ca^{2+} dependence of BK channels is influenced by the membrane potential, with the K_d for Ca^{2+} in the micromolar range at resting potentials, and in the nanomolar range at depolarised membrane potentials (Latorre et al., 1989; Cui et al., 1997). Upon strong depolarisation, BK channels can also open in the absence of Ca^{2+}, indicating that they can function as purely voltage-dependent channels (Horrigan and Aldrich, 2002). The effects of Ca^{2+} and voltage on channel opening seem to consist of two independent processes, both increasing the open probability of the channels (Horrigan et al., 1999; Horrigan and Aldrich, 2002). BK channels are sensitive to inhibition by several compounds. They are blocked by micromolar concentrations of tetraethylammonium (TEA), charybdotoxin and by specific agents, including the scorpion toxin, iberiotoxin, and the mycotoxin, paxilline (Marty, 1989; Galvez et al., 1990; Sanchez and McManus, 1996; Wu, 2003).

The pore forming α subunit of BK channels contains a core domain similar to the one of voltage-gated K^+ channels, with six transmembrane segments S1-S6, including the voltage sensor S4 (Papazian et al., 1991). Additionally the subunit contains the amino-terminal S0 transmembrane segment and a long carboxy-terminal domain (Meera et al., 1997). Although the voltage sensitivity is generated by mechanisms similar to the ones described for other voltage-gated K^+ channels, the

mechanisms underlying the Ca^{2+} sensitivity have not been completely understood. One Ca^{2+} binding site of the BK α subunits has been located in a highly conserved region named "Ca^{2+} bowl", in the carboxy-terminal cytoplasmic tail (Wei et al., 1994; Schreiber et al., 1997; Schreiber et al., 1999). An additional Ca^{2+} sensing domain has been located in the RCK (regulator of K^+ conductance) domains (RCK1 and RCK2), which share high homology with regulatory elements present in bacterial K^+ channels, and are present in the amino-terminal part of the carboxy-terminal cytoplasmic tail (Xia et al., 2002). However, a further study reports that the removal of the complete carboxy-terminal domain of BK does not disrupt the Ca^{2+} sensitivity of the channel, indicating that the Ca^{2+} sensitivity domains in the carboxy-tail are not necessary for the effect of Ca^{2+} on channel opening (Piskorowski and Aldrich, 2002).

Native BK channels display a broad range of functional properties. Despite this high diversity, only one gene encodes the mammalian BK α subunit. Several mechanisms generate diversity of native BK channels, including assembly with modulatory β subunits (Orio et al., 2002), alternative splicing (Shipston, 2001) and phosphorylation (Weiger, 2002).

To date, four β subunits have been cloned (Knaus, et al., 1994; Tseng-Crank et al., 1996; Brenner et al., 2000; Meera et al., 2000; Uebele et al., 2000; Weiger et al., 2000). They are membrane proteins containing two transmembrane domains connected by a loop. The assembly of the BK β subunits modifies the pharmacology, the gating kinetic or the voltage dependence of the principal BK α subunits (Orio et al., 2002). Co-expression of the BK α and β1 subunits shifts the voltage dependence of activation to more negative membrane potentials, increases the Ca^{2+} sensitivity and influences the toxin binding (McManus et al., 1995; Dworetsky et al., 1996; Nimigean and Magleby, 1999; Wallner et al., 1999). The co-expression of BK α subunits with β2/β3 subunits results in channels that exhibit a reduced sensitivity to charybdotoxin and show rapid inactivation (Wallner et al., 1999; Brenner et al., 2000). In contrast, the α subunit alone or co-expressed with β1/β4 produces currents that do not inactivate (Wallner et al., 1999; Meera et al., 2000). The β4 subunit, which is mainly expressed in the brain, renders the α subunit insensitive to iberiotoxin and charybdotoxin (Brenner at al., 2000; Weiger et al., 2000; Meera et

al., 2000). Alternative splicing of BK transcripts can generate channels that exhibit distinct functional features. Inclusion of STREX exon (STRess axis-regulated exon) speeds the activation and slows the deactivation kinetics, and results in channels with increased voltage and Ca^{2+} sensitivity (Xie et al., 1998). Furthermore, STREX introduces in the BK α subunit a PKA phosphorylation site that, in heterologous expression system, switches the channel from being activated to being inactivated by PKA (Tian et al., 2001).

The current corresponding to the activation of BK channels has been named I_C, which, in neurones, participates in action potential repolarisation and is responsible for the fast afterhyperpolarization (Storm, 1987; Storm, 1990; Sah, 1996) In many central neurones, BK channels are present in somata, dendrites and presynaptic terminals (Edgerton and Reinhart, 2003; Hu et al., 2001) where they can be activated by intracellular Ca^{2+} increase mediated by voltage-gated Ca^{2+} channels (Womack et al., 2004; Edgerton and Reinhart, 2003), NMDA receptors (Isaacson and Murphy, 2001) or intracellular Ca^{2+} release (Chavis et al., 1998). At axon terminals, BK channels contribute to repolarisation of the presynaptic action potential and function as feedback regulators of Ca^{2+} influx and neurotransmitter release (Hu et al., 2001).

1.3.2 IK channels

IK channels are voltage-insensitive, Ca^{2+}-dependent K^+ channels and they are mainly expressed in some non-neuronal cells such as epithelial cells and lymphocytes (Ishii et al., 1997a; Joiner et al., 1997; Logsdon et al., 1997). IK channels exhibit a single channel conductance of 30-40 pS, are blocked by charybdotoxin and clotrimazole (Ishii et al., 1997a; Logsdon et al., 1997) and are sensitive to the enhancer EBIO (1-ethyl-2-benzimidazolinone) (Devor et al., 1996; Jensen et al., 1998; Pedersen et al., 1999). Currents due to the activation of IK channels have not been characterised in central neurones. In myenteric neurones, IK channels have been proposed to underlie a slow afterhyperpolarisation (Vogalis et al., 2002).

1.4 SK channels cloning and structure

Three members of the SK channel family have been cloned in 1996 by Kohler and colleagues: SK1 ($K_{Ca}2.1$), SK2 ($K_{Ca}2.2$) and SK3 ($K_{Ca}2.3$) (Kohler et al., 1996). The three genes have a complex gene structure, with the coding region of SK1 containing nine exons, and the coding regions of SK2 and SK3 containing 8 exons (Fig. 1.3). The exon-intron boundaries, which are conserved across species, are represented as black arrows in the Figure 1.3.

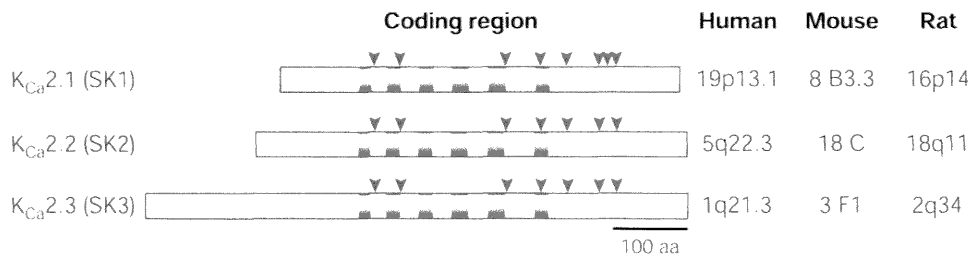

FIGURE 1.3: Genomic structure of SK1, SK2 and SK3 genes. The bars represent the coding sequences of the three genes. The black arrows indicate the exon-intron boundaries, and the blue boxes represent the 6 transmembrane domains. On the right, the chromosomal localisation of the three genes in the human, mouse and rat genomes is reported. (From Stocker, 2004)

When expressed as homomultimers, the three identified subunits form ion channels that respond rapidly to Ca^{2+} applied on the cytoplasmic side, are voltage-independent and exhibit a small single channel conductance of ~10 pS (Kohler et al., 1996). The Ca^{2+} concentration required for the half maximal activation of SK channels (EC_{50}) is approximately 300-700 nM (Xia et al., 1998; Hirschberg, 1998).

Structurally, the SK channel subunits have a membrane topology similar to the voltage-gated K^+ (Kv) channels. The S4 transmembrane segment, which in Kv channels is the voltage sensor, presents a reduced number of positive charges, only two, compared to the seven basic residues of Kv channels (Kohler et al., 1996). This difference might represent the molecular basis for the voltage insensitivity of SK channels. The sequences of the three subunits are highly conserved in the transmembrane domains, as shown in the alignment of Figure 1.4, but diverge in length and sequence in the amino and carboxy terminals. SK channels contain multiple phosphorylation consensus sites for several protein kinases but no conserved N-linked glycosylation site and no Ca^{2+} binding domain (Kohler et al., 1996). Because of the structural homology of SK α subunits and voltage-gated K^+

channel α subunits, which assemble in tetramers to form functional channels, it is likely that native SK channels are composed of four α subunits.

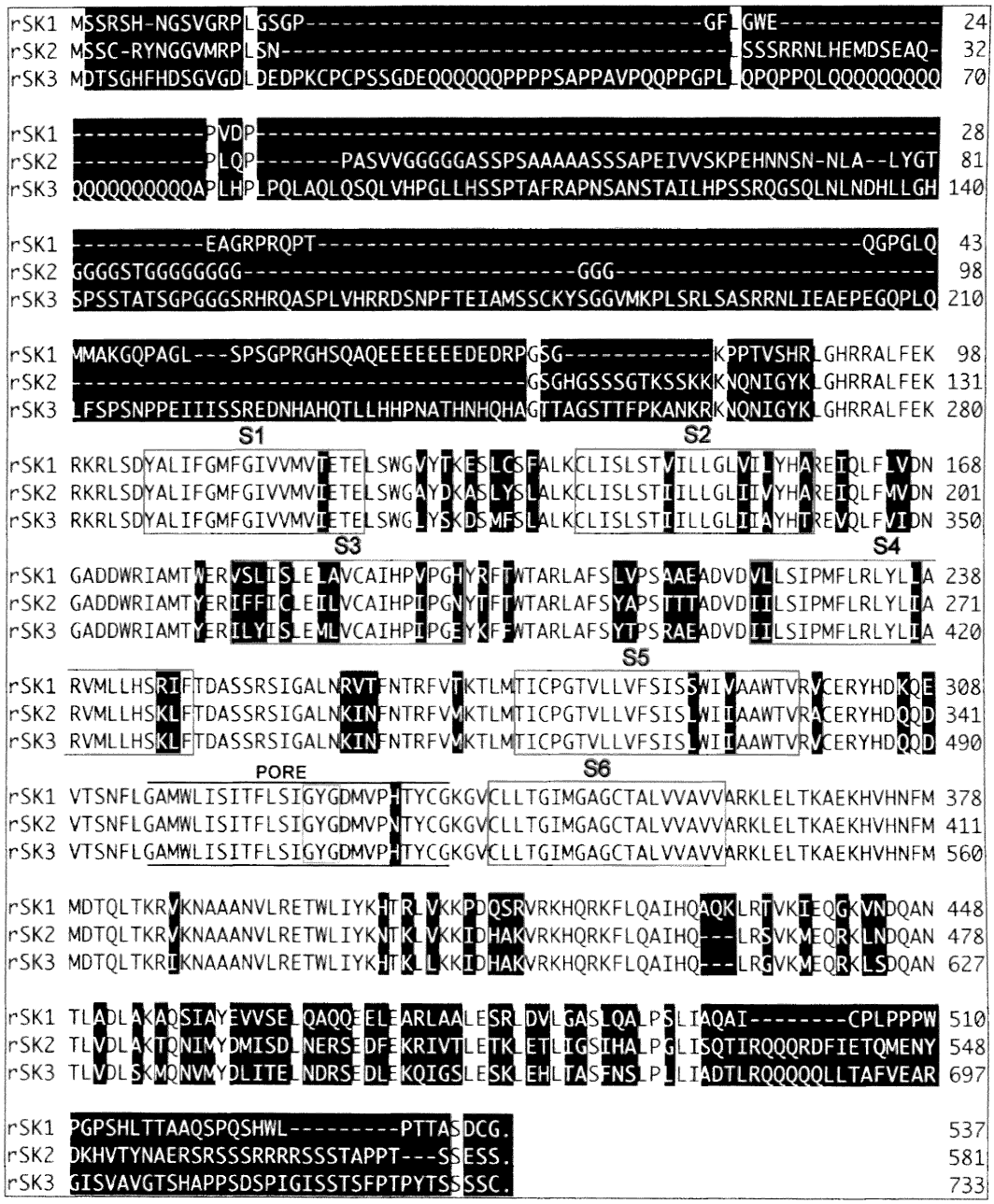

FIGURE 1.4: Sequence alignment of rSK1, rSK2 and rSK3. The S1-S6 transmembrane domains are indicated as blue boxes. The pore region is indicated with black lines, and the red box indicates the pore signature sequence GYG.

1.5 Gating of SK channels

The SK α subunits do not possess intrinsic Ca^{2+} binding domains (Kohler et al., 1996); therefore, the Ca^{2+} sensitivity of the SK channels cannot be explained by direct binding of Ca^{2+}. The work performed by Xia and colleagues revealed that SK channels use calmodulin as a high affinity Ca^{2+} sensor (Xia et al., 1998). Ca^{2+} gating is accomplished by the constitutive association of calmodulin to a region immediately adjacent to S6, in the carboxy terminal domain of each of the 4 SK α subunits (Keen et al., 1999; Xia et al., 1998). This region is highly conserved in all SK channel subunits and is responsible for the Ca^{2+}-independent binding of calmodulin to the SK subunits. Calmodulin contains 4 Ca^{2+} binding EF-hand motifs: the EF hands 1 and 2, located in the amino-terminal lobe (N-lobe), and the EF hands 3 and 4 in the carboxy-terminal lobe (C-lobe). Mutagenesis studies revealed that the C-lobe of calmodulin interacts with the SK α subunits in a Ca^{2+}-independent manner, whereas the N-lobe interacts with the SK subunits only in the presence of Ca^{2+}. The crystal structure of the calmodulin/α subunits complex, published by Schumacher and colleagues in 2001, confirmed these findings and indicated a model for the gating of SK channels (Schumacher et al., 2001). The structure of the SK2 channel calmodulin binding domain (CaMBD) consists of 2 α-helices, α1 and α2, connected by a loop, and organised in an antiparallel configuration (Fig.1.5 A, B). The crystal structure revealed a dimeric structure of the CaMBD in presence of Ca^{2+} (Fig.1.5 A, B), where two calmodulins are bound to the CaMBD dimer, and each calmodulin interacts with both CaMBDs. As shown in the Figure 1.5 A, the C-lobe of calmodulin grips the CaMBD α1 and α2 helices of one subunit, whereas the N-lobe interacts with the α2' helix of the neighbour SK subunit.

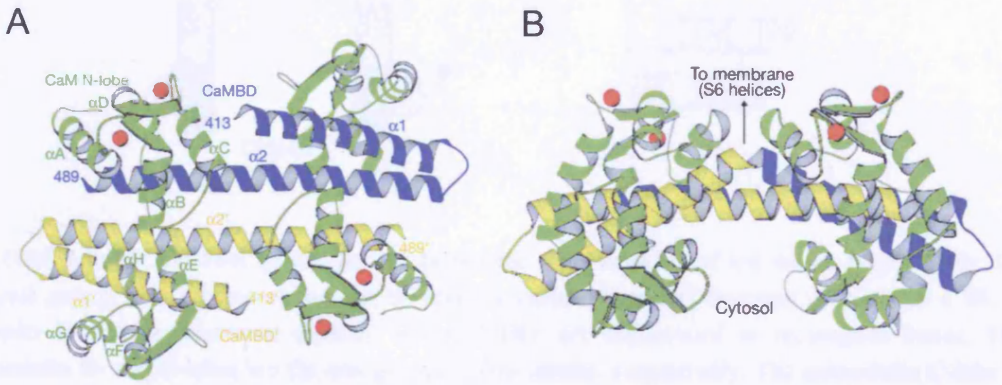

FIGURE 1.5: Ribbon diagram of the structure of the calmodulin/CaMBD dimeric complex. A: One CaMBD is shown in yellow, the other in blue. Each CaMBD consists of a short α helix (α1 or α1'), a long α helix (α2 or α2') and a loop between them. The calmodulin molecules are represented in green. The N-lobe of calmodulin contains Ca^{2+} ions, depicted in red. (From Schumacher et al., 2001). **B**: A 90° rotation of the structure reported in A is shown.

Although the crystallization was performed in the presence of Ca^{2+}, only the EF hands 1 and 2 (N-lobe) contained Ca^{2+} ions, whereas the EF hands 3 and 4 of the C-lobe did not, supporting previous observations of the constitutive binding of the calmodulin C-lobe, and of the Ca^{2+}-dependent interactions of the N-lobe with the SK subunits. Moreover, biochemical data indicated that in the absence of Ca^{2+} the calmodulin/CaMBD complex is monomeric. Taken together, all these data suggested a model for the gating of SK channels, shown in the schematic representation of Figure 1.6. The calmodulin C-lobe is bound to the carboxy-terminus of the SK α subunit. The binding of Ca^{2+} to the N-lobe causes structural rearrangements that allow its interaction with the CaMBD of a neighbouring SK α subunit. Because each N-lobe of adjacent monomers contacts the CaMBD of the neighbouring SK subunit, the rearrangement results in a rotatory movement transmitted to the channel gate. The deactivation of the channel is the opposite process and occurs when the Ca^{2+} dissociates from calmodulin (Keen et al., 1999; Xia et al., 1998).

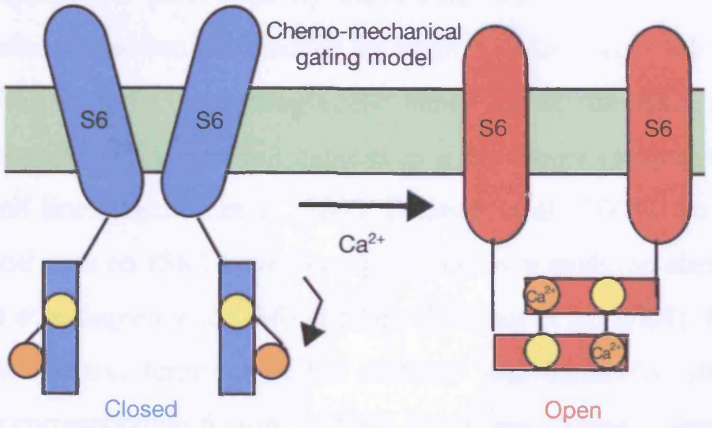

FIGURE 1.6: SK channel gating model. Schematic representation of the model proposed for SK channel gating. The scheme shows the S6 and the carboxy-terminal domains of 2 of the 4 SK α subunits forming a functional channel. The CaMBDs are represented as rectangular boxes. The calmodulin N- and C-lobes are the orange and yellow circles, respectively. The calmodulin C-lobe is bound to the CaMBD. Upon Ca^{2+} binding, the N-lobe interacts the CaMBD of a neighbouring SK

channel subunit and generate a rotatory movement responsible of the channel gating. (From Shumacher et al., 2001)

Recently, the study of Bildl and colleagues reported that, in addition to calmodulin, the SK channel subunits seem to form multiprotein complexes with two regulatory proteins, the protein kinase CK2 and the protein phosphatase 2A (Bildl et al., 2004). In this complex, protein kinase CK2 phosphorylates calmodulin. Phosphorylation of calmodulin reduces the Ca^{2+} sensitivity of the SK channel by ~5 times and accelerates its deactivation kinetic (Bildl et al., 2004).

1.6 SK channel pharmacology

The distinctive feature of SK channel family is that they are selectively blocked by the bee venom toxin, apamin, an 18 amino acids peptide isolated from the apis millifera (Habermann, 1972; Haberman et al.,1979). Pharmacologically, the SK channels present distinct profiles. SK2 displays high sensitivity to apamin, in the picomolar range (IC_{50} = 27-140 pM) (Table 1), whereas SK3 is less sensitive to the toxin and is blocked by apamin concentrations in the nanomolar range (IC_{50} = 0.6-4 nM) (Table 1). In contrast, initial expression studies of the hSK1 in Xenopus oocytes showed that this subunit produced functional channels insensitive to apamin at concentrations up to 100 nM (Kohler et al., 1996; Ishii et al., 1997b). However, subsequent experiments performed by expressing hSK1 in mammalian cell lines revealed that also this subunit is blocked by apamin, with IC_{50} in the range between 0.7 and 12 nM (Table 1). Interestingly, the behaviour of the rSK1 subunit differs from hSK1, because rSK1 does not express as a functional channel in oocytes and mammalian cell lines (Benton et al., 2003; D'hoedt et al., 2004). To date, the only pharmacological data on rSK1 have been provided by a study on chimeric channels containing the core sequence (S1-S6) of rSK1 (D'hoedt et al., 2004). By substituting either only the carboxy-terminus or the carboxy- and amino-terminal domains of rSK1 with the corresponding regions of SK2, functional channels were obtained, but the resulting currents were not sensitive even to 100 nM apamin (D'hoedt et al., 2004).

In addition to apamin, other scorpion venoms toxins target SK channels. These include: scyllatoxin (Chicchi et al., 1988) (Table 1); P05 (Zerrouk et al., 1993); the recently identified tamapin (Pedarzani et al., 2002) (Table 1); and Lei-Dab, a

compound highly selective for SK2 that was obtained by substituting the amino acid in position 7 of scyllatoxin with the non-natural amino acid di-aminobutanoic acid (Dab) (Shakkottai et al., 2001). Moreover, SK channels are inhibited by several organic compounds, such as d-tubocurarine (Table 1), quaternary salts of bicuculline, dequalinium, UCL 1684 and UCL 1848 (Stocker et al., 2004a).

The molecular basis of apamin and d-tubocurarine binding has been investigated using chimeras and mutagenesis studies (Ishii et al., 1997). Two amino acids (D341 and N368 in rSK2), which are located on opposite sides of the outer vestibule of SK channels, have been found to be crucial for apamin and d-tubocurarine sensitivity (Ishii et al., 1997). Similarly to apamin, the sensitivity to scyllatoxin is mediated by amino acids in the outer pore region (Jager and Grissmer, 2004). Moreover, mutant cycle analysis has suggested that the Dab at position 7 in Lei-Dab directly interacts with one amino acid in the outer pore of SK2 (Shakkottai et al., 2001). Mutagenesis studies of the pore region of SK channels showed that a single amino acid in the outer pore of SK2 conferred sensitivity to the Kv channel blockers charybdotoxin and kaliotoxin (Jager and Grissmer, 2004). This suggests that a general architecture of the SK channel pore is similar to the one of Kv channels (Jager and Grissmer, 2004).

TABLE 1.1: Pharmacological properties of SK channels. (From Stocker et al., 2004)

	IC_{50}	SK1	SK2	SK3
Apamin	nM	0.70[5],1.3[12], 2.9[3], 5.1[3], 7.7[4], 8[10] 12.2[4], >100[1,2]	0.027[5],0.063[1], 0.07[12], 0.083[3], 0.095[13], 0.14[10]	0.63[7], 1[12], 1.1[10],1.4[8], 2[2], 4[5]
Scyllatoxin	nM	80[3], 325[9]	0.29[3]	1.1[9], 8.3[8]
Tamapin	nM	42[11]	0.024[11]	1.7[11]
d-Tubocurarine	µM	23.5[4], 27[3], 76.2[1], 354[2]	2.4[1], 5.4[2], 17[3]	210[6]

(1) Kohler et al., 1996; (2) Ishii et al., 1997b; (3) Strobaek et al., 2000; (4) Shah and Haylett, 2000; (5) Grunnet et al., 2001a; (6) Terstappen et al., 2001; (7) Grunnet et al., 2001b; (8) Hosseini et al., 2001;

(9) Shakkottai et al., 2001; (10) Dale et al., 2002; (11) Pedarzani et al., 2002; (12) Castle et al., 2003; (13) Benton et al., 2003;

Besides SK channel blockers, some SK channels enhancers have also been reported. The typical SK channel enhancer is EBIO (1-ethyl-2-benzimidazolinone), which was initially characterised on IK channels natively expressed in colonic epithelial cells (Devor et al., 1996). EBIO was subsequently shown to enhance the activity of IK channels heterologously expressed in cultured cells (Jensen et al., 1998; Pedersen et al., 1999). The application of EBIO on SK1 and SK2 channels increases the Ca^{2+} sensitivity of the channels by ~ 7 fold and slows the channel deactivation (Pedarzani et al., 2001). EBIO has also been extensively used as a pharmacological tool for the investigation of the physiological role of native SK channels (Stocker, 2004b). Other compounds have also been shown to enhance the activity of SK2 as well as of IK channels, such as chlorzoxazone and zoxazolamine (Stocker et al., 2004a).

1.7 Alternative splicing of SK channels

Alternative splicing represents an important mechanism that contributes to the molecular diversity of the K^+ channel family. To date, numerous splice variants of principal and accessory K^+ channel subunits have been described. Some of them have been related to different functional consequences such as changes of the cellular targeting, differential tissue expression, or changes of the channel electrophysiological properties (Coetzee et al., 1999).

Recent evidence indicates that alternative splicing occurs also within the SK channel family. In particular, extensive alternative splicing has been reported for the mouse SK1 gene (Shmukler et al., 2001). RT-PCR studies showed that 20 SK1 alternatively spliced transcripts are found in brain tissue. The 20 variants code for 16 putative polypeptides arising from the combination of 2 different amino-terminal amino acid sequences and 8 different carboxy-terminal amino acid sequences, some of which do not preserve the ability to bind calmodulin (Shmukler et al., 2001). Although the transcripts for 16 putative polypeptides have been detected, it has still to be determined whether these proteins exist *in vivo* and whether they contribute to the generation of functional SK channels. Recent studies reported also the existence of several SK3 splice variants. An hSK3 variant, named hSK3_ex4, containing an

additional exon between the third and fourth exons of hSK3, has been identified (Figure 1.7 A) (Wittekindt et al., 2004). The inclusion of the new exon 4 results in the insertion of 15 amino acids between the S5 segment and the P-loop of the hSK3 α subunit (Figure 1.7 A). Pharmacological studies revealed that the hSK3_ex4 is insensitive to the classical SK channel blockers such as apamin, scyllatoxin and d-tubocurarine. Transcripts coding for hSK3_ex4 were found in neuronal and non-neuronal human tissues but were expressed at lower levels when compared with hSK3. Additionally, two more SK3 variants, named SK3-1B (Tomita et al., 2003) and SK3-1C (Kolski-Andreaco et al., 2004), have been described. These variants use alternative first exons, termed 1B and 1C, which are localised downstream to the first exon of SK3 (Fig. 1.7 B). Consequently, the resulting proteins lack the amino-terminal domain and the S1 transmembrane segment. Interestingly, the heterologous expression of SK3-1B and of SK3-1C does not produce functional channels, but the two variants have been shown to act as dominant negative inhibitors of members of the SK-IK channel family (Tomita et al., 2003; Kolski-Andreaco et al., 2004). Little is known about the native expression and the functional role of these SK splice variants *in vivo*, and more work is needed to understand the physiological consequences of alternative splicing within the SK channel family. SK3-1B has been used to generate transgenic animals (see also 1.10) to study the physiological roles of SK channels (Shakkottai et al., 2004; Villalobos et al., 2004).

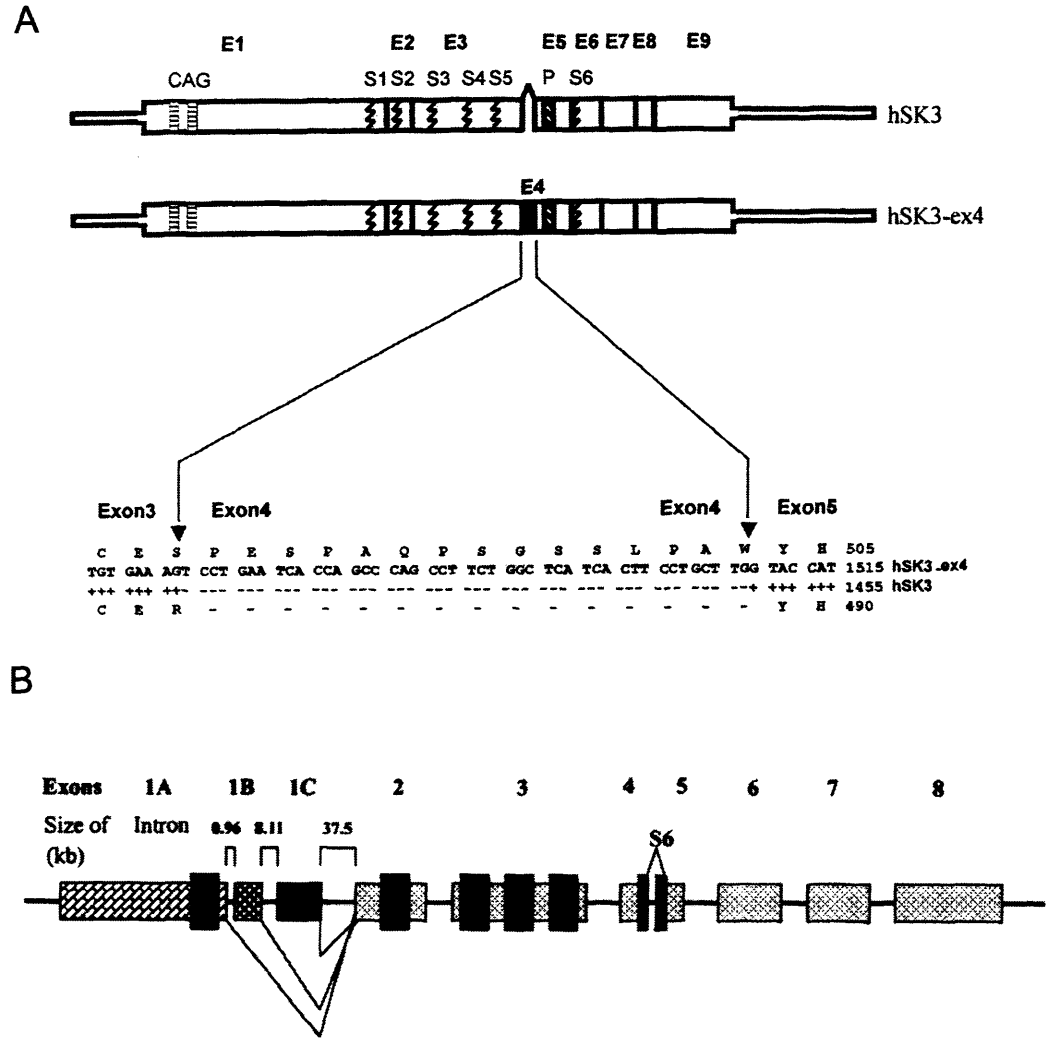

FIGURE 1.7: **Alternative splicing of the SK3 gene. A**: Schematic representation of the cDNAs of hSK3 and of the hSK3_ex4 splice variant. The thick boxes represent the coding region, whereas the thin boxes represent the 5' and 3' untranslated regions. The exon-intron boundaries are indicated as straight lines whereas the jagged lines depict the transmembrane segments S1-S6. The inclusion of the exon 4, represented as a filled black box, results in the insertion of 15 amino acids between the S5 segment and the pore region. The sequence of the 15 amino acids insertion is reported below (From Wittekindt et al., 2004). **B**: Schematic representation of the SK3 gene, indicating the localisation of the three alternative first exons, 1A, 1B and 1C. The lines below indicate the splicing events occurring between exons 1A, 1B or 1C and exon 2. The 6 transmembrane domains are represented as dark grey boxes. SK3 uses 1A as the first exon, whereas 1B and 1C are the first exons used by the SK1-1B and SK3-1C, respectively. (Adapted from Kolski-Andreaco et al., 2004).

1.8 Trafficking and assembly of SK channel subunits

The investigation of trafficking and multimerisation of SK channels has revealed a complex picture where the molecular determinants involved in these processes are different, making their analysis particularly complicated. Several studies suggest that the carboxy-terminal domain of SK channels has a relevant role both in trafficking and tetramerisation (Lee et al., 2003; Kolski-Andreaco et al., 2004; Roncarati et al., 2005). However, more recent evidence proposes that molecular determinants for the correct targeting are also present in other regions of the SK α subunits (Miller et al., 2001; Roncarati et al., 2005; Jones et al., 2005). The constitutive association between SK α subunits and calmodulin is necessary not only for gating but also for trafficking (Lee et al., 2003). In SK2 α subunits, the mutation of the amino acids responsible for the constitutive interaction with calmodulin results in SK2 channels that, besides having reduced affinity for calmodulin, display incorrect membrane trafficking. In fact, the mutant SK2 subunits are not expressed in the membrane but are retained in intracellular compartments (Lee et al., 2003). Coexpression of the mutated channel with calmodulin overcomes the reduced affinity to calmodulin and results in membrane expression. Membrane targeting is also obtained by coexpressing the mutant SK2 with a mutant calmodulin (CaM 1, 2, 3 and 4) that is unable to bind Ca^{2+}, indicating that only the Ca^{2+}-independent interactions with calmodulin are necessary for surface expression (Lee et al., 2003). Moreover, deletion of CaMBD causes retention of the SK3 α subunits in the endoplasmic reticulum and no membrane expression, but does not interfere with oligomerisation of the channel subunit (Roncarati et al., 2005). These observations indicate that the interaction with calmodulin is important for the trafficking of the SK channels but not for subunit assembly. A possible role of the amino-terminal domain in membrane targeting has also been proposed, as the expression of a dominant negative SK3 amino-terminal fragment has been shown to oligomerise with native SK2 currents in Jurkat cells (Miller et al., 2001). Moreover, the complete truncation of the amino-terminal domain in SK3 results in the lack of membrane expression of the channel (Roncarati et al., 2005). More recently, the cytoplasmic linker S4-S5 of IK and SK3 channels has been reported to be involved in channel trafficking (Jones et al., 2005). In particular, the mutation of a lysine in the S4-S5 linker (K197 of hIK and K453 of SK3) results in channels that fail to traffic to the plasma membrane, accumulate in

the endoplasmic reticulum, but can assemble in multimeric complexes (Jones et al., 2005).

The identification of a region involved in the assembly of SK channels has emerged from the study of the amino-terminal truncated splice variant SK3-1C (Kolski-Andreaco et al, 2004). The variant sequesters SK-IK channels and retain them in intracellular compartments, thereby preventing their functional membrane targeting (see also 1.6) (Kolski-Andreaco et al., 2004). Deletion analysis identified a 30 amino acid fragment, localised in the carboxy-terminus of SK3-1C, as the region responsible for this effect. The identified domain, which is called dominant inhibitory segment (DIS), covers part of the CaMBD (Fig. 1.8), but experimental evidence indicates that the segment does not interfere with calmodulin binding. The DIS is very conserved among the members of the SK channel family and resembles a coiled-coil domain known to mediate specific multimerisation of many K^+ channels (Jenke et al., 2003), suggesting that it could be involved in SK subunit assembly.

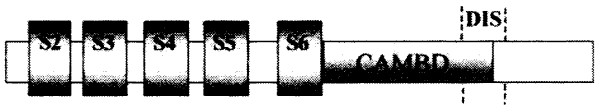

FIGURE 1.8: Localisation of the DIS domain. Schematic representation of the topological structure of the SK α subunits, indicating the location of the calmodulin binding domain and of the dominant inhibitory segment (DIS). (From Kolski-Andreaco et al., 2004).

Several studies indicate that the heteromeric assembly between members of the SK channel family occurs. Ishii and colleagues have shown that coexpression of rSK2 and hSK1 in oocytes results in functional channels with an apamin sensitivity that is intermediate between the sensitivity measured for homomeric SK2 and for homomeric hSK1 (Ishii et al., 1997b). More recent studies indicate that, although rSK1 subunits alone do not form functional channels, they can form heteromers with rSK2. These heteromeric channels generate larger currents but reduced apamin sensitivity when compared to SK2 homomers (Benton et al., 2003). Additionally, the coexpression of rSK3 and SK1 subunits (both human and rat) reduces the expression levels of functional rSK3 channels, suggesting heteromultimerisation of the two

subunits (Monaghan et al., 2004). Interestingly the most dramatic effect on SK3 expression is induced by hSK1 which completely suppressed the SK3 currents (Monaghan et al., 2004). Also, there is evidence for heteromeric assembly of SK2 and SK3 subunits (Miller et al., 2001). In Jurkat cells, the expression of an SK3-amino-terminal fragment suppresses native SK2 currents, supporting that coassembly between the two subunits might occur (Miller et al., 2001). A further indication comes from pharmacological data based on the use of an SK3 mutant insensitive to apamin and to UCL1848 (Monaghan et al., 2004). The heterologous expression of this SK3 mutant and SK2 results in channels with sensitivity to apamin and UCL1848 intermediate between the sensitivity that was measured when the two subunits were expressed alone (Monaghan et al., 2004). Although heteromeric association of SK α subunits seems to occur in recombinant expression systems, it is not clear whether such interactions occur *in vivo*. In fact, biochemical techniques based on the use of specific antibodies for SK2 and SK3 did not detect the presence of SK2-SK3 heteromers in rat brain (Sailer et al, 2002). Therefore, the existence and the physiological role of heteromers of SK subunits *in vivo* have still to be determined.

1.9 SK channel distribution

SK channels are predominantly expressed in the brain, as supported by Northern blot, *in situ* hybridisation and RT-PCR analysis (Kohler et al., 1996; Stocker and Pedarzani, 2000; Hosseini et al., 2001; Bosh et al., 2002). However, transcripts coding for the different SK subunits have also been detected in some peripheral tissues including the heart, which expresses SK1, SK2 and SK3 mRNA (Kohler et al. 1996, Hosseini, 2001; Xu et al., 2003); the adrenal gland, where SK1 and SK3 transcripts have been detected (Kohler et al., 1996); superior cervical ganglia, liver and the skeletal muscle which display SK3 mRNA expression (Hosseini et al., 2001). *In situ* hybridisation and recent immunohistochemical studies reported that in the mature rat brain the three SK subunits present a distinct distribution profile (Stocker and Pedarzani, 2000; Tacconi et al, 2001; Bosch et al., 2002; Sailer et al., 2002; Sailer et al., 2004; Sarpal et al., 2004). In many brain regions, the expression profile of SK1 and SK2 subunits overlaps, whereas SK3 has a complementary distribution (Fig. 1.9). In particular, high levels of SK1 and SK2 are detected in the neocortex, in

the hippocampus and in the thalamus. At the cellular level, immunolocalisation of SK2 has shown that this subunit has a preferential localization in Purkinje cell somata and dendrites at early stages of postnatal development (Cingolani et al., 2002; Womack and Khodakhah, 2003). Somatodendritic localisation has also been described for SK1 subunits in CA1 primary cultures (Bowden et al., 2001) but this observation differs from the localisation of this subunit in the brain tissue, where SK1 immunoreactivity was associated with the dendrites but not to the somata of CA1 hippocampal neurones (Sailer et al., 2002; Sailer et al., 2004). SK3 is abundantly expressed in many subcortical areas such as most thalamic nuclei, the lateral septum, the hypothalamus and in different monoaminergic neurones. Somatodendritic localisation of SK3 in dopaminergic neurones of the substantia nigra pars compacta emerged from immunhistochemical studies with an SK3 specific antibody (Wolfart et al., 2001). Moreover, axonal and presynaptic localization has been proposed for SK3 in primary cultures of hippocampal neurones, where the SK3 protein co-localises with presynaptic marker proteins (Obermair et al., 2003). These observations suggest that, despite their similarity, the different SK subunits not only are localised in different brain areas but also might be targeted to specific cellular compartments in different neuronal types.

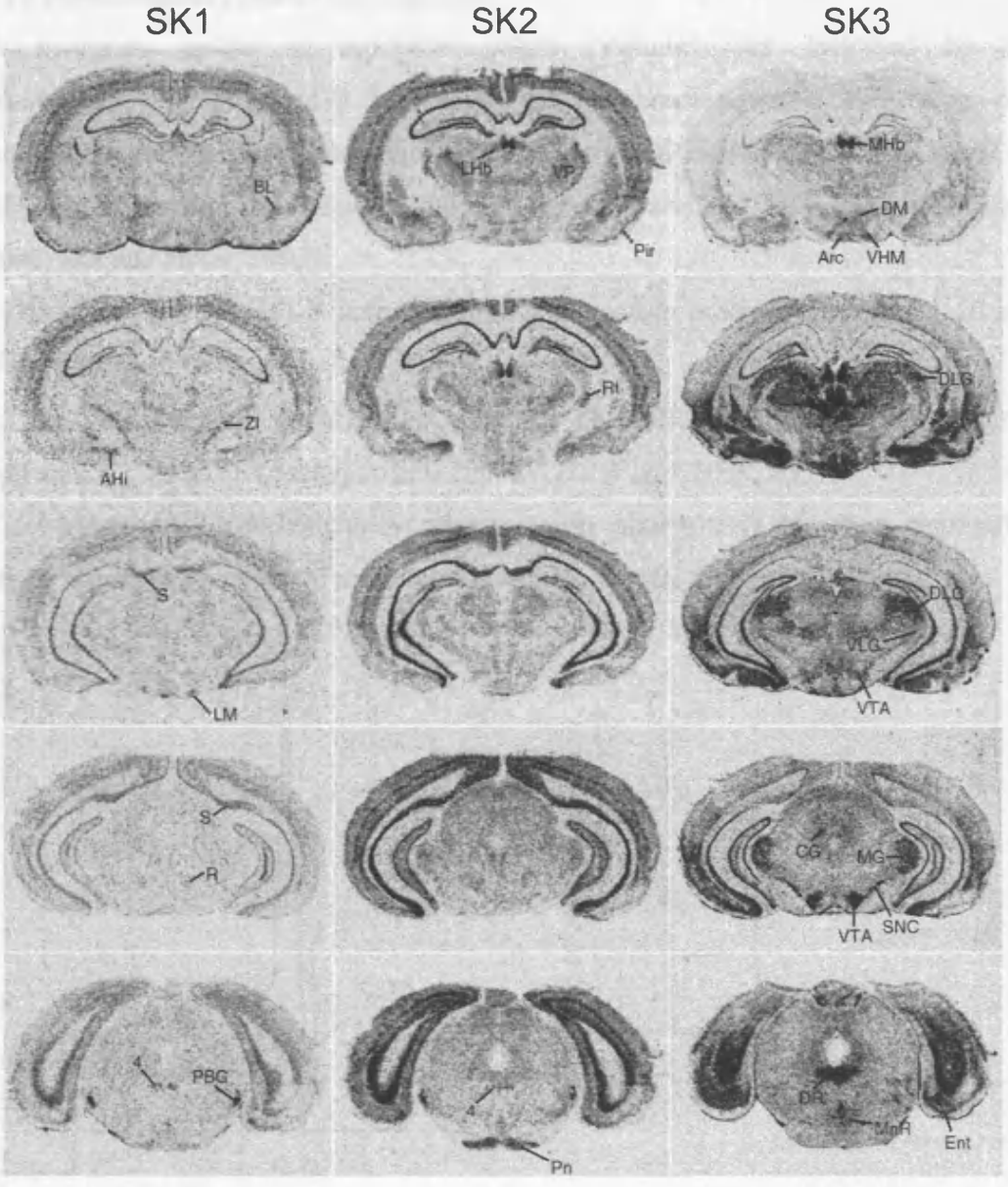

FIGURE 1.9: *In situ* hybridisation of SK channel α subunits in the adult rat brain. Overview pictures showing the distribution profile of SK1, SK2 and SK3 mRNA analysed by *in situ* hybridisation in the rat brain. (From Stocker and Pedarzani, 2000).

1.10 Physiological roles of SK channels

In neurones, single or repetitive action potentials are followed by an afterhyperpolarisation (AHP) that moves the membrane potential away from the action potential threshold, therefore reducing neuronal excitability. Three types of AHP have been classified according to their time course (Sah, 1996; Sah and Davies, 2000; Sah and Faber, 2002):

- the fast AHP (fAHP) is activated during the action potential and lasts 1-10 ms (Fig. 1.10 A);
- the medium AHP (mAHP) activates rapidly following one or more action potentials (1-5 ms) and decays within 200-400 ms (Fig. 1.10 A, B);
- the slow AHP (sAHP) can be observed only after a train of action potentials, peaks in several hundreds of milliseconds and can last up to 5 s (Fig. 1.10 B).

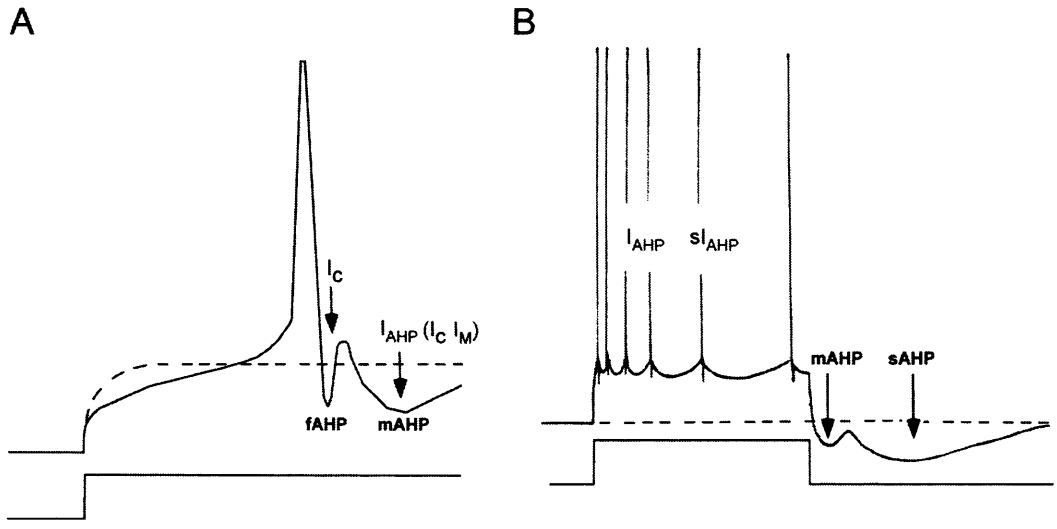

FIGURE 1.10: Representation of the three types of AHP that follow single or repetitive action potentials. A: Single action potentials are followed by a fast afterhyperpolarisation (fAHP), generated by the Ca^{2+}-activated K^+ current Ic. An afterhyperpolarising phase called mAHP follows the fAHP. The apamin-sensitive I_{AHP} current underlies the mAHP. Depending on the brain region, other currents are also involved in the generation of the mAHP. For example, in hippocampal CA1 pyramidal neurones, the voltage sensitive I_M and the voltage- and Ca^{2+}-sensitive I_C currents contribute to the generation of the mAHP. **B**: Train of action potentials elicited by constant current injection in hippocampal pyramidal neurones. The mAHP is maximally activated after a few action potentials, whereas the sAHP develops only after a train of action potentials (Adapted from Storm, 1990).

SK channels contribute to the generation of the mAHP, underling the I_{AHP} current, that is Ca^{2+}-activated, voltage-insensitive and selectively blocked by apamin, d-

tubocurarine and scyllatoxin (Kawai and Watanabe, 1986; Schwindt et al., 1988; Osmanovic et al., 1990; Stocker et al., 1999; Stocker et al., 2004a). Although SK channels have also been proposed to be involved in the generation of the sI_{AHP} current, which underlies the sAHP, there is no clear evidence for this hypothesis and, to date, the molecular determinants of this current are still a matter of debate (Vogalis et al., 2003; Bond et al., 2004; Stocker, 2004a-b; Villabos et al., 2004).

The I_{AHP} has been described in a large number of central neurones, in agreement with the broad distribution profile of the SK channel subunits in the central nervous system (Stocker and Pedarzani, 2000). The I_{AHP} displays a variety of functional roles, depending on the neuronal type, on the coupling to different Ca^{2+} sources, on the SK channel subunit composition and, possibly, on their subcellular localisation (Stocker et al., 2004b). The correlation between the SK channel distribution and the pharmacological properties of the I_{AHP} in various neuronal types provides information on the molecular composition of the channels underlying the I_{AHP}. Moreover, the use of immunohistochemical techniques for the analysis of the SK channel cellular distribution is starting to increase the information on how separate populations of SK channels, localised in specific neuronal compartments, contribute to different physiological roles.

In the hippocampus, the pyramidal neurones of the CA1 hippocampal region exhibit an apamin-sensitive I_{AHP} current, that controls the early frequency of firing (Stocker et al., 1999). In these neurones, the high mRNA levels of the SK2 subunit (Stocker and Pedarzani, 2000) and the apamin sensitivity of the I_{AHP} current (IC_{50} of 480 pM) suggested that SK2 is one of the main molecular determinants of the channels underlying the I_{AHP} (Stocker et al., 1999). The IC_{50} for apamin in hippocampal neurones is higher than that measured for heterologously expressed SK2 subunits (Stocker et al., 1999). This observation, together with the presence of SK1 transcripts in the CA1 pyramidal neurones, indicated the possibility that SK1/SK2 heteromeric channels underlie the I_{AHP} in these brain region (Stocker et al., 1999; Stocker and Pedarzani, 2000). However, electrophysiological studies on transgenic animals that lack either SK2 or SK1 channels indicate that SK2 alone can generate the I_{AHP} current in CA1 pyramidal neurones (Bond et al., 2004). CA3 pyramidal neurones

have also been shown to express an I_{AHP} current of similar amplitude to the one measured in CA1 pyramidal neurones, whereas a smaller I_{AHP} is present in dentate gyrus granule cells (Sailer et al., 2002). This difference in the current amplitude correlates with the observation that CA1 and CA3 regions display higher SK2 expression levels than the dentate gyrus (Stocker et al., 2000; Sailer et al., 2002; Sailer et al., 2004) and support the notion that SK2 channels contribute to the generation of the apamin-sensitive I_{AHP}. Also, hippocampal interneurones of CA3 stratum radiatum exhibit an I_{AHP} current that is involved in the regulation of the tonic firing activity (Savic et al., 2001). The selective detection of SK2 mRNA in these neurones indicates that SK2 homomeric channels are likely to be responsible for the generation of the I_{AHP} (Savic et al., 2001).

SK channels are involved in the regulation of the spontaneous firing in several neuronal types. For example, SK3 is the predominant subunit underlying the I_{AHP} current in dopaminergic neurones of the substantia nigra pars compacta. In this area, the current has a determinant role in controlling the frequency of spontaneous firing (Stocker and Pedarzani, 2000; Wolfart et al, 2001) and is selectively activated by T-type Ca^{2+} channels (Wolfart et al., 2002). The I_{AHP} contributes to the regulation of the spontaneous firing also in motor neurones of the dorsal vagal nucleus (Pedarzani et al., 2000). Pharmacological studies and *in situ* hybridisation indicate that SK3 homomeric channels underlie the I_{AHP} current in these neurones (Pedarzani et al., 2000). In the supraoptic neurones, an apamin-sensitive I_{AHP} current is involved in the control of the phasic firing of the supraoptic neurosecretory neurones (Bourque and Brown, 1987; Kirkpatrick and Bourque, 1996). The current has been reported to have an estimated apamin sensitivity in the nanomolar range (IC_{50} of 1.3 nM) (Bourque and Brown, 1987). This observation, together with the selective detection of SK3 mRNA (Stocker and Pedarzani, 2000) in this brain region, suggests that the current is likely to be mediated by SK3 homomeric channels. In Purkinje neurones of the cerebellum, SK2 channels have been shown to mediate the I_{AHP} current that regulates the tonic firing pattern of these cells (Cingolani et al., 2002; Womack and Khodakhah, 2003; Edgerton et al., 2003). The selective activation of P/Q type Ca^{2+} channels seems to be responsible for the activation of the SK channels in these neurones (Womack et al., 2004).

Recently, a new role for SK channels in the modulation of the synaptic activity of the hippocampal pyramidal neurones has been proposed (Ngo-Anh et al., 2005; Faber et al., 2005; Cai et al., 2004). In individual spines of hippocampal CA1 neurones, the Ca^{2+} entry during synaptic activation opens SK channels that, in turn, reduce the NMDA receptor-mediated Ca^{2+} transients within the spine, resulting in the reduction of the amplitude of excitatory postsynaptic potentials at the soma (Ngo-Anh et al., 2005). A similar physiological role of SK channels has been described in neurones of the lateral amygdaloid nucleus (Faber et al., 2005), where SK channels, localised in the dendritic spines, function as feed-back regulators of synaptic response to glutamate. Moreover, recent evidence shows that, in organotypic hippocampal cultures, SK channels are responsible for the repolarization of local dendritic plateau potentials triggered by focal glutamate application to CA1 pyramidal neurone distal apical dendrites (Cai et al., 2004).

Further information on the physiological function of SK channels are derived from the generation of transgenic animals with enhanced or reduced expression of the SK channel α subunits. The generation of a mouse model where the expression of the SK3 gene was regulated by dietary administration of a tetracycline derivative showed that suppression of SK3 did not produce any phenotypic change (Bond et al., 2000). On the contrary, the overexpression of SK3 resulted in mice with abnormal respiration and abnormal parturition (Bond et al., 2000). Also, the splice variant SK3-1B (see also 1.6), which suppresses SK and IK channels, was used to generate transgenic animals. The mouse model was engineered to express the SK3-1B under the control of a neuronal promoter, resulting in the expression of the transgene in several brain regions (Shakkottai et al., 2004). The transgenic mice developed severe cerebellar ataxia due to an increased excitability of the deep cerebellar nuclei. This enhanced excitability was shown to be generated by downregulation of SK1 and SK2 channel expression in the deep cerebellar nuclei of the cerebellum, which resulted in the reduction of the apamin-sensitive I_{AHP} (Shakkottai et al., 2004). The SK3-1B transgene was also expressed in pyramidal neurones of neocortical layer V. The expression of the transgene in these neurones caused a strong reduction of the apamin-sensitive I_{AHP} measured in this brain region (Villalobos et al., 2004).

Moreover, electrophysiological studies on mice models lacking SK1 or SK3 revealed that the I_{AHP} current measured in CA1 pyramidal neurones was unchanged (Bond et al., 2004). On the contrary, the lack of SK2 subunit abolished the I_{AHP} current in CA1 pyramidal neurones, confirming that SK2 is the principal SK subunit contributing to the generation of that current (Bond et al., 2004).

1.11 Aims of this thesis

The principal aim of this thesis was the study of different aspects of the distribution of SK subunits in the rat brain:

- the subcellular distribution of the SK2 α subunit was analysed in different central neurones by using a site-directed SK2 antibody, anti-NSK2, in immunohistochemistry studies;

- the distribution pattern and the targeting of a newly identified SK2 splice variant, called SK2-860, were investigated. For this purpose, an antibody specifically recognising this new variant was characterised and used in combination with the anti-NSK2 antibody to assess the distribution of the SK2-860 protein in native tissue and in transfected neuronal cells;

- after the characterisation of an SK3-specific antibody, immunohistochemical studies were performed to assess the cellular distribution of the SK3 subunit in various brain regions;

- the developemental distribution of the SK3 subunit was analysed in the rat brain monoaminergic regions such as the substantia nigra-ventral tegmental area, the locus coeruleus and the dorsal raphe.

In the last chapter of this thesis, the aim was to refine the understanding of the differences in apamin-sensitivity between the members of the SK channel family.

CHAPTER 2

Materials and methods

2.1 Materials

2.1.1 Consumables

Glass coverslips	∅ 13 and 22 x 22 mm, Menzel-Glässer
Glass coverslips for mounting sections	24 x 60 mm, Menzel-Glässer
Glass capillaries (1.2 mm O.D. x 0.69 mm I.D.)	Clark Electromedical Instruments (GC120F-10)
Immuno-plates, 96 wells	Maxisorp, Nunc (442404)
Mini spin handy columns	Pierce
Multiple well plates: 4, 6, & 24	Nunc
12 well plates	Corning
15 mm Netwell™ inserts (74 µm mesh size polyester membrane)	Corning (3477)
Netwell™ 12 well carrier kit for 15 mm inserts	Corning (3520)
Nitrocellulose membrane	Protran®, Schleicher & Schuell
Petri dish, 92 x 19 mm	Sarstedt
35 mm dishes	Nunc
Slides 76 x 26 mm	Menzel-Glässer
Stericup filters, 150 & 500 ml	Millipore
SuperFrost®Plus slides	041300, VWR International
Serological pipette; 5, 10 & 25 ml	Sarstedt
Tissue culture flask: T25 & T75	Nunc
1.5, 2, 15 & 50 ml tubes	Sarstedt
12 ml PS tubes screw caps	Greiner
Syringe filters, 0.22 µm PES-membrane	Millex®-GP, Millipore
Ultra-Clear centrifuge tubes 25 x 89 mm	Beckman (344058)
Whatman paper 3 MM	Whatman
VectaSpin Micro filters	Whatman
Films	Kodak BioMax

2.1.2 Equipment

CCD camera	QImaging, MicroPublisher
Cell culture incubator	Heraeus Instruments
Centrifuge	J2-MI, Beckman
	5415R, Eppendorf
	MiniSpin Plus, Eppendorf
Ultra-centrifuge	XL-80, Beckman
Computer	eMac
Confocal microscope	Axiovert 200, Zeiss/ LSM 510
Zeiss Filters	HFT UV488/543/633,LP650, BP 560-615
Hood for tissue culture	BioMAT-2
Hood for dissection	Envair VLF
Homogeniser	RWI6 basic IKA Labortechnik
X-Ray Film processor RG II	FUJI
Microinjector 5246	Eppendorf
Micromanipulator 5171	Eppendorf

Micropipette puller	Sutter Instrument P-80
Microscope	Axiophot, Zeiss
Fluorescence filter for Axiophot:	
Zeiss set 10 (excitation: BP 450-490; beamsplitter: FT 510; emission: BP 515-565)	
Zeiss set 15 (excitation: BP 546-512; beamsplitter: FT 580; emission: LP 590)	
PCR System 2400	Applied Biosystems
Sequencer ABI PRISM® 3100-*AVANT*	Applied Biosystems
Shaker	Innova 4230, New Brunswick
Sliding microtome SM2000 R	Leica
Spectrophotometer	SmartSpec 3000, Bio-Rad
Tissue-Tek slide holder	Miles
Tissue-Tek slide staining set	Sakura
Thermo-max microplate reader	Molecular Devices
UV trans-illuminator (750-M)	International Biotechnologies 4W Model UVL-24, (365 nm), UVP

2.1.3 Kits and reagents

BigDye™ Terminator (version 1.1)	Applied Biosystem
BioRad DC Protein Assay kit	Bio-Rad
DAB Substrate kit for peroxidase	Vector Laboratories
ECL chemiluminescent system	Amersham Pharmacia Biotech
Gel filtration NAP™10 Columns	Amersham Pharmacia
Immobilised TCEP Disulphide Reducing Gel	Pierce (77712)
Lipofectamine™ 2000	Invitrogen
Nucleobond PC 100 & PC 500	Macherey-Nagel
NucleoSpin Extract	Macherey-Nagel
NucleoSpin Plasmid	Macherey-Nagel
ProLong Antifade kit	Molecular Probes
SulfoLink® Coupling Gel	Pierce (20401)
Tyramide Signal Amplification Kit (TSA)	Molecular Probes
TSA™ Biotin System	PerkinElmer
Vectastain Elite ABC Kit (PK-6100)	Vector Laboratories

2.1.4 Enzymes, commercial antibodies and proteins

Alkaline Phosphatase	Roche
Anti-c-myc (clone 9E10)	Roche
BSA, protease-free, fraction V (for immunofluorescence)	Sigma (A-3294)
BSA, protease, peroxidase, alkaline phosphatase-free, fraction V (for antibody purification)	Serva, (11926)
Swine anti-rabbit FITC-conjugated	DAKO
Goat anti-rabbit IgG HRP-conjugated antibody (PepSpot)	BioRad
Goat anti-rabbit IgG HRP-conjugated antibody (ELISA)	Sigma
Goat anti-rabbit IgG HRP-conjugated antibody	

(Western Blot)	Jackson (111-035-008)
KOD hot start DNA-polymerase (1 U/µl)	Novagen
Pfu DNA-polymerase (2.5 U/µl)	Stratagene
Protease inhibitors: PMSF, Leupeptin, Pepstatin, Aprotinin	Roche
RNase A	Sigma
T4-DNA ligase (1U/µl)	Roche

Restriction enzymes were purchased from Roche and NewEnglandBiolabs.

2.1.5 Antibodies, fusion proteins and peptides

Anti-NSK2 antibody (raised against GST-NSK2 fusion protein)	aa 23–83, GenBank accession no. U69882
Anti-N860 antibody (raised against GST-N7 fusion protein)	aa 68-249, GenBank accession no.AK033158.1
Anti-CSK3 antibody	aa 706-719, H_2N-CSHAPPSDSPIGISS-amide
pET-NSK2	aa 1-165 Trx, aa 166-227 NSK2 (aa 23-83)
GST-NSK2	aa 1-227 GST, aa 228-289 NSK2 (aa 23-83)
NSK2 PepSpot peptide	acetyl-QPLQPPASVVGGGC-amide

2.1.6 DNA and protein molecular weight markers

DNA ladders:
1 kb DNA-ladder: 12,216; 11,198; 10,180; 9,162; 8,144; 7,126; 6,108; 5,090; 4,072; 3,054; 2,036; 1,636; 1,018; 506; 396; 344; 298; 220; 201; 154; 134; 75 bp

100 bp DNA-ladder: 2,072; 1,500; 1,400; 1,300; 1,200; 1,100; 1,000; 900; 800; 700; 600; 500; 400; 300; 200; 100 bp

The DNA-ladders were obtained from Gibco BRL.

Protein standards:
Prestained broad range protein standard (BioRad): 250, 150, 100, 75, 50, 37, 25, 15, 10 kDa
Prestained protein molecular weight marker (Fermantas): 118, 85, 47, 36, 26, 20 kDa

2.1.7 Cell culture

B27 supplement (50 x)	Invitrogen (17504044)
BSA (SCG neurones)	Sigma (A4161)
Collagenase type 1A (SCG neurones)	Sigma (C9891)
DMEM/F12	Invitrogen (21331-020)
Foetal Calf Serum	Invitrogen (10108-165)
Glucose (45%)	Sigma (G8769)
HEPES (1M) (hippocampal neurones)	Invitrogen (15630-049)
HEPES (1M) (SCG neurones)	Sigma (H 0887)
HBSS	Invitrogen (14170-070)

Horse Serum	Invitrogen (26050-070)
L15	Sigma (L5520)
Laminin	Sigma (L2020)
L-Glutamine 200 mM	Invitrogen (15039-027)
MEM with Earl's salts	Invitrogen (21090-022)
$NaHCO_3$ (7.5%)	Invitrogen (25080-060)
Neurobasal	Invitrogen (2110-3049)
NGF 7S	Sigma (N0513)
OPTI-MEM1	Invitrogen (51985-026)
Penicillin/Streptomycin (Pen-Strep) (10000 U/ml)	Invitrogen (15140-148)
PBS	Invitrogen (20012-019)
Pyruvic acid (100 mM)	Invitrogen (11360-039)
Trypan blue	Sigma (T8154)
Trypsin-EDTA (HEK Cells)	Invitrogen (25300-054)
Trypsin, bovine type XII S (SCG neurones)	Sigma (T9935)
Trypsin (2.5%) (hippocampal neurones)	Invitrogen (15090-046)

2.1.8 Chemicals

Acrylamide (AA)/bisacrylamide (BA), 30%	Bio-Rad
Select-Agar	Gibco-BRL
Agarose Ultra-Pure	Gibco-BRL
Ammonium persulfate (AP)	Kodak
Ampicillin	Roche
2,2'-Azinobis (3-ethylbenzothiazoline-6-sulfonicacid) (ABTS)	Pierce
DePex mounting medium	BDH
Dithiothreitol (DTT)	Biomol
HiDi formamide	Applied Biosystems
Histo-Clear	National Diagnostic
H_2O_2 30%	BDH
Hematoxylin (Mayer solution)	Fluka
Hemoglobin	Sigma
Heparin sodium salt (151 U/mg)	Sigma
HEPES	Fluka
Iodacetamide	Sigma
Luria Broth (LB)	Gibco-BRL
2-Mercaptoethanol	BDH
Milk powder	Frema
N, N ,N', N'-tetramethylenediamine (TEMED)	BDH
Paraformaldehyde (PFA), granular	Electron Microscopy Sciences
Poly-D-Lysine (MW 70,000-150,000)	Sigma
Ponceau S Solution (0.1% Ponceau S in 5% acetic acid)	Sigma
Sodium dodecylsulfate (SDS)	USB
TAE (50X)	National Diagnostics
Triton X-100	Fluka
Tween-20	Calbiochem

All other chemicals were purchased from BDH, Fluka, Merck and Sigma.

2.1.9 Buffers

PB (0.1M)	70	mM	Na_2HPO_4
	30	mM	NaH_2PO_4
	(pH 7.4)		
PBS (10x)	1300	mM	NaCl
	70	mM	Na_2HPO_4
	30	mM	NaH_2PO_4
	(pH 7.4)		
TBS (10x)	1.4	M	NaCl
	200	mM	Tris-HCl (pH7.5)
	(pH 7.5)		

2.2 Methods

2.2.1 Membrane purification of antibody

2.2.1.1 Membrane preparation. The anti-NSK2 antibody, raised against GST-NSK2 fusion protein (2.1.5), was purified using the Trx-NSK2 fusion protein in which the same region of SK2 used to raise the antibody was fused to Thioredoxin (Trx). 100 µg of Trx-NSK2 fusion protein were solubilized in 0.5 ml PBS-Azide and adsorbed to nitrocellulose membrane (Protran® Schleicher & Schuell, 1.4 x 1.4 cm) at room temperature for 2 hours, in a sealed plastic bag under slow rotation. After rinsing in PBS-Azide, the membrane was blocked with 10 ml of 5% dry milk in PBS-Azide for 2 hours in a Petri dish (92 x 19 mm). The membrane was then washed twice for 5 min in PBS-Azide, once in wash buffer, and twice in 1% BSA (Sigma, A-3294)/PBS-Azide. All washes were performed with 10 ml of the indicated solution, in a Petri dish (92 x 19 mm). After moving the membrane into a clean 2 ml tube, the fusion protein weakly bound to the membrane was removed by vortexing the membrane for 1 min in 500 µl of acidic elution buffer and three times for 1 min in 500 µl of alkaline elution buffer. After discarding the last time the alkaline buffer, the membrane was moved back in a Petri dish, and washed first for 5 min with PBS-Azide and then for 5 min with 5% dry milk/PBS-Azide.

2.2.1.2 Antibody purification. The binding of the antibody was performed by incubating the membrane (2.2.1.1) with the anti-NSK2 serum (50 µl antiserum diluted in 500 µl of 5% dry milk/PBS-Azide) in a sealed plastic bag, over night at 4°C, under slow rotation. The next morning the membrane was washed for 5 min in wash buffer and twice for 5 min in 1% BSA (Sigma, A-3294)/PBS-Azide. The antibody elution was performed by vortexing the membrane for exactly 1 min with 500 µl acidic buffer, and, right away, the eluted antibody was neutralized with 125 µl Tris-HCl (1 M, pH 8.0). This elution step was repeated a second time and, after removing the second eluate, the membrane was washed twice for 1 min in 1% BSA (Sigma, A-3294)/PBS-Azide. Two more elutions were performed, as described before, by adding 500 µl of alkaline buffer and neutralising each eluate in 50 µl Tris-HCl (1 M, pH 8.0). All the eluates were combined.

2.2.1.3 Desalting of the purified antibody. The combined fractions were desalted by gel filtration using NAP-10 columns (AmershamPharmacia). The columns were equilibrated with 15 ml of equilibration buffer and loaded with 1.25 ml of the

sample. The elution was carried out with 1.5 ml of equilibration buffer. Finally, 100 µl aliquots of purified antibody were snap frozen in liquid nitrogen and stored at -80°C

PBS-Azide	130	mM	NaCl
	7	mM	Na_2HPO_4
	3	mM	NaH_2PO_4
	0.01	%	Azide
	(pH 7.4)		
Wash buffer	1	%	BSA (Sigma, A-3294)
	1	x	PBS-Azide
	0.5	%	Triton X-100
Acidic elution buffer	200	mM	Glycine
	150	mM	NaCl
	(pH 2.5)		
	1	mg/ml	BSA
Alkaline elution buffer	100	mM	Triethylamine
	(pH 11.5)		
PBS-Azide	130	mM	NaCl
	7	mM	Na_2HPO_4
	3	mM	NaH_2PO_4
	0.01	%	Azide
	(pH 7.4)		
Equilibration buffer	1	%	BSA (Serva)
	1	x	PBS
	0.01	%	Azide

2.2.2 Column purification

2.2.2.1 Column preparation. SulfoLink coupling gel was used to immobilize the fusion protein Trx-NSK2 (2.1.5), the NSK2-pepspot peptide (2.1.5) or the peptide SK3 (2.1.5) that were used for the affinity purification of the anti-NSK2 and anti-NSK3 sera. SulfoLink enables the covalent immobilisation of sulphydryl-containing peptides or proteins to an agarose gel support. The coupling is mediated by the reaction of the iodoacetyl groups of the matrix with the reduced sulphydryl group of the terminal cysteine of the peptide or other free sulphydryl groups. Before immobilization, the peptide was reduced using the immobilized TCEP disulphide

Reducing Gel, where the reducing agent TCEP is linked to agarose beads which allow an easy separation from the reducing agent.

2.2.2.2 Peptide reduction. All the solutions used for this procedure were deoxygenated by bubbling N_2 through the solutions for 15 min. 1 mg of peptide was dissolved in 200 µl of sterile dH_2O; EDTA was added to the peptide solution at the final concentration of 10 mM and Tris-HCl (pH 7.5) was added at the final concentration 5 mM. 750 µl of TCEP reducing gel (corresponding to 1.5 ml of 50% slurry) was equilibrated at room temperature, centrifuged at 50 x g for 1 min and the supernatant was removed. The reducing gel was washed three times with 750 µl of deoxygenated reducing buffer. Each wash was performed by adding reducing buffer, vortexing, centrifuging at 50 x g for 1 min and, finally, removing the supernatant. After the last wash, the peptide solution and 150 µl of reducing buffer were added to the TCEP-agarose beads, mixed by vortexing, and incubated for 15 min at room temperature under slow rotation. To recover the reduced peptide, the beads were sedimented as before and the supernatant was collected. The TCEP reducing gel was washed three times with 200 µl of reducing buffer and the collected supernatants were combined. To remove any residue of agarose, the solution containing the reduced peptide was finally filtered using a spin column (mini spin handy, Pierce) by centrifugation at 50 x g for 1 min. The flow through, which contained the reduced peptide, was collected and Tris-HCl (pH 8.5) was added at the final concentration of 50 mM.

Reducing buffer	10	mM	EDTA
	5	mM	Tris-HCl
	(pH 7.5)		
	(deoxygenated before use)		

2.2.2.3 Peptide coupling to SulfoLink affinity matrix. After equilibrating the SulfoLink coupling gel at room temperature, 2 ml of 50% slurry were moved into a tube and washed three times with 1 ml of deoxygenated coupling buffer. Washes were performed by adding coupling buffer, vortexing, centrifuging at 50 x g for 1 min and discarding the supernatant. After the last wash, the solution containing the reduced peptide was added to the SulfoLink gel and incubated for 15 min under slow rotation followed by 30 min without rotation. The agarose beads were sedimented at

50 x g for 1 min, and, after removing the supernatant, they were washed with coupling buffer. In order to block non-specific binding sites on the gel, 1 ml of coupling buffer containing 50 mM cysteine was added to the gel matrix and incubated for 15 min under slow rotation, at room temperature, followed by further 30 min incubation without rotation. The matrix was finally transferred into a column (500 µl per column), washed first with 16 matrix volumes of 1 M NaCl and then with 16 volumes of 0.05% Azide. The column was stored at 4°C in TBS-0.005% Azide and was washed with 5 ml TBS before starting the purification.

Coupling buffer	5	mM	EDTA
	50	mM	Tris-HCl
	(pH 8.5)		
	(deoxygenated before use)		

2.2.2.4 Column purification. 500 µl of serum were diluted in 4.0 ml solution A, incubated at 56°C for 30 min and centrifuged at 16000 x g for 15 min at 4°C. The diluted serum was then loaded onto the affinity column (2.2.2.3) with a flow rate of 5 column volumes per hour. The eluate was collected and loaded three more times onto the column. The flow through after the fourth repetition was stored at 4°C. In order to remove the antibody not specifically bound to the fusion protein, the column was first washed four times with 1 ml of solution A and then four times with 1 ml of a high salt buffer (solution B). The first elution of the antibody was performed using an acidic solution: 6 x 500 µl of solution C were loaded on the column and each eluate was immediately neutralised with 75 µl 1 M Tris-HCl (pH 8.0). After washing the column four times with 1 ml of solution A, the alkaline elution was performed: 6 x 500 µl of solution D were loaded on the column and each 500 µl eluate was collected in 1.5 ml tubes containing 150 µl 1 M Tris-HCl (pH 6.8) for neutralisation. The column was finally washed five times with 1 ml of solution A, once with TBS-0.005% Azide and stored at 4°C. OD measurements at 280 nm were performed to assess the protein concentration of each elution fraction, the flow through and each washing step, in order to estimate the progress of the purification. Elution fractions with the highest protein concentration were pooled and desalted by gel filtration using NAP10 columns (2.2.1.3). 100 µl aliquots of purified antibody were snap frozen in liquid nitrogen and stored at -80°C.

Solution A	100	mM	NaCl
	10	mM	Tris-HCl
	(pH7.5)		
Solution B	500	mM	NaCl
	10	mM	TrisHCl
	(pH7.5)		
Solution C	100	mM	Glycine
	(pH 2.4)		
Solution D	100	mM	Na_2HPO_4
	160	mM	NaCl
	(pH 11.5)		

2.2.3 Peptide coupling to Imject® Maleimide Activated BSA

The PepSPOT peptide was coupled to Imject® Maleimide Activated BSA carrier protein in order to perform ELISA experiments. The PepSPOT peptide (1 mg) was dissolved in 150 µl of BSA reducing buffer and reduced as described in 2.2.2.2, but using BSA coupling buffer in place of the reducing buffer. The Imject® Maleimide Activated BSA was reconstituted in 200 µl of deoxygenated dH_2O and mixed to the reduced peptide. The mix was incubated for 2 hours at room temperature under slow rotation to allow the binding of the peptide to the BSA. After the incubation, aliquots of BSA-peptide were snap frozen in liquid nitrogen and stored at -80°C.

BSA reducing buffer	100	mM	Sodium Phosphate
	150	mM	NaCl
	20	mM	EDTA
	(pH 7.1)		
	(deoxygenated before use)		

2.2.4 ELISA

The success of the antibody purification was tested with an ELISA assay. 3 µg/ml of antigen in coating buffer were adsorbed overnight at 4°C on 96-well Maxisorp plates (60 µl/well). The next morning the antigen solution was removed, the wells were washed in ELISA wash buffer and then blocked for 30 min in ELISA blocking solution (250 µl/well). After 3 rinses in ELISA wash buffer, the wells were incubated with serial dilutions of primary antibody diluted in ELISA blocking solution (60 µl/well) for 2 hours at room temperature. After removing the antibody, the wells were washed twice in ELISA wash buffer, once in PBS, and then incubated for 45 min with the secondary goat anti-rabbit IgG HRP-conjugated antibody (1:1000, Sigma) diluted in PBS supplemented with 1 mg/ml Hemoglobin (60 µl/well). The secondary antibody was removed and the wells were washed three times with PBS. Afterwards, the HRP substrate ABTS (1 mg/ml) plus 0.006% H_2O_2 in incubation buffer was added (100 µl/well). The reaction was carried out for 5-7 min in the dark, and then stopped with 100 µl of 10% SDS solution. The absorbance was read at the wavelength of 405 mm with a Thermo-max microplate reader (Molecular Devices). Data were analysed using Microsoft Excel.

Coating buffer	17	ml	Na_2CO_3 200 mM
	8	ml	$NaHCO_3$ 200 mM
	75	ml	dH_2O
	(pH 9.6)		
ELISA Wash buffer	50	mM	NaH_2PO_4
	150	mM	NaCl
	(pH 7.2)		
	0.05	%	Tween 20
	0.02	%	NaN_3
ELISA blocking solution	1	mg/ml	Hemoglobin
	1	x	ELISA Wash buffer
Incubation buffer	50	mM	NaH_2PO_4
	100	mM	CH_3COONa
	(pH 4.2)		

2.2.5 Primary antibody preadsorption

To demonstrate the specificity of the primary antibodies, the affinity-purified anti-NSK2 and anti-CSK3 antibodies (2.1.5) were preadsorbed with the corresponding antigens (pET-NSK2 and SK3 peptide) (2.1.5). The amount of purified antibody needed for the final dilution was incubated in 100 µl 1xTBS supplemented with 2% BSA (Sigma, A-3294)/5% NGS either with Trx-NSK2 (20 µg/ml) or with the SK3 peptide (30 µg/ml). The pre-adsorption was carried out for 4 hours at room temperature or over night at 4°C, under slow rotation. This mixture was then adjusted to the final volume with the buffer used for the primary antibody incubation in Western, immunocytochemistry or immunohistochemistry experiments. The given peptide concentrations refer to the final volume used in each experiment. In parallel the anti-NSK2 and anti-CSK3 antibody were incubated under the same conditions but omitting the fusion protein or peptide.

The preadsorption of the anti-N860 antibody was performed by immobilising the pET-N7 antigen on nitrocellulose membrane (Protran® Schleicher & Schüll, 1.0 x 1.0 cm). The binding of the antigen to the membrane was performed as described in 2.2.1.1, in a 0.5 ml tube under slow rotation. Afterwards, the membrane was washed, blocked for 2 hours and then washed again as described in 2.2.1.1. In order to remove the pET-N7 antigen weakly bound to the membrane, three acidic elutions were performed followed by washes with PBS-0.01% Azide and with 5% dry milk/PBS-0.01% Azide (2.2.1.1). Afterwards, the membrane was incubated with the anti-N860 antibody diluted (1:200) in 300 µl of 2% BSA/5% NGS in TBS. The incubation was performed in a 0.5 ml tube, overnight at 4°C. In parallel, the anti-NSK2 antibody was treated in the same way but the membrane was coated with pET protein, in order to test non-specific binding of the antibody. The following day the supernatant was collected and used as control in immunohistochemistry experiments.

2.2.6 Synaptosomal membranes preparation

Synaptosome membrane preparation is based on the method described in Dodd et al. (Dodd et al., 1981). A 35 days old rat was terminally anaesthetised by a rising concentration of CO_2. The brain was removed from the skull and placed immediately in ice-cold PBS. After removing brain stem and cerebellum, the brain was homogenised in 10 ml homogenisation buffer, with 15 strokes, using a glass Teflon

homogeniser. The homogenate was centrifuged for 5 min at 1000 x g. The resulting P1 pellet was resuspended in 5 ml homogenisation buffer, homogenised again with 10 strokes and centrifuged as before. The supernatants of both centrifugations were combined, moved into a thin-walled ultracentrifuge tube and membranes were sedimented by centrifugation at 100,000 x g, for 1 hour (28,000 rpm in SW28 rotor), at 4°C. The resulting P2 pellet was resuspended in 5 ml of wash buffer, homogenised with five strokes and stirred on ice at 4°C for 15 min, in order induce hypotonic lysis of vesicles. Subsequently, 2 M sucrose was added to the homogenate to reach a final concentration of 0.8 M sucrose. A step gradient of sucrose was prepared as follows: the homogenate was placed at the bottom of a thin-walled ultracentrifuge tube and carefully overlaid with 10 ml of homogenisation buffer (0.3 M sucrose). This gradient was centrifuged at 100,000 x g for 2 hours. Myelin rich membranes, forming a white thick band, were retained at the interphase between the 0.8 M and 0.3 M sucrose, whereas membranes of higher density were sedimented and formed a big beige pellet. The 0.3 M and 0.8 M sucrose phases were removed and the high density membrane pellet was resuspended in 10 ml of wash buffer containing 1.2 M sucrose. The resuspension was homogenised with five strokes to give a homogeneous membrane suspension, and then adjusted to 15 ml with wash buffer containing 1.2 M sucrose. This suspension was transferred to the bottom of a 38.5 ml thin-walled ultracentrifuge tube and carefully overlaid with 9 ml of wash buffer containing 0.8 M sucrose and 9 ml of homogenisation buffer (0.3 M sucrose). This second step gradient was centrifuged for 2.5 hours at 100,000 x g. Synaptosomes were retained at the interphase between 0.8 M and the 1.2 M sucrose, whereas mitochondria were pelleted. All fractions of the preparation were collected, resuspended in wash buffer in order to reduce the sucrose content, sedimented by centrifugation for 30 min at 19,800 x g. The pellets were resuspended in 0.5-1.5 ml of wash buffer and snap-frozen in liquid nitrogen.

Homogenisation buffer	320	mM	Sucrose
	10	mM	HEPES
	2	mM	EDTA (pH 8.0)
	(pH 7.5)		
	0.1	mM	PMSF
	1	µM	Leupeptin
	1	µM	Pepstatin
	1	µg/ml	Aprotinin
	(pH 7.5)		
Wash buffer	10	mM	HEPES
	2	mM	EDTA (pH 8.0)
	(pH 7.5)		
	0.1	mM	PMSF
	1	µM	Leupeptin
	1	µM	Pepstatin
	1	µg/ml	Aprotinin

2.2.7 Estimation of protein concentration

The concentration of the extracted proteins was estimated using the BioRad DC Protein Assay Kit, which is based on the Lowry assay (Lowry et al., 1951). The assay is based on the reaction between proteins and an alkaline copper tartrate solution, and the subsequent reduction of Folin reagent by the copper-treated protein. The reduced Folin reagent has a characteristic blue colour with a maximum absorbance at the wavelength of 750 nm. Six dilutions of the standard protein BSA were prepared, containing 1, 0.8, 0.6, 0.4, 0.2 and 0.1 mg/ml of protein. The samples were diluted 1:1, 1:2, 1:4 and 1:10. All dilutions of the standard protein as well as of the samples were prepared in dH_2O and LDS at the final concentration of 2.5%. The reagent A (alkaline copper tartrate solution) was premixed with the reagent S (20 µl/ml reagent A), and 100 µl of this mix were combined with 20 µl of each sample dilution. 800 µl of reagent B (Folin reagent) were added and, after 15 min, the absorbance was read at the wavelength of 750 nm with a SmartSpec 3000 spectrophotometer (Bio-Rad). According to the Beer-Lambert's law, the relationship between absorbance and protein concentration is linear. Therefore, the absorbances corresponding to the standard protein dilutions are used to fit a linear standard curve. The slope and the intercept of this linear standard curve are used to calculate the concentration of the samples.

2.2.8 Western blot

2.2.8.1 SDS-polyacrylamide gel electrophoresis. Proteins were separated on a SDS-polyacrylamide gel that was prepared and run in a mini-gel apparatus (Mini-Protean III, Bio-Rad). The stacking gel was made of 3.5% acrylamide (AA)/bisacrylamide (BA) and 1 x Upper Tris, whereas the separating gel was made of 7.5% or 12% AA/BA and 1 x Lower Tris (Table 1). The polymerization of stacking and separating gel was carried out at room temperature using ammonium persulfate (AP) and TEMED to start and catalyse the reaction (Table 1). Samples containing 100 µg protein were supplemented with 6 x Laemmli buffer, DTT (made fresh) at the final concentration of 25 mM and dH_2O to reach the final volume of 15-40 µl. Samples were incubated for 10 min at 75°C and then supplemented with iodacetamide (made fresh) at the final concentration of 50 mM. After an incubation of 15-30 min in the dark the samples were loaded on the gel. A pre-stained, broad range molecular marker (2.1.6) was run in parallel to the samples to estimate the molecular weight of the proteins. The electrophoresis was carried out in running buffer at a constant voltage of 80 V for the stacking gel and at a constant current of 17 mA for the separating gel.

TABLE 2.1: Separating (7.5%, 12%) and stacking gel preparation. All volumes given in ml.

	7.5% AA/BA	**12% AA/BA**	**Staking gel (3.5%)**
AA/BA	2.5	4.0	0.5
Lower Tris	2.5	2.5	-
Upper Tris	–	–	1.25
AP (10%)	0.07	0.07	0.07
dH_2O	4.92	3.42	3.21
TEMED	0.01	0.01	0.01

Upper Tris (4x)	0.4	%	SDS
	500	mM	Tris-HCl
	(pH 6.8)		
Lower Tris (4x)	0.4	%	SDS
	1.5	M	Tris-HCl (pH 8.8)

Laemmli buffer (6x)	7	ml	4 x Upper Tris
	3	ml	Glycerol
	1	g	SDS
	25	mM	DTT (added fresh to the sample)
	1.2	mg	Bromphenol blue
	dH_2O ad 10 ml		
Running buffer (10x)	144	g/l	Glycine
	30	g/l	Tris-base
	1	%	SDS

2.2.8.2 Transfer of proteins to nitrocellulose membranes by tank blot. Proteins were transferred from the gel to a nitrocellulose membrane (Protran® Schleicher & Schüll) by standard tank blot, using a Mini Trans-Blot Cell (Bio-Rad). Following SDS-PAGE, the stacking gel was removed. The separating gel was equilibrated for 10 min in transfer buffer. Nitrocellulose membrane was cut to the size of the gel and equilibrated for 5-10 min in dH_2O, and then for 10 min in transfer buffer. The blot was assembled as follows (from the anode to the cathode): one sheet of Whatman paper soaked in transfer buffer, the gel, the nitrocellulose membrane and a second sheet of Whatman paper soaked in transfer buffer. Care was taken not to trap air bubbles. The transfer was carried out in the cold room. The blotting tank was filled with pre-cooled transfer buffer and placed on a magnetic stirrer. This allowed the continuous mixing of the transfer buffer during the transfer, which was performed for 50 min at a constant voltage of 100 V. After the transfer, the blot was disassembled, the membrane was quickly rinsed in dH_2O, and occasionally stained for 2 min in the Ponceau S solution, under slow agitation. Afterwards, the membrane was rinsed twice in dH_2O, to remove the excess of Ponceau S solution, and the transfer efficiency was assessed. The membrane was destained by washing the membrane 2-3 times in PBS until the red staining was completely removed. After further rinses with dH_2O, the membrane was placed on a piece of Whatman paper and dried. At this step the membrane could be stored overnight at 4°

Transfer buffer	10	%	Running buffer (10x)
	20	%	Methanol

2.2.8.3 Transfer of proteins to nitrocellulose membrane by semi-dry transfer. Proteins were transferred to Hybond-ECL nitrocellulose membrane using a semi-dry transfer cell (Trans-Blot SD, Bio-Rad). A piece of membrane was cut to the same size of the separating gel and equilibrated for 10 min in dH_2O. Afterwards, the blot was assembled as follow (from the anode to the cathode): one sheet of Whatman paper soaked in anode buffer 1, two sheets of Whatman paper soaked in anode buffer 2, the nitrocellulose membrane soaked in anode buffer 2, and 3 sheets of Whatman paper soaked in cathode buffer. Proteins were transferred at constant current of 2.5 mA/cm^2 for 20 min. The efficiency of the transfer was evaluated with Ponceau S staining as described above (2.2.8.2).

Anode buffer 1:	0.3 (pH10.4)	M	Tris-HCl
	10	%	Methanol (add just before use)
Anode buffer 2:	25 (pH 10.4)	mM	Tris HCl
	10	%	Methanol (add just before use)
Cathode buffer:	25 (pH9.4)	mM	Tris-HCl
	40	mM	6-amino-n-caproic acid
	20	%	Methanol (add just before use)

2.2.8.4 Antibody incubation and staining procedure. After a short rinse in dH_2O, the membrane was blocked for 1 hour in 10 ml of buffer A (in a plastic container) and then incubated for 3 hours with the primary antibody diluted in buffer A, in a sealed plastic bag (5 ml, for a complete mini-gel blot). Afterwards, the membrane was washed twice for 5 min with 10 ml of buffer A, twice for 10 min with 10 ml of buffer B and then incubated for 50 min with the anti-rabbit horse-radish peroxidase conjugated secondary antibody (Jackson ImmunoResearch) at the dilution of 1:10,000 in buffer A (10 ml, in a plastic container). Finally, the membrane was washed two times in 10 ml of buffer A (5 min), two times in 10 ml of buffer B (10 min) and once for 10 min in 10 ml of TBS. The ECL solution (Amersham Biosciences) was prepared by mixing 1 ml of reagent A with 1 ml of reagent B and

immediately applied on the blot, which was placed on a glass plate. After the incubation of exactly 1 min, the glass plate was slightly tilted in order to remove the excess of ECL solution. The membrane was then placed in a film cassette, covered with a plastic transparent sheet and exposed to Kodak BioMax Light Film for 2-10 min. Films were developed using a film processor.

Buffer A	5	%	NGS
	5	%	Milk powder
	0.1	%	Tween 20
	1	x	TBS
Buffer B	0.1	%	Tween 20
	1	x	TBS

2.2.9 Immunoblot of PepSpot membrane

Immunoblot on the PepSpot membrane was performed following the manufacturer's instructions. The membrane was rinsed for 5 min with 5 ml of methanol, washed three times for 10 min with 5 ml of TBS, and then blocked for 2 hours with 5 ml of buffer A (2.2.8.4) at room temperature, in a small plastic container. Incubation of the immunopurified anti-NSK2 serum diluted in 5 ml of buffer A was carried out for 3 hours at room temperature in the plastic container. Afterwards, the membrane was washed twice for 10 min with 5 ml of TBS-Tween-20 and incubated for 1 hour in the secondary antibody (BioRad) solution diluted in buffer A (1:6000, 5 ml). After two washes with 5 ml of TBS-Tween-20 (5 min each) and two washes with 5 ml of TBS (5 min each), the membrane was incubated for 1 min with 1 ml of ECL solution (500 µl reagent A plus 500 µl reagent B). Afterwards, the membrane was treated like the nitrocelluose membrane for the Western analysis (2.2.8.4). The exposure was between 2-10 min. Directly after the exposure, the membrane was regenerated by washing three times for 10 min with sterile dH_2O, 30 min with regeneration buffer I, three times for 10 min with 10 x PBS, three times for 10 min with TBS-Tween-20 and three times for 5 min with TBS. All the washes were performed at room temperature, with 5 ml of the indicated solution in the small plastic container. The membrane was stored at 4°C in TBS-Tween-20.

Regeneration buffer I	2	%	SDS
	62.5	mM	Tris-HCl (pH 6.7)
	0.7	%	2-Mercaptoethanol
TBS-Tween	1	x	TBS
	0.05	%	Tween

2.2.10 HEK 293 cell culture

2.2.10.1 Maintenance and splitting of HEK 293. HEK 293 cells expressing the SK2 channel and HEK 293 wild-type were maintained in T25 tissue culture flasks, in HEK 293 medium. The culture was maintained in a cell culture incubator at 37°C, 5% CO_2 and 95% humidity. When the cells reached 80-90% confluence they were split. The growth medium was aspirated and cells were washed once with 2 ml of sterile PBS (Invitrogen). Afterwards, 1 ml of trypsin-EDTA was added to the cells, the flask was tilted to uniformly distribute the trypsin-EDTA solution and, right away, the solution was removed. The flask was placed in the incubator for 1-2 min and, afterwards, 3 ml of HEK 293 medium were added and the cells were resuspended. 2-3 drops of cell suspension were added to 5 ml of fresh medium in a new T25 flask to maintain the cultures.

HEK 293 medium	1	x	DMEM/F12
	10	%	FCS
	2	mM	glutamine
	100	U/ml	Pen-Strep

2.2.10.2 Plating HEK 293 cells for immunocytochemistry

2.2.10.2.1 Coating coverslips: 22 mm x 22 mm coverslips were washed for 45 min in absolute ethanol and then rinsed 3 times with 75% ethanol. After completely removing the ethanol, they were baked at 200°C for 6 hours. Before use, coverslips were placed in 6 well plates and coated for 10-30 min with ~500 µl of poly-D-Lysine (0.1 mg/ml), at room temperature. Afterwards, coverslips were washed three times with ~2 ml of sterile dH_2O.

2.2.10.2.2 Plating HEK 293 cells on coverslips: HEK 293 cells were split (2.2.10.1) and 100 µl of cell suspension were used to determine the cell density using

a Neubauer hemacytometer. For immunocytochemistry, cells were plated on 22 x 22 mm coverslips coated with poly-D-Lysine (2.2.10.2.1), at the density of 120,000 cells/coverslip, in HEK 293 medium without serum (2 ml of medium/coverslip in 6 wells plates). 48 hours after plating immunofluorescence was performed.

2.2.11 Superior cervical ganglion (SCG) neurones

2.2.11.1 Coverslip preparation. 13 mm diameter coverslips were washed and baked at 200°C as described in 2.2.10.2.1. The coverslips used for micro-injection of SCG neurones were placed inside SCG culture chambers (2.2.11.2). Alternatively, coverslips were placed inside 4 well plates. The coverslips were coated with poly-D-lysine and laminin. Coverslips were first incubated for 20-30 min with 250 µl of poly-D-lysine solution (0.1 mg/ml) at room temperature. After removing the poly-D-lysine solution, coverslips were washed three times with sterile dH_2O. Subsequently, coverslips were incubated with 250 µl of 10 µg/ml of laminin in HBSS for 2-3 hours in a cell culture incubator (5% CO_2, 37°C, 95% humidity). The laminin solution was aspirated, replaced with 250 µl of fresh SCG culture medium (2.2.11.3) and left in the incubator until the SCG neurones were plated. Before plating, the coverslips were washed once more with SCG culture medium.

2.2.11.2 SCG culture chambers preparation. The chambers were made of a 16 mm ∅ glass ring fixed with Sylgard 184 to 22 x 22 mm coverslips. To prepare them, Sylgard 184 was distributed on one side of a 16 mm ∅ glass ring, which was then positioned on a 22 x 22 mm coverslip and baked for 2 hours at 200°C. Afterwards, the chambers were washed, baked as described in 2.2.10.2.1 and, working under the tissue culture hood, placed into sterile 35 mm dishes with sterile forceps. As long as the chambers were not damaged, they were re-used several times. After each experiment, the chambers were washed in dH_2O for ~1 hour, washed with ethanol, baked (2.2.10.2.1) and placed in 35 mm dishes as described above.

2.2.11.3 Primary SCG culture preparation. One 17-21 days old male Sprague-Dawley rat was terminally anaesthetised by a rising concentration of CO_2 and decapitated. The head was fixed with needles onto a dissecting board so that the throat area was exposed. One needle was placed through the skin on each side of the neck, and one under the mouth. Another needle was inserted through the trachea and pulled gently toward the nose. Artery clamps were used to grip the spinal cord and

were bent downwards. The two SCGs are positioned within the carotid artery bifurcation on each side of the neck. Fine forceps were used to find the carotid artery and the SCGs were removed. The two ganglia were placed in a 35 mm dish containing ~2 ml of fresh L15, and were cleaned from the surrounding fibres using small forceps. After cutting the ganglia in four pieces using small scissors, the L15 was removed from the dish with a plastic Pasteur pipette. The tissue was washed twice with 2 ml of dissection medium using a plastic Pasteur pipette and, afterwards, treated enzymatically in two steps. First, the pieces of ganglia were incubated for 15 min in a 35 mm dish containing 2 ml of collagenase solution. The incubation was performed in the cell culture incubator (5% CO_2, 37°C, 95% humidity). After removing the collagenase solution, the pieces of ganglia were washed twice with 2 ml of dissection medium, and then incubated with 2 ml of Trypsin solution, for 30 min in the cell culture incubator. Afterwards, the ganglia pieces were collected with a glass pipette and transferred, capturing as little trypsin solution as possible, into a fresh 15 ml tube containing 2 ml of SCG culture medium. Neurones were dissociated by sequential mechanical trituration, using a fire polished glass pipette with an open tip diameter of 1-0.5 mm. After pipetting up and down 15-20 times, cells were centrifuged shortly at 120 x g, stopping the centrifugation as soon as the set g-force was reached. The supernatant, containing the dissociated neurones, was transferred into a fresh 15 ml tube; the pellet, containing undissociated tissue, was resuspended in further 2 ml of SCG culture medium and triturated and centrifuged as described above. The supernatants were combined and the procedure was repeated three more times. Finally, the combined cell suspension (10 ml) was centrifuged for 5 min at 120 x g and, after discarding the supernatant, the neurones were resuspended in 1.5 ml of SCG culture medium. 250 µl of cell suspension were plated on poly-D-lysine and laminin coated coverslips (13 mm diameter) (2.2.10.2.1), and incubated in the cell culture incubator for 4 hours. Afterwards, 400 µl of SCG culture medium were added to each coverslip. The culture was maintained in the cell culture incubator for up to four days.

Dissection medium	1	x	HBSS
	10	mM	HEPES

SCG culture medium:	42	ml	L-15
	8.5	ml	$NaHCO_3$ (1.26%)
	5	ml	FCS
	1.15	ml	Glucose (30%)
	0.61	ml	L-Glutamine (200 mM)
	1.15	ml	5000 u Penicillin/5000 u Streptomycin
	100	µl	NGF-7S stock solution (25µg/ml)
NGF-7S stock solution	100	µg	NGF
	3.9	ml	sterile dH_2O
	0.1	ml	FCS
	aliquot and store at -20°C		
Collagenase solution	0.6	ml	Dissection medium
	0.2	ml	Collagenase type 1A (Sigma, 10 mg/ml)
	1.2	ml	BSA stock solution
	sterile filtrate with 25 mm syringe filter with HT TuffrynA® Membrane		
Trypsin solution	0.8	ml	Dissection medium
	2	mg	Trypsin bovine, type XII S (Sigma)
	1.2	ml	BSA stock solution
	sterile filtrate with 13 mm syringe filter with HT TuffrynA® Membrane		
BSA stock solution	1	x	Dissection medium
	10	mg/ml	BSA (Sigma, A4161)

2.2.11.4 cDNA microinjection. Microinjection of cDNA plasmids into SCG neurones was performed using an Eppendorf 5246 microinjector and an Eppendorf 5171 micromanipulator, 24-48 hours after plating. The cDNA was diluted at the concentration of 100 ng/µl in injection solution and filtered with Whatman VectaSpin Micro filters. The cDNA injection was performed with injection needles pulled from capillary glass (1.2 mm O.D. x 0.69 mm I.D.) using a micropipette puller (Sutter Instrument, program: heat 525, pull 40, vel.60, time 250). The injection was performed applying a constant pressure resulting in a constant flow of the injection solution. The injection needle was gently driven into the neuronal nucleus and retracted as soon as a slight enlargement of the nuclus was observed (~ 1-2 s).

Injection solution	154	mM	NaCl
	5	mM	HEPES
	2.5	mM	KCl
	0.5	mM	$MgCl_2$
	(pH 7.4)		

2.2.12 Embryonic hippocampal and cortical neurones

2.2.12.1 Coating coverslips. 13 mm diameter coverslips were treated as described in 2.2.10.2.1. Before use, the coverslips were placed in 4 or 24 well plates and coated for 1 hour at 37°C or over night at room temperature with ~300 µl of poly-D-lysine (0.1 mg/ml). After removing the poly-D-lysine, coverslips were washed three times over a time of 2 hours (~500 µl sterile dH_2O/wash). The washing was performed in the incubator. After the last wash 500 µl of attachment medium was added and equilibrated in the incubator (5% CO_2, 37°C, 95% humidity) during the preparation of the neuronal cultures.

2.2.12.2 Primary hippocampal and cortical neuronal culture preparation. Hippocampal and cortical neurones were prepared following the method described by Brewer (1997). The dissection was performed in a vertical laminar flow hood (Envair VLF), wearing gloves and working as sterile as possible. The working surface was cleaned with 70% ethanol before starting the dissection. All the tools were placed in a plastic beaker containing 70% ethanol and kept under the hood during the dissection. An E17 pregnant rat was sacrificed, the abdomen of the animal was wiped with 70% ethanol and the skin of these region was removed using sharp scissors. The muscular layer of the abdominal wall was cut using sterile instruments, the uterus was removed and placed in a sterile petri dish. The foetuses were removed from the uterus, decapitated, and the heads were transferred in a petri dish containing cold dissection medium. The brains were isolated as follows: the heads were grasped with a curved forceps inserted in the eyes, a rostro-caudal cut beginning from the mouth was made through the skin and the skull, with fine scissors; the brains were pushed out from the skull by lightly wringing the forceps, collected with a small spatula and transferred in cold dissection medium. Each brain was dissected under a light microscope in order to isolate the hippocampus and the cortex. After cutting off

the cerebellum and the brainsteam, the two hemispheres were separated and cleaned from the meninges using fine forceps. The thalamus was removed from each hemisphere in order to uncover the hippocampus, which was then separated from the cortex using fine forceps. The dissected hippocampi and cortices were collected separately in petri dishes containing ice-cold dissection medium. After all brains were dissected, hippocampi and cortices were moved into two different 15 ml plastic tubes. The tissue was allowed to settle to the bottom of the tube for 1-2 min, after which the dissection medium was removed using a sterile Pasteur pipette and replaced with 4.5 ml fresh dissection medium plus 0.5 ml trypsin (2.5%). The incubation in the trypsin solution was carried out at 37°C for 15 min followed by two washes with 5 ml of dissection medium and one with 5 ml of attachment medium to stop the enzymatic activity of the trypsin. After removing the medium of the last wash, fresh attachment medium was added (1 ml/dissected embryo cortex, 1.5 ml in total for the hippocampi). The mechanical trituration was performed first with a 5 ml pipette (15 times) and then with a fire polished glass pipette with the tip reduced to half of its normal size, until no obvious particles of tissue were left in the solution. An aliquot of cells was mixed with 1/10 volume of trypan blue, and the number of living cells was determined using a Neubauer hemacytometer. Neurones were plated in 500 µl of attachment medium, on poly-D-Lysine coated coverslips (13 mm diameter) (2.2.12.1). Neurones were plated at a density of 20,000-40,000cells/coverslip in 4 or in 24 wells plates. After 4 hours the attachment medium was removed and replaced with maintenance medium. Neurones were maintained in a cell culture incubator (5% CO_2, 37°C, 95% humidity) up to 3 weeks. Half of the medium was replaced with fresh maintenance medium every 5 days.

Dissection medium	1	x	HBSS
	10	mM	HEPES
Attachment medium	1	x	MEM
	10	%	Horse serum
	0.59	%	Glucose
	1	mM	Pyruvic acid
	2	mM	L-Glutamine
Maintenance medium	1	x	Neurobasal
	2	%	B27
	0.59	%	Glucose
	100	U/ml	Pen-Strep
	2	mM	L-Glutamine**2.2.12.3**

2.2.12.3 Transfection using lipofectamine. Lipofectamine™ 2000 was used to transfect hippocampal or cortical embryonic cultures between 5 and 8 DIV. 1 μg of DNA was mixed to 49 μl of Opti-MEM I, and, in parallel, 1 μl of Lipofectamine™ 2000 was mixed to 49 μl of Opti-MEM I. After 5 min the two solutions were combined, mixed, and incubated for 20 min at room temperature. Afterwards, the maintenance medium was removed from the neurones and replaced with 400 μl of fresh maintenance medium plus the 100 μl mixture of DNA and Lipoectamine™ 2000 in Opti-MEM I. The neurones were incubated for 2 hours at 37°C in the cell culture incubator (5% CO_2, 37°C, 95% humidity). After the incubation, the medium containing the Lipofectamine solution was removed and replaced with 500 μl of fresh maintenance medium, and the neurones were maintained in the incubator. Immunofluorescence experiments were performed starting from 24 hours after transfection.

2.2.13 Post-natal hippocampal neurones

7-8 Sprague-Dawley rats were dissected on the day of the birth (P0). Each pup was decapitated, the skin of the head was cut off and, after doing a lateral cut in the skull with fine scissors, the skull was removed using forceps. The brain was isolated, transferred in a dish containing ice cold dissection medium and the hippocampus was dissected as described in 2.2.12.2. After all the brains were dissected, a small scalpel was used to cut each hippocampus in three-four pieces. The tissue was then

transferred into a fresh 15 ml tube, the dissection medium was removed and replaced by 5 ml of fresh dissection medium (2.2.12.2). After removing again the dissection medium, 5.4 ml of fresh dissection medium plus 0.6 ml trypsin (2.5%) were added to the tissue. The incubation in trypsin was carried out for 10 minutes in the incubator, gently shaking the tube every 2 minutes. Afterwards, the tissue was washed twice with 5 ml of dissection medium and twice with 5 ml of attachment medium (2.2.12.2). After removing the last washing solution, 3 ml of attachment medium was added and neurones were mechanically dissociated by pipetting up and down with a P1000 Gilson pipette, until the medium turned turbid, indicating dissociated neurones. Undissociated tissue was allowed to sediment at the bottom of the tube for ~2 min. The supernatant, containing the dissociated neurones, was collected with a plastic Pasteur pipette and transferred into a fresh 15 ml tube. 2 ml of attachment medium were added to the undissociated tissue and triturated with a glass Pasteur pipette ~15 times. Undissociated tisuse was left to settle (~ 2 min) and the supernatant was combined with the one from the first trituration step. This procedure was repeated a third time with a fire polished pipette whose tip was reduced to half the normal size. Finally, the collected cellular suspension (7 ml) was centrifuged at 120 x g for 5 minutes and the pellet was resuspended in 3 ml of fresh attachment medium. The cell density was determined as described in 2.2.12.2. Neurones were plated on poly-D-Lysine coated coverslips (13 mm diameter) (2.2.12.1) in 4 well plates, at the density of 45,000 neurones/coverslip for electrophysiology experiments or 15,000-30,000 neurones/coverslip for immuocytochemistry experiments. After 4 hours the attachment medium was removed and replaced with maintenance medium (2.2.12.2). Neurones were maintained as described in 2.2.12.2.

2.2.14 Immunocytochemistry

2.2.14.1 Immunocytochemistry on HEK 293 cells. HEK 293 cells were plated as described in 2.2.10.2.2. Immunofluorescence was performed in the 6 well plates, 48 hours after plating. Cells were rinsed 3 times with ~2 ml of PBS using a plastic Pasteur pipette and, afterwards, fixed with 1 ml of 4% PFA-PBS for 10 min at room temperature. After rinsing the cells twice with ~2 ml of PBS, they were permeabilised with 1 ml of 0.2% Triton X-100 in PBS for 2 min and then washed four times (5 min each) with ~2 ml of PBS. 300 µl of blocking buffer were applied

on the coverslips, the six well plate containing the coverslips was placed in a humidified box and incubated for 30 min at 37°C. Subsequently, the blocking buffer was replaced by 300 µl of the primary antibody diluted in blocking buffer (antibody dilutions are reported in the results section) and incubated for 1 hour at 37°C. Cells were rinsed five times and washed three times with ~2 ml of PBS (5 min each) before incubation for 30 min at 37°C with the FITC-conjugated swine anti-rabbit secondary antibody (1:30) (Dako) (300 µl/coverslip). Cells were rinsed five times followed by three more washes with PBS (five min each) in the dark. Coverslips were mounted using ProLong Antifade (Molecular Probes), dried overnight and sealed the next day with nail polish. Slides were examined with a fluorescence microscope (Axiophot, Zeiss). Pictures were taken with a MicroPublisher camera (QImaging).

4% PFA-PBS	80	ml	dH_2O
	200	µl	NaOH (1M)
	heat to 65°C and add 4g of PFA, stir until dissolved		
	10	ml	PBS 10x
	200	µl	HCl (1M)
	adjust to pH 7.4, and store at -20°C		
Blocking buffer	1	x	PBS
	10	%	FCS
	2	%	BSA

2.2.14.2 Immunocytochemistry on SCG neurones. The immunofluorescence on SCG neurones was performed either in the 4 well plates or in the SCG culture chambers (2.2.11.2). 300 µl of 4% PFA-PBS (2.2.14.1) containing 10% sucrose were carefully added to the growth medium. After an incubation time of 30 min at room temperature the medium/fixation solution was removed using a plastic Pasteur pipette and cells were rinsed twice in ~500 µl of PBS. Permeabilisation was performed by adding 500 µl of 0.2% Triton X-100 in PBS for 2 min at room temperature. Cells were then washed four times with ~500 µl of PBS (5 min each). The immunocytochemistry was performed as described in 2.2.14.1, using a total volume of 200 µl for blocking, primary and secondary antibody incubation. The

primary and secondary antibody dilutions used for the different experiments are reported in the results section. Coverslips were mounted as described above (2.2.14.1). Samples were examined with a confocal microscope (Axiovert 200, LSM 510, Zeiss) and pictures were taken with the LSM 510 software. The images were analysed using ImageJ and Adobe Photoshop 6.0 software.

2.2.14.3 Immunocytochemistry on embryonic hippocampal and cortical neurones. Hippocampal and cortical neurones, plated on 13 mm coverslips, were treated for immunofluorescence experiments inside 4 well plates. Neurones were gently rinsed once with ~500 µl of PBS using a plastic Pasteur pipette and subsequently fixed for 10 min with 500 µl of 4% PFA-PBS (2.2.14.1) supplemented with 4% sucrose at room temperature. After two rinses in PBS, the neurones were blocked with 200 µl of blocking buffer for 30 min at room temperature. The primary antibodies were diluted in 200 µl of blocking buffer (see results sections for antibody dilutions), applied to the coverslips and incubated overnight at 4°C, in a humidified box. The day after, cells were rinsed twice and then washed three times with ~500 µl PBS (5 min each) to remove the unbound primary antibodies. Subsequently, the FITC-conjugated swine anti-rabbit (1:30, Dako) or Cy3 conjugated goat anti-rabbit secondary antibody (1:600, Jackson ImmunoResearch) were diluted in incubation buffer (200µl/coverslip) and applied to the coverslips for 1 hour at room temperature, in the dark. Neurones were finally rinsed two times and washed three times, in the dark, in PBS (5 min each). Coverslips were mounted, examined and pictures were taken as described in (2.2.14.1).

Blocking buffer	1	x	PBS
	5	%	NGS
	0.2	%	BSA
	0.2	%	TritonX100
Incubation buffer	1	x	PBS
	5	%	NGS
	0.2	%	BSA

2.2.14.4 Immunofluorescence on post-natal hippocampal neurones. The Tyramide Amplification System (TSA, Molecular Probes) was used to visualise the SK2 protein in post-natal hippocampal cultures. TSA is an enzyme based detection method which utilizes the enzymatic activity of horseradish peroxidase (HRP) to catalyse the deposition of a fluorophore labeled tyramide reagent. After the binding of the primary antibody to the target protein, the secondary detection is performed using a HRP-conjugated antibody. The amplification of the signal is conferred by the turnover of multiple dye-tyramide substrates per peroxidase, which results in the deposition of numerous fluorophore labels in vicinity of the immobilised HRP- target interaction site.

Hippocampal neurones, plated on 13 mm coverslips, were treated for immunofluorescence experiments inside 4 well plates. The growth medium was gently removed from the wells using a Pasteur pipette, neurones were gently rinsed once with PBS, and then fixed for 10 min at room temperature with ~500 µl of 4% PFA-PBS (2.2.14.1) supplemented with 4% sucrose. After two washes with PBS (5 minutes each), neurones were permeabilised with ~500 µl of 0.3% Triton X-100 for 15 min. After rinsing the cultures twice and washing two times with PBS (5 min each), the neurones were incubated for 1 hour, at room temperature, with 200 µl of 2% H_2O_2 to block the activity of the endogenous HRP. The H_2O_2 solution was removed and the cultures were blocked with 200 µl of 1% blocking reagent (Molecular probes) in PBS. The affinity-purified anti-NSK2 was applied in blocking buffer (200 µl/coverslip), and incubated overnight at 4°C. Neurones were rinsed twice and washed in PBS for 3 times (5 min each) to remove the unbound primary antibodies, and then incubated for 1 hour at room temperature with 200 µl of HRP-conjugated anti-rabbit secondary antibody (1:200, T20922, Molecular Probes) in blocking buffer. After rinsing the cultures twice and washing for 3 times in PBS (5 min each), the Tyramide-Alexa Fluor 488 reagent (1:100 in amplification buffer containing 0.0015% H_2O_2) (Molecular probes) was added to the neurones (100 µl/coverslip) and incubated in the dark for 5 min. Neurones were washed in the dark three times (5 min each). Coverslips were mounted, examined and pictures were taken as described in (2.2.14.1 and 2.2.14.2).

2.2.15 Immunohistochemistry

2.2.15.1 Tissue preparation and slicing. Male Sprague Dawley rats at the age of P1, P3, P6, P12, P21 and P25 were anesthetised with an intraperitoneal injection of pentobarbital sodium (Euthanal, Merial) at the dose of 4.5 mg/100 g of body weight. When the animals were completely asleep they were intracardially perfused in order to preserve a good morphology of the tissues. Briefly, the anesthetised animals were fixed on a metal grid by tying the arms and the legs to the grid. The skin on the chest and the abdomen of the animal was removed. Afterwards, the muscular layer was cut horizontally with a small scalpel on the bases of the chest, in order to expose the end of the sternum. The end of the sternum was gripped with artery clamps and pulled up gently while cutting the muscular layer parallel to the ribs, and then laterally on both sides upward across the ribs and parallel to the lungs. Afterwards, the diaphragm was cut from the left to the right side and, working fast, the canula (drawing up needle 18G 1 1/2 for P21-P25; needle 23G 1 1/4 for P12; needle 25G 5/8 for P1, P3 and P6) was introduced in the left ventricle while holding the heart with the fingers. Ice-cold phosphate buffer (PB) containing 50 U/ml heparin was infused, and, right away, the right atrium was cut for drainage. After most of the blood had been flushed out of the system (~100 ml for P21 animals, ~50 ml for P1, P3, P6 and P12 animals), the PB was substituted by an ice cold, freshly made, solution of 4% PFA-PB. The perfusion was carried out until the neck of the animal became stiff (~100 ml PB for P21 animals, ~50 ml PB for P1, P3, P6 and P12 animals). The brains were dissected out of the skull, post-fixed by immersion in 4% PFA-PB for 1-4 hours and stored in PB-0.01% Azide containing 30% sucrose, at 4°C, for up to 2 weeks. Alternatively the brains were stored at -80°C after cryoprotection for 3 days at 4°C in 30% sucrose in PB-0.01% Azide and freezing in powdered dry ice. Coronal and sagittal sections (45 µm thickness for P21 brains, 55-60 µm thickness for P1, P3, P6, P12 brains) were cut using a sliding microtome (Leica SM2000 R), collected with a soft brush and transferred in 24 well plates filled with PBS-0.01% Azide. Sections were stored up to 2 weeks at 4°C.

4% PFA-PB	800	ml	dH_2O
	2	ml	NaOH (1M)
	heat to 65°C and add 40 g of PFA, stir until dissolved		
	100	ml	PB (1M)
	2	ml	HCl (1M)
	adjust to pH 7.4, use fresh		

2.2.15.2 Immunohistochemistry. The immunohistochemistry experiments were performed on free floating sections in 24 well plates. Sections, stored in PBS-0.01% Azide, were transferred by means of a brush into a fresh 24 well plate containing 300 µl/well of IHC blocking solution and incubated for 1 hour at room temperature, with slow agitation. Subsequently, sections were transferred with a brush into another 24 well plate containing 300 µl/well of the affinity-purified primary antibody diluted in incubation buffer A. The incubation was performed overnight at 4°C, on a shaking platform. All the following incubations were performed at room temperature. The day after, sections were washed with ~500 µl of TBS (2 x 15 min and 1 x 30 min). Washes were performed on a rotating platform and the solution exchange was performed by moving the sections into 24 well plates containing fresh TBS. When many sections were processed at the same time, 15 mm Netwell™ inserts in combination with 12 well plates were used to perform the washes. After the washes, sections were incubated with 300 µl of the biotinylated secondary antibody (Vectastain Elite ABC Kit) diluted 1:200 in incubation buffer B for 1 hour, with slow agitation. After 1 hour of washes (performed as before: 2 x 15 min and 1 x 30 min) the sections were incubated with 300 µl of ABC (Vectastain Elite ABC Kit, 10 µl A+ 10 µl B per ml of TBS) for 1 hour on the shaking platform and then washed again in TBS (2 x 15 min and 1 x 30 min). The antibody binding was visualised by using DAB as substrate of the peroxidase enzyme (DAB substrate kit for peroxidase) plus nickel, which was added to the reaction in order to obtain a grey-black stain. The staining reaction was carried out by applying 300 µl of DAB solution to the sections for 4-6 min, in the 24 well plates, in the dark. Afterwards, DAB was removed with a pipette, sections were shortly rinsed in dH_2O and then washed three times for 10 min with TBS.

IHC blocking solution	1	x	TBS
	10	%	NGS
	0.3	%	Triton X-100
	0.3	%	H_2O_2
Incubation buffer A	1	x	TBS
	2	%	NGS
	0.2	%	TRITONX-100
	0.01	%	Azide
Incubation buffer B	1	x	TBS
	1.5	%	NGS

2.2.15.3 Immunohistochemistry in the absence of Triton X-100. Sections of P1 and P3 brains were cryoprotected with sucrose (10% sucrose in PB for 10 min at room temperature and then 30% sucrose overnight at 4°C) and permeabilised by temperature shock in dry ice as follows. A beaker containing acetone was equilibrated on dry ice. Sections were placed into a 10 ml tube using a brush (two or three sections can be processed at the same time). The tube containing the sections was immersed in the beaker containing cold acetone for 30 s. The sections were removed right away from the tube by using a brush and washed three times for 10 minutes in TBS. Sections were blocked in IHC blocking solution for 1 hour at room temperature and then incubated over night at 4°C with the primary antibody diluted in Incubation buffer A. Secondary antibody incubation and DAB staining were performed as described in 2.2.15.2.

IHC blocking solution	1	x	TBS
	10	%	NGS
	0.3	%	H_2O_2
Incubation buffer A	1	x	TBS
	2	%	NGS
	0.01%	Azide	

2.2.15.4 Immunhistochemistry using the TSA™ Biotin System. Immunohistochemistry experiments with anti-N860 antibody were performed using the TSA™ Biotin System (PerkinElmer), which is based on the use of the biotin-

labelled tyramide reagent in combination with the Vectastain Elite ABC Kit (Fig. 1). After the blocking, primary antibody and secondary antibody incubations (performed as described in 2.2.15.2), the sections were incubated with 300 µl of the ABC reagent (4 µl A+ 4 µl B per ml of TBS) for 1 hour, on a rotating platform. After washing four times for 10 minutes, 250 µl of the biotin-labelled tyramide reagent solution (13.3 µl tyramide reagent per ml of amplification buffer, PerkinElmer) was applied on the sections for 7 min. The sections were washed three times for 10 minutes with slow agitation, and then incubated again for 1 hour with the ABC reagent, on the shaking platform. Finally, after washing the sections (2.2.15.2) the antibody binding was visualised by using DAB (2.2.15.2).

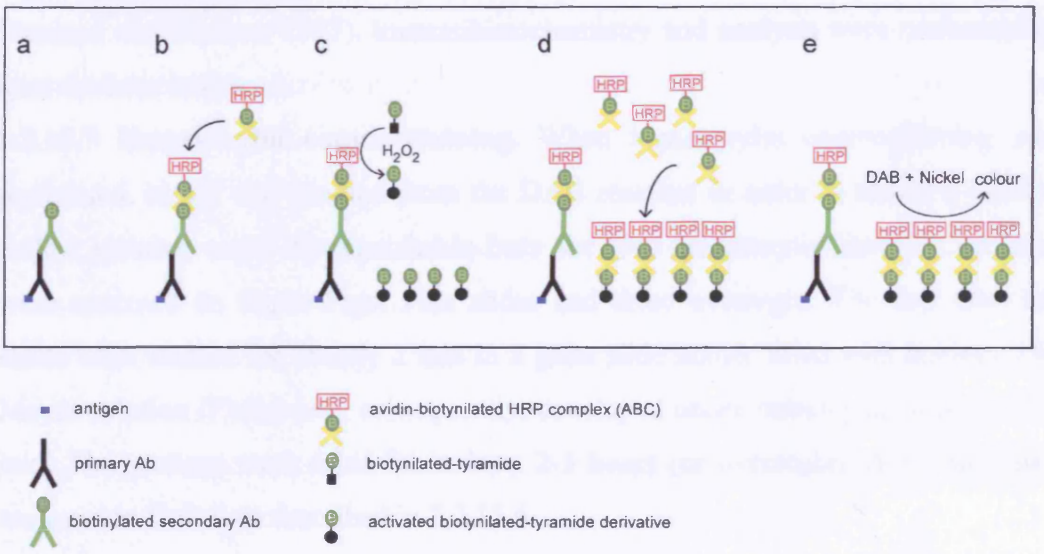

FIGURE 2.1. Schematic representation of the immunohistochemistry with the TSA™ Biotin System (PerkinElmer) in combination with the ABC Vectastain Kit. **A**: Binding of the primary antibody to the antigen followed by the binding of the anti-rabbit biotinylated secondary antibody (Vectastain). **B**: the biotinylated HRP-avidin complex (ABC) binds to the biotinylated secondary antibody. **C**: the HRP-mediated reaction activates the biotinylated-tyramide resulting in the precipitation of the activated biotinylated-tyramide derivatives in proximity of the antigen. **D**: the ABC complex is added again and it binds to the precipitated activated biotinylated-tyramide derivatives. **E**: DAB and Nickel are used to visualise the localisation of the tyramide precipitates.

2.2.15.5 Immunofluorescence using the TSA™ Biotin System. The TSA™ Biotin System (PerkinElmer) was also used for immunofluorescence experiments on brain sections. The experiment was performed as described in 2.2.15.4 until the incubation in ABC reagent (step d of Fig. 2.1). Afterwards, sections were washed and incubated for 2 hours in 200 µl of FITC-avidin (1.67 µl per ml of TBS), in the dark. Sections

were washed three times for 20 min with TBS, mounted on Super Frost Plus slides and air-dried overnight, in the dark. The sections were mounted with Pro-Long Antifade mounting medium.

2.2.15.6 Mounting and analysis. The free floating sections were mounted on Super Frost Plus slides and air-dried overnight. A Tissue-Tek slide staining unit was used, the day after, to dehydrate the sections in an ascending series of ethanol (50%, 70%, 95% and 2 x 100%, 5 min each), followed by two incubations (5 min) in Histo-Clear. Afterwards, the slides were mounted with DePex mounting medium and covered with glass coverslips (24 x 60 mm). Sections were examined with a Zeiss Axiophot microscope and pictures were taken with a MicroPublisher camera (QImaging). Brain regions were identified using "The Rat Brain in Stereotaxic Coordinates" (Paxinos and Watson, 1997). Immunihistochemistry and analysis were performed at least on three brains.

2.2.15.7 Hematoxylin counterstaining. When hematoxylin counterstaining was performed, nickel was omitted from the DAB reaction in order to obtain a brown-yellow staining easily distinguishable from the blue hematoxylin staining. Sections were mounted on Super Frost Plus slides and dried overnight. The day after the slides were stained for exactly 2 min in a glass slide holder filled with hematoxylin Mayer solution (Fluka) and, subsequently, developed under running tap water for 10 min. The sections were dried for at least 2-3 hours (or overnight), dehydrated and mounted in DePex as described in 2.2.15.6.

2.2.16 Standard molecular biology techniques

2.2.16.1 Restriction enzyme digest of plasmid DNA. Digests were performed in a 1.5 ml tube containing DNA, the appropriate restriction enzyme, buffer and dH_2O. For analytical digests 200-300 ng of DNA were used in a volume of 20 µl. For digests of vector and fragment isolation, 1 µg of DNA was used in a volume of 40 µl. The digest was incubated for 1 hour at a temperature optimal for the selected restriction enzyme. The reaction was stopped by adding DNA sample buffer (2.2.16.3).

2.2.16.2 Dephosphorylation of plasmid DNA. Following restriction digest, cloning vectors were subjected to dephosphorylation in order to prevent self ligation of plasmid DNA. Alkaline phosphatase was used to remove terminal 5'-phosphate groups. The dephosphorylation mixture contained the digest, 1 U of alkaline phosphatase and the alkaline phosphatase buffer. The dephosphorylation was carried out at 37°C for 1 hour and the reaction was stopped by adding sample buffer (2.2.16.3).

2.2.16.3 Agarose gel electrophoresis of cDNA. Separation of the digested DNA was carried out by agarose gel electrophoresis. DNA was separated on 0.7-2% TAE agarose gels containing 40 µg/ml ethidium bromide. The electrophoresis was carried out at 80-100 mV for 30-60 min. 1 kb and/or 100 bp DNA ladders (2.1.6) were used as molecular weight standards. The DNA was visualised under UV-light. Gel images were documented as video prints using a gel documentation system.

DNA sample buffer (5x)	20	%	Ficoll 400
	100	mM	EDTA (pH 8.0)
	0.25	%	Bromphenoblue
	0.25	%	Xylencyanol

2.2.16.4 Gel extraction of DNA fragments. DNA fragments were visualised using UV light (365 nm) and the fragment of interest was excised from the agarose gel using a scalpel. To recover the DNA, the Nucleospin Extract kit was used according to the manufacturer's instructions. Briefly, agarose gel slices were melted at 65°C in buffer NT1 (300 µl/100 mg agarose gel) and the resulting dissolved mixture was loaded on a column. After two washes with buffer NT3, the DNA bound to the column membrane was eluted with buffer NE pre-heated at 70°C to increase the yield of DNA elution.

Buffer NE (Macherey-Nagel)	5	mM	Tris-HCl (pH 8.5)

2.2.16.5 Phenol/chloroform extraction of DNA. Occasionally, phenol/chloroform extraction was performed to remove proteins following the restriction digestion. DNA samples were mixed with an equal volume of phenol and two-three drops of chloroform, vortexed for 30 seconds and centrifuged for 2 min at maximum speed (14,000 x g). The aqueous phase was transferred into another tube and the same volume of chloroform was added. The mixture was vortexed and centrifuged again for 2 min at maximum speed. The aqueous phase was transferred into a new tube and DNA was precipitated.

2.2.16.6 Ethanol precipitation of DNA. The DNA solution was adjusted to 400 mM LiCl and three volumes of 100% ethanol were added. DNA was precipitated at -80°C for at least 30 min or at -20°C overnight. Afterwards samples were centrifuged for 15 min at 14.000 x g and the resulting pellet was washed with 75% ethanol. After the washes the pellet was air-dried and resuspended in sterile dH_2O.

2.2.16.7 Ligation of DNA fragments. Ligation was performed in 20 µl containing 20 ng of dephosphorylated vector, 3 molar excess of DNA fragment, 1µl T4 DNA ligase, 5 µl ligation buffer and dH_2O. As control a ligation of the dephosphorylated vector without DNA fragments was performed. The reactions were carried out in a water bath at 14°C for at least 3 hours. 10 µl of the reaction were used for transformation of competent DH5α bacteria, the remaining 10 µl were left in the water bath for 12-18 hours and then stored at 4°C.

Ligation buffer (5x)	50	mM	$MgCl_2$
	50	mM	DTT
	5	mM	ATP
	100	mM	Tris-HCl (pH 7.5)

2.2.16.8 Transformation of competent bacteria DH5α. 10 µl of ligation reaction were added to 100 µl of competent bacteria and placed on ice for 15 min. Afterwards the mixture was heat shocked for 5 min in a heat block at 37°C , mixed with an equal amount of LB medium and incubated further for 15 min at 37°C. The bacteria were spread onto LB-agar plates containing ampicillin (100 µg/ml) and incubated overnight in an incubator at 37°C. The day after, 4-8 single colonies were picked to start bacteria cultures.

LB plates/ampicillin	25	g	LB
	15	g	Agar
	1	l	dH_2O

autoclave, cool to 50°C and add ampicillin at 100µl/ml

2.2.16.9 Isolation of DNA from bacterial cultures

Small scale preparation of plasmid DNA: For small scale preparation of plasmid DNA, single colonies were grown overnight at 37°C in 5 ml LB medium containing 100 µg/ml of ampicillin. DNA was isolated using the Nucleobond Plasmid kit, following the manufacturer's protocol. Briefly, the 5 ml culture was centrifuged for 5 min at 3,200 x g and the pellet was resuspended in 250 µl of buffer A1. 250 µl of lysis buffer A2 was added and, after inverting the tubes 6-8 times, 300 µl of neutralisation buffer A3 was added and gently mixed. The cell debris was precipitated by centrifugation at 11,000 x g for 5 min and the clear lysate was loaded into a NucleoSpin column. After centrifugation (30 s at 11,000 x g), the flow through was discarded and the membrane was washed with 600 µl buffer A4. Plasmid DNA was eluted from the membrane with 50 µl of AE buffer pre-warmed at 70°C.

Medium scale preparation of plasmid DNA: For medium scale plasmid DNA preparation, single colonies were grown in 40 ml of LB medium containing 100 µg/ml of ampicillin and the Nucleobond AX 100 kit was used for plasmid DNA

extraction. The cultures were harvested by centrifugation at 7,000 x g for 10 min and the pellet was resuspended in ice-cold 4 ml buffer S1. Subsequently, 4 ml of the lysis buffer S2 were added, mixed and then 4 ml of S3 buffer were added. The mix was centrifuged at 3,200 x g for 10 min at 4°C and the cleared lysate was filtered through a paper filter (Macherey-Nagel). The flow through was collected and loaded on a Nucleobond AX 100 cartridge pre-equilibrated with 2.5 ml of buffer N2. Subsequently, the cartridge was washed twice with 5 ml of buffer N3 and the DNA was then eluted with 5 ml of buffer N5. The plasmid DNA was precipitated by mixing the eluate with 0.7-0.8 volumes of isopropanol and centrifuging at 16,000 x g for 30 min at 4°C. The precipitated DNA was then washed with 75% ethanol and centrifuged at 15,000 x g for 10 min at 4°C. The plasmid DNA pellet was dissolved in dH_2O at the final concentration of 1 µg/µl.

Buffer S1	10	mM	EDTA (pH 8.0)
(Macherey-Nagel)	100	µg/ml	RNase A
	50	mM	Tris-HCl
	(pH 8.0)		
Buffer S2	200	mM	NaOH
(Macherey-Nagel)	1	%	SDS
Buffer S3	2.8	M	KAc (pH 5.1)
(Macherey-Nagel)			
Buffer N2	100	mM	Tris-H_3PO_4
(Macherey-Nagel)	15	%	Ethanol
	900	mM	KCl
	0.15	%	Triton X-100
	(pH 6.3)		
Buffer N3	100	mM	Tris-H_3PO_4
(Macherey-Nagel)	15	%	Ethanol
	1.15	M	KCl
	(pH 6.3)		
Buffer N5	100	mM	Tris-H_3PO_4
(Macherey-Nagel)	1	M	KCl
	(pH 6.3)		

2.2.16.10 Amplification of DNA using PCR. Specific DNA sequences were amplified by Polymerase Chain Reaction (PCR). The reaction was performed using either KOD Hot Start DNA or Pfu DNA polymerases.

PCR with KOD Hot Start DNA polymerase: KOD Hot Start DNA Polymerase is a premixed complex of KOD Hi Fi DNA polymerase and two monoclonal antibodies that inhibit the enzyme's DNA polymerase and 3' exonuclease activities during PCR assembly and initial denaturation step. Reactions were made in a final volume of 100 µl containing: 1 x KOD buffer, 1 mM $MgSO_4$, 0.2 mM dNTPs, 100 pmol of each primer, 10-20 ng of template DNA, 1 U of KOD DNA Polymerase and sterile dH_2O.

PCR with Pfu DNA polymerase: Reactions were made in a final volume of 100 µl. A mix (60 µl) was prepared containing: 0.2 mM dNTPs, 100 pmol of each primer, 10-20 ng of template DNA and sterile dH_2O. This mix was denatured for 3 min at 94°C, and then a second mixture (40 µl) was added containing: 10 µl of Pfu buffer (10 x), 2.5 U of Pfu and sterile dH_2O. Then the PCR was started.

The reagents were assembled on ice in 0.5 ml PCR tubes. PCRs were performed in a PCR System 2400 thermocycler (Applied Biosystems) under the following conditions:

- Initial denaturation: 94°C, 3 min
- Denaturation: 94°C, 30 s
- Annealing: X°C (T_M), 30-45 s
- Elongation: 72°C, 20 s/kb for KOD Hot Start - 1 min/kb for Pfu
- Repeats of steps 2 through 4: 15 cycles or occasionally 30
- Final elongation: 72°C, 10 min

The annealing temperature (T_M) was depending on the melting temperature of the primer with the lowest T_M and was calculated following the formula: T_M= 4 x (G+C) + 2x (A+T).

2.2.16.11 Splicing by overlap extensions. Splicing by overlap extensions (SOE) (Horton et al., 1989; Ho, 1989) was used to introduce single or multiple amino acids mutations (Fig. 2.2 A) and to generate chimeras (Fig. 2.2 B). SOE consists of three separate PCRs. KOD Hot Start DNA polymerase was employed in the PCR reactions (1) and (2) (Fig 2.2 A and 2.2 B) following the protocol described at 2.2.16.10. The two PCR products were separated on an agarose gel, extracted as described in 2.2.16.4 and used as template for the third PCR reaction ((3) in Fig 2.2 A and 2.2 B).

1/3 of each of the two extracted fragments were assembled in a tube with 1 x KOD buffer , 1 mM $MgSO_4$ and 45 µl of dH_2O. The tube was submerged in a beaker with 800 ml of boiling water until the water reached room temperature. This procedure maximises the annealing of complementary sequences. Afterwards, 0.2 mM dNTPs and 1 u KOD DNA polymerase were added and a 10 min elongation step at 72 °C was performed. In this step, the extension of the annealed area by DNA polymerase produces a double-stranded DNA molecule in which the original molecules are spliced together. After the elongation, the two flanking primers (100 pmol/100 µl) were added to the reaction mix and a PCR reaction was performed as described in 2.2.16.10.

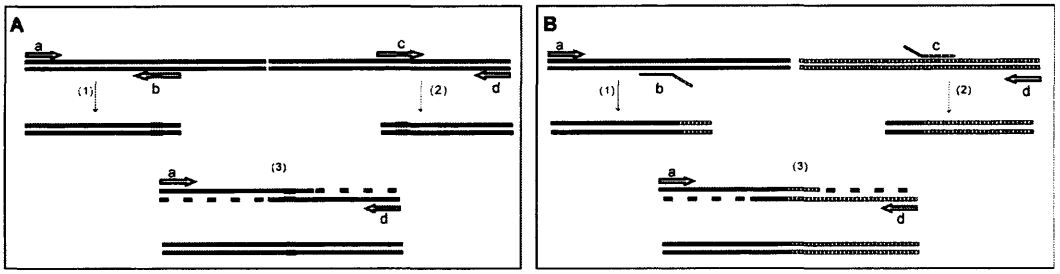

FIGURE 2.2: Schematic representation of SOE for site-directed mutagenesis and chimeras generation. A: Schematic representation of site-directed mutagenesis. The dsDNA are represented by lines and primers are represented by arrows. The hybrid primers b and c introduce the desired mutations (grey box) and are used in two separate PCRs, (1) and (2), in combination with the two flanking primers a and d. The PCR products of the reactions (1) and (2), carrying the mutated region (grey box) and having complementary ends, are used as template in PCR (3). After denaturation, the two PCR products anneal at the overlapping region, are extended 3' by DNA polymerase (dashed line) and then they are further amplified by the PCR with the flanking primers a and d. **B**: Schematic representation of chimeras generation by SOE. Two different dsDNA are represented as solid lines (left) or as a broken lines (right). The hybrid primers b and c match their template cDNAs at their 3' portions whereas the 5' portions are designed so that they are complementary to each other. In PCR (1) the primer b is used in combination with the flanking primer a, and, in PCR (2), c is used in combination with the flanking primer d. The PCR products of the PCRs (1) and (2) are used as template in PCR (3). The two PCR products are denatured, the 3' is extended by the DNA polymerase activity (dashed line) and then they are amplified by PCR with the flanking primers a and d.

2.2.16.12 Sequencing of DNA. Purified DNA plasmids containing modified sequences were verified by sequencing with the BigDye Terminator Cycle Sequencing Kit 1.1 or 2 and an ABI PRISM® 3100-*AVANT* automated DNA capillary sequencer (Applied Biosysems). When the BigDye Kit 1.1 was used, the sequencing reaction was performed in a volume of 10 µl, containing: 200 ng of

DNA, 2 µl of BigDye Kit 1.1, 3.2 pmol primer and sterile dH_2O. Alternatively, when the BigDye Kit 2 was used, the reaction was performed in 20 µl, containing: 300-600 ng DNA, 4 µl of BigDye Kit 2, 3.2 pmol primer and sterile dH_2O. The PCR was performed in a PCR System 2400 thermocycler (Applied Biosystems). Initial denaturation was 30 s at 94°C followed by 25 cycles: denaturation (94°C, 30 s), annealing (50°C, 30 s) and extension step (60°C, 4 min). The reaction was stopped by cooling to 4°C. 10 µl of sterile dH_20 were added to the 10 µl reactions performed with Big Dye 1.1. Afterwards, the PCR product was precipitated by adding 2 µl of NaAc (3M NaAc, pH 5.2, in combination with BigDye Kit 1.1; 3M NaAc, pH 4.6, in combination with BigDye Kit 2), 50 µl of 100% ethanol and 10 min incubation on ice. The mix was centrifuged at 4°C for 15 min, at 16,000 x g. The supernatant was discarded, the pellet washed with 250 µl of 75% ethanol and centrifuged at 4°C for another 15 min at 16,000 x g. The supernatant was removed, the pellet was air-dried and resuspended in 10 µl of HiDi formamide loading buffer. Sequences were analysed using the Lasergene (DNASTAR) analysis suite.

2.2.17 Cloning strategies

2.2.17.1 Oligonucleotides

T7: 5' TAATACGACTCACTATAGGG 3'

SP6: 5' GATTTAGGTGACACTATAG 3'

P1361: 5' CCAATGTACTCAGGGAAACG 3'

P1392: 5' AAGCGGCTCAGCGACTATGC 3'

P2049: 5' GGCCACTGACGGGGCGTACGTGAAGGCCAGCCGCGCCGTCC 3'

P2048: 5' CTTCACGTACGCCCCGTCAGTGGCCGAGGCGGATGTGGATG 3'

P2051: 5' TGGGGCGTGTACACCAAGGAGTCTCTGTATTCATTCG 3'

P2052: 5' CAGCTCGGTCTCGATGACCATGACGACGATGCCAAACATGCC 3'

P2053: 5' GGCATGTTTGGCATCGTCGTCATGGTCATCGAGACCGAGCTG 3'

P2054: 5' GAACATGGGGATGGACAGCAGCACATCCACGTCTGCAGTGGT
TGTGGA 3'

P2055:5'TCCACAACCACTGCAGACGTGGATGTGCTGCTGTCCATCCCCATGTTC3'

P2071: 5' GTGCCCGGCAATTACCGCTTCAC 3'

P2072: 5' GTGAAGCGGTAATTGCCGGGCAC 3'

P2073: 5' CGGCCACTACACGTTCACGTGGACG 3'

P2074: 5' CGTCCACGTGAACGTGTAGTGGCCG 3'

P2075: 5' CCTGGCCTTCTCCTACGCGCCCTC 3'

P2076: 5' GAGGGCGCGTAGGAGAAGGCCAGG 3'

P2077: 5' CGCGCCCTCGACAACCGAGGCCGACG 3'

P2078: 5' CGTCGGCCTCGGTTGTCGAGGGCGCG 3'

P2079: 5' CTCGGTGGCCACTGCCGACGTG 3'

P2080: 5' CACGTCGGCAGTGGCCACCGAG 3'

P2081: 5' CGACGTGGACATTATTCTGTCCATCC 3'

P2082: 5' GGATGGACAGAATAATGTCCACGTCG 3'

P2083: 5' GCTCTAGAGCCAAGATTTAGGGGTCTG 3'

P2084: 5' CGTGGACGGCGCGCCTGGCCTTCAC 3'

P2085: 5' GTGAAGGCCAGGCGCGCCGTCCACG 3'

2.2.17.2 Cloning strategy for L1-hSK1.

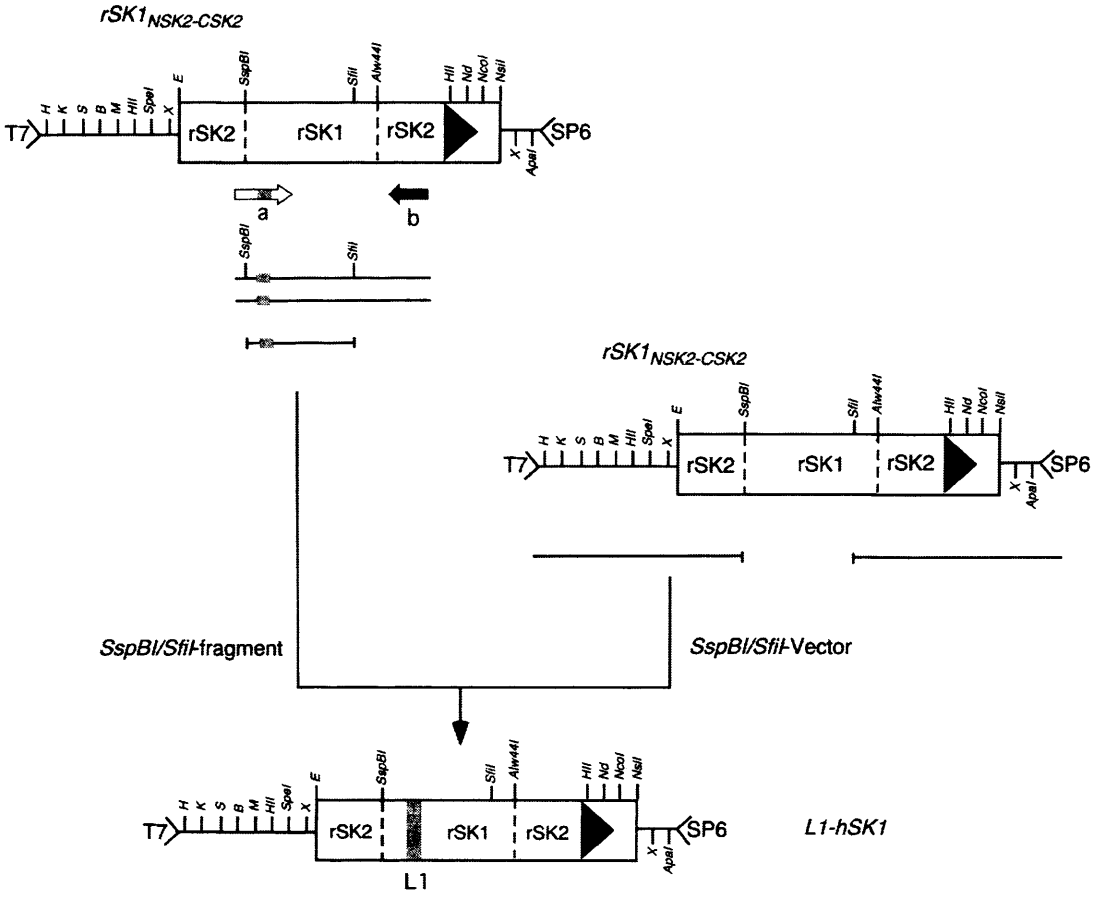

The following primers were used: primer a, P2051; primer b, P1361. The mutation C167Y was introduced and is represented as a grey box in the picture.

2.2.17.3 Cloning strategy for L3-hSK1.

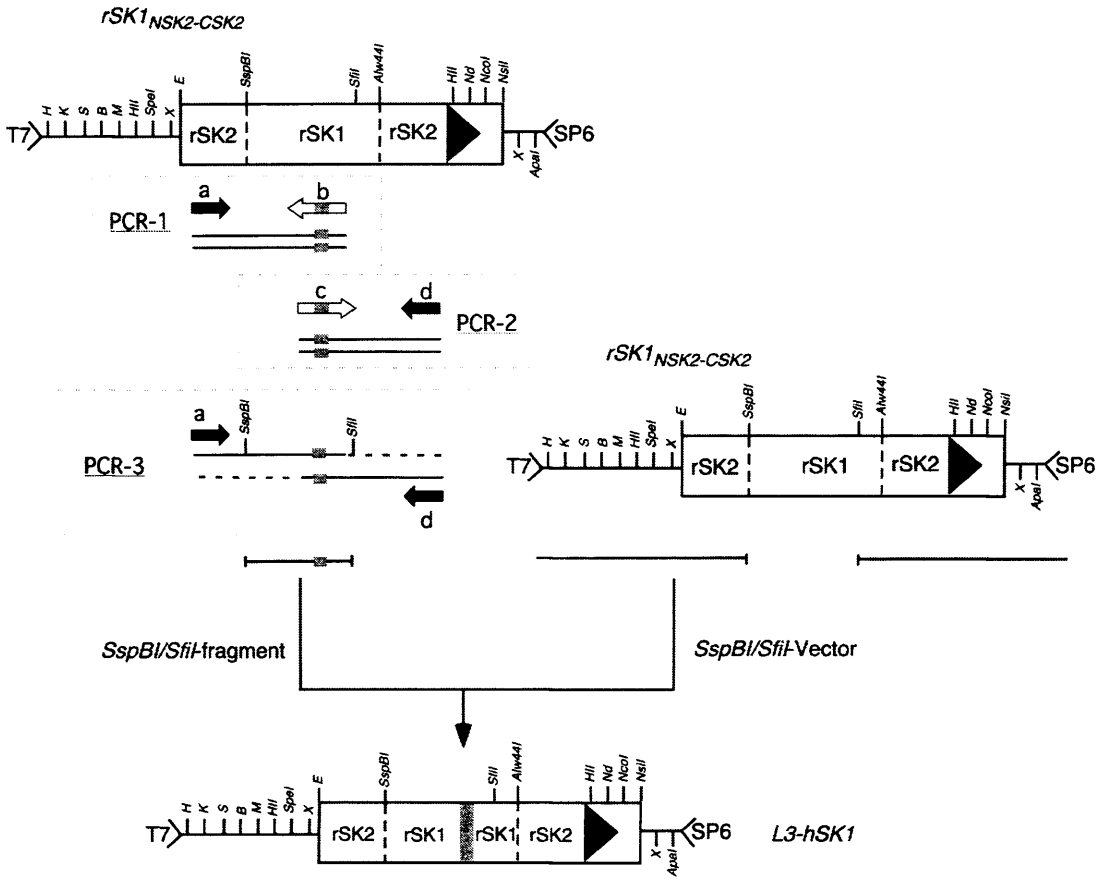

The following primers were used: primer a, P1392; primer b, P2049; primer c, P2048; primer d, P1361. The mutation SLVA245/246/247/250TYAV was introduced, and is represented as a grey box in the picture.

2.2.17.4 Cloning strategy for hSK1-SK2-hSK1.

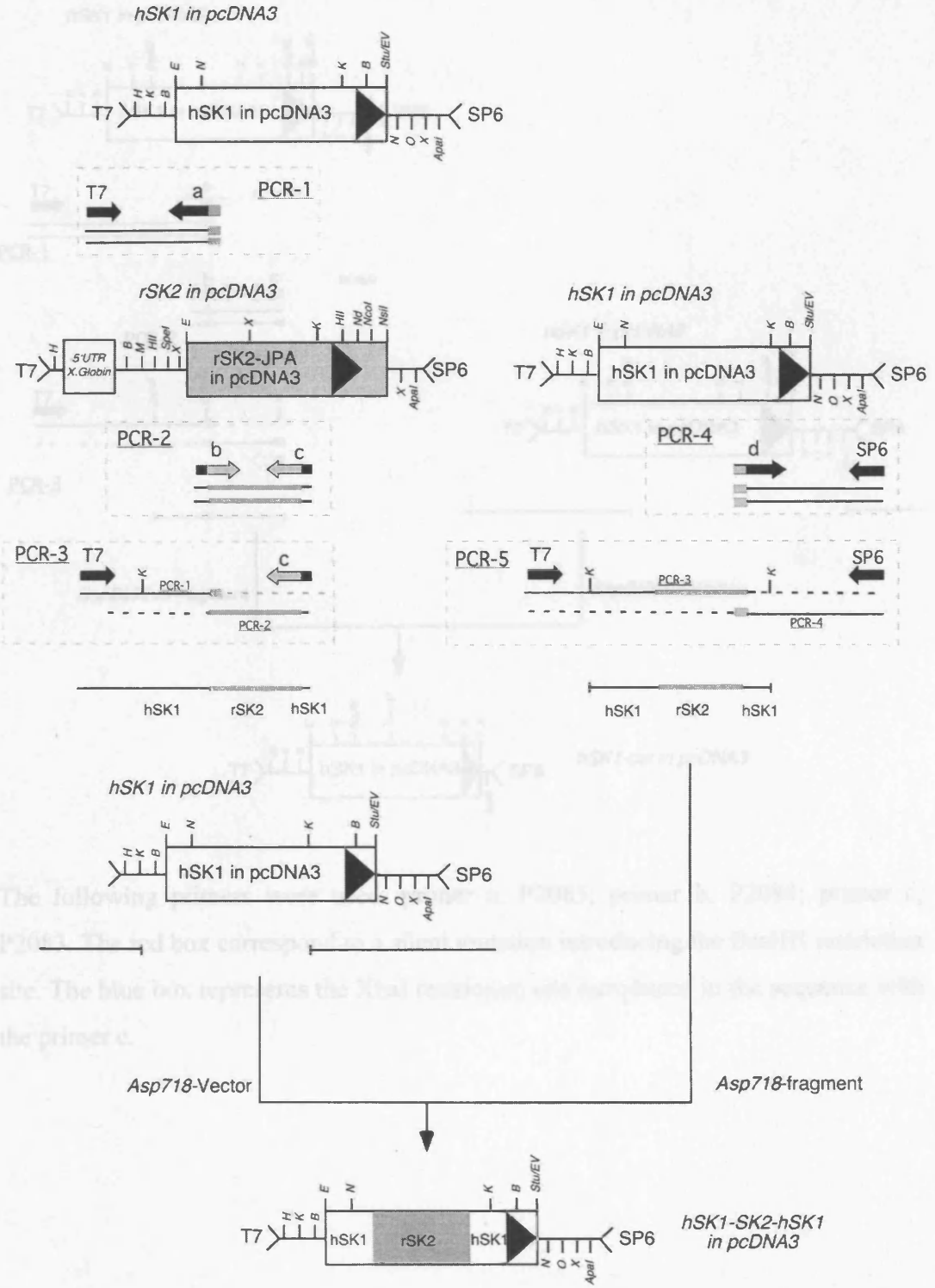

The following primers were used: primer a, P2052; primer b, P2053; primer c, P2054; primer d, P2055. Grey boxes represent SK2 sequences, whereas black lines correspond to hSK1 sequences.

2.2.17.5 Cloning strategy for hSK1-del

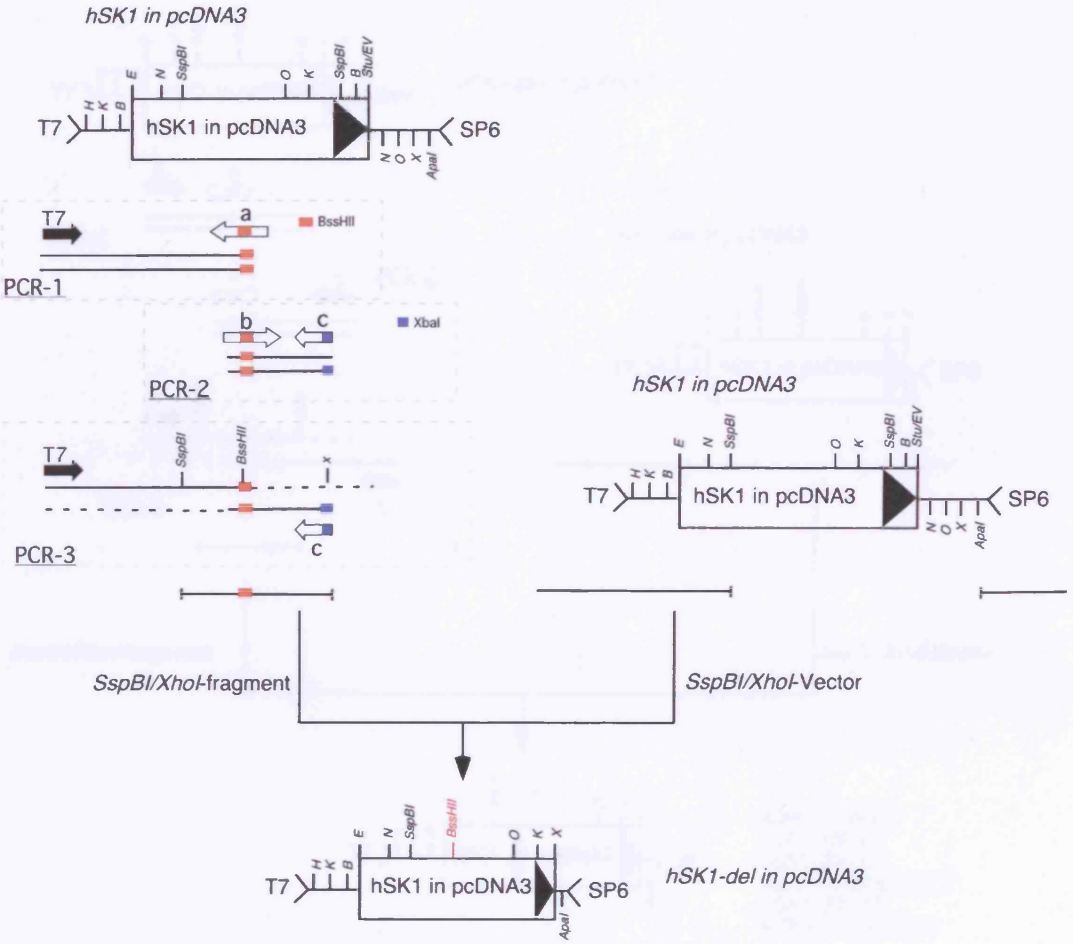

The following primers were used: primer a, P2085; primer b, P2084; primer c, P2083. The red box correspond to a silent mutation introducing the BssHII restriction site. The blue box represents the XbaI restriction site introduced in the sequence with the primer c.

2.2.17.6 Cloning strategy for hSK1 L3 mutants

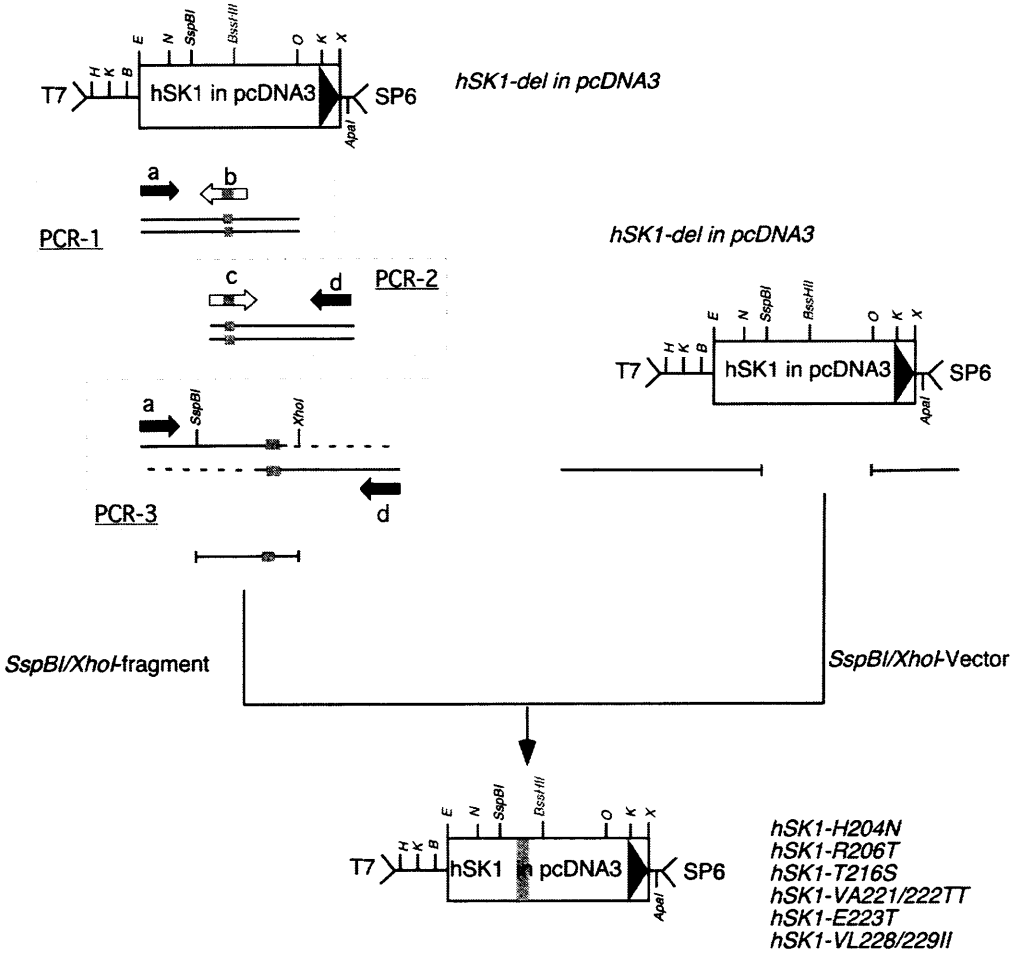

Primer a and d were the same for all the mutations: a, P2070; primer b, P272. The following primers were used to introduce the mutations in hSK1-del:

- hSK1 H204N: c, P2071; b, P2072
- hSK1 R206T: c, P2073; b, P2074
- hSK1 T216S: c, P2075; b, P2076
- hSK1 VA221/222TT: c, P2077; b, P2078
- hSK1 E223T: c, P2079; b, P2080
- hSK1 VL228/229II: c, P2081; b, P208

The grey box in the figure corresponds to the mutated amino acids.

Abbreviations of restriction enzymes

NotI = N

BamHI = B

SacI, SstI = S

EcoRI = E

EcoRV = EV

SmaI = M

HindIII = H

XbaI = X

KpnI, Asp718 = K

XhoI = O

NdeI = Nd

CHAPTER 3

Characterisation of the anti-NSK2 antibody

3.1. Introduction

One of the aims of this thesis is the study of the distribution of SK2 α subunit in the rat brain. For this purpose, a rSK2-directed polyclonal antibody was generated. This chapter describes the affinity purification and characterisation of this antibody performed in order to: (1) test the ability of the antibody to recognise native rSK2 protein in immunocytochemistry and in Western analysis; (2) demonstrate the specificity of the antibody; and (3) identify the epitope to which the antibody specifically binds.

3.2 Antibody purification

A specific antibody was raised in rabbit against a fusion protein of glutathione-S-transferase (GST) and a region of the N-terminal domain of rSK2 α subunit (Fig. 3.1 A). This sequence, corresponding to the amino acids (aa) 23–83 (GenBank accession no. U69882), is unique to SK2, as no significant homology to the corresponding region of SK1 and SK3 was found. Two animals were immunized with the GST-NSK2 fusion protein; therefore, two different sera, named 1973g and 1974g, were obtained (Biogenes, Germany). ELISA assays, performed by Biogenes to determine the antibody titer to the GST-NSK2 antigen, indicated that there was no difference between the two sera. The experiments shown in this chapter refer to the 1973g serum, unless specified.

In order to remove anti-GST and other non-specific immunoglobulins present in the generated sera, the antibody was affinity-purified. The affinity purification was employed using the pET-NSK2 fusion protein, which comprises the same region of the channel used to raise the antibody (NSK2) fused with thioredoxin (Trx) (Fig. 3.1 A). The pET-NSK2 fusion protein was immobilised on a solid support. When the serum was applied, only the immunoglobulins that recognised the NSK2 antigenic determinant were retained on the support and purified. Two different affinity purification methods were used. To purify small amounts of serum (20-50 μl), the membrane purification method (2.2.1) was used. The pET-NSK2 fusion protein was adsorbed to a nitrocellulose membrane. The serum was then incubated with the membrane and, subsequently, the bound antibody was eluted with acidic and alkaline buffers. Larger amounts of serum (500 μl) were purified by the column purification method (2.2.2). In this case, the antibody was purified over columns of SulfoLink

agarose beads coupled to the pET-NSK2 fusion protein. The elutions were performed as described in 2.2.2.4, and the OD_{280} was measured. The three eluates with the highest antibody concentration were mixed in a fraction called E1; the three eluates with the next highest concentration of antibody were combined in E2 and so on. The eluates contained the following amount of antibody: E1 ~100 μg, E2 ~49 μg, E3 ~32 μg and E4 ~25 μg.

Following every purification, ELISA assays were performed to determine the titer of the purified antibody. All the elution fractions and the unpurified serum were used in ELISA experiments to test the sensitivity to the pET-NSK2 fusion protein and, in parallel, to GST. Figure 3.1 B, C shows a representative ELISA experiment of a membrane purification of the anti-NSK2 1974g serum. The ELISA performed with pET-NSK2 fusion protein (Fig 3.1 B) showed that the elution fractions contained high titers of antibody directed against NSK2, with the acidic elution exhibiting higher sensitivity for pET-NSK2 compared with the basic fraction. The ELISA performed against GST indicated that the high levels of GST-directed antibodies, present in the unpurified serum, were removed with the purification and hardly any signal for GST was measured in the two elution fractions (Fig. 3.1 C), suggesting that the antibody purification was achieved. After ELISA, the acidic and alkaline elutions were pooled and used in the experiments reported in 3.4. Comparable results were obtained using ELISA assay on the membrane purified anti-NSK2 1973g serum, which was employed in some of the experiments shown in 3.3. Moreover, a typical ELISA experiment performed with a column purification of the anti-NSK2 1973g serum is shown in Figure 3.1 D and E. The assay was performed on the E1-E4 elution fractions and on the serum. As reported in Figure 3.1 D, E1 and E2 were the elution fractions that contained the highest levels of the antibodies directed against NSK2, whereas a lower signal was detected in E3 and E4. Figure 3.1 E shows that only a very low sensitivity for GST was detected in all the elution fractions, indicating, also in this case, that the antibody purification was accomplished. The elution fraction E1 was used for the experiments described later in this chapter (3.3 and 3.4).

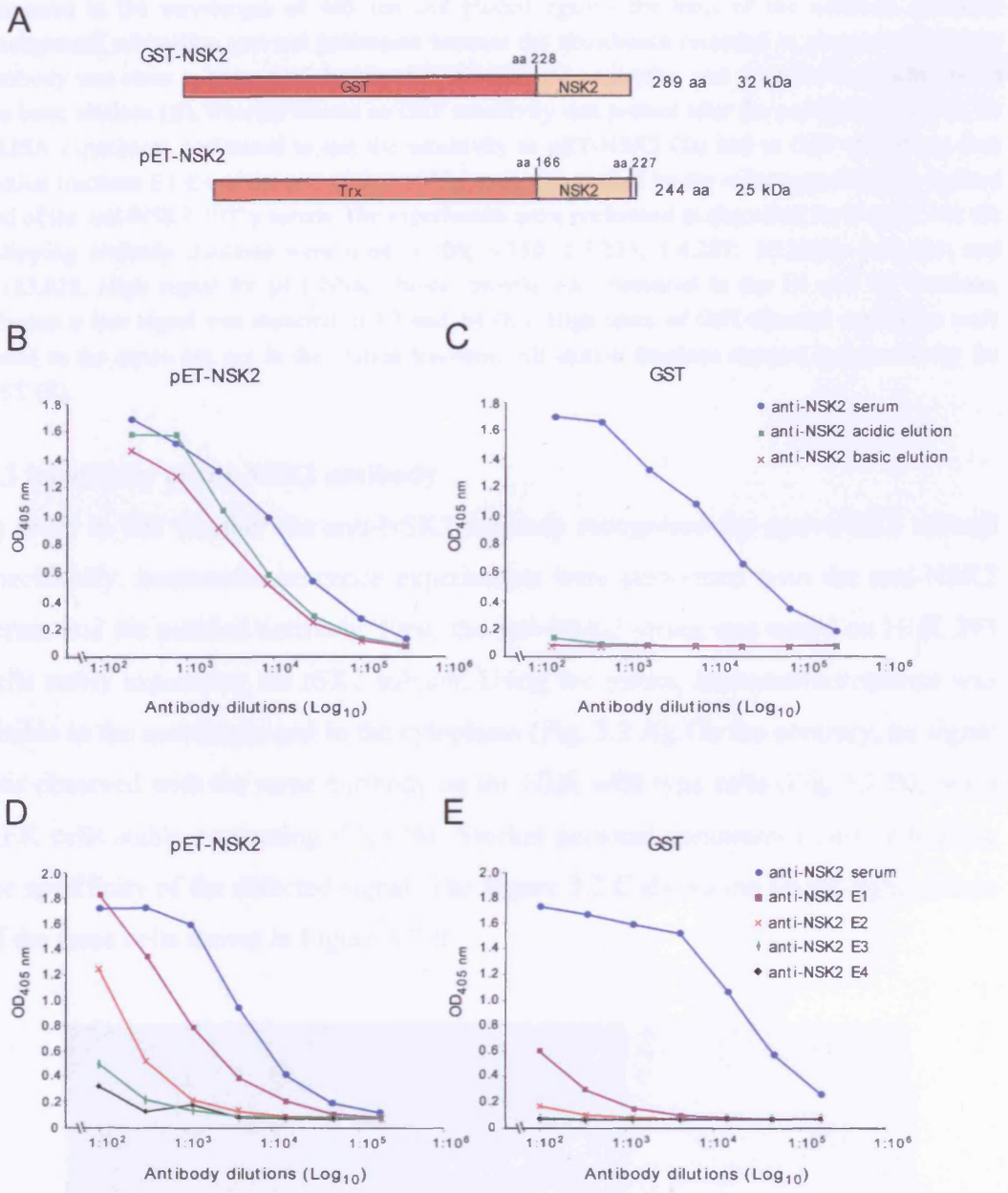

FIGURE 3.1: **Affinity purification of the anti-NSK2 antibody**. **A**: Schematic representation of the GST-NSK2 fusion protein, which was used to generate the anti-NSK2 polyclonal antibody, and of the pET-NSK2 fusion protein, where the same rSK2 region (aa 23–83, GenBank accession no. U69882) was fused to Trx. **B**, **C**: ELISA experiment performed to determine the titer to pET-NSK2 (**B**) and to GST (**C**) of the acidic and basic elutions of the anti-NSK2-1974g membrane-purified antibody and of the anti-NSK2-1974g serum. 96 well immuno-plates were adsorbed either with pET-NSK2 fusion protein (**B**) or with GST (**C**) at the concentration of 3µg/µl. This concentration was shown to give maximum signal in initial tests that were performed by coating the 96 well plates with different concentrations of protein. Seven serial dilution steps were prepared for the anti-NSK2-1974g serum and for the acidic and basic elutions. The starting dilution was 1:150 and the dilution factor of 3.5 was used, leading to the following dilutions: 1:150; 1:525; 1:1,837; 1:6,431; 1:22,509; 1:78,782; and 1:275,739. The background signal was measured in the absence of primary antibody. Absorbance was

measured at the wavelength of 405 nm and plotted against the $\log_{10}$ of the antibody dilutions. Background subtraction was not performed because the absorbance recorded in absence of primary antibody was close to zero. A high titer of NSK2-directed antibodies was found in the acidic and in the basic elutions (**B**), whereas almost no GST sensitivity was present after the purification (**C**). **D, E:** ELISA experiment performed to test the sensitivity to pET-NSK2 (**D**) and to GST (**E**) of the four elution fractions E1-E4 of the anti-NSK2 1973g antibody purified by the column purification method and of the anti-NSK2-1973g serum. The experiments were performed as described for B and C but the following antibody dilutions were used: 1:100; 1:350; 1:1,225; 1:4,287; 1:15,006; 1:52,521; and 1:183,826. High signal for pET-NSK2 fusion protein was measured in the E1 and E2 fractions, whereas a low signal was detected in E3 and E4 (D). High titers of GST-directed antibodies were found in the serum but not in the elution fractions. All elution fractions showed low sensitivity for GST (**E**).

3.3 Specificity of the NSK2 antibody

In order to test whether the anti-NSK2 antibody recognised the native SK2 subunit specifically, immunofluorescence experiments were performed with the anti-NSK2 serum and the purified antibody. First, the anti-NSK2 serum was tested on HEK 293 cells stably expressing the rSK2 subunit. Using the serum, immunofluorescence was visible in the membrane and in the cytoplasm (Fig. 3.2 A). On the contrary, no signal was observed with the same antibody on the HEK wild type cells (Fig. 3.2 B), or on HEK cells stably expressing rSK3 (M. Stocker personal communication), indicating the specificity of the detected signal. The Figure 3.2 C shows the bright-light picture of the same cells shown in Figure 3.2 B.

FIGURE 3.2: Immunocytochemistry with the anti-NSK2 serum on HEK 293 cells stably expressing rSK2. A, B: Immunofluorescence using the anti-NSK2 serum (1:1000) on HEK 293 cells stably expressing rSK2 (**A**) or wild type HEK 293 cells (**B**). In A, membrane and cytoplasmic staining was observed whereas no immunostaining was detected in B. **C**: Bright-light picture of the cells pictured in B. **A-C**: FITC-conjugated anti-rabbit secondary antibody was used for signal detection (1:30). Scale bar: 20 µm.

The same cell line that expresses rSK2 was used in immunofluorescence experiments with the affinity-purified anti-NSK2 antibody (membrane purification, 1:200) and, as

shown in Figure 3.3 A, a clear immunofluorescence signal was observed in the cell membrane and cytoplasm. This result was similar to the signal observed in experiments performed with the serum. The specificity of this immunostaining was also confirmed by preadsorption experiments. Indeed, preincubation of the purified antibody with saturating amounts of the fusion protein pET-NSK2 completely abolished the ability of the antibody to detect SK2 in the rSK2-expressing cells (Fig. 3.3 B). In addition to preadsorption experiments, a control experiment was performed where the purified antibody was preincubated under the same conditions but the fusion protein was omitted. This experiment was performed to demonstrate that the lack of signal observed in the preadsorption experiments is due to specific binding of the antibody to the fusion protein and not to non-specific adsorption of the antibody to the plastic tube in which the preadsorption was carried out. As expected, when the antibody preincubation was performed in absence of fusion protein, the detected signal (Fig. 3.3 D) was similar to the staining shown in Figure 3.3 A. Identical results were obtained when immunofluorescence experiments were performed using the anti-NSK2 antibody purified by column purification. Immunocytochemistry that was performed with this purified antibody on rSK2-expressing HEK 293 cells showed the same distribution pattern observed using the membrane purification. Taken together, these experiments indicate that the serum and the immunopurified anti-NSK2 antibody were able to recognise recombinantly expressed rSK2 α subunits. Furthermore, the experiments demonstrated that the detected signal was specific, as no staining was generated by the serum in untransfected HEK 293 cells or by the purified antibody preadsorbed with the antigen in rSK2-expressing cells.

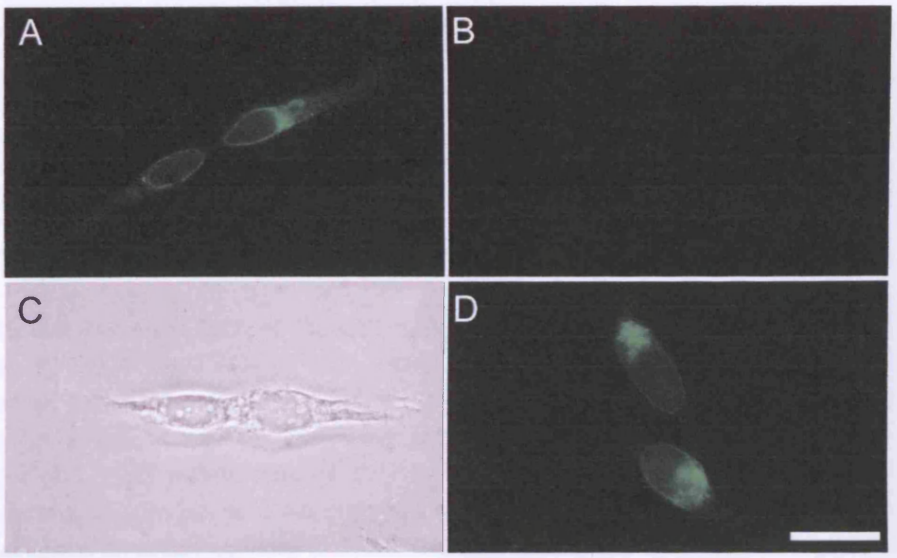

FIGURE 3.3: Immunocytochemistry with the affinity-purified anti-NSK2 antibody on HEK 293 cells stably expressing rSK2. A: Immunofluorescence on HEK 293 cells that express rSK2 using the affinity-purified anti-NSK2 antibody (1:200). A membrane purification preparation was used in this experiment. Membrane and cytoplasmic staining was observed. B: Antigen blocking: the anti-NSK2 antibody (1:200) was preincubated with 20 µg/µl pET-NSK2 fusion protein for three hours at room temperature. No immunofluorescence signal was detected. C: Bright-light picture of the cells pictured in B. D: Control for the antigen blocking: the anti-NSK2 antibody (1:200) was preincubated in the same conditions indicated in B but the pET-NSK2 fusion protein was omitted. A, D: FITC-conjugated anti-rabbit secondary antibody was used for signal detection (1:30). Scale bar: 20 µm.

Subsequently, the anti-NSK2 antibody was used in Western blot analysis in order to estimate the antibody sensitivity in this assay. The unpurified and the purified anti-NSK2 antibody were tested in immunoblots of serial dilutions of the fusion protein pET-NSK2. The lowest amount of fusion protein detected by the unpurified anti-NSK2 antibody was 0.5 ng (Fig. 3.4 A). The lowest amount of fusion protein detected by the purified anti-NSK2 antibody was ~5 ng (Fig. 3.4 B). However, taking into consideration the signal intensity of the band, it is possible that 2-3 ng of fusion protein might be still detected. Moreover, as shown in Figure 3.1 A, the rSK2 sequence corresponds to ~25% of the total length of the pET-NSK2 fusion protein. This has to be considered for the actual detection limit of the antibodies, which is four times higher than the detection limit observed. Therefore, the purified antibody should be able to detect around 20 fmol of SK2 protein.

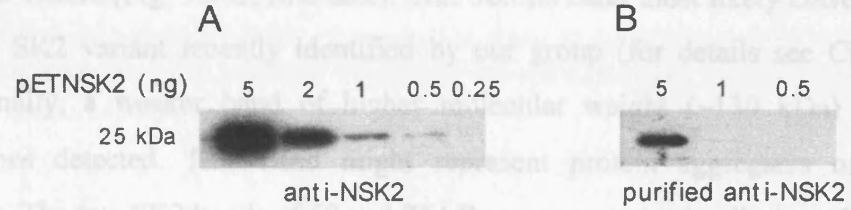

FIGURE 3.4: Detection limit of the anti-NSK2 serum and of the affinity-purified anti-NSK2 antibody. 5, 2, 1, 0.5 and 0.25 ng (A) or 5, 1 and 0.5 ng of pET-NSK2 fusion protein (B) were separated on 12% SDS page and transferred to nitrocellulose membrane by semi-dry transfer. A: Immunoblot performed with the anti-NSK2 serum (1:1,000) showed that 0.5 ng was the lowest amount of pET-NSK2 protein detected. B: Western blot using the membrane affinity-purified anti-NSK2 antibody (1:300) indicated that 5 ng was the lowest amount of fusion protein detected. **A, B:** HRP-conjugated secondary antibody (1:5,000; BioRad) and ECL chemiluminescent system were used for signal detection.

After estimating the detection limit, the subunit specificity of the anti-NSK2 antibody was assessed in Western analysis. HEK 293 cells were transiently transfected with the plasmids that code for rSK1, rSK2 or rSK3 subunits, and lysates were prepared. These lysates and the lysate from untransfected HEK 293 cells were then analysed in Western blot using the anti-NSK2 serum. As shown in Figure 3.5 A, the antibody recognised a single band of ~50 kDa in rSK2-transfected cells (Fig. 3.5 A, third lane). The molecular weight of this band deviates from the 63 kDa predicted from the primary sequence of rSK2 α subunit. However, no bands were detected in untransfected cells (Fig 3.5 A, first lane) and no cross-reactivity was observed with the other SK subunits, as no bands were detected on cells that were transfected with rSK1 (Fig. 3.5 A, second lane) or with rSK3 cDNA (Fig. 3.5 A, fourth lane). Moreover, the immunopurified anti-NSK2 antibody was used in Western blot of rSK2-expressing HEK 293 cells to demonstrate that also the purified antibody detected a band of the same molecular weight (Fig. 3.5 B). These analyses show that the immunopurified antibody is subunit-specific. Furthermore, these experiments confirmed that the unpurified and purified anti-NSK2 antibody recognise the SK2 α subunit, which shows a smaller molecular weight than expected.

Finally, the affinity-purified anti-NSK2 antibody was used to study the native expression of the SK2 subunit in the rat brain by Western blot of rat brain synaptosomal membranes. This antibody detected two predominant bands. In addition to the ~50 kDa band, which is likely to represent SK2, a second band of ~75

kDa was visible (Fig. 3.5 C, first lane). This second band most likely corresponds to a novel SK2 variant recently identified by our group (for details see Chapter 5). Additionally, a weaker band of higher molecular weight (~130 kDa) was also sometimes detected. This band might represent protein aggregates of SK2 α subunits. The two SK2 bands of 50 and 75 kDa were completely eliminated when the antibody was preadsorbed with saturating amount of pET-NSK2 protein (Fig. 3.5 B, second lane), confirming the specificity of the antibody in the native tissue. Surprisingly, the band that corresponds to protein aggregates was not preadsorbed.
In conclusion, all these experiments indicated that the affinity-purified anti-NSK2 antibody is a specific tool to study the immunohistochemical distribution of SK2 α subunit in the rat brain.

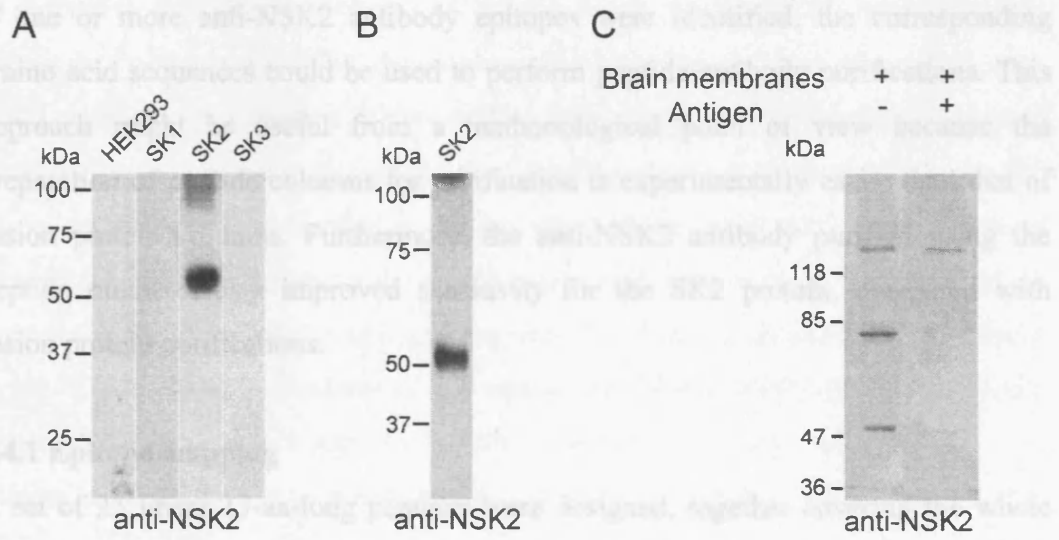

FIGURE 3.5: Characterisation of the anti-NSK2 antibody in Western blot analysis. A: Crude membrane lysates of untransfected HEK 293 cells and HEK 293 cells transiently transfected with plasmids coding rSK1, rSK2 or rSK3 α subunits were separated on SDS page and transferred to nitrocellulose membrane by tank blot. Immunoblot was performed using the unpurified antibody. No bands were detected in untransfected HEK 293 (first lane) and in cells transfected with rSK1 (second lane) or with rSK3 (fourth lane); a single band of ~50 kDa was detected in rSK2-expressing cells (third lane). **B:** Western blot on HEK 293 cells transiently transfected with rSK2. The lysates were separated on SDS gel and transferred to nitrocellulose membrane as described in A. Immunoblot was performed with the column purified anti-NSK2 antibody. A single band of ~50 kDa was visible. **C**: 100 µg of synaptosomal membranes of 35-days-old rat brain were separated on 7.5% SDS page and transferred to nitrocellulose membrane as described in A. Immunoblot was performed with column purified anti-NSK2 antibody (1:300). Two immunoreactive bands were detected: a ~50 kDa band, corresponding to SK2, and a ~75 kDa band, corresponding to a novel SK2 variant (Chapter 5). A

third, less intense band of ~130 kDa was also detected. In the second lane, the preadsorbtion control, performed with 20 µg/ml pET-NSK2, is shown. The signal of the 50 kDa and 75 kDa bands was abolished, whereas the higher molecular weight band was still visible. The Western blots were kindly provided by Dr. K. Hirzel

3.4 Epitope mapping of anti-NSK2 antibody

To characterise the anti-NSK2 antibody further, epitope mapping was performed to identify antibody binding sites. The method employed for this purpose is the so called "peptide scan". In this method, a set of linear overlapping peptides, that were designed to cover the entire primary sequence of the antigen, were synthesized on a solid support. Subsequently, the antibody was used in immunoblot-like experiments together with this solid support to test whether specific regions within the antigen could be recognised.

If one or more anti-NSK2 antibody epitopes were identified, the corresponding amino acid sequences could be used to perform peptide antibody purifications. This approach might be useful from a methodological point of view because the preparation of peptide columns for purification is experimentally easier than that of fusion protein columns. Furthermore, the anti-NSK2 antibody purified using the peptide might display improved sensitivity for the SK2 protein, compared with fusion protein purifications.

3.4.1 Epitope mapping

A set of 25 linear 13-aa-long peptides were designed, together covering the whole NSK2 part of the fusion protein that was used to generate the antibody (Fig. 3.1 A). The peptides overlapped by 11 aa and were shifted of two aa along the NSK2 sequence, from the amino- to the carboxyl-terminus (Fig. 3.6 A). The 25 peptides were synthesized by "SPOT synthesis" directly on Whatman 50 cellulose membrane support, from the carboxyl to the amino-terminus, with the carboxyl-terminus covalently bound to the membrane (Jerini Peptide Technologies). We obtained a membrane with 25 spots (PepSPOTs™), each spot consisting of ~5 nmol of peptide. The spots were numbered from 1 to 25, corresponding to the peptides covering the antigen (Fig. 3.6 B).

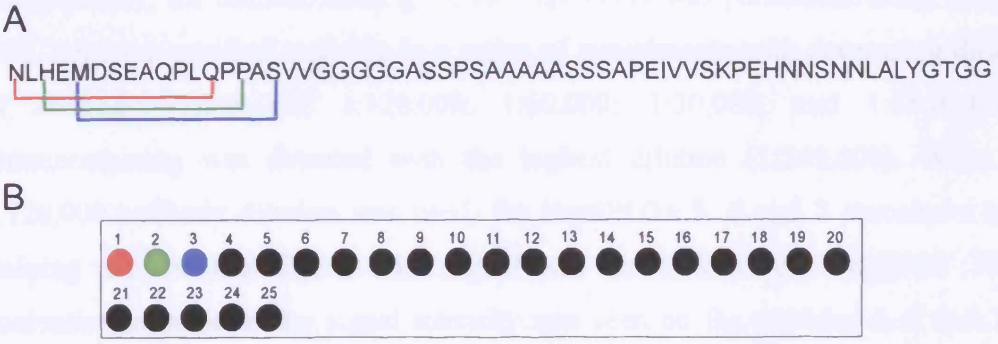

FIGURE 3.6: Schematic representation of the PepSPOTs™ membrane. A: Sequence of the NSK2 antigenic determinant. The red, green and blue lines below the sequence indicate the 13-aa-long peptides 1, 2 and 3, each overlapping of 11 aa. 25 peptides were designed to cover the entire NSK2. **B**: Schematic illustration of the 25 PepSPOTs on the membrane support. The red, green and blue dots represent the peptides 1, 2 and 3, respectively, which are indicated in A with the same colours.

To determine the epitope to which the antibody binds, the PepSPOTs membrane was employed in immunoblot-like experiments (2.2.9) using the immunopurified anti-NSK2 antibody for detection. Before testing the antibody on the PepSPOTs, a set of control experiments were carried out on a membrane where no peptide was bound. These controls were performed to assess whether the anti-NSK2 antibody alone generated background signal and, in case any non-specific staining was detected, to test whether the regeneration of the membrane (2.2.9) might efficiently eliminate the signal. The following dilutions of the column purified anti-NSK2 antibody were tested: 1:249,000; 1:219,000; 1:150,000; 1:90,000; 1:30,000; and 1:6,000. No staining was visible up to the antibody dilution of 1:30,000. When the 1:30,000 dilution was applied, a diffused staining was visible with long exposure times of the membrane (20 min), whereas short exposures (1 min) did not show any signal. Following this experiment, the membrane was successfully regenerated (2.2.9). Also, the experiment with the dilution of 1:6,000 revealed background signal only at long exposure time (20 min). Therefore, we concluded that long exposure combined with antibody dilutions lower than 1:30,000 could result in non-specific staining of the membrane and, in turn, mask any real signal. Additionally, it was tested whether the secondary antibody showed any cross-reactivity with the PepSPOTs. In this control experiment, the PepSPOTs membrane was used in the immunoblot experiment but the primary antibody was omitted. No signal was detected, indicating that the secondary detection system used was suitable for the experiments.

Subsequently, the immunostaining on the PepSPOTs was performed using the anti-NSK2 column purified antibody in a series of experiments with decreasing dilution of antibody: 1:249,000; 1:120,000; 1:60,000; 1:30,000; and 1:15,000. No immunostaining was detected with the highest dilution (1:249,000). When the 1:120,000 antibody dilution was used, the PepSPOTs 5, 6 and 7 revealed a clear staining and, additionally, a faint signal was detected on the PepSPOT 18. A qualitative increase of the signal intensity was seen on the peptides 5, 6 and 7 by decreasing the antibody dilution from 1:60,000 to 1:15,000. Moreover, a slight increase of the signal on the PepSPOT 18 was observed and a weak staining appeared on the PepSPOT 4. Starting from the second experiment, performed with the 1:120,000 antibody dilution, the membrane was regenerated immediately after each immunoblot to remove the antibody bound to the PepSPOTs. Figure 3.7 shows a representative PepSPOTs immunoblot experiment performed with antibody dilution of 1:30,000, which gave the best signal to noise ratio.

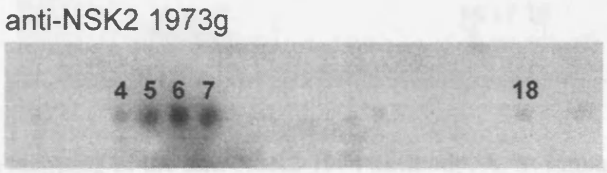

FIGURE 3.7: Epitope mapping of the anti-NSK2 antibody. Immunoblot experiment performed on the PepSPOTs™ membrane. The experiment was performed with the anti-NSK2 antibody column purification (1:30,000). The antibody bound to the peptides was detected with anti-rabbit HRP-conjugated secondary antibody (1:6,000 BioRad). The ECL chemiluminescent system was used to reveal the signal; the membrane was exposed to the film for five minutes. PepSPOTs 5, 6 and 7 showed a strong immunostaining. PepSPOTs 4 and 18 revealed a weak signal, whereas all the other PepSPOTs were not detected by the antibody.

As mentioned in 3.2, two anti-NSK2 sera were raised in two rabbits against the same fusion protein NSK2-GST: 1973g immune serum, which is the one used in all the experiments shown in this chapter, and 1974g. In order to test whether the two sera recognised the same or different epitopes of the NSK2 antigenic determinant, the immunopurified 1974g antibody (3.2) was also tested in the immunoblot on the PepSPOTs membrane. Before performing this experiment, a control immunoblot was preformed omitting the primary antibody. The absence of a signal indicated the complete regeneration of the PepSPOT membrane (Fig. 3.8 A). When the purified

1974g antibody (1:60,000) was used in the immunoblot, an intense staining appeared on PepSPOTs 5, 6 and 7 and, with less intensity, on 16. Moreover, a weak signal was also detected on the PepSPOTs 4, 17, and 18.

Altogether, the epitope mapping experiments suggest that the main region recognised by both anti-NSK2 immune sera (1973g and 1974g) corresponds to the sequence of the peptides 5, 6 and 7. A second sequence corresponding to PepSPOTs 16, 17 and 18 was identified with the serum 1974g. The signal intensity of these PepSPOTs was significantly lower.

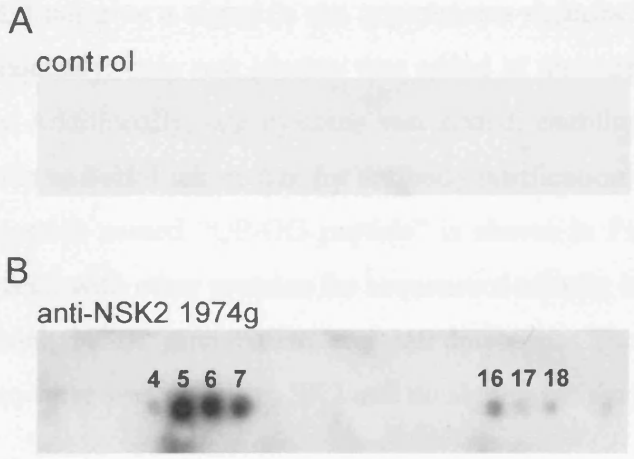

FIGURE 3.8: Epitope mapping of the anti-NSK2-1974 antibody. A, B: Immunoblot experiment on the PepSPOTs™ membrane performed either omitting the primary antibody (**A**) or with the anti-NSK2-1974g antibody membrane purification (1:60,000) (**B**). In A, no signal was detected. In B, the PepSPOTs 5, 6, 7 and, to less extent, 4 showed immunostaining. A second region of NSK2 corresponding to the PepSPOTs 16, 17 and 18 revealed a weaker signal. All the other PepSPOTs were not detected by the antibody. The experiments were performed as described in Figure 3.7.

3.4.2 Anti-NSK2 antibody purification

After identifying the linear epitope recognised by the affinity-purified anti-NSK2 1973g and 1974g sera, the amino acid sequence corresponding to the epitope was used to purify the 1973g serum.

The sequences of the peptides 5, 6 and 7, which revealed intense immunoreactivity in the immunoblot experiments, (Fig. 3.7 and 3.8) were inspected. The sequence QPPASVVGG (Fig 3.9 A, red) is present in all three peptides and represents the central part of the linear epitope. As shown in Figure 3.9 A, in all three peptides this core sequence is flanked by a few amino acids: four amino acids at the amino-

terminus in peptide 5; two amino acids at the amino-terminus and two amino acids at the carboxyl-terminus in peptide 6; four amino acids at the carboxyl-terminus in the peptide 7. These amino acids might contribute to the binding of the antibody. Therefore, the peptide designed for the antibody purification contained the core sequence and the amino acids QPL at the amino-terminus, as shown in Figure 3.9. At the carboxyl-terminus of the core sequence a stretch of glycine residues is present, which gives high flexibility to that region. Antibodies frequently do not bind to regions of high flexibility; therefore, we do not expect that the anti-NSK2 antibody binds to the stretch of glycine residues. This is also supported by the fact that PepSPOTs 8-11 did not give a signal in the experiments described above (Fig. 3.7 and 3.8 B). Consequently, only one glycine was added at the carboxyl-terminus to the core sequence. Additionally, one cysteine was added, enabling the coupling of the designed peptide to SulfoLink matrix for antibody purification (Fig. 3.9 B). The sequence of the peptide named "QP-GG peptide" is shown in Figure 3.9 B. This peptide was compared with other proteins for sequence similarity by BLAST search against the GenBank NCBI mammalian and rat databases. The BLAST search showed that the sequence was unique to SK2 and no significant similarity (E-value < 1) was found.

FIGURE 3.9: Sequence analysis of the anti-NSK2 antibody epitope. **A:** Alignment of the sequences of PepSPOT peptides 5, 6 and 7 which are recognised by the anti-NSK2 sera 1973g and 1974g. The core sequence present in all peptides is shown in red. **B**: Sequence of the QP-GG peptide, designed for the antibody purification. An additional cysteine was added at the carboxy-terminus of the peptide.

The QP-GG peptide, obtained from Alta Bioscience (University of Birmingham) was coupled to SulfoLink agarose beads and the anti-NSK2 1973g serum was immunopurified (2.2.2). Surprisingly, the protein concentration measured in the eluates was extremely low (0.06-0.01 OD_{280nm}/ml), compared with that of other purifications performed with the same amount of serum, using the pET-NSK2 fusion

protein. Nevertheless, the flow through, one eluate and the serum were tested in an ELISA assay. Since the QP-GG peptide alone is too small to adsorb efficiently to the plate used for the ELISA assay, the peptide was coupled to a BSA carrier protein (Imject Maleimide Activated BSA, 2.2.3). As shown in Figure 3.10, the eluate showed a clear signal above background up to a dilution of 1:10,000, whereas the flow through gave a signal comparable with the background even at low dilutions. These two observations indicate that all the antibodies recognising the anti-QP-GG peptide were purified from the serum. Additionally, we tested whether the eluate still contained antibody that detected GST. As shown in Figure 3.10 B, no anti-GST antibodies were present in the purification, whereas the flow through fraction showed a signal for GST comparable with that of the serum. The antibody purification performed with the peptide was also used in immunoblot on the PepSPOTs membrane (1:30,000) and, as shown in Figure 3.10 C, intense staining was visible only on the PepSPOTs 5, 6 and 7, which correspond to the region of the NSK2 used for the antibody purification, whereas no signal was detected on PepSPOT 18.

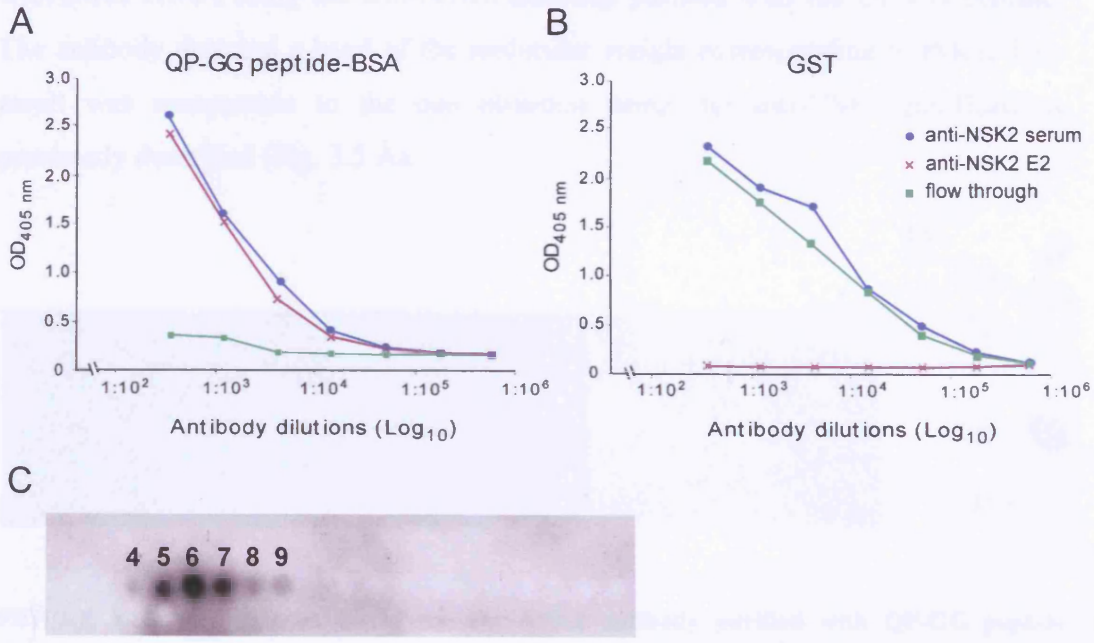

FIGURE 3.10: Affinity purification of the anti-NSK2 antibody using the QP-GG peptide. A, B: ELISA experiment performed to determine the titer of the anti-NSK2 column purification using the QP-GG peptide coupled to SulfoLink matrix. In this purification, the eluates were not pooled as described in 3.1 but they were kept separate. One eluate, the serum and the flow through were tested to titer the antibodies directed against either the QP-GG peptide (**A**) or the GST (**B**). In ELISA assays,

the BSA-conjugated QP-GG peptide (QP-GG peptide-BSA) and GST (3 µg/ml) were adsorbed to a 96 well immuno-plate. The experiment was performed as described in Figure 3.1. **B, C:** Seven serial dilution steps were tested for the anti-NSK2 serum, for the eluate and for the flow through (1:350; 1:1,225; 1:4,287; 1:15,006; 1:52,521; and 1:183,826). The background signal, measured in the absence of primary antibody was close to zero. Antibodies that recognised the QP-GG peptide were found in the eluate, whereas little or no antibodies against GST were present. **C:** Immunoblot experiment performed on the PepSPOTs membrane with the E2 fraction of the QP-GG peptide column purification of the anti-NSK2 antibody (1:30,000). The experiment was performed as described in Figure 3.7. Intense immunostaining was detected on the PepSPOTs 5, 6 and 7.

After the successful antibody purification, despite the low protein content in the eluates, the antibody was employed in immunocytochemistry experiments to test its ability to recognise SK2 α subunit recombinantly expressed in HEK 293 cells. Figure 3.11 A shows that the purified antibody revealed a clear membrane signal in the HEK 293 cells stably expressing SK2 subunit. This signal was identical to the one previously obtained with the anti-NSK2 antibody purified with the pET-NSK2 fusion protein. Moreover, no staining was detected in wild type HEK 293 cells (Fig. 3.11 B), indicating the specificity of the signal. Additionally, Western analysis was performed on lysates that were obtained from HEK 293 cells transiently transfected with rSK2 cDNA using the anti-NSK2 antibody purified with the QP-GG peptide. The antibody detected a band of the molecular weight corresponding to rSK2. This result was comparable to the one obtained using the anti-NSK2 purifications previously described (Fig. 3.5 A).

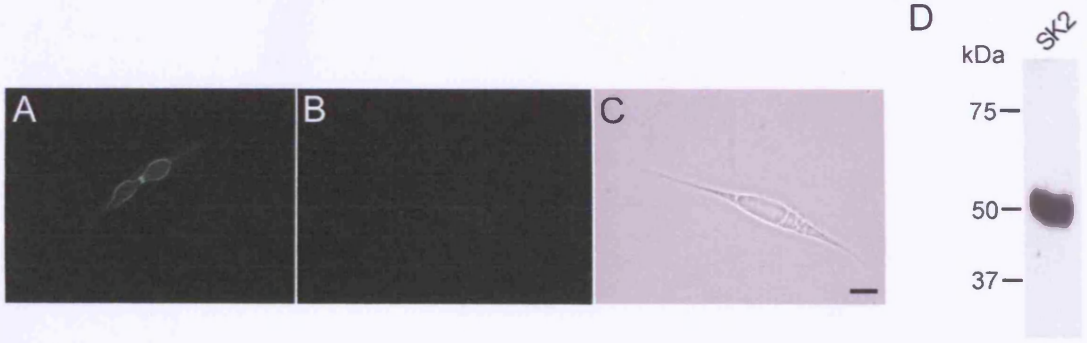

FIGURE 3.11: Characterisation of the anti-NSK2 antibody purified with QP-GG peptide columns. A-C: Immunofluorescence experiment using the antibody purified with the QP-GG peptide (1:150) on HEK 293 cells expressing SK2 (**A**) or wild type HEK cells (**B**). In C, the bright-light picture of the cell reported in B is shown. Scale bar: 10 µm. **D:** Crude membrane lysates of SK2-transfected HEK 293 cells were separated on 7.5% SDS page and transferred to nitrocellulose membrane by semi dry blot. Immunoblot was performed using the antibody purified with the QP-GG peptide. A single band was detected.

All these experiments indicated that the anti-NSK2 antibody purified using the QP-GG peptide was able to recognise recombinant SK2 protein. However, when the antibody was used in Western blot analysis of adult rat brain synaptosomal membranes, results were in contrast with observations made using the pET-NSK2 purified antibody. In these experiments, a band of ~90 kDa was detected (K. Hirzel personal communication), which is in contrast with previous results where two bands of ~50 kDa and 75 kDa were detected (Fig. 3.5 B). In the absence of a logical explanation for the ~90 kDa band, taking into consideration the surprisingly low protein content of the QP-GG peptide antibody purification and the results presented in Chapter 5, this antibody preparation was not further used in the study of the SK2 distribution in native tissues.

CHAPTER 4

Distribution of SK2 in the rat brain

4.1 Introduction

In situ hybridisation studies have recently reported the detailed distribution of SK channels mRNA in the rat brain (Stocker and Pedarzani, 2000). The studies showed that the three SK channels are widely expressed in the central nervous system and display differential distribution throughout the rat brain. In particular, SK2 mRNA is abundantly expressed; high levels of SK2 transcript are detected in the neocortical layer V and in hippocampal CA1-CA3 pyramidal neurones. However, little is known about the subcellular localisation of SK channels in specialised neuronal compartments. The study of the differential distribution of these channels in neuronal somata, dendrites or axons is important to understand their function in the regulation of firing patterns, integration of synaptic inputs or the regulation of synaptic activity. In this chapter, the immunohistochemical distribution of SK2 α subunit will be reported. In particular, the subcellular localisation of SK2 protein was analysed in brain regions such as the hippocampus, the neocortex, the amygdala, the thalamus and the habenula. The distribution profile of SK2 in post-natal hippocampal cultures will also be described.

4.2 Immunohistochemical localisation of SK2 in the rat brain

The distribution of SK2 α subunit in the rat brain was investigated by immunohistochemistry using the specific, affinity-purified anti-NSK2 antibody (Chapter 3). The experiments were performed as described in 2.2.15.2 on sagittal and coronal sections of P21-P25 rats (2.2.15.1). As shown in Figure 4.1, the SK2 protein was widely distributed throughout the rat brain. Particularly high levels of expression were observed in the cortex and in the hippocampal formation. Additionally, intense immunostaining was detected in the amygdala and in thalamic regions. When immunohistochemistry experiments were performed with the anti-NSK2 antibody preincubated with saturating amount of pET-NSK2 fusion protein, the immunostaining was completely abolished, confirming the specificity of the antibody (Fig 4.1 B).

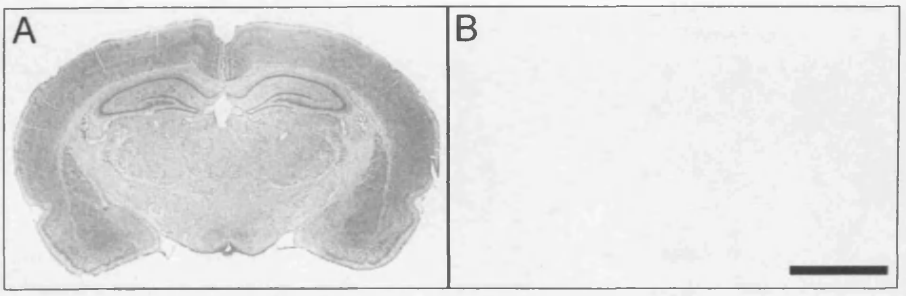

FIGURE 4.1: Distribution pattern of SK2 α subunit in the rat brain. Immunohistochemistry of rat coronal sections (P21), performed either with the affinity-purified anti-NSK2 antibody (1:2,100) (**A**) or with the primary antibody preincubated with 20 µg/ml pET-NSK2 fusion protein (**B**). The Vectastain Elite ABC kit was used for signal detection. **A:** The affinity-purified anti-NSK2 antibody revealed widespread signal in the rat brain. The most prominent signal was observed in the cortex and in the hippocampus. **B:** No signal was detected in the preadsorption control. Scale bar: 3 mm.

4.2.1 SK2 distribution in hippocampus and cerebral cortex

The hippocampal formation and the cortex are among the brain areas that showed the highest levels of SK2 α subunit expression in the rat brain. In the hippocampal formation, the most intense SK2 immunostaining was detected in CA1, CA2 and CA3 regions, as shown in Figure 4.2 A. High magnification analysis of the CA1 pyramidal layer (Fig. 4.2 B) showed that the SK2 signal was localised in the membrane of somata and in the proximal part of apical dendrites of pyramidal neurones. In contrast, the nuclei did not show any staining. Similar cellular distribution was observed in CA2 and CA3 pyramidal neurones. Additionally, intense signal was present in scattered neurones in the stratum oriens and radiatum, indicating that there is expression of SK2 channels in hippocampal interneurones. Furthermore, high SK2 immunoreactivity was detected in the subiculum. Within the dentate gyrus, the granule cell layer and the molecular layer displayed a very weak signal (Fig. 4.2 A), whereas SK2 labelling was detected in scattered neurones of the polymorphic layer.

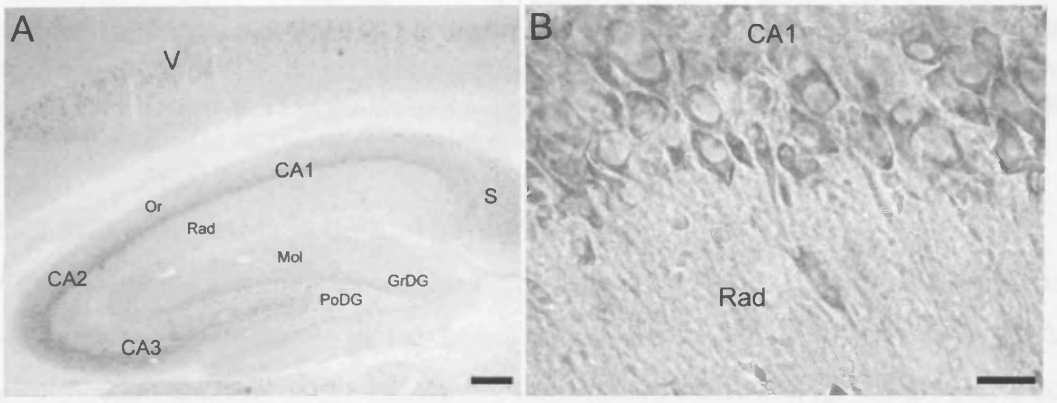

FIGURE 4.2: Distribution of the SK2 α subunit in the rat hippocampus. A: Immunohistochemistry on a rat brain sagittal section (P25) using the affinity-purified anti-NSK2 antibody (1:2,100). CA1, CA2 and CA3 regions and the layer V of the neocortex displayed a very intense immunostaining. SK2 signal was also observed in scattered neurones in the stratum oriens and radiatum, in the subiculum and in scattered neurones of the polymorphic layer of the dentate gyrus. Weak signal was observed in the granule cell layer and molecular layer of the dentate gyrus. **B**: Cellular distribution of SK2 in pyramidal neurones of the CA1 hippocampal region. The experiment was performed on a rat brain coronal section (P21) with the affinity-purified anti-NSK2 antibody (1:2,100). The SK2 signal was distributed in the soma and in the proximal portion of apical dendrites. Or, stratum oriens; Rad, stratum radiatum; GrDG, granular layer of the dentate gyrus; Mol, molecular layer of the dentate gyrus; PoDG, polymorphic layer of the dentate gyrus; S, subiculum; V, neocortical layer V. Scale bars: A, 200 μm; B, 20 μm.

Figure 4.3 A shows the expression profile of SK2 within the neocortex. The most intense signal was detected in the neocortical layer V, whereas moderate levels of SK2 signal were detected in the neocortical layer II-IV and VI. In pyramidal neurones of layer V, SK2 protein was localised in the soma and in the apical and basal dendritic branches (Fig. 4.3 B). Additionally, intense SK2 signal was observed in the piriform and entorhinal cortex.

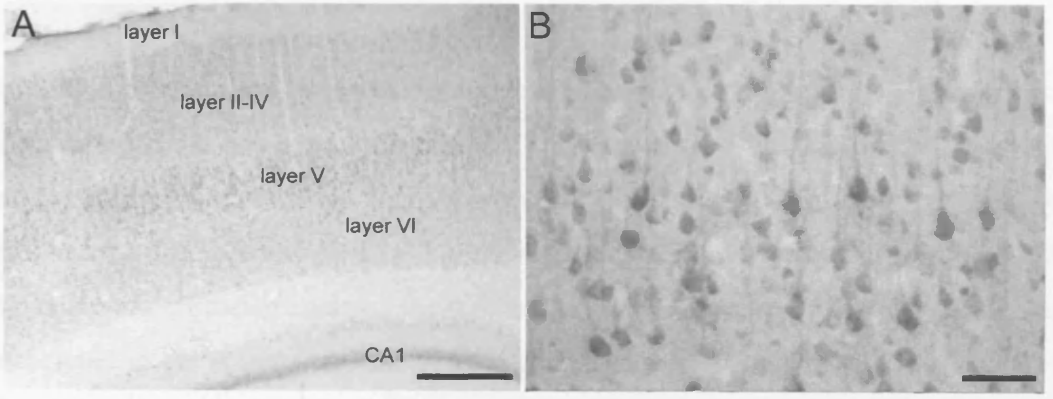

FIGURE 4.3: Distribution of the SK2 α subunit in the rat neocortex. Immunohistochemistry with the affinity-purified anti-NSK2 antibody (1:2,100) on rat coronal sections. **A:** SK2 immunoreactivity was detected in layers II-VI of the neocortex. The most intense signal was observed in layer V. **B:** Cellular distribution of SK2 protein in neocortical layer V. Scale bars: A, 400 μm; B, 100 μm.

4.2.2 SK2 distribution in the amygdala

Within the amygdala complex a dense signal was observed in the basolateral nucleus and, with lower intensity, in the lateral amygdaloid nucleus (Fig. 4.4 A). High magnification analysis of the basolateral amygdaloid nucleus (Fig. 4.4 B) indicated that in this area the staining was not homogeneous, because some neurones revealed a more intense signal than others. Figure 4.4 B shows a somato-dentritic localisation of SK2 protein at cellular level. The nuclei were completely free of staining.

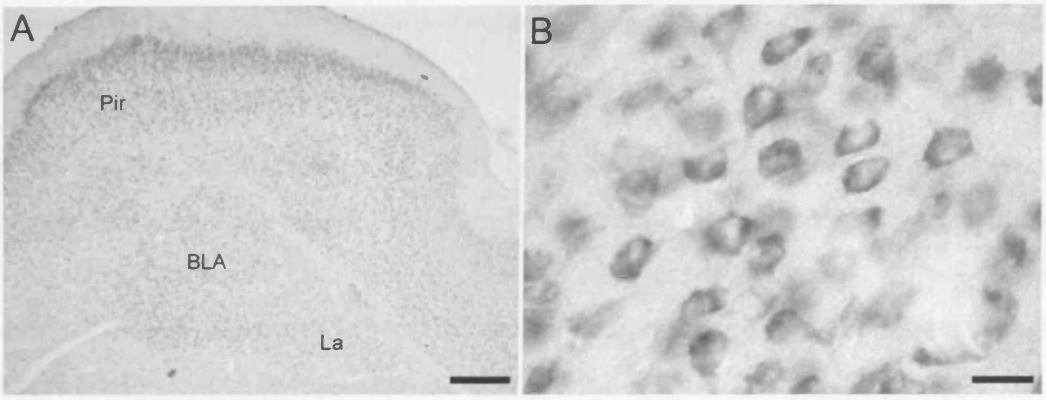

FIGURE 4.4: Expression of the SK2 α subunit in the basolateral and lateral amygdaloid nuclei. The immunostaining was performed on rat coronal sections (P21) using the affinity-purified anti-NSK2 antibody (1:2,100). **A:** The basolateral amygdaloid nucleus displayed an intense SK2 signal. Moderate staining was detected in the lateral amygdaloid nucleus. **B:** High magnification picture of the basolateral amygdaloid nucleus, somato-dendritic localisation of the SK2 protein is observed. **A-B:** BLA, basolateral amygdaloid nucleus; La, lateral amygdaloid nucleus; Pir, piriform cortex. Scale bars: A, 200 μm; B, 20 μm.

4.2.3 SK2 distribution in the thalamus and habenula

High to moderate levels of SK2 expression were detected throughout the thalamus. Intense SK2 immunolabeling was observed in the reticular thalamic nucleus (Rt), the laterodorsal thalamic nuclei (LDVL), the anterior and posterior nuclei (Po) (Fig. 4.4 A). High magnification analysis throughout the thalamus revealed that the signal was associated to the somata and the proximal dendrites of neurones. Figure 4.5 B and show the subcellular localisation of the SK2 signal in the reticular thalamic nucleus and in the lateral part of the laterodorsal thalamic nucleus, respectively.

FIGURE 4.5: Distribution analysis of the SK2 α subunit in the thalamus. Immunohistochemistry performed on rat (P25) sagittal sections (**A**) or on rat (P21) coronal sections (**B**, **C**) using the affinity-purified anti-NSK2 antibody (1:2,100). **A**: Overview picture showing that high to moderate immunostaining was detected throughout the thalamic nuclei. **B**: Somato-dendritic localisation of the SK2 protein in the reticular thalamic nucleus. **C**: High magnification picture showing SK2 somato-dentritic distribution in the laterodorsal thalamic nucleus, lateral part. LDVL, laterodorsal thalamic nucleus, ventrolateral; LP, lateroposterior thalamic nucleus; Po, posterior thalamic nucleus group; Rt, reticular thalamic nucleus; VPL, ventral posterolateral thalamic nucleus; VPM, ventral posteromedial nucleus. Scale bars: A, 300 μm; B, 40 μm.

In the epithalamus (habenula), the densely packed neurones of the medial habenula presented the most prominent SK2 staining. Moderate signal intensity was observed in the lateral habenula (Fig. 4.6 A). The SK2 signal was mainly restricted to the neuronal somata, as shown in the high magnification picture of the medial habenula (Fig. 4.6 B).

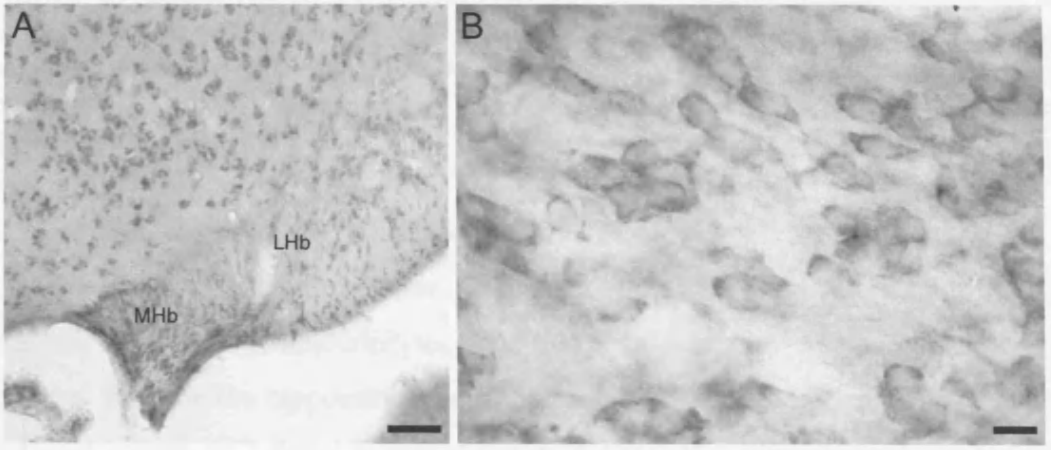

FIGURE 4.6: Localisation of the SK2 α subunit in the habenula. Immunohistochemistry performed on rat (P21) coronal sections with the affinity-purified anti-NSK2 antibody (1:2,100). **A**: Intense immunostaining was detected in the medial habenula, whereas the lateral habenula displayed moderate signal. MHb, medial habenula; LHb, lateral habenula. **B**: High magnification picture showing SK2 somato-dentritic distribution in the medial habenula. Neuronal nuclei were free of SK2 signal. Scale bars: A, 100 μm; B, 10 μm.

4.2.4 SK2 distribution in the nucleus accumbens and caudate putamen

The nucleus accumbens and the caudate putamen were the brain regions displaying the lowest SK2 expression levels. In particular, the nucleus accumbens was almost completely devoid of SK2 signal (Fig. 4.7) and only weak, diffuse staining was visible in the caudate putamen. These data were in agreement with *in situ* hybridisation studies (Stocker and Pedarzani, 2000), that detected no SK2 mRNA in the nucleus accumbens and only a weak SK2 signal in the caudate putamen.

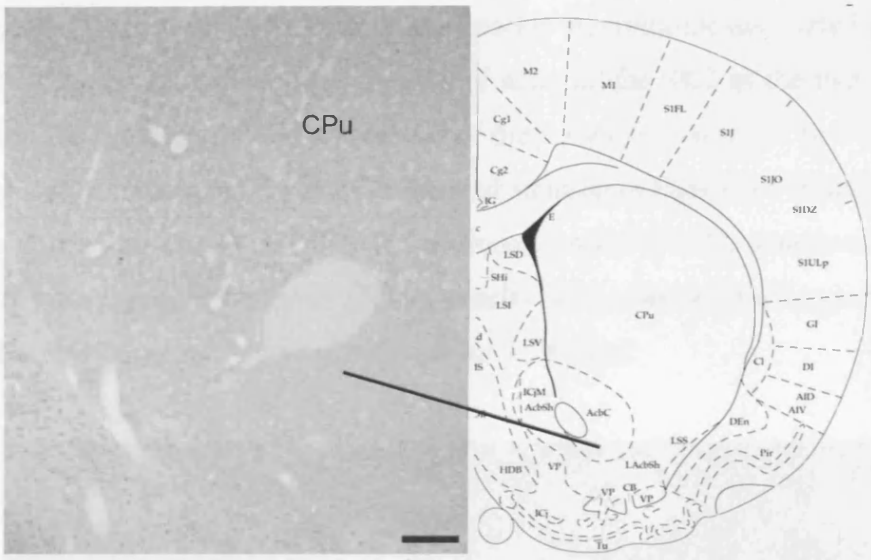

FIGURE 4.7: Distribution of SK2 in the nucleus accumbens. Immunohistochemistry of a P21 rat coronal section (anti-NSK2 antibody, 1:2,100) showed that no signal was detected in the nucleus accumbens. A weak signal was detected in the caudate putamen. The scheme on the right corresponds to panel 15 of "The Rat Brain in Stereotaxic Coordinates", (Paxinos and Watson, 1997). CPu, caudate putamen;cortex. Scale bar: 200 μm.

4.3 Localisation of SK2 in rat neuronal cultures

To define in more detail the cellular localisation of the SK2 α subunit, the anti-NSK2 antibody was used in immunocytochemistry experiments on rat neuronal primary cultures. Because the hippocampus and the neocortex were the brain areas showing the most intense SK2 signal in the immunohistochemistry, hippocampal and cortical primary cultures were used.

Initial immunocytochemistry experiments (2.2.14.3) were performed on embryonic cortical and hippocampal cultures. The experiments were performed at different stages of the culture development to investigate if developmental regulation of the

protein expression occurred. On these cells, the affinity-purified anti-NSK2 antibody did not detect any SK2 immunostaining, suggesting that either the SK2 protein was not expressed or the expression level was under the detection limit of the antibody. To test whether low levels of SK2 protein were expressed, signal amplification was attempted using a Tyramide based amplification system (TSA) (2.2.14.4). Also under these experimental conditions, SK2 signal was not detected in these cultured neurones, and only a faint background staining was observed on glia cells. Figure 4.8 shows a typical example of immunostaining performed with the TSA amplification system on hippocampal neurones at day 22 in culture. In this experiment, double staining was performed with the neuronal marker microtubule-associated protein 2 (MAP2). Figure 4.8 A shows the absence of staining for SK2 in the two neurones present in the field of view. The presence of these two neurones can be observed in the light field photograph (Fig. 4.8 C). The red staining in Figure 4.6 B indicates that both cells were instead labelled by the neuronal marker MAP2, demonstrating that these cells were indeed neurons. Similar results were obtained for hippocampal or cortical neurones, when they were cultured for 7-28 days.

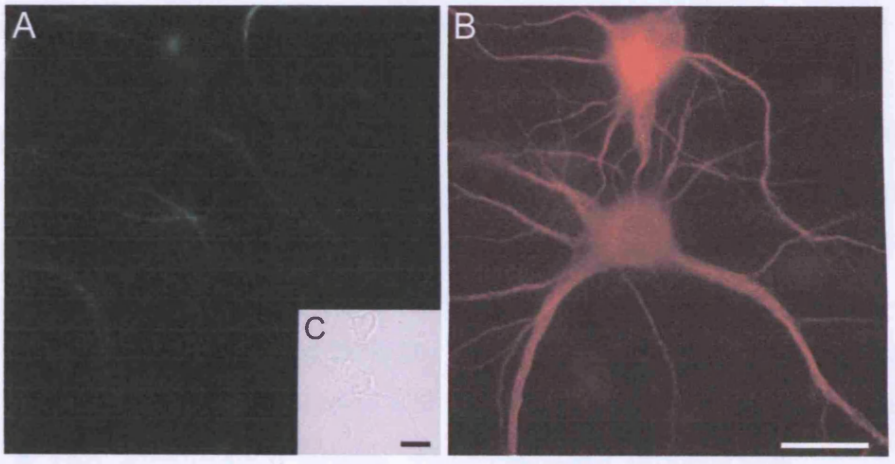

FIGURE 4.8: Immunofluorescence of hippocampal neurones at day 22 in culture. Co-labelling of SK2 (**A**) and MAP2 (**B**). **A**: The affinity-purified anti-NSK2 antibody (1:150) was used in combination with the TSA amplification system. No signal was detected in the neurones. **B**: The anti-MAP2 antibody was used at the dilution of 1:3,000; anti-mouse secondary Cy3 antibody (1:600) was used for signal detection. **C**: Bright-light picture of the cells pictured in A and B. Scale bar: 20 µm.

Since no SK2 signal was detected in embryonic cultures, hippocampal neurones prepared from P0 rats were cultured, and the expression of SK2 α subunits was analysed by immunofluorescence with the affinity-purified anti-NSK2 antibody.

Using the cultures from postnatal animals in combination with the TSA amplification system (2.2.14.4) no immunostaining was observed in neurones after 24 hours in culture (Fig. 4.9 A). However, from day 2, an increase of the SK2 protein signal was observed. At this stage, an SK2 immunostaining was present in the soma of the neurones (Fig. 4.9 C). By day 4 and 6 in culture, the SK2 signal increased in intensity, (Fig. 4.9 D, E) and between day 10 and 13, maximal expression was observed (Fig. 4.9 F). As shown in Figure 4.9 F, the SK2 staining was restricted to the soma and to the proximal portion of the dendrites of hippocampal neurones. The preabsorption of the anti-NSK2 antibody with the pET-NSK2 fusion protein and the omission of the primary antibody (data not shown) resulted in the complete loss of fluorescent staining (Fig 4.9 G), confirming the specificity of the detected signal.

Immunohistochemical experiments on brain sections showed also that a specific SK2 signal was present in interneurones in the stratum oriens and radiatum of the hippocampus (Fig. 4.2 A). Since primary cultures of hippocampal neurones contain both pyramidal cells and interneurones, we investigated whether the SK2 protein was expressed in the interneurones. These interneurones can be differentiated morphologically from pyramidal neurones. Pyramidal cells represent 85-90% of the total neuronal population and are characterised by a complex, highly branched dendritic tree. In contrast, interneurones are ~10% of the neurones in culture and have only few dendritic branching points. Moreover, immunohistochemically, the two neuronal populations can be distinguished by the expression of the enzyme glutamic acid decerboxylase (GAD), which is involved in the synthesis of GABA. GAD is expressed in the GABA-ergic interneurones but not in the glutamatergic pyramidal cells. Double staining with the monoclonal GAD6 antibody and with the affinity-purified anti-NSK2 antibody was performed. The SK2 signal was amplified using the TSA amplification system. The experiment revealed that ~10% of the neurones in culture were labelled by the anti-GAD antibody and these cells displayed the morphological features of interneurones, described above. About half of the interneurones revealed immunostaining also for SK2. Figure 4.10 shows the double-staining in an interneuron. The SK2 signal (Fig. 4.10 A, green) was localised in the soma and in the proximal portion of the dendrites of the anti-GAD-positive interneuron (Fig. 4.10 B, red), similar to the distribution pattern observed in the pyramidal cells.

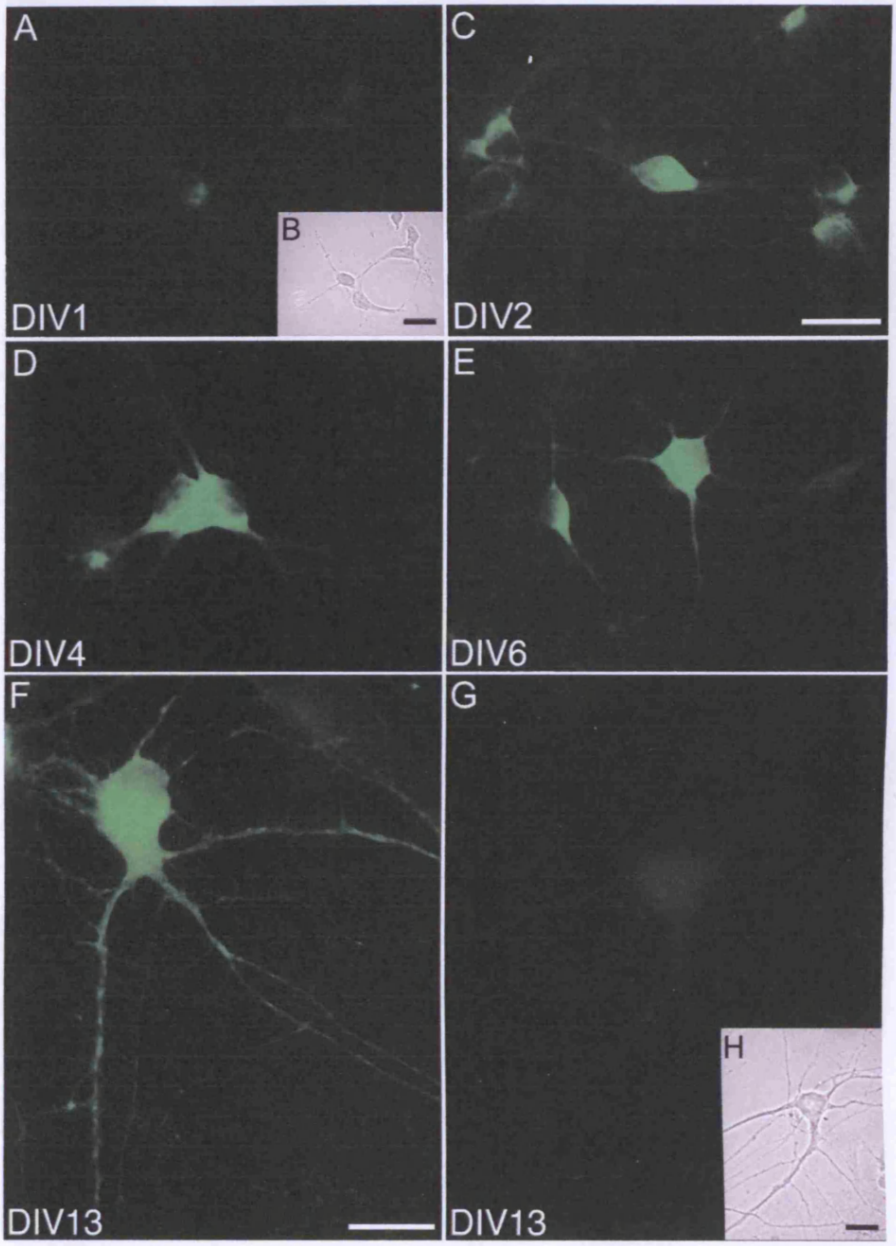

FIGURE 4.9: Developmental expression of SK2 in cultured postnatal hippocampal neurones. Immunohistochemistry performed with the affinity-purified anti-NSK2 antibody (1:270) and TSA amplification system. SK2 signal was absent at 1 day in culture (**A**). In B the cells pictured in A are shown. At day 2 in culture, SK2 immunostaining was detected (**C**) and its expression increased at day 4 (**D**) and 6 (**E**). In F the distribution of the SK2 protein at day 13 is shown. No staining is visible with antibodies preadsorbed with pET-NSK2 fusion protein (**G**). In H the bright-light pictures of the cell reported in G is shown. Scale bar: A-E, 20 μm; F-H, 10 μm.

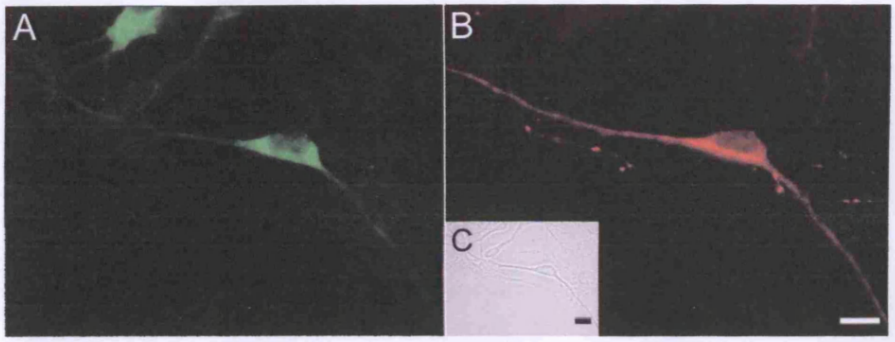

FIGURE 4.10: SK2 expression in hippocampal interneurones in culture. **A-B**, Co-labelling experiment with affinity-purified anti-NSK2 antibody (1:270) (**A**), and anti-GAD antibody (1:500) (**B**). The SK2 signal (**A**) was detected using the TSA amplification system. SK2 was expressed in the soma and in the dendrites of a GAD positive neurone (**B**). The anti-GAD antibody signal was detected using anti-mouse Cy3 secondary antibody (1:600). In **C**, the bright light picture of the neurones pictured in A and B is shown. Scale bars: 10 μm.

CHAPTER 5

Characterisation of a new rSK2 variant: rSK2-860

5.1 Introduction

Studies recently performed in our group identified a new rSK2 variant, called rSK2-860 because the corresponding primary sequence is 860 amino acids long. The rSK2-860 differs from the originally cloned SK2 subunit because it has a 275 amino acids longer amino terminal domain. The rSK2-860 was identified by cDNA cloning from the rat brain. Its existence was verified by RNase protection, which indicated the presence of SK2 transcripts containing an additional 5' exon and having a longer open reading frame (Kerscenstein, 2003) compared to the published rSK2 sequence (Kohler et al., 1996). Furthermore, RNase protection showed that this SK2 transcript is the predominant one in the rat brain (Kerscenstein, 2003). Electrophysiological recordings in HEK 293 cells expressing rSK2-860 showed that the protein assembles into functional channels that generate a Ca^{2+}-dependent and apamin-sensitive K^+ current (D. D'hoedt personal communication). Nevertheless, immunocytochemical studies on different cell lines expressing rSK2-860 revealed a peculiar distribution pattern. When cDNA plasmids coding for rSK2-860 were transfected in HEK 293, CHO or COS cells, the protein was present in clusters localised throughout the cytoplasm (D'hoedt, 2004). The mechanism responsible for this distribution pattern of the rSK2-860 subunit has not been yet elucidated.

In this chapter, the study of the native distribution of the rSK2-860 protein will be presented. An antibody directed against the novel rSK2-860 subunit was raised and characterised. This antibody was used to assess the expression of the rSK2-860 variant in the rat brain by Western analysis and to study its distribution profile in immunohistochemical experiments. Moreover, the subcellular targeting of the rSK2-860 subunit exogenously expressed in different neuronal types was analysed and compared with the distribution profile of the originally cloned rSK2 subunit.

5.2 Western analysis of rSK2-860

As described above, the only difference between the rSK2 α-subunit and the rSK2-860 consists in the amino terminal 275 amino acids long stretch, whereas the rest of the sequence is identical (Fig. 5.1). Therefore, a region within the extended amino terminal domain of the rSK2-860 subunit was selected to generate an antibody that distinctively binds to the rSK2-860. This antibody, called anti-N860, was raised against a fusion protein consisting of GST and amino acids 68-249 (light blue box in

Fig. 5.1) of the rSK2-860 sequence (GenBank accession no. AK033158.1). To study the distribution of the new rSK2-860 variant in the rat brain, the anti-N860 antibody was used in combination with the anti-NSK2 antibody described in Chapter 3, which recognises both the rSK2 and the rSK2-860 subunits (Fig. 5.1).

FIGURE 5.1: Schematic illustration of rSK2 and rSK2-860 subunits. The upper scheme represents the cloned SK2 (Kohler et al., 1996). The lower scheme corresponds to the rSK2-860, with the 275 aa extended amino terminus represented as a dark blue box. The yellow boxes represent the six S1-S6 transmembrane domains. The red box marks the region used to generate the anti-NSK2 antibody and the light blue box indicates the region used to generate the anti-N860 antibody.

Similar to what has been described in Chapter 3 for the anti-NSK2, the anti-N860 serum was affinity-purified to eliminate GST-directed and other unspecific antibodies. Column antibody purification (2.2.2) was performed using a fusion protein where the N860 region, which was used to raise the antibody, was fused to thioredoxin (Trx) (pET-N860). The purification was tested in ELISA assays. The ELISA indicated that GST-directed antibodies were eliminated and anti-N860 immunoglobulins were purified.

The anti-NSK2 and anti-N860 antibodies were characterised in Western analysis to test their ability to recognise native rSK2-860 subunit. Crude membrane lysates of HEK 293 cells transfected with cDNA plasmids that code the rSK2-860 were prepared and used in Western blots. In parallel, lysates of HEK 293 cells expressing the originally cloned rSK2 subunit were also used. The anti-NSK2 serum recognised a single band of ~85 kDa on rSK2-860-expressing cells (Fig. 5.2 A, first lane). When the rSK2 subunit was expressed, a single band of ~50 kDa could be observed (Fig. 5.2 A, second lane), as already described in Chapter 3. Additionally, as shown in Figure 5.2 B, the same high molecular weight band detected by the serum (~85 kDa) was revealed by the affinity-purified anti-NSK2 antibody on lysates of HEK 293 cells expressing rSK2-860. This result confirmed that also the purified antibody retained its ability to recognise the recombinantly expressed rSK2-860 protein.

Furthermore, lysates of HEK 293 untransfected or transfected with rSK2-860, rSK2 or rSK3 cDNA plasmids were used in Western blots to test the anti-N860 serum. Figure 5.2 C (second lane) shows that, similar to the results obtained with the anti-NSK2 antibody, a single band of ~85 kDa was detected in rSK2-860-expressing cells. As expected, no bands were detected in un-transfected HEK 293 (Fig. 5.2 C, first lane) and in cells expressing either rSK2 (Fig. 5.2 C, third lane) or rSK3 (Fig. 5.2 C, fourth lane). This observation indicates that the antibody did not cross-react with other SK subunits. The affinity-purified anti-N860 was also tested in Western blot of lysates from rSK2-860-expressing HEK 293 cells. When the affinity-purified anti-N860 antibody was used in the immunoblot, it recognised the single high molecular weight band of ~ 85 kDa corresponding to the rSK2-860 subunit (Fig. 5.2 D).

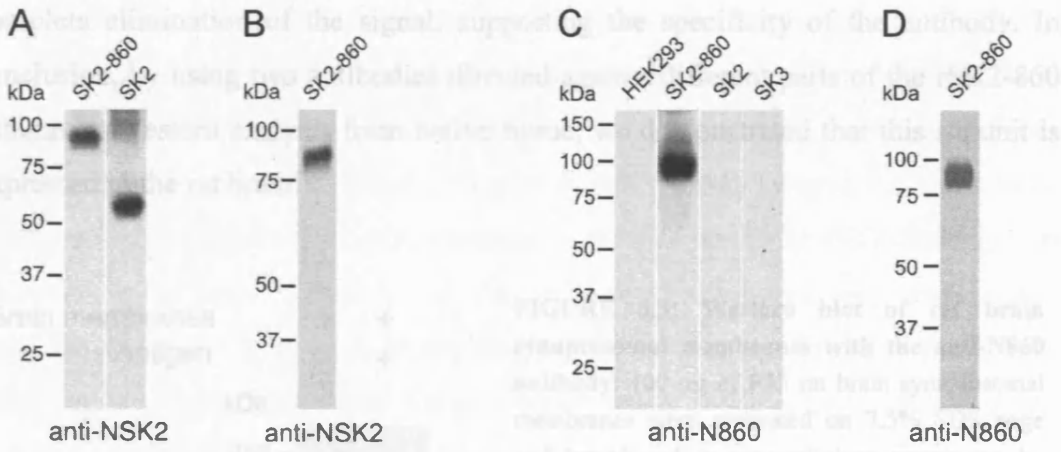

FIGURE 5.2: Western blot of HEK 293 cells expressing SK2 or SK2-860 subunits. A, B: Western blot (2.2.8) of crude membrane lysates of HEK 293 cells transiently transfected with plasmids encoding rSK2-860 or rSK2 α subunit. Proteins were separated on SDS page and transferred to nitrocellulose membrane by tank blot. The immunoblot was performed with the anti-NSK2 serum (**A**) or with the affinity-purified anti-NSK2 antibody (**B**). **A:** A single high molecular weight band was detected in the rSK2-860-expressing HEK 293 cells (first lane) and a ~50 kDa band was visible in HEK 293 cells transfected with rSK2 (second lane). **B**: A single band of ~85 kDa was detected in the HEK 293 cells transfected with rSK2-860. **C**: Lysates of HEK 293 cells untransfected or transiently transfected with plasmids that code for the rSK2-860, rSK2 or rSK3 α-subunits were used in Western blot with the anti-NSK2 serum. No bands were detected in untransfected HEK 293 (first lane), and in cells transfected either with rSK2 (third lane) or with rSK3 (fourth lane). A single band (~85 kDa) was detected in rSK2-860-expressing cells (second lane). **D:** Western blot of rSK2-860-expressing HEK 293 cells performed with the affinity-purified anti-N860 antibody (1:600).

Taken together, these experiments show that the affinity-purified anti-NSK2 antibody recognised the rSK2-860 subunit, in addition to rSK2 protein. Moreover, the experiments performed with the affinity-purified anti-N860 indicate that the antibody is sensitive and specific for the rSK2-860. Therefore, the two antibodies were used for the study of the expression of rSK2-860 subunits in the rat brain.

To assess the expression of the rSK2-860 subunit in the rat brain, Western analysis was performed on rat brain synaptosomal membranes using the two available antibodies. As shown in Chapter 3 (Fig. 3.5 D), the affinity-purified anti-NSK2 antibody detected two specific bands: one of ~50 kDa, which corresponds to rSK2, and a second one of higher molecular weight (~80 kDa). When the affinity-purified anti-N860 was used in the Western analysis on rat brain, a single band of ~80 kDa was detected, confirming that this band represents the rSK2-860 subunit (Fig. 5.3). Preincubation with saturating amounts of pET-N860 fusion protein resulted in the complete elimination of the signal, supporting the specificity of the antibody. In conclusion, by using two antibodies directed against different parts of the rSK2-860 subunit in Western analysis from native tissue, we demonstrated that this subunit is expressed in the rat brain.

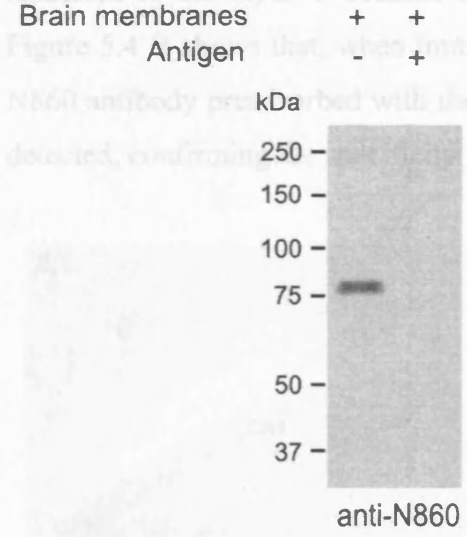

FIGURE 5.3: Western blot of rat brain synaptosomal membranes with the anti-N860 antibody. 100 µg of P35 rat brain synaptosomal membranes were separated on 7.5% SDS page and transferred to nitrocellulose membrane by tank blot. Immunoblot was performed with the affinity-purified anti-N860 antibody. A single ~80 kDa band was detected. The signal was abolished by pre-adsorbing the primary antibody with pET-N860 fusion protein.

5.3 Immunohistochemical distribution of the rSK2-860 subunit

The distribution of the rSK2-860 subunit was investigated by immunohistochemical studies. In particular, the expression pattern was analysed in the hippocampal formation and in the cortex. In these regions, an intense signal was detected using the anti-NSK2 antibody, which recognises both SK2 variants (Fig. 4.2 and 4.3). By using the anti-N860 antibody, we wanted to investigate whether the newly characterised rSK2-860 was also expressed in these regions.

Initial experiments performed with the affinity-purified anti-N860 antibody did not show any signal in immunohistochemistry. Therefore, the TSA™ Biotin System was used in combination with the ABC detection system to amplify a potential rSK2-860 immunostaining (2.2.15.4). In CA2 and CA3 layers of the hippocampus, the expression pattern observed with the affinity-purified anti-N860 antibody (Fig. 5.4 A) is similar to that observed with the anti-NSK2 antibody (Fig. 4.2 A). In contrast, the signal in the CA1 and in the subiculum is weaker than the one observed with the anti-NSK2 antibody. This indicates that the predominant subunit expressed in these regions is rSK2. rSK2-860 immunostaining was also detected in scattered neurones of the stratum oriens and radiatum, suggesting that the two variants are likely to be co-expressed in hippocampal interneurones. In the neocortex, the rSK2-860 signal is restricted to the layer V because all the other layers displayed very weak signal. Figure 5.4 B shows that, when immunohistochemistry was performed with the anti-N860 antibody preadsorbed with the pET-N860 fusion protein (2.2.5), no signal was detected, confirming the specificity of the antibody.

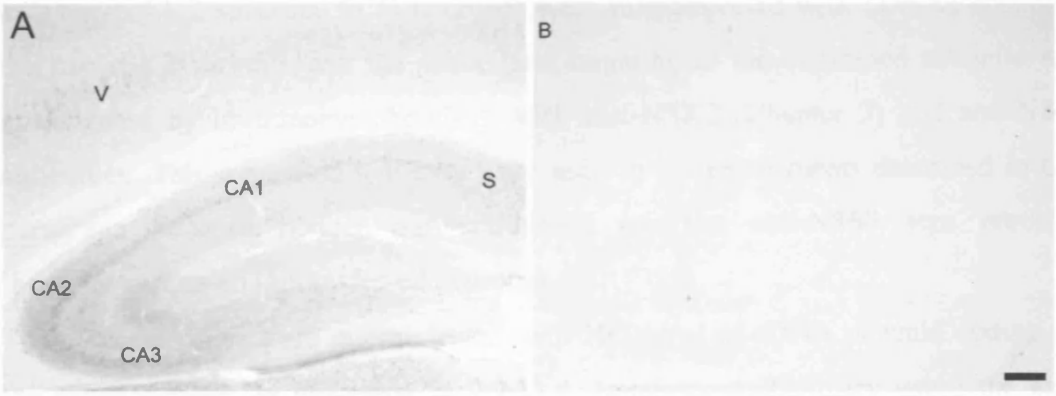

FIGURE 5.4: Distribution of the rSK2-860 α-subunit in the rat hippocampus. Immunohistochemistry was performed on rat brain (P25) sagittal sections using the affinity-purified anti-N860 antibody (1:875) (**A**) or the affinity-purified anti-N860 antibody preincubated with the

pET-N860 fusion protein (20 μg/ml) (**B**). **A:** CA2 and CA3 hippocampal regions and the layer V of the neocortex displayed SK2-860 immunostaining. Weak signal was detected in the CA1 region. SK2-860 signal was also observed in scattered neurones of the stratum oriens and radiatum. **B**: No signal was detected in the pre-adsorbtion control. V, neocortical layer V. Scale bars: 200 μm.

5.4 Exogenous expression of rSK2 and rSK2-860 subunits in neuronal cells

Studies performed in our laboratory indicated that the expression of the rSK2-860 variant in different cell lines, such as HEK 293, COS and CHO cells, resulted in a distinctive distribution pattern. The rSK2-860 protein formed numerous clusters localised in the cytoplasm of cells and no plasma membrane localisation was observed. However, the molecular mechanisms underlying the intracellular retention and the clustering of the rSK2-860 subunit are still unknown. Several retention signal sequences present in the extended 275 aa amino terminus were analysed but none of them was found to be responsible for the retention of the protein in the intracellular clusters (D'hoedt, 2004).

In order to study the targeting of the rSK2-860 variant in neurones, the protein was expressed in two different neuronal types. By using the two antibodies anti-NSK2 and anti-N860 the distribution of the exogenously expressed protein was analysed and compared with the distribution profile of rSK2 α-subunit.

5.4.1 Expression of rSK2 and rSK2-860 subunits in SCG neurones

Immunocytochemistry experiments initially performed on SCG neuronal cultures indicated that the SK2 protein was not detected using the anti-NSK2 antibody (data not shown). Therefore, these cells were used as a neuronal expression system for exogenous SK2 subunits. SCG neurones were microinjected with cDNAs encoding the two rSK2 variants, and the subcellular targeting of the expressed subunits was investigated by immunocytochemistry with anti-NSK2 (Chapter 3) and anti-N860 antibodies. The unpurified antibody were used in the experiments described in this paragraph because neither the anti-NSK2 nor the anti-N860 sera revealed immunostaining on untransfected neurones

The SCG neurones were microinjected with 100 ng/μl of cDNA plasmid coding for the rSK2 subunit, as described in 2.2.11.4. Immunocytochemistry using the anti-NSK2 serum (2.2.14.2) was performed 24-48 hours after the injection. Figure 5.5 shows that, when the SK2 subunit was expressed in SCG neurones, a uniformly

distributed immunostaining was observed in cell bodies and in dendrites. The signal in different sections of the cell clearly indicates that the SK2 subunit was localised in the membrane of neurones.

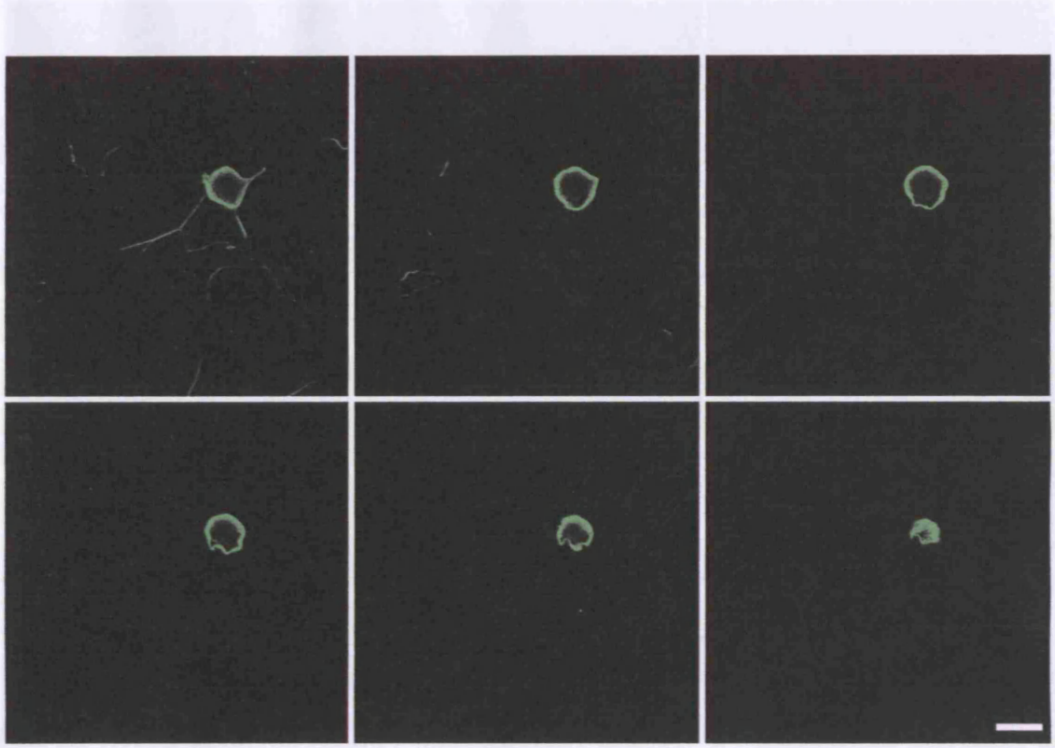

FIGURE 5.5: Immunocytochemistry of SCG neurones microinjected with SK2 cDNA. Selection of six confocal sections of an SCG neuron expressing the rSK2 subunit. Immunocytochemistry was performed with the anti-NSK2 serum (1:1,000). The signal was detected by using the anti-rabbit Cy3-conjugated secondary antibody (1:600). Scale bar: 20 μm

In parallel, rSK2-860 subunit cDNA was injected in SCG neurones, as described above, and the distribution of the expressed protein was analysed by immunostaining using anti-NSK2 and anti-N860 sera. Figure 5.6 shows the immunostaining performed with the anti-NSK2 serum. Experiments revealed that in all the injected neurones the protein was present in numerous ring-shaped clusters localised in the soma and in the proximal part of the dendrites. In the soma, the clusters were distributed throughout the cytoplasm but not in the nucleus. In some of the injected neurones, a uniform signal in the plasma membrane was also detected, indicating that some rSK2-860 protein did not form clusters and was targeted to the membrane. The neuron reported in Figure 5.6 is an example that shows a diffuse membrane signal (white arrowheads in the inset of Fig. 5.6), in addition to the staining in the clusters. Comparable results were obtained when the anti-N860 serum was used for the

immunostaining of SCG neurones expressing the rSK2-860 subunit. A large number of cytoplasmic clusters was observed (Fig. 5.7).

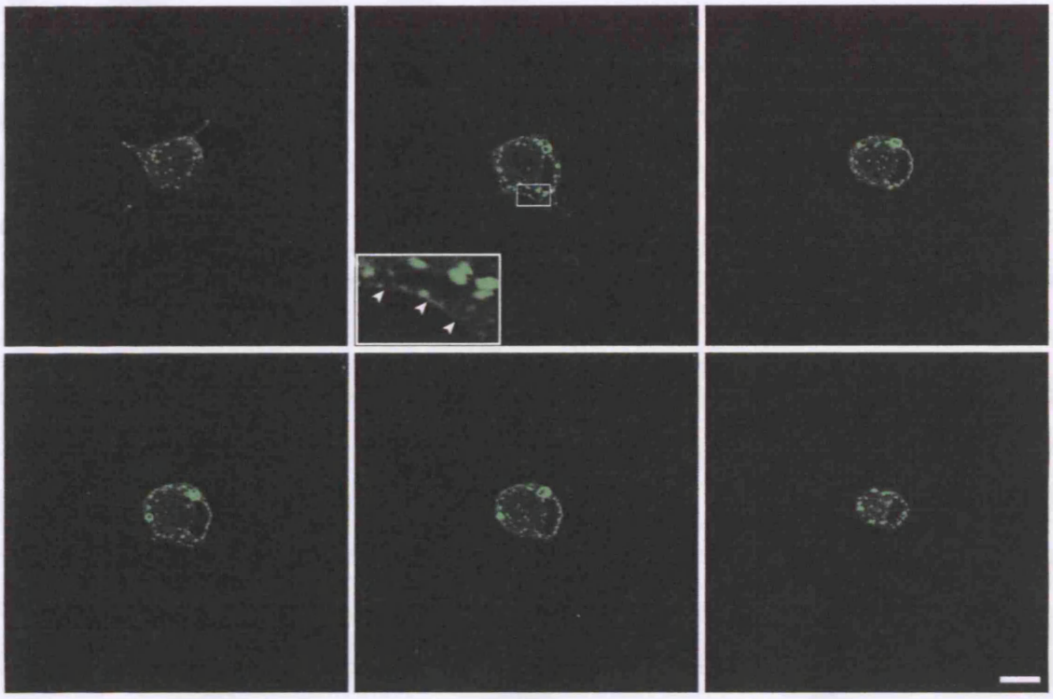

FIGURE 5.6: Immunocytochemistry with anti-NSK2 antibody of SCG neurones expressing the SK2-860 subunit. SCG neurones microinjected with rSK2-860 cDNA plasmids. Six confocal sections of an SCG neuron expressing the rSK2-860 and immunostained with anti-NSK2 serum (1:1,000) are shown. The signal was detected by using the anti-rabbit Cy3-conjugated secondary antibody (1:600). The inset shows the 4 x magnification of the region marked in the figure. Scale bar:10 μm.

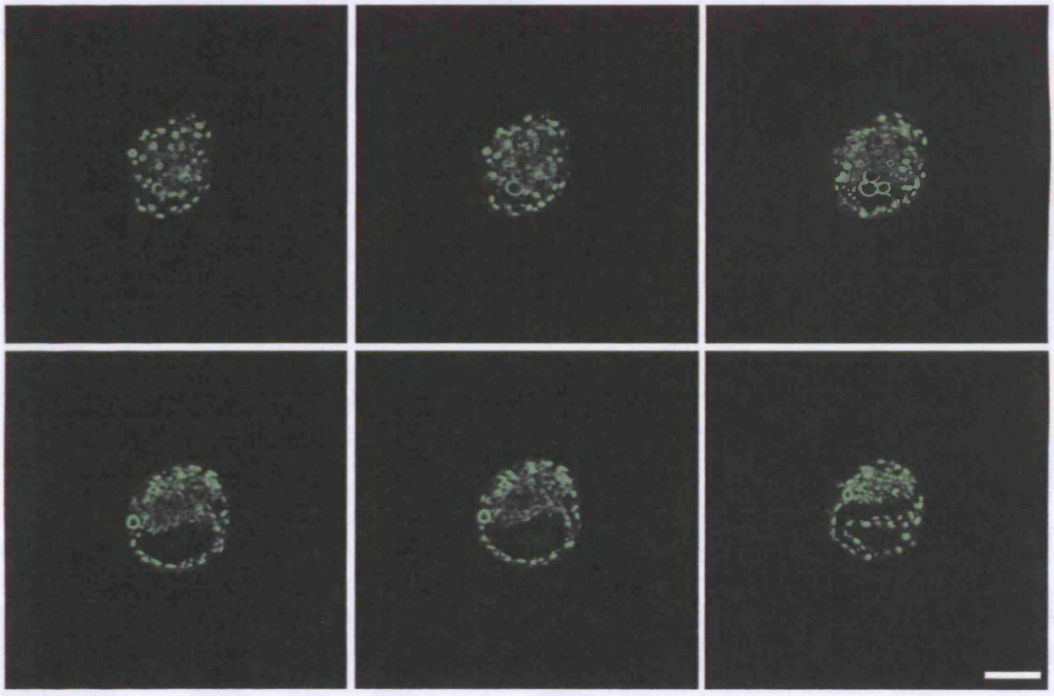

FIGURE 5.7: Immunocytochemistry with anti-N860 antibody of SCG neurones microinjected with the SK2-860 cDNA. A selection of six confocal sections of an SCG neuron expressing the rSK2-860 are shown. Immunostaining was performed with the anti-N860 antibody (1:1,000). Anti-rabbit Cy3-conjugated secondary antibody (1:600) was used for signal detection. Scale bar: 10 μm.

Because the protein was overexpressed, we wanted to test whether the formation of the rSK2-860 protein clusters was related to the saturation of the sorting machinery that might lead to mislocalisation of the expressed subunit. This hypothesis was addressed by decreasing up to 20 times the amount of rSK2-860 cDNA injected in SCG neurones. When 5-10 ng/μl of rSK2-860 plasmid were injected, the distribution pattern of the protein did not change. Figure 5.8 shows the immunostaining performed with the anti-NSK2 serum on a neuron injected with 10 ng/μl of rSK2-860 plasmid. As visible in the selected confocal sections, the protein formed clusters throughout the cytoplasm, similar to the ones shown in the Figures 5.6 and 5.7. However, the number of clusters was reduced compared with that of the injections with higher amounts of plasmids. These observations indicated that, even when the rSK2-860 subunit was expressed at extremely low levels, its targeting profile did not changed.

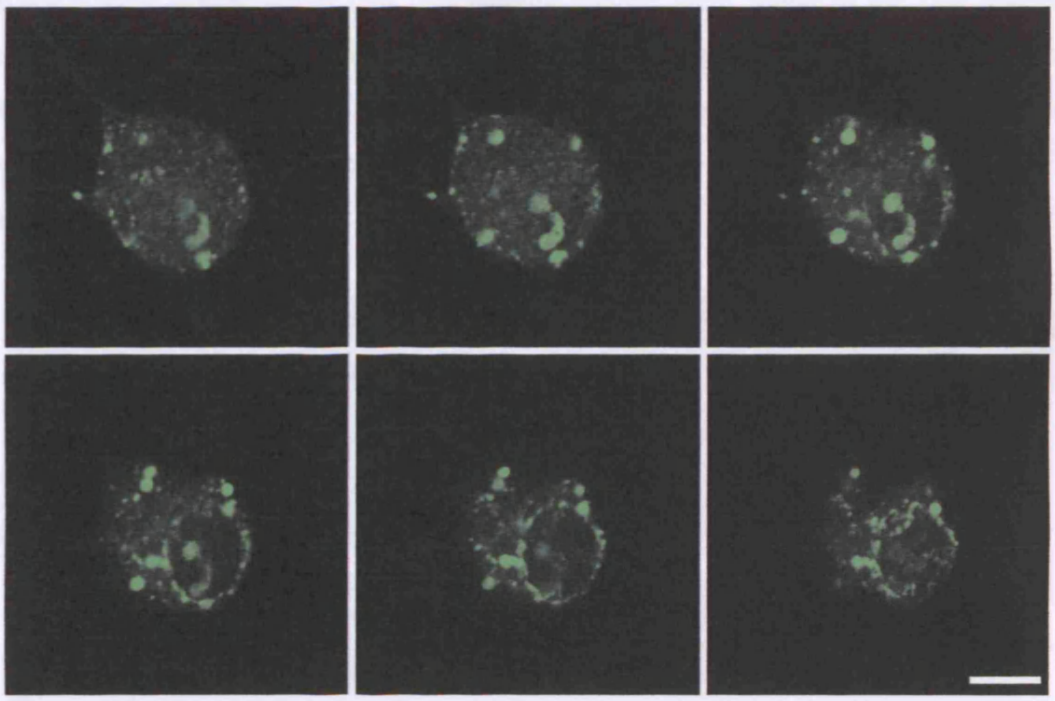

FIGURE 5.8: Immunofluorescence on SCG neurones microinjected with 10 ng/μl of rSK2-860 cDNA plasmid. The immunostaining was performed with the anti-NSK2 serum (1:1,000). The figure

shows six confocal sections of an injected SCG neuron. Anti-rabbit Cy3-conjugated secondary antibody (1:600) was used for signal detection. Scale bar: 10 µm.

5.4.2 Co-expression of rSK2 and rSK2-860 subunits in SCG neurones

An interesting aspect of the potential function of the rSK2-860 is that this subunit might form heteromeric channels with the rSK2. To test this hypothesis, myc-tagged rSK2 subunits were co-expressed with rSK2-860 in SCG neurones. Immunofluorescence experiments were performed by using an anti-myc monoclonal antibody to detect the rSK2-myc, and the anti-N860 serum to detect specifically the rSK2-860 subunit.

When the two subunits were expressed together, the rSK2-860 subunit was retained in the cytoplasm of all the injected neurones and, in some cases, also a membrane signal was detected. The rSK2-860 that was retained in the cytoplasm exhibited a different distribution profile compared to the one observed when rSK2-860 was expressed alone. In fact, a reduced number of clusters and a more diffused rSK2-860 distribution were observed throughout the cytoplasm. As shown in Figure 5.9 A and B, an overlapping signal of the rSK2-860 (blue) and the rSK2-myc (red) was observed throughout the sections, indicating assembly of the two subunits. The inset in the Figure 5.9 A shows that overlapping signals were found in the ring shaped clusters present in the area indicated in the figure, supporting a partial retention of the rSK2 subunit together with the rSK2-860 in the clusters. The overlapping signal of the two subunits was also detected in the plasma membrane of injected SCG neurons (Fig. 5.9 B).

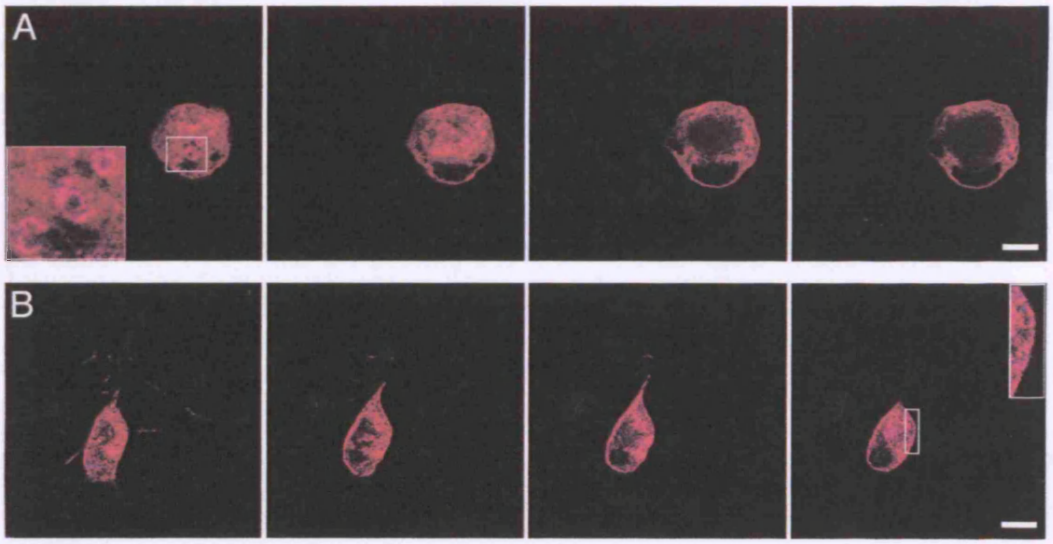

FIGURE 5.9: Immunofluorescence on SCG neurones microinjected with rSK2-myc and rSK2-860 cDNA plasmids. SCG neurones were microinjected with rSK2-myc (25 ng/µl) and rSK2-860 (25 ng/µl) cDNA plasmids. The immunostaining was performed with the mouse anti-myc monoclonal antibody (1:400) and the anti-N860 serum (1:1,000). Anti-mouse Cy3-conjugated secondary antibody (1:600) was used to detect the rSK2-myc signal (red); anti-rabbit-Cy5-conjugated secondary antibody (1:600) was used to detect the rSK2-860 subunit (blue). **A, B:** Five confocal sections of two injected SCG neurones are shown. The insets show the high magnification of the regions marked in the images in A and B. The inset in A is 2.6 x magnification and the inset in B is 4 x magnification. Scale bar: 10 µm.

5.4.3 Exogenous co-expression of rSK2 and rSK2-860 subunits in cortical neurones

The expression of rSK2 and rSK2-860 subunits was also analysed in primary cultures of cortical embryonic neurones. As reported in 4.3, the immunocytochemistry with the affinity-purified anti-NSK2 antibody on the cortical primary cultures revealed no SK2 immunostaining. Therefore, these cultures were used as an expression system to analyse whether the rSK2-860 subunit exhibited a different distribution than the one observed in SCG neurones.

Neurones were transfected with Lipofectamine™ 2000 (2.2.12.3) and cDNA plasmids coding either for rSK2 or rSK2-860 subunits. The anti-NSK2 antibody was used in immunocytochemistry experiments to determine the targeting pattern of the expressed subunits.

Figure 5.10 shows that, when the rSK2 subunit was expressed in cortical neurones, a uniform immunofluorescence signal was detected in the soma. The protein is probably localised in the membrane. Moreover, SK2 expression was found in the complex dendritic tree of transfected pyramidal neurones and in the distal part of the dendrites (Fig. 5.10 A).

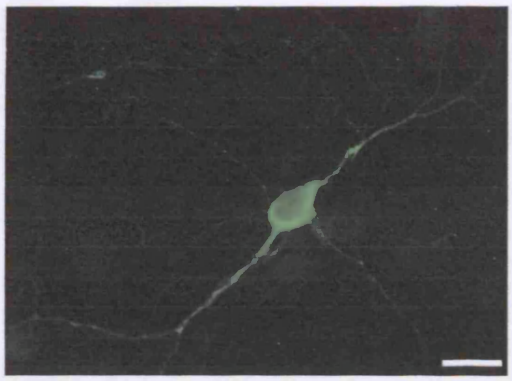

FIGURE 5.10: Immunofluorescence on cortical neurones transfected with cDNA plasmids coding rSK2 α-subunit. The anti-NSK2 antibody (1:1,000) was used for the immunostaining. The signal was detected with anti-rabbit FITC-conjugated secondary antibody (1:30). Scale bar: 20 μm.

When the rSK2-860 cDNA was transfected, the subcellular distribution of the subunit was similar to that observed in SCG neurones. Immunofluorescence experiments were performed two and six days after transfection to determine whether any change in the targeting of the protein in the different subcellular compartments occurred. Figure 5.11 A shows the immunocytochemistry performed 48 hours after transfection. The rSK2-860 subunit was mainly localised in clusters. However, some signal was present also in the neuronal membrane. Numerous clusters were distributed throughout the soma and along the dendrites (Fig. 5.11 B). No change in the protein distribution was observed when the experiment was performed six days after transfection (Fig. 5.11 C, D). The protein was still present in numerous clusters in the soma and in the dendrites of transfected neurones.

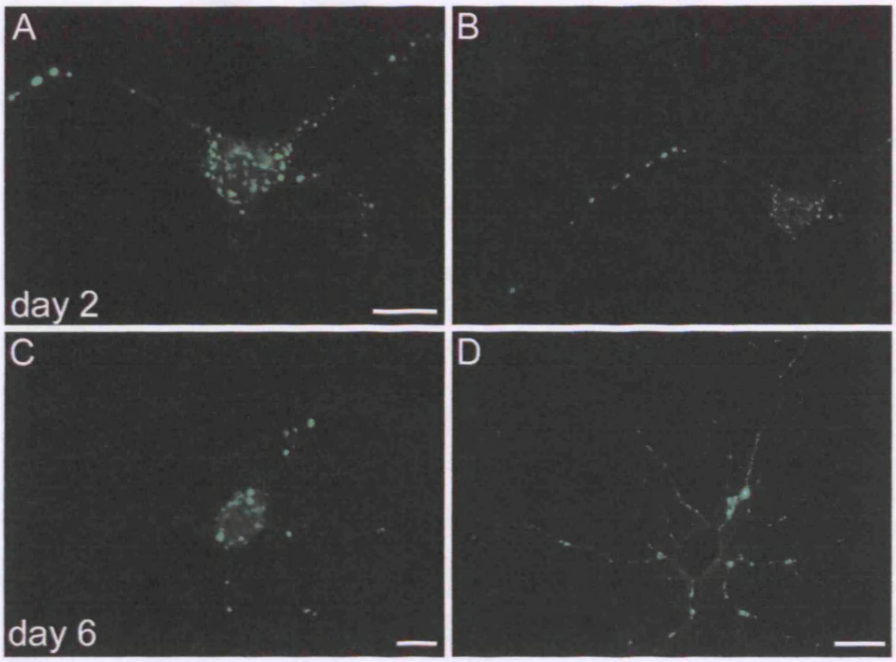

FIGURE 5.11 Immunofluorescence on cortical neurones transfected with cDNA plasmids coding the rSK2-860 α-subunit. Immunostaining was performed with the affinity-purified anti-NSK2 antibody (1:380) at day 2 (**A-B**) or 6 (**C-D**) after the transfection. Anti-rabbit FITC-conjugated secondary antibody was used for signal detection (1:30). In D the neurone soma was blanked out because the picture was obtained by overexposing the specimen. Scale bar: A-C, 10 μm; D: 20 μm.

CHAPTER 6

Immunohistochemical distribution of SK3 α subunit in the rat brain

6.1 Introduction

In this chapter, the immunohistochemical localisation of SK3 α subunit in the rat brain will be reported. To study the protein distribution, an anti-SK3 antibody was generated and characterised. The antibody was used in immunohistochemistry experiments to determine the regional distribution of the SK3 protein throughout the rat brain and to assess the subcellular distribution of the channel in various central neurones.

In situ hybridisation studies of SK channels in the rat brain revealed that the overall distribution of SK3 α subunit is complementary to the distribution of SK1 and SK2 α subunits (Stocker and Pedarzani, 2000; Tacconi et al., 2001; Bosch et al., 2002; Sarpal et al., 2004). Among the brain regions displaying high levels of SK3 mRNA are the lateral septum, the dorsal and central thalamic nuclei, the medial habenula, the dorsal motor nucleus of the vagus and, in the hypothalamus, the supraoptic and suprachiasmatic nuclei. Moreover, SK3 mRNA expression was observed in regions containing monoaminergic neurones such as the substantia nigra pars compacta, the locus coeruleus and the dorsal raphe. In some of these brain regions, the expression pattern described for the SK3 mRNA has been correlated with native I_{AHP} currents. For example, in the dorsal vagal nucleus, pharmacological studies indicate that homomeric SK3 channels underlie the apamin-sensitive I_{AHP} expressed by these neurones (Pedarzani et al., 2000). In dopaminergic neurones of the substantia nigra pars compacta, SK3 homomeric channels are the main determinants of the I_{AHP}, which are important in the control of the spontaneous firing frequency in these neurones (Wolfart et al., 2001).

However, the precise subcellular localisation of SK3 channels in different neuronal types has still to be determined. Recent studies have proposed that SK3 might have presynaptic localisation in the neuromuscular junction (Roncarati et al., 2001) and in hippocampal neuronal primary cultures (Obermair et al., 2003). These observations, together with the data reported in Chapter 4, indicating that SK2 is a somatodendritic channel, suggest that different SK subunits might target specific neuronal compartments and contribute differently to neuronal function.

6.2 Characterisation of the carboxy-terminal anti-SK3 antibody

A sequence-specific peptide antibody was raised against a region that is unique to rSK3, corresponding to the amino acids 706-719 and located in the carboxyl-terminal domain of SK3 α subunit. The antibody was immunopurified following the column purification method (2.2.2) by using SulfoLink agarose beads coupled to the SK3 peptide that was used to generate the antibody.

Western blot experiments showed that the immunopurified antibody recognised rSK3 subunits that are recombinantly expressed in HEK 293 cells and it did not cross-react with rSK2 and rSK2-860 α subunits (K. Hirzel personal communication). The immunopurified anti-CSK3 antibody was also used in Western analysis on rat synaptosomal membrane preparations in order to test the specificity of the antibody on native tissue. As shown in Figure 6.1, the antibody detected a single immunoreactive band of ~75 kDa, in good agreement with the molecular weight predicted from the primary sequence of rSK3 α subunit. Similar results were obtained in Western analysis of mouse synaptosomal membranes, where a commercial anti-NSK3 antibody (Alomone) detected a single band of ~75 kDa (Bond et al., 2004). Taken together, these observations indicated that the affinity purified anti-CSK3 antibody specifically recognised only the rSK3 channel protein in rat brain tissue.

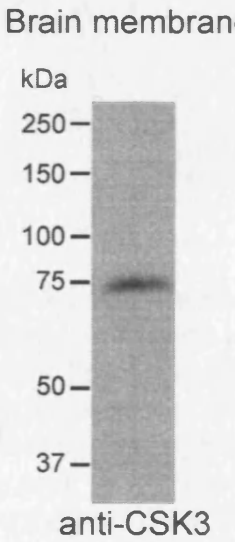

FIGURE 6.1: Western analysis of SK3 α subunit in the rat brain. 50 µg of synaptosomal membrane preparation were separated on a 7.5 % SDS page. Proteins were transferred to nitrocellulose membrane and immunoblot was performed as described in 2.2.8 using the affinity purified anti-CSK3 antibody (1:1,200). A single immunoreactive band of 75 kDa was detected.

6.3 Distribution of SK3 in the rat brain

After showing its specificity in Western analysis, the affinity purified anti-CSK3 antibody was used to study the immunohistochemical distribution of SK3 α subunit in the rat brain. Immunohistochemistry experiments were performed on coronal and sagittal brain sections of P25 rats (2.2.15.1), following the protocol described in 2.2.15.2.

As shown in the overview pictures in Figure 6.2, the white matter tracts were completely devoid of SK3 immunoreactivity and, generally, SK3 signal was restricted to neuronal structures and not to glial cells. Moreover, the overall expression pattern detected by the anti-CSK3 antibody was in good agreement with the distribution profile previously described by *in situ* hybridisation studies (Stocker and Pedarzani, 2000). High levels of SK3 expression were detected in the septum, in most thalamic nuclei, in supraoptic and suprachiasmatic nuclei and in the medial habenula. High SK3 immunoreactivity was also detected in brainstem regions containing monoaminergic neurones such as the substantia nigra pars compacta, the ventral tegental area, the locus coeruleus and the dorsal raphe.

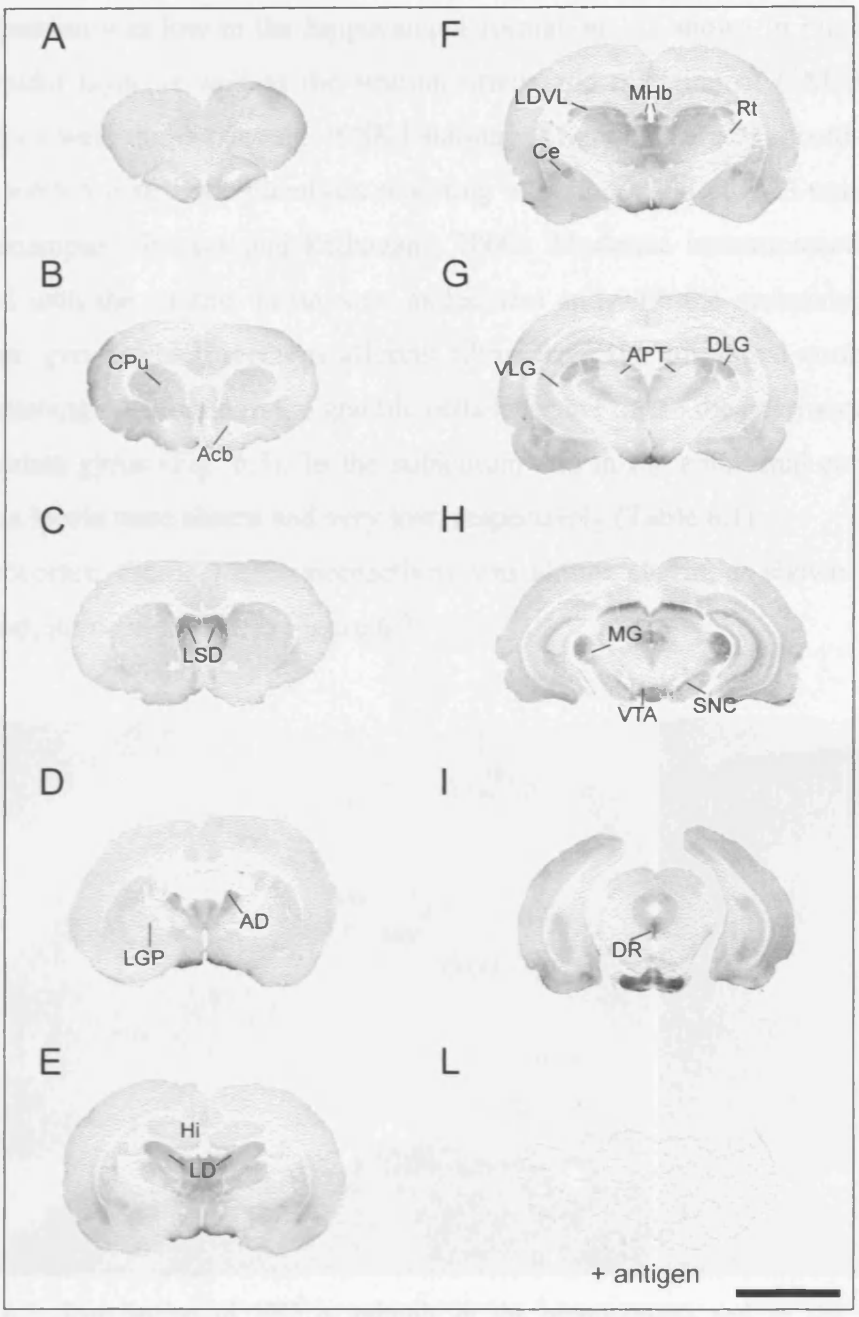

FIGURE 6.2: Immunohistological localisation of SK3 α subunit in the rat brain. Immunohistochemistry performed on rat (P25) coronal sections using either the affinity purified anti-CSK3 antibody (1:17,500) (**A-I**) or the same antibody preadsorbed with 30µg/ml of the SK3 peptide (**J**). The signal was visualised using the Vectastain ABC Kit and DAB staining (2.2.15.2). Acb, nucleus accumbens; AD, anterodorsal thalamic nucleus; APT, anterior pretectal nucleus; Ce, central amygdala; CPu, caudate putamen; DLG, dorsal lateral geniculate nucleus; DR, dorsal raphe; LGP, lateral globus pallidus; LDVL, laterodorsal thalamic nucleus, ventral part; LSD, lateral septal nucleus, dorsal part; MG, medial geniculate nucleus, MHb, medial habenula; MG; Rt, reticular thalamic nucleus; SNC, substantia nigra pars compacta; VLG, ventral lateral geniculate nucleus; VTA, ventral tegmental nucleus. Scale bar: 5 mm.

6.3.1 SK3 distribution in the hippocampus and cerebral cortex

SK3 expression was low in the hippocampal formation. As shown in Figure 6.3 A, the pyramidal layer as well as the stratum oriens and radiatum of CA1, CA2 and CA3 regions were almost devoid of SK3 staining. These data are in accordance with previous mRNA distribution analysis reporting weak detection of SK3 transcripts in the hippocampus (Stocker and Pedarzani, 2000). Moderate immunoreactivity was associated with the stratum lacunosum moleculare and with the molecular layer of the dentate gyrus, which receives afferent fibres from the entorhinal cortex. Weak immunostaining was found in the granule cells layer but not in the polymorphic layer of the dentate gyrus (Fig. 6.3). In the subiculum and in the entorhinal cortex, SK3 expression levels were absent and very low, respectively (Table 6.1).

In the neocortex, the SK3 immunoreactivity was almost absent, as shown in Figure 6.2 A-I and, in more details, in Figure 6.3.

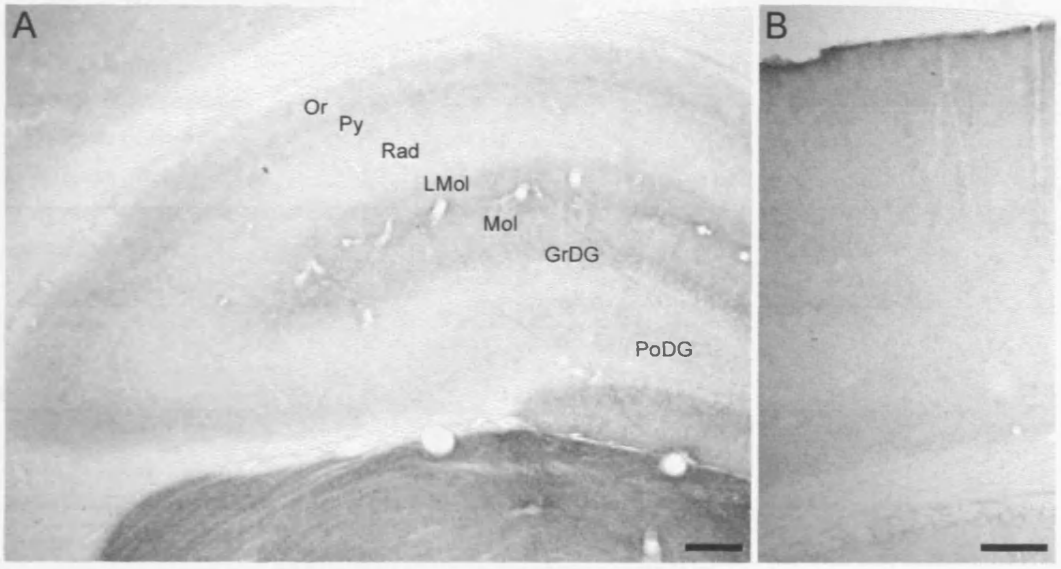

FIGURE 6.3: Distribution of SK3 α subunit in the hippocampus and in the neocortex. Immunohistochemistry with the anti-CSK3 affinity purified antibody (1:17,500) on P25 rat coronal sections. **A**: Weak immunostaining was observed in the hippocampus. **B**: No signal was observed in layers I-IV of the neocortex. GrDG, granular layer of the dentate gyrus; LMol, lacunosum moleculare layer; Mol, molecular layer of the dentate gyrus; Or, stratum oriens; PoDG, polymorphic layer of the dentate gyrus; Py, pyramidal cell layer of the hippocampus; Rad, stratum radiatum. Scale bars: A, 200 μm; B, 100 μm.

TABLE 6.1: Distribution of SK3 α subunit in the rat brain.

Brain region	SK3	Subcellular localisation
Olfactory system		
Min olfactory bulb		
Granular layer	+	
Int. plexiform layer	+	
Mitral cell layer	++	
Glomerular layer	+++	
Ext plexiform layer	+++	
Anterior olfactory nuclei	++	
Olfactory tuberclei	++++	neuropil
Islands of Calleja	++	
Neocortex		
Piriform cortex	+	neuropil
Entorhinal cortex	+	neuropil
Subiculum	-	
Alternative layer II/III/IV	-	
Alternative layer V	(+)	
Alternative layer VI	-	
Hippocampus		
CA1-CA3 region:		
stratum pyramidale	(+)	
stratum radiatum	-	
stratum oriens	(+)	
stratum lacunosum moleculare	++	
Dentate gyrus:		
granule cell layer	+	
molecular layer	++	
hilus	-	
Basal nuclei		
Caudate putamen	++	neuropil
Globus pallidus	(+)	
Ventral pallidum	++	neuropil
Nucleus accumbens	++	neuropil
Claustrum	+	
Subthalamic nucleus	+	
Substantia nigra		
pars reticulata	+++	somata/dendrites
pars compacta	++ sc	somata/dendrites
Septum		
Lateral septal nucleus, dorsal part	++++	somata/dendrites/fibres
Lateral septal nucleus, intermediate part	++	fibres
Medial septal nucleus	+	
Triangular septal nucleus	(+)	
Nucleus of the diagonal band	++	
Bed nucleus stria terminalis	++	

Table 6.1- *continued*

Brain region	SK3	Subcellular localisation
Amygdala		
Posterior cortical amygdaloid nucleus	(+)	
Lateral amygdaloid nucleus	-	
Basolateral amygdaloid nucleus	-	
Basomedial amygdaloid nucleus	-	
Central amygdaloid nucleus	++++	neuropil
Thalamus		
Reticular thalamic nucleus	-	
Anterodorsal nucleus	++++	neuropil
Anteroventral nucleus	+++	neuropil
Anteromedial nucleus	++++	neuropil
Laterodorsal nucleus, ventrolateral nucleus	++++	neuropil
Laterodorsal nucleus, ventromedial nucleus	++++	neuropil
Paratenial nucleus	+++	neuropil
Mediodorsal nucleus	+	neuropil
Ventrolateral nucleus	(+)	
Paraventricular nucleus–anterior	+++	neuropil
Paraventricular nucleus–posterior	+++	neuropil
Central medial nucleus	++	neuropil
Ventromedial nucleus	+	neuropil
Ventroposterolateral thalamic n.	++	neuropil
Ventroposteromedial thalamic n.	++	neuropil
Posterior thalamic nuclei	+++	neuropil
Anterior pretectal nucleus	(+)	
Parafascicular nucleus	+	neuropil
Lateral geniculate nucleus–dorsal	++++	neuropil
Lateral geniculate nucleus–ventral	+	neuropil
Medial geniculate nucleus	+++	neuropil
Lateroposterior nucleus	++++	neuropil
Habenula		
Medial habenula	++++	somata/dendrites
Lateral habenula, medial part	+	neoropil
Lateral habenula, lateral par	-	
Hypothalamus		
Lateral preoptic area (LPO)	-	
Anterior hypothal. area, anterior part	(+)	
Lateral hypothal. area	-	
Suprachiasmatic nucleus	+++	
Supraoptic nucleus	++++	somata/dendrites/ filamentous structures
Arcuate nucleus	++++	
Ventromedial hypothal. nucleus	(+)	
Dorsomedial hypothal. nucleus	-	

Table 6.1- *continued*

Brain region	**SK3**	**Subcellular localisation**
Premammillary nucleus	+	
Med. mammillary nucleus	(+)	
Lateral mammillary nucleus	+++	neuropil
Supramammillary nucleus	+	
Zona incerta	+	
Brain stem		
Lateral reticular nucleus	++++	
Parvicellular reticular nucleus	++	
Dorsal Raphe nucleus	++	somata/dendrites
Locus coeruleus	+++	somata/dendrites/fibres
Ventral tegmental area	++	somata/dendrites
Nucleus of the solitary tract	+++	neuropil
Lateral parabrachial nucleus	(+)	
Dorsal motor nucleus of vagus	+++	somata/dendrites
Hypoglossal nucleus	+++	somata/dendrites/ fibres
Accessory abducens/facial nucleus	++	
External cuneate nucleus	++++	
Cuneate nucleus	+++	
Mesencephalic trigeminal nucleus	+++	somata/dendrites
Central nucl. of the inf. culliculus	(+)	
External cortex of the inf. culliculus	(+)	
Periaqueductal gray	++	neuropil
Red nucleus	+++	somata/dendrites
Pontine nuclei	++++	neuropil
Reticulotegmental nucleus of the pons	++	
Inferior olive, subnucleus B of medial n.	++++	
Superior paraolivary nucleus	(+)	
Cerebellum		
Deep nuclei	++	somata/dendrites
Purkinje cell layer	+	
Molecular layer	+	
Granule cell layer	-	

Immunoreactivity is graded as follows: ++++ very high signal; +++ high signal; ++ moderate signal; + low signal; (+) signal very low if any; - signal below detection limit.

6.3.2 SK3 distribution in the thalamus and in the epithalamus

Most thalamic nuclei revealed intense SK3 immunoreactivity. A high signal was detected in the anterior thalamic nuclei complex (Fig. 6.4 A-C; Table 6.1) and in the laterodorsal nuclei (Fig. 6.5 A-B; Table 6.1). High to moderate levels of SK3 expression were found in the posterior, central medial, paraventricular and paratenial thalamic nuclei (Fig. 6.5 A; Table 6.1). At the cellular level, SK3 immunoreactivity in the thalamus was diffuse and neuronal profiles were not visible. As shown in the high magnification picture of the anterodorsal thalamic nucleus (Fig. 6.4 C), SK3 immunostaining was distributed in the perisomatic neuropil and, in some cases, in fibre-like structures.

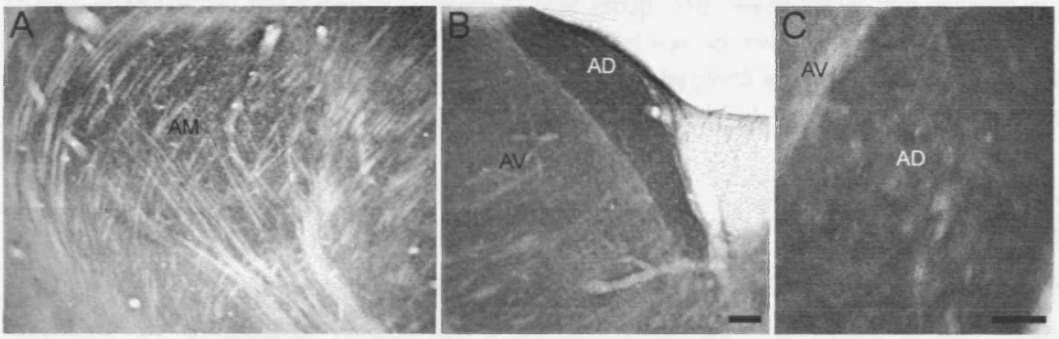

FIGURE 6.4: Distribution of the SK3 channel in the anterior thalamic nuclei. Immunohistochemistry on sagittal (**A**) and coronal (**B, C**) sections of P25 rats, using the affinity purified anti-CSK3 antibody (1:17,500). **A**: SK3 signal was observed in the anteromedial thalamic nucleus (AM). **B**: Very intense signal was observed in the anterodorsal thalamic nucleus (AD) and, to a lower degree, in the anteroventral nucleus (AV). **C:** High magnification picture of AD showing that SK3 signal was associated to the neuropil. Scale bars: A, B, 200 µm; C, 40 µm.

The reticular thalamic nucleus was among the few thalamic regions devoid of SK3 immunostaining (Fig. 6.5 B). Other nuclei expressing low SK3 immunoreactivity were the medial dorsal nucleus and the ventral thalamic nuclei complex (Fig. 6.5 A-B; Table 6.1).

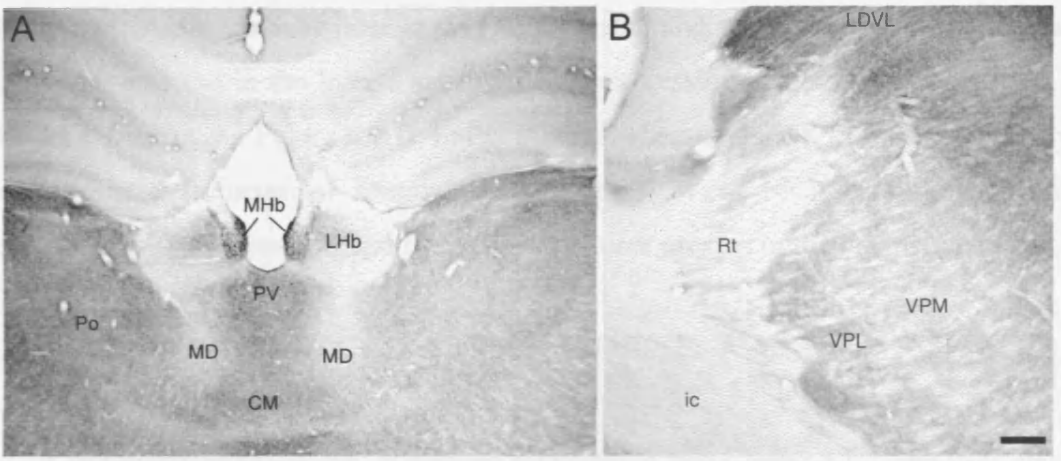

FIGURE 6.5: SK3 distribution in the thalamus. Immunohistochemistry on coronal sections of P25 rats, using the affinity purified anti-CSK3 antibody (1:17,500). **A**: SK3 signal was intense in the medial habenula (MHb), in the paraventricular thalamic nucleus (PV); in the central medial thalamic nucleus (CM) and in the posterior thalamic nuclear group (Po). Weak signal was detected in the mediodorsal thalamic nucleus (MD). **B**: Very intense signal was observed in the laterodorsal thalamic nucleus (LDVL), whereas the ventral posterior thalamic nuclei (VPL and VPM) displayed a weaker staining. The reticular thalamic nucleus (Rt) was devoid of SK3 signal. ic, internal capsule. Scale bar: 100 μm.

Among the geniculate nuclei, the dorsal lateral geniculate nucleus displayed intense SK3 expression, whereas low staining was observed in the ventral lateral nucleus (Fig. 6.6 A). Moreover, intense SK3 immunoreactivity was found in the medium geniculate nucleus (Fig. 6.6 B). Similar to the cellular distribution pattern observed in other thalamic nuclei, SK3 immunoreactivity was associated to the neuropil and neuronal profiles were not visible.

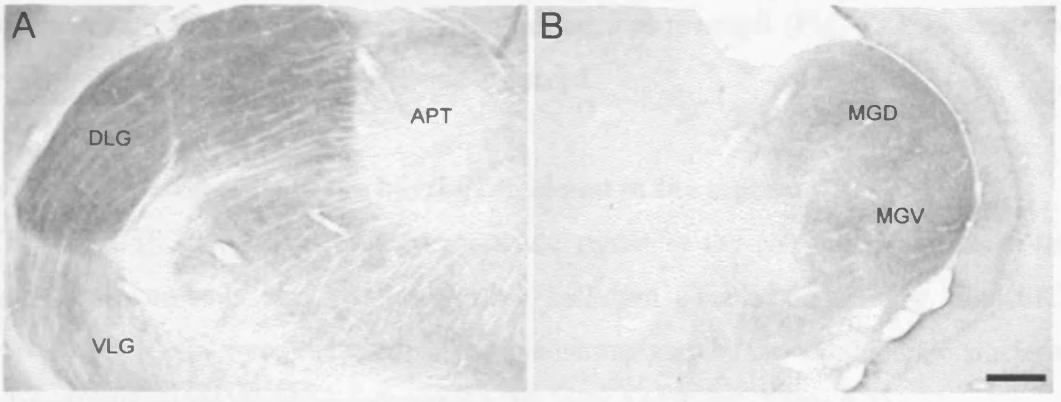

FIGURE 6.6: SK3 distribution analysis in the geniculate nuclei. A: SK3 was highly expressed in the dorsal lateral geniculate nucleus (DLG) whereas lower expression levels were detected in the ventral lateral geniculate nucleus (VLG). APT, anterior pretectal nucleus. **B**: SK3 immunoreactivity was present in the medial geniculate dorsal (MGD) and ventral (MGV) nucleus. Scale bar: 300 μm.

In the epithalamus, a very intense SK3 immunostaining was observed in the medial habenula, whereas in the lateral habenula SK3 expression levels were low (Fig. 6.7 A). As shown in the Figure 6.7 B, in the medial habenula the SK3 immunoreactivity was localised in neuronal somata and processes. Weak SK3 staining was also associated with the neuropil and fibre-like structures present in the lateral habenula.

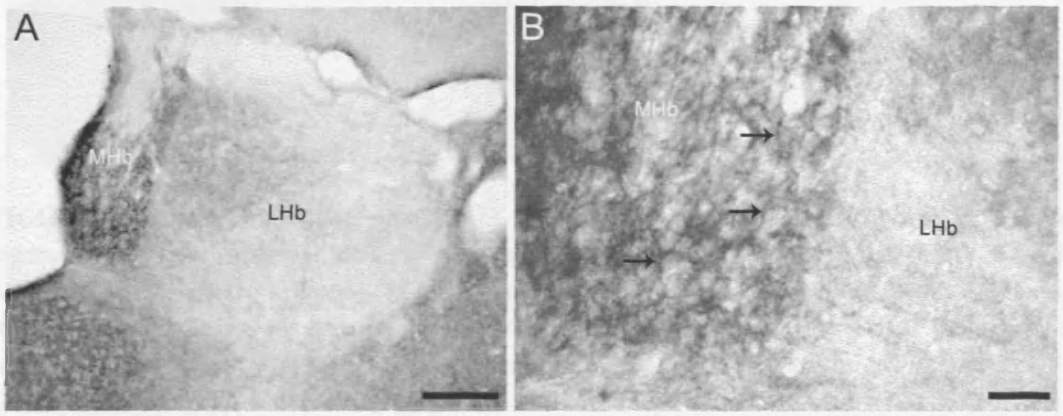

FIGURE 6.7: SK3 α subunit expression in the habenula. Immunohistochemistry on P25 rat coronal sections with the affinity purified anti-CSK3 antibody (1:17,500). **A**: Intense expression was detected in the medial habenula (MHb), in contrast to the lateral habenula (LHb) where the signal was weak. **B**: High magnification picture showing subcellular distribution of the SK3 protein in the MHb. The black arrows indicate neuronal somata and processes labelled with SK3 immunoreactivity. Scale bars: A, 200 µm; B, 40 µm.

6.3.3 SK3 distribution in the amygdala

No SK3 expression was observed throughout the amygdala complex (Table 6.1) apart from the central amygdaloid nucleus. In this region, a dense SK3 immunoreactivity was associated to the perinuclear neuropil (Fig. 6.8), whereas no evident somatic or fibres staining was observed.

6.3.4 SK3 distribution in the basal ganglia and in the septum

The anti-CSK3 antibody revealed moderate signal in the caudate putamen, in the nucleus accumbens and in the ventral pallidum (Table 6.1). Very low SK3 expression levels were detected in the claustrum and in the subthalamic nucleus, whereas almost no signal was present in the globus pallidus (Table 6.1).

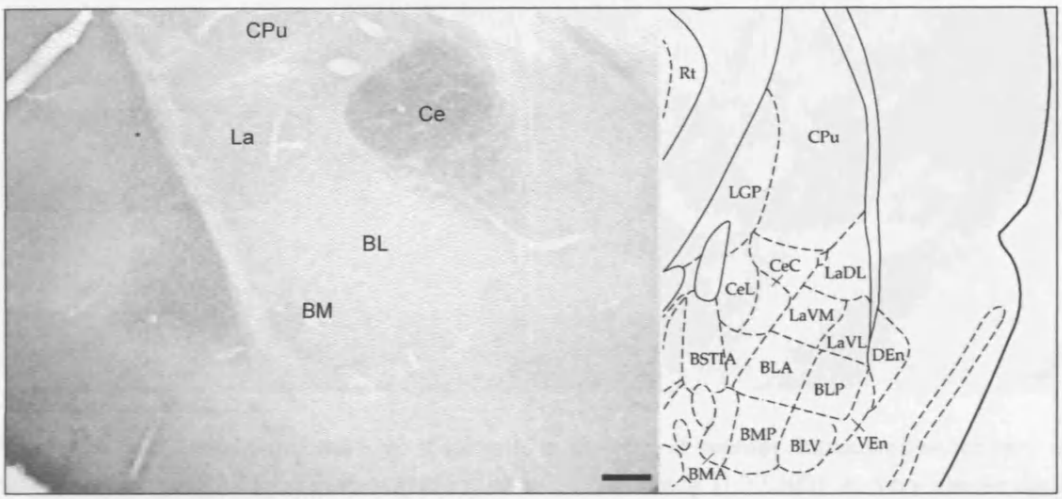

FIGURE 6.8: SK3 distribution analysis in the amygdala. Immunohistochemistry on P25 rat sagittal sections was performed with the immunopurified anti-CSK3 antibody (1:17,500). Very weak SK3 signal was detected in lateral (La), basolateral (BL) and basomedial (BM) amygdaloid nuclei. Intense neuropil staining was present in the central amygdaloid nuclei (Ce). The scheme on the right is adapted from panel 30 of "The Rat Brain in Stereotaxic Coordinates" (Paxinos and Watson, 1997). Scale bar: 200 μm.

In the substantia nigra, intense SK3 immunostaining was observed in the pars compacta (SNC) and in scattered neurones of the pars reticulata (SNR). SNC dopaminergic neurones exhibit an apamin-sensitive I_{AHP}, which has a central role in setting the regular spiking activity of these neurones (Worfart et al., 2001). Pharmacological (Worfart et al., 2001) and *in situ* hybridisation studies (Stocker and Pedarzani, 2000) indicated that SK3 is the principal molecular determinant of the SNR I_{AHP}. Immunohistochemistry performed with the anti-CSK3 antibody confirmed that SK3 is highly expressed in these neurones and somatodendritic subcellular localisation was observed (See paragraph 6.3.7, Fig. 6.12 A).

Very dense SK3 immunostaining was detected in the septum. The SK3 α subunit exhibited a very intense expression in the dorsal part of the lateral septal nucleus (Fig. 6.9 A), whereas the medium and triangular septal nuclei were almost completely devoid of signal. In the lateral septum, the immunostaining was associated to neuronal somata, dendrites and varicose fibres resembling axonal profiles (Fig. 6.9 B).

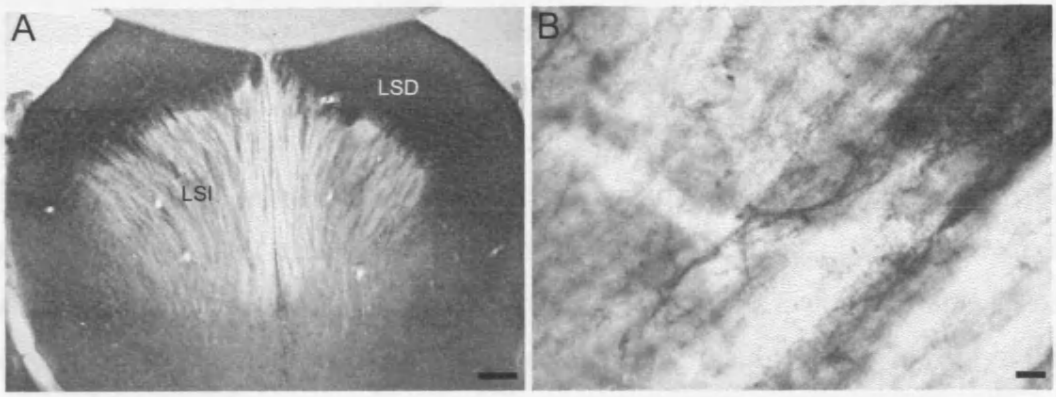

FIGURE 6.9: Expression of the SK3 α subunit in the lateral septum. Immunohistochemistry on P25 coronal sections with the immunopurified anti-CSK3 antibody (1:17,500). **A**: Very intense signal was detected in the dorsal part of the lateral septal nucleus (LSD), whereas much weaker immunostaining was present in the intermediate part (LSI). **B**: SK3 immunostaining was detected on fibres in LSD and LSI. Scale bar: A, 200 μm; B, 20 μm.

6.3.5 SK3 distribution in the hypothalamus

In the hypothalamus SK3 was generally expressed at low levels. Exceptions were represented by the supraoptic, suprachiasmic, arcuate and the lateral mamillary nuclei (Table 6.1).

Particularly interesting was the study of the subcellular distribution of the SK3 channel in the supraoptic nucleus (SO). The SO contains neurosecretory neurones that produce and secrete oxytocin and vasopressin. These cells display an apamin-sensitive I_{AHP} (Bourque and Brown, 1987), which is important for the regulation of the SO-neurones rhythmicity and, therefore, influences the secretion of hormones (Kirkpatrick and Bourque, 1996). The pharmacological properties of this current and *in situ* hybridisation indicated that SK3 is likely to be the channel underlying the I_{AHP} in SO neurones (Bourqueand Brown, 1987; Stocker and Pedarzani 2000).

Immunohistochemistry performed with the anti-CSK3 antibody indicated that the SO exhibited one of the highest levels of SK3 expression in the rat brain. In this area, SK3 immunoreactivity was very dense and cellular structures were hardly visible. In some neurones (such as the one marked with a black arrow in Figure 6.10 B), immunostaining was associated with somata and dendrites, whereas nuclei appeared clearer. However, the most intense signal within the supraoptic nucleus was visible at the base of the nucleus (black arrowheads in Fig. 6.10 A), which is a region rich in glial cells, and was associated to thick filamentous structures (white arrows in Fig. 6.10 B). These observations indicated that in the supraoptic nucleus the SK3 α

subunit might be expressed not only in neurones but also in glial processes. In order to test this hypothesis, co-labelling immunofluorescence experiments (2.2.15.5) were performed by using the affinity purified anti-CSK3 antibody together with the glial marker anti-GFAP monoclonal antibody (Fig. 6.10 C). In this experiment, SK3 immunofluorescence staining was detected using the TSA™ Biotin System to amplify the signal (green in the Fig. 6.10 C). SK3 signal overlapped with the GFAP signal at the base of the supraoptic nucleus, indicating that glial cells present in this area express the SK3 protein (Fig. 6.10 C).

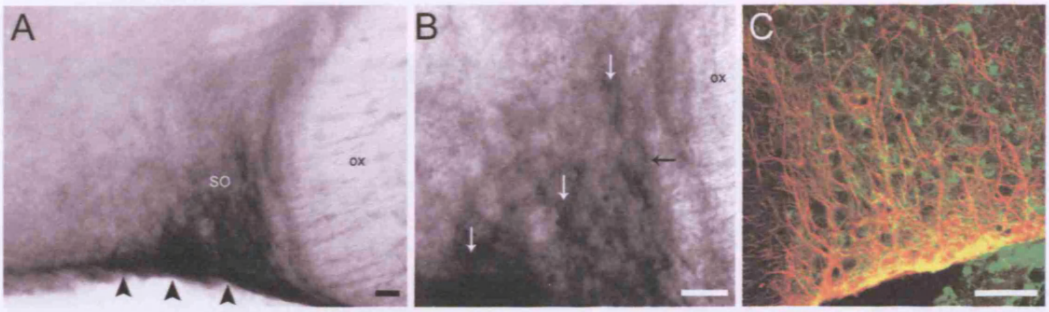

FIGURE 6.10: SK3 expression in the supraoptic nucleus. Immunohistochemistry with the affinity purified anti-CSK3 (1:17,500) was performed on P25 sagittal (**A**, **B**) and coronal (**C**) sections of rat brain. **A**: SK3 immunoreactivity in the supraoptic nucleus (SO) was particularly intense at the base of the nucleus (black arrowheads). **B**: High magnification picture of SO. A neuronal profile is indicated with a black arrow. The white arrows mark the signal associated to filamentous structures distributed throughout the SO. **C**:. Immunofluorescence using the affinity purified anti-CSK3 antibody (1:2,500) and the anti-GFAP monoclonal antibody (1:500). SK3 signal was detected using the TSA™ Biotin System in combination with the ABC system and with FITC-conjugated Avidin. Anti-mouse Cy3 antibodies (1:600) were used to detect the GFAP signal. The picture was kindly provided by H. Morgan. ox, optic chiasm. Scale bar: A, B, 20 µm; C, 50 µm.

6.3.6 SK3 distribution in the dorsal vagal nucleus and in the hypoglossal nucleus

Within the brainstem, a particularly intense SK3 signal was observed in the dorsal vagal nucleus (DVN) and in the hypoglossal nucleus.

Pharmacological studies indicated that, in DVN neurones, homomeric SK3 channels underlie the I_{AHP}, which regulates the spontaneous firing frequency of these cells (Pedarzani et al., 2000). As shown in Figure 6.11 A, immunohistochemistry experiments indicated that high levels of SK3 expression were detected in DVN neurones. The signal was associated to the somata and proximal dendrites. Moreover, SK3 signal was present in the fibre bundles that exit the DVN nucleus laterally (Fig. 6.11 A, black arrows). These fibres are likely to represent DVN neurone axons that

form the vagus nerve. Figure 6.11 B, where immunostained fibres are clearly visible, shows a high magnification of the region labelled in Figure 6.11 A (black arrows). These observations indicate axonal localisation of SK3 α subunit in DVN neurones.

In the hypoglossal nucleus, intense SK3 immunoreactivity was restricted to somata and to numerous thin varicose fibres (Fig. 6.11 C, black arrows). Neuronal nuclei were devoid of immunostaining. Prominent SK3 immunoreactivity was also visible in numerous fibres that exit the hypoglossal nucleus ventrally (Fig. 6.11 D). These fibres are likely to represent the axons that project ventrally from the hypoglossal neurones and converge in the hypoglossal nerve. (Fig. 6.11 D).

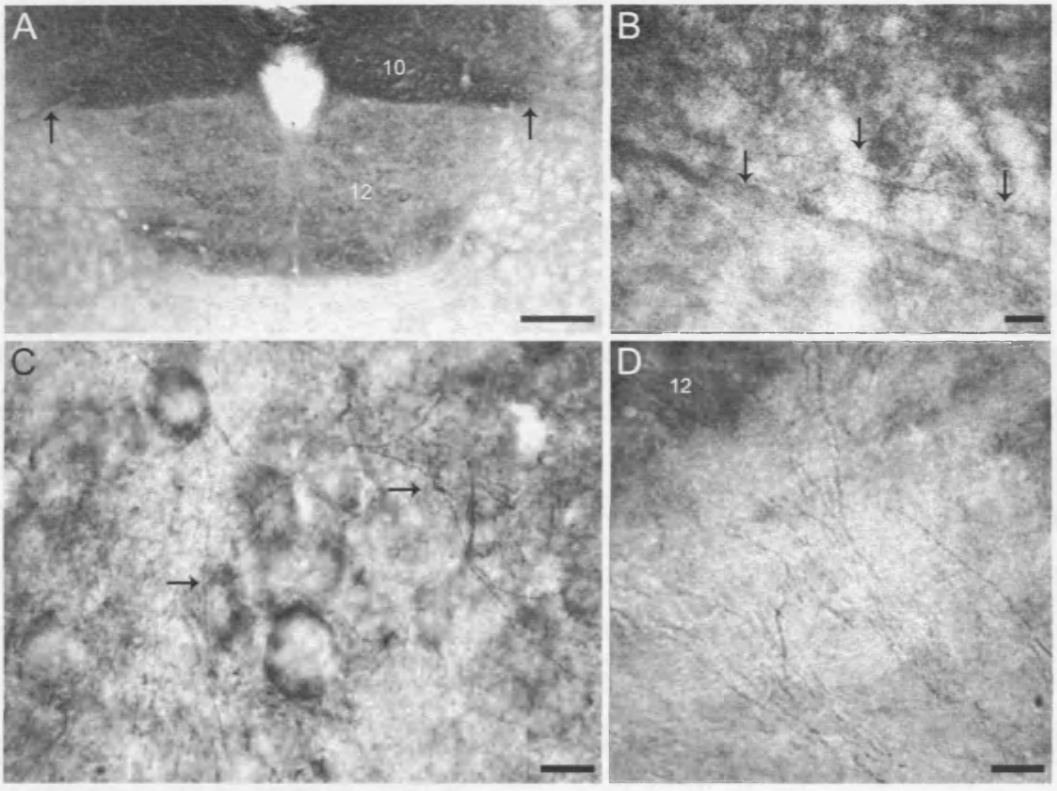

FIGURE 6.11: SK3 α subunit distribution in the dorsal motor nucleus of the vagus and in the hypoglossal nucleus. Immunohistochemistry on P25 rat coronal sections using the anti-CSK3 affinity purified antibody (1:17,500). **A**: Intense signal was visible in the DVN (10) and in fibres groups (black arrows). SK3 was highly expressed also in the hypoglossal nucleus (12). **B**: High magnification picture of the DVN fibres that are labelled with SK3 immunoreactivity. **C**: SK3 labelled neuronal somata and fibres in the hypoglossal nucleus. The arrows indicate the fibres. **D**: Fibres immunostained with SK3 signal are located ventrally to the hypoglossal nucleus. Scale bars: A, 200 μm; B, 40 μm; C, D, 20 μm.

6.3.7 SK3 distribution in monoaminergic neurones

High to moderate SK3 immunoreactivity was detected in monoaminergic brain areas such as the substantia nigra (SNC)-ventral tegmental (VTA) area dopaminergic system, the locus coeruleus and the dorsal raphe. We analysed the subcellular localisation of the SK3 α subunit in these areas and correlated the protein expression with the monoaminergic neurone profiles.

As mentioned earlier, a prominent SK3 immunoreactivity was observed in SNC and in scattered neurones of SNR. The SNC is composed of a layer of densely packed dopaminergic neurones that revealed intense SK3 immunorectivity (Fig. 6.12 A and B). Immunostained somata were visible throughout the SNC dopaminergic neurones layer (Fig.6.12 A and B). Additionally, SK3 immunoreactivity was associated to the long apical dendrites invading the pars reticulata and to the basal dendrites laterally spread within the pars compacta (Fig. 6.12 C). A somato-dendritic distribution was also visible in scattered neurones of the SNR (Fig. 6.12 A and D). In this region, in addition to the principal GABA-ergic neurones, a subpopulation of scattered multipolar dopaminergic neurones is present. The scattered pattern (Fig. 6.12 A) and the morphologic features (Fig. 6.12 D) of SK3-labelled neurones in the SNC suggest that SK3 α subunit is selectively expressed in the dopaminergic neurones of this area.

SK3 immunoreactivity was also observed in the VTA (Fig. 6.12 A). However, the signal in this area was less intense than that in the SNR. This observation correlates with electophysiological studies reporting that a smaller SK-mediated I_{AHP} is detected in the VTA compared with the current recorded in dopaminergic neurones of the SNC (Wolfart et al., 2001). At the subcellular level, SK3 signal was associated to somato-dendritic neuronal profiles.

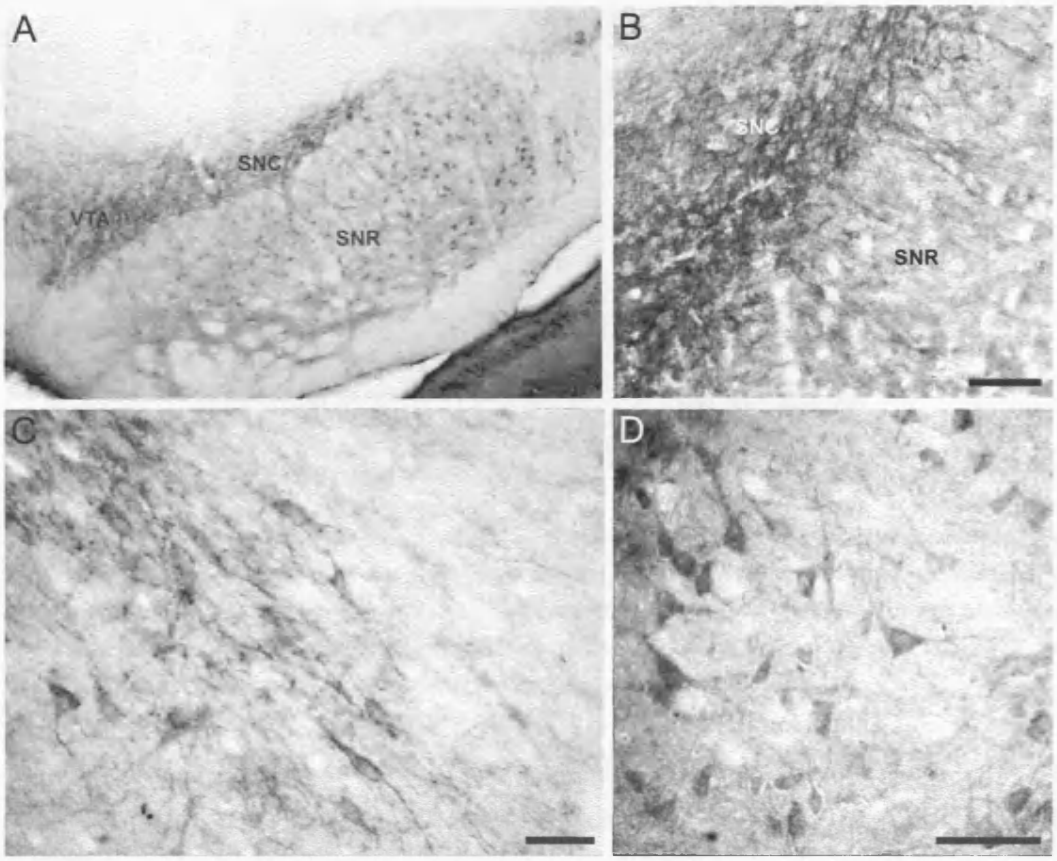

FIGURE 6.12: Expression of SK3 in the substantia nigra and the ventral tegmental nucleus. Immunohistochemistry was performed on coronal sections of P25 rats with the affinity purified anti-CSK3 antibody (1:17,500). **A:** SK3 immunoreactivity was detected in the substantia nigra pars compacta (SNC), in scattered neurones of the substantia nigra pars reticulata (SNR) and in the ventral tegmental nucleus (VTA). The subcellular localisation of SK3 channels was somato-dendritic in the SNC (**B**, **C**) and in scattered neurones of the SNR (**D**). Scale bars: A, 200 μm; B, 100 μm; C, 40 μm; D, 20 μm.

The locus coeruleus (LC) is composed of a homogeneous group of noradrenergic neurones. In this region, the SK3 immunoreactivity was very dense. The signal was distributed in somata of most LC neurones (Fig. 6.13), whereas cellular nuclei were free of SK3 signal. Additionally, SK3 immunostaining was associated with thick neuronal processes (Fig. 6.13, white arrows). Numerous thin fibres that were positive to SK3 immunostaining were also visible throughout the LC, indicating axonal localisation of SK3 α subunit (Fig. 6.13, black arrows). Given the complexity of the afferent/efferent projections of LC neurones, it is difficult to assess the origin of the SK3-positive axons within the LC.

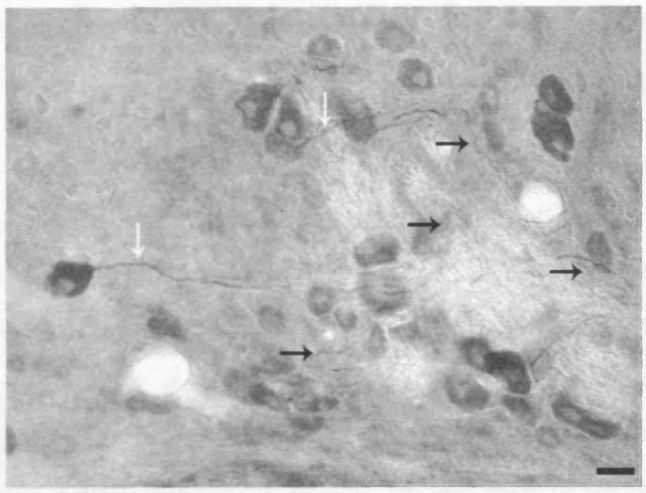

FIGURE 6.13: Cellular localisation of SK3 α subunit in neurones of the locus coeruleus. Immunohistochemistry on P25 sagittal sections with the immunopurified anti-CSK3 antibody (1:17,500) revealed that the SK3 protein was distributed in locus coeruleus neuronal somata and processes. The white arrows indicate neuronal dendrites; the black arrows indicate fibres that were immunostained with SK3 immunoreactivity. Scale bar: 20 μm.

Finally, the distribution of SK3 was analysed in the dorsal raphe (DR) serotonergic neurones, where the anti-CSK3 antibody detected moderate expression of the channel. As shown in the Figure 6.14, immunoreactivity was restricted to somata and proximal dendrites of small DR neurones.

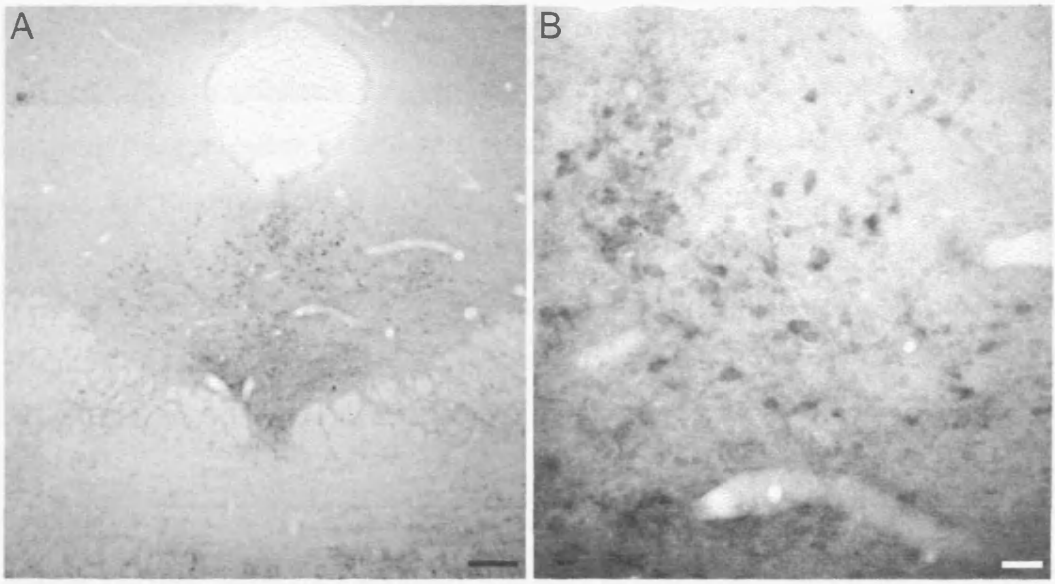

FIGURE 6.14: Expression of SK3 channels in the dorsal raphe. Immunohistochemistry on coronal sections with the anti-CSK3 immunopurified antibody (1:17,500) revealed that SK3 was expressed in the dorsal raphe (A). High magnification analysis indicated that the SK3 protein was localised in

somata and in the proximal portion of dendrites of dorsal raphe neurones. Scale bars: A, 200 μm, B, 40 μm.

6.4 Developmental regulation of SK3 distribution in monoaminergic neurones

Changes in ion channel composition and electrical excitability are crucial during the development of the central nervous system. In particular, fluctuations of intracellular Ca^{2+} have been shown to have a central role in the maturation of single neurones and neuronal networks (Spitzer et al.,1995). Given their high sensitivity to Ca^{2+}, SK channels might have an important role in the regulation of Ca^{2+} transients. However, limited information is available on the role of SK channels in neuronal development. Developmental downregulation of the expression of SK2 channels has been shown to influence the firing properties of developing Pukinje neurones and possibly contribute to the regulation of Ca^{2+} transients and oscillations during the first two weeks after birth (Cingolani et al., 2002). We investigated whether any change in the distribution of SK3 α subunit occurs during the first stages of postnatal development in substantia nigra-VTA, locus coeruleus and dorsal raphe. In the previous paragraph, we have shown that SK3 channels are expressed in monoaminergic neurones of these areas. In all three regions, the expression of the channel has been shown to affect the firing properties of these neurones (Worfart et al, 2001; Osmanovich et al., 1990; Osmanovic et al., 1993; Freedman and Aghajanian, 1987) and, possibly, to influence the release of the different monoamines. An intriguing aspect of the expression of SK3 monoaminergic neurones is related to the proposed, but still controversial, involvement of the gene that encodes SK3 in schizophrenia (Chandy et al., 1998; Gargus et al., 1998; Jobber et al., 1999). This adds a further level of interest to the analysis of the developmental regulation of SK3 expression, given the numerous lines of evidences indicating a role of developmental processes in schizophrenia (Rapoport et al., 2005).

The distribution of the SK3 channel was analysed in P1 and P3 rat brains. The affinity purified anti-CSK3 antibody was used in immunohistochemistry experiments following the protocol described in 2.2.15.2, which is based on the use of detergent (Triton-X-100) to permeabilise the tissue during the blocking and the primary antibody incubation. However, generally, sections of tissue from young animals

exhibited a higher background compared with that of P25 rat brains and displayed poor cellular resolution. Therefore, we tested also a protocol where the tissue was permeabilised by freeze/thawing omitting Triton-X100 (2.2.15.3). When this protocol was used, the distribution pattern of the SK3 protein was identical to the one observed with the protocol 2.2.15.2, but the signal to background ratio and the cellular definition were improved. Therefore, results obtained using both protocols are reported in this paragraph.

The signal intensity obtained in the immunohistochemistry experiments on postnatal brains was generally weaker than that in P25 rats. However, in the substantia nigra, SK3 α subunit displayed high expression in dopaminergic neurones of the SNC and in scattered neurones of the SNR (Fig. 6.15 A and B). Similar to the results obtained on P25 rats, SK3 immunoreactivity was localised in the somato-dendritic compartment of these neurones. A less intense SK3 immunostaining was observed in the VTA, where, owing to the low intensity of the signal, it was difficult to assess the subcellular localisation of the protein. A similar difference in SK3 expression levels between VTA and SN has been observed also in P25 brains. Taken together, these results indicate that SK3 is expressed in the early phases of postnatal development in the SN-VTA dopaminergic system, with a similar expression profile to the one observed in P25 rats. Moreover, no change in the subcellular localisation of the SK3 channel was observed in the SN dopaminergic neurones.

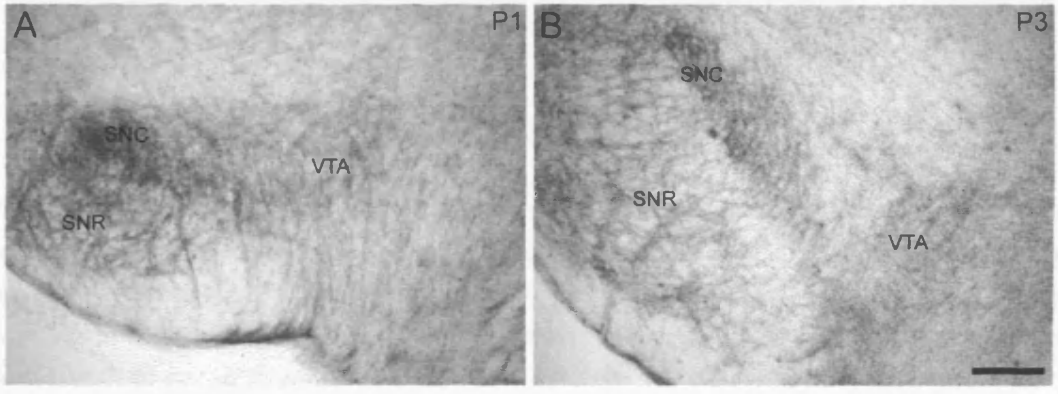

FIGURE 6.15: Developmental regulation of the SK3 channel expression in the substantia nigra-ventral tegmental area dopaminergic system. The affinity purified anti-CSK3 antibody (1:17,500) was used in immunohistochemistry experiments on coronal sections of P1 (**A**) and P3 (**B**) rat brains. SK3 immunoreactivity was detected in the substantia nigra pars compacta (SNC) and in scattered neurones of the substantia nigra pars reticulate (SNR). Somato-dendritic immunostaining was

observed in SNC dopaminergic neurones, whereas a lower intensity signal was detected in the ventral tegmental area. Scale bar: 200 µm.

In noradrenergic neurones of the locus coeruleus, SK3 immunoreactivity was detected on P1 and P3 brain tissue (Fig. 6.16). In both developmental stages, an intense signal was present in the neuronal somata and in numerous processes resembling axonal profiles (Fig 6.16 B, D). Also in this case, the cellular localisation of the SK3 channel that was observed in these postnatal stages is similar to the localisation in P25 rats.

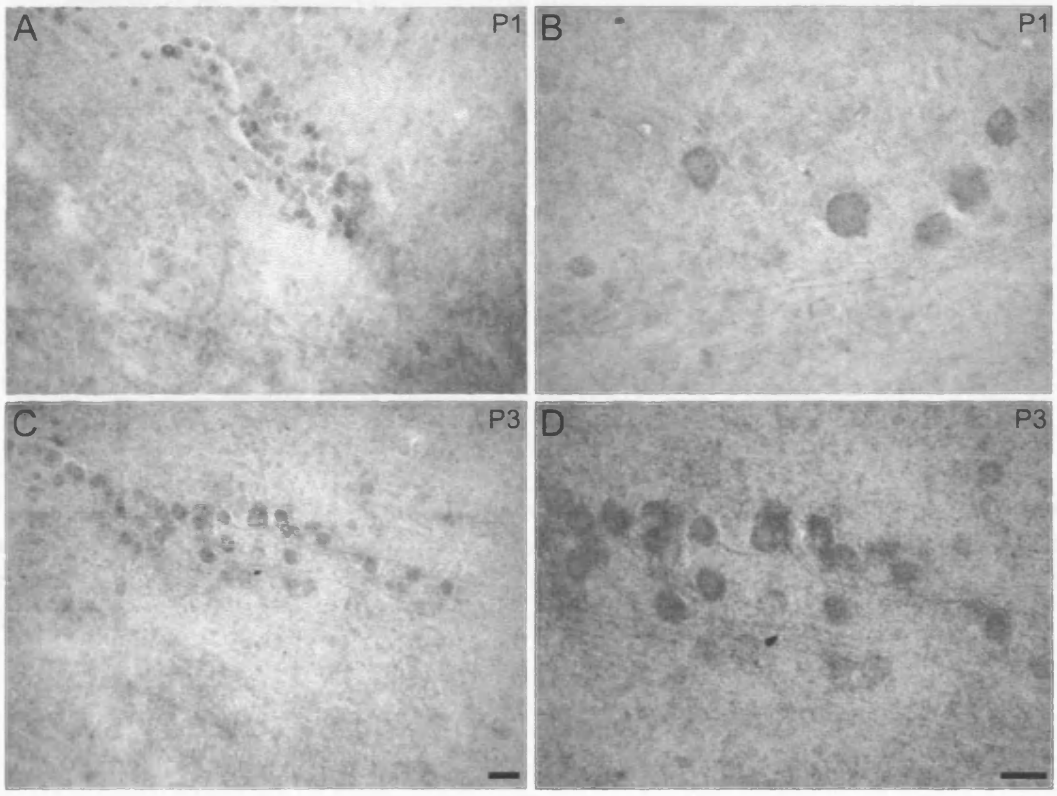

FIGURE 6.16: Developmental regulation of the SK3 channel expression in the locus coeruleus. Immunohistochemistry experiments on coronal sections of P1 (**A, B**) and P3 (**C, D**) rat brains using the affinity purified anti-CSK3 antibody (1:17,500). SK3 immunoreactivity was detected in the locus coeruleus in P1 and P3 sections. SK3 immunostaining was present in neuronal somata and in fibres. Scale bar: C, 40 µm; D, 20 µm.

Serotoninergic neurones of the dorsal raphe revealed a very weak SK3 signal in P1 and P3 animals (Fig. 6.17). Given the low intensity of the immunostaining, it is not possible to determine the subcellular localisation of the protein. Comparison of this signal with the one in P25 animals (Fig. 6.14) suggests that, in this brain region, there might be a developmental upregulation of the expression of the SK3 α subunit.

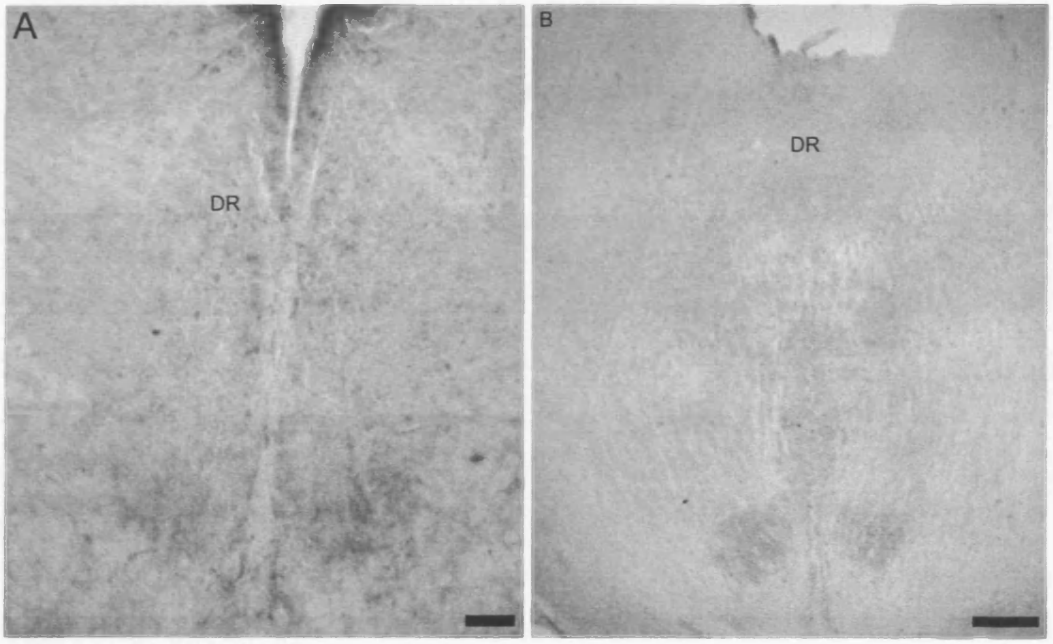

FIGURE 6.17: Developmental regulation of the SK3 channel expression in the dorsal raphe. Immunohistochemistry on coronal sections of P1 (**A**) and P3 (**B**) rat brains using the affinity purified anti-CSK3 antibody (1:17,500). Very weak SK3 signal was detected in the dorsal raphe neurones (DR) in P1 and P3 sections. Scale bar: A, 40 μm; B, 200 μm.

CHAPTER 7

Determinants of apamin sensitivity in SK channels

7.1 Introduction

The three members of the SK channel family, SK1, SK2 and SK3, differ in their apamin sensitivity. Homomeric SK2 channels from rat (rSK2), mouse (mSK2) and human (hSK2) exhibit the highest sensitivity, whereas homomeric human SK1 channels (hSK1) are the least apamin sensitive channels of the SK channel family (Kohler 1996, Strobaek 2000, Shah 2000, Stocker et al., 2004a-b). The behaviour of the rat rSK1 subunit is different than hSK1, because rSK1 is not expressed as a functional channel either in oocytes or in mammalian cell lines (Benton et al., 2003; D'hoedt et al., 2004). The chimeric rSK1 α subunit, $rSK1_{NSK2\text{-}CSK2}$, where the carboxy- and amino-terminal domains of rSK1 have been replaced with the corresponding regions of rSK2, forms functional channels (D'hoedt et al., 2004). However, the current generated by the $rSK1_{NSK2\text{-}CSK2}$ chimera is only marginally inhibited by 100 nM apamin, whereas apamin inhibits hSK1 with an IC_{50} of 3nM (D'hoedt et al., 2004). The difference in apamin sensitivity between this chimera and hSK1 is surprising because: (i) the molecular determinants of apamin sensitivity have been allocated in the region between transmembrane segment S5 and S6, which comprises the pore of potassium channels (Ishii, 1997; Shakkottai, 2001); (ii) the primary sequence of the S5-S6 region of hSK1 and of $rSK1_{NSK2\text{-}CSK2}$ chimera is identical (Fig. 7.1). Altogether these observations suggest that amino acids located outside the pore are most likely involved in the sensitivity to apamin.

In this chapter, we address the question as to whether regions other than the pore of the α subunit of SK channels influence the apamin sensitivity of these channels. The present work has been done in collaboration with Drs. A. Nolting and D. D'hoedt who performed the electrophysiological experiments.

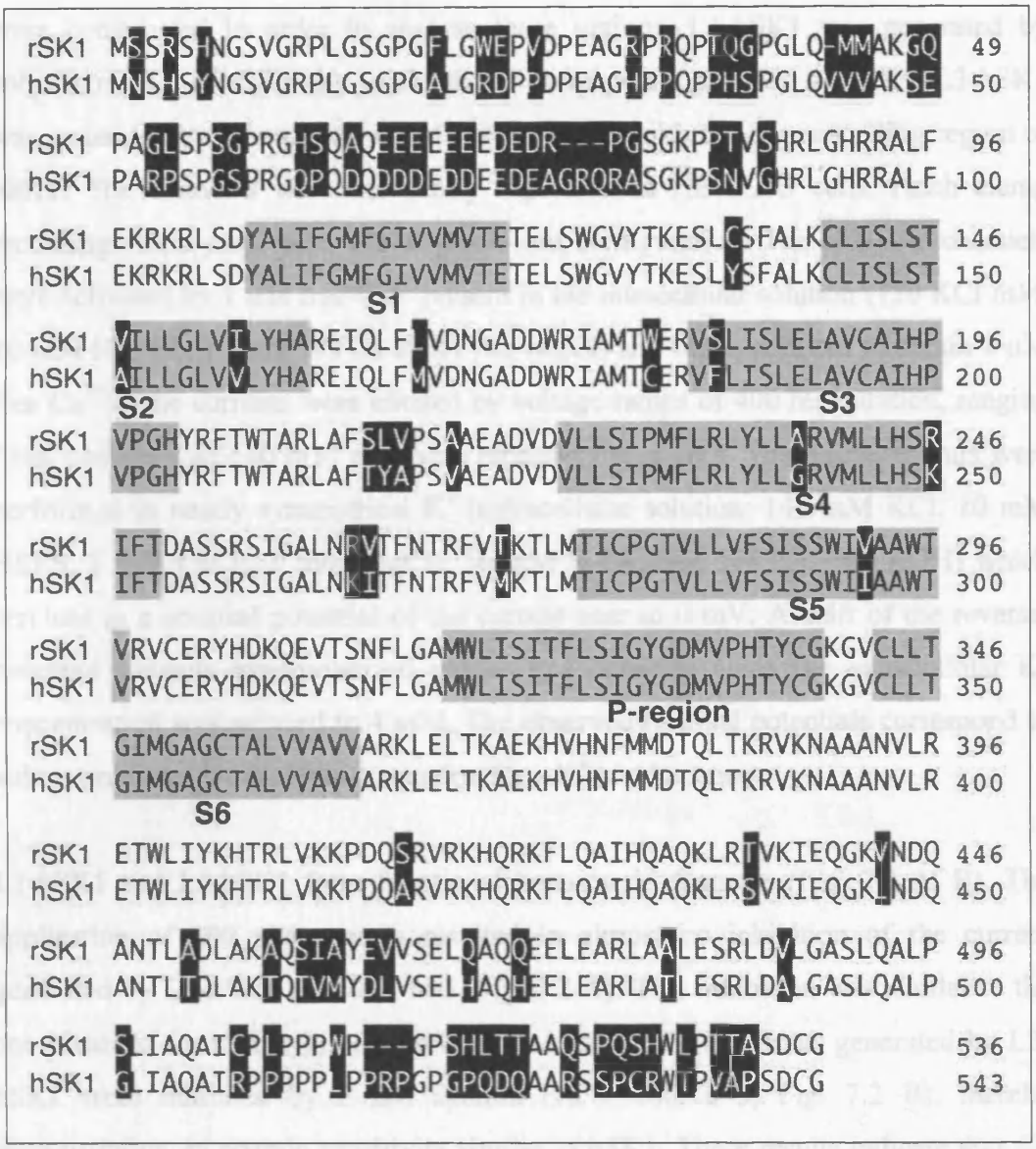

FIGURE 7.1: Alignment of the primary sequence of rSK1 and hSK1. The alignment shows that the primary sequence of the S5-S6 region is identical in hSK1 and rSK1. The six transmembrane segments (S1-S6) and the pore region (P-region) are represented as grey boxes. The different amino acids are labelled in black.

7.2 Apamin sensitivity of SK channels is affected by regions outside the pore

The most obvious regions outside the pore that might have an influence on apamin-sensitivity are the extracellular loops L1, that connects transmembrane segment S1 and S2, and L3, which is located between transmembrane segment S3 and S4. Inspection of the primary sequences of L1 and L3 revealed that one amino acid is different between hSK1 and $rSK1_{NSK2\text{-}CSK2}$ in L1, and four amino acid are different in L3 (Fig. 7.1). Therefore, two chimeras, L1-hSK1 (2.2.17.2) and L3-hSK1 (2.2.17.3),

were constructed in order to analyse these regions. L1-hSK1 was generated by substituting L1 of $rSK1_{NSK2\text{-}CSK2}$ with the corresponding region of hSK1. L3-hSK1 was generated by substituting L3 of $rSK1_{NSK2\text{-}CSK2}$ with the corresponding region of hSK1. The chimeras were transiently expressed in HEK 293 cells. Patch clamp recordings were performed in the whole-cell configuration. The chimeric channels were activated by 1 µM free Ca^{2+} present in the intracellular solution (130 KCl mM, 10 mM HEPES, 10 mM EGTA at pH 7.2, $MgCl_2$ and $CaCl_2$ adjusted to obtain 1 µM free Ca^{2+}). The currents were elicited by voltage ramps of 400 ms duration, ranging from –140 mV to +40 mV, and were repeated every 10 s. The measurements were performed in nearly symmetrical K^+ (extracellular solution: 144 mM KCl, 10 mM HEPS, 2 mM $CaCl_2$, 1 mM $MgCl_2$, 10 mM D-Glucose, pH 7.4 with KOH) which resulted in a reversal potential of the current near to 0 mV. A shift of the reversal potential towards hyperpolarized values was obtained when the extracellular K^+ concentration was reduced to 4 mM. The observed reversal potentials correspond to values predicted by the Nernst equation for a K^+ conductance.

L1-hSK1 and L3-hSK1 form functional homomeric channels (Fig. 7.2 A, B). The application of 100 nM apamin resulted in almost no inhibition of the current generated by L1-hSK1 (7 ± 9%, n=5, Fig. 7.2 A). This inhibition was similar to the one obtained for $rSK1_{NSK2\text{-}CSK2}$. In contrast, ~50% of the currents generated by L3-hSK1 were inhibited by 5 nM apamin (52 ± 5%, n=3, Fig. 7.2 B), thereby demonstrating an apamin sensitivity similar to hSK1. These results indicate that the extracellular loop between S3 and S4 influences apamin sensitivity and might explain the observed difference in apamin sensitivity between hSK1 and rSK1.

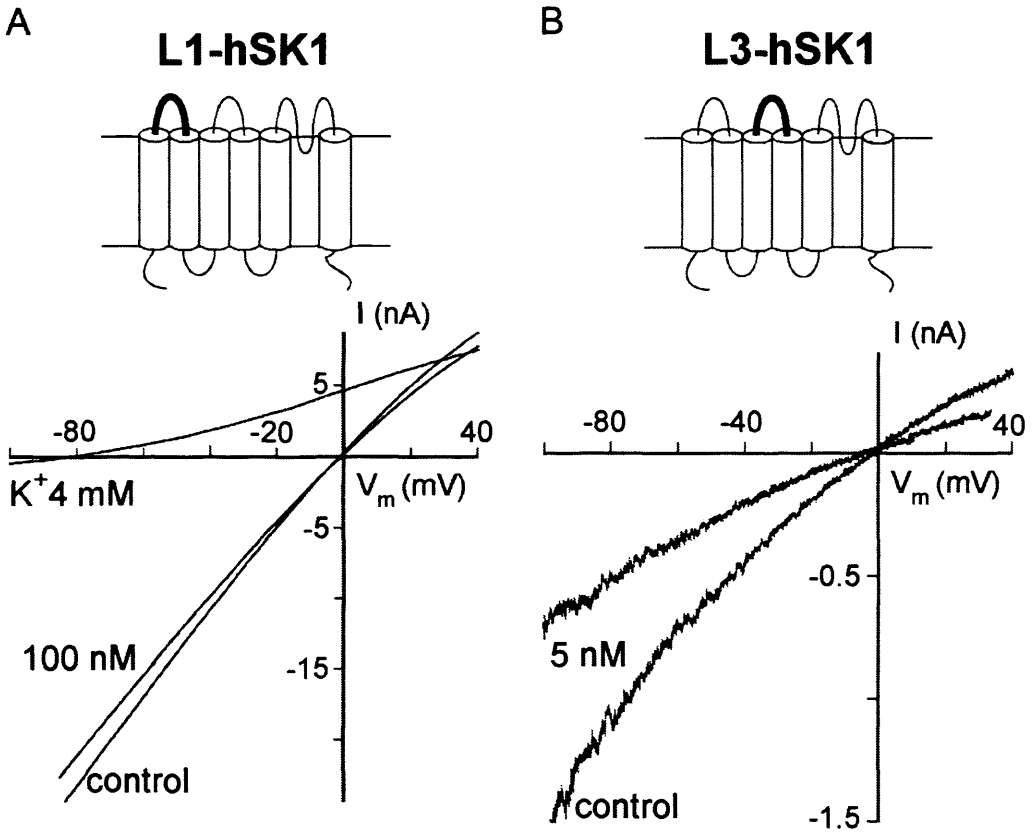

FIGURE 7.2: Amino acids located in the extracellular loop between transmembrane segments S3 and S4 affect apamin sensitivity. Schematic representation of the chimeric SK α subunits L1-hSK1 (**A**) and L3-hSK1 (**B**). Thin lines correspond to regions of $rSK1_{NSK2\text{-}CSK2}$ α-subunit and thick lines represent regions of hSK1 α-subunit. Patch clamp experiments were performed in the whole-cell configuration on HEK 293 cells that express L1-hSK1 (**A**) and L3-hSK1 (**B**). Channels were activated in the presence of 1 μM intracellular Ca^{2+}. 400 ms voltage ramps from −100 mV to +40 mV are shown. **A**: Representative current traces of HEK 293 cells that express L1-hSK1 (control). The application of 100 nM apamin does not inhibit the current. In the same cell, when $[K^+]_e$ is reduced to 4 mM, a left shift of the current-voltage relation is observed. Currents generated by L1-hSK1 are not affected by the application of 100 nM apamin (residual current: 93±9%, n=3). **B:** Representative current traces of HEK 293 cells that express the chimera L3-hSK1. 5 nM apamin inhibited 52 ± 5% (n=3) of the current.

7.3 Identification of amino acids outside the pore that affect apamin sensitivity of SK channels

Because amino acids that are located outside the pore influence apamin sensitivity of the $rSK1_{NSK2\text{-}CSK2}$ chimera, we were interested in knowing whether this property is a peculiarity of the chimera or also a feature of other SK channels. To address this question, we generated another chimera of hSK1, which is the least apamin-sensitive SK subunit, and of SK2, which is the most apamin-sensitive SK subunit. The chimera, named hSK1-SK2-hSK1 (2.2.17.4), was generated by substituting the region that starts from the end of S1 and ends at the beginning of transmembrane segment S4 of hSK1 with the corresponding region of SK2 (Fig. 7.2). If regions that are located outside the pore affect the apamin sensitivity of the channel, then hSK1-SK2-hSK1 should be more sensitive to apamin than hSK1. On the contrary, if the pore is the only region of the channel involved in apamin binding, then the chimera should have similar apamin sensitivity than hSK1. To test these two possibilities, hSK1-SK2-hSK1 was transiently expressed in HEK 293 cells and Ca^{2+}-activated K^+ currents were elicited as described earlier. hSK1-SK2-hSK1 formed functional homomeric channels; its apamin sensitivity was tested by applying 300 nM apamin, a concentration that is known not to affect hSK1 but inhibits SK2 almost completely. As shown in Figure 7.2, 300 nM apamin suppressed >50% of the current generated by hSK1-SK2-hSK1 (58 ± 3%, n=5), indicating that the chimera is more sensitive to apamin than hSK1. From these experiments we conclude that regions located outside the pore contribute to the different apamin sensitivity of hSK1 and rSK2. Moreover, these results suggest the involvement of regions other than the pore in apamin sensitivity might be a feature of all the SK subunits.

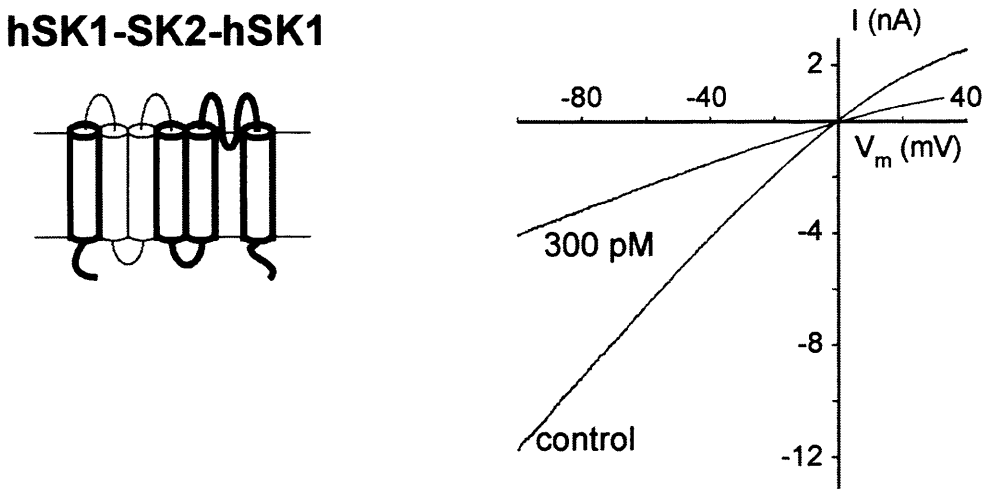

FIGURE 7.3: Substitution of the extracellular loops L1 and L3 of hSK1 with the corresponding regions of rSK2 increases apamin sensitivity. Schematic representation of the chimera hSK1-SK2-hSK1 generated by substituting the region between the transmembrane segments S1 and S4 of hSK1 with the corresponding sequence of rSK2. Thick lines represent hSK1, whereas thin lines indicate rSK2. Current traces obtained from HEK 293 cells expressing the hSK1-SK2-hSK1 chimera. Recordings were performed in the presence of 1 µM intracellular Ca^{2+} and in symmetrical K^+, as described in the legend of Figure 7.2. After application of 300 nM apamin, 58 ± 3% current inhibition was observed (n=5).

Following these observations, we aimed to identify the amino acids outside the pore which contribute to apamin sensitivity of the SK channels α subunits. In hSK1-SK2-hSK1, the complete region between the end of the transmembrane segment S1 and the beginning of transmembrane segment S4 was exchanged with the corresponding region of rSK2. However, the amino acids that are most likely to be responsible for the increased sensitivity of the chimera are located in L1 or L3. Based on the observation that the extracellular loop L3, but not L1, influences the apamin-sensitivity of $rSK1_{NSK2\text{-}CSK2}$ (Fig. 7.2), we decided to focus on differences in the amino acid sequences of hSK1 and SK2 in L3.

As shown in the alignment of Figure 7.4 A, eight amino acids differ between the L3 loop of hSK1 and the L3 loop of rSK2. These eight different amino acids in hSK1 were replaced with the corresponding amino acids of rSK2. In four mutants a single amino acid was exchanged, whereas in two mutants we introducing double amino acid exchanges. The following six mutants were therefore generated (2.2.17.6):

- in hSK1-H204N, hSK1-R206T and hSK1-E223T, a charged amino acid of hSK1 was substituted with a neutral amino acid in the corresponding positions of rSK2;
- in hSK1-VA221/222TT, two hydrophobic amino acids in hSK1 were replaced with two hydrophilic residues in the corresponding position of rSK2;
- in hSK1-T216S and hSK1-VL228/229II, hydrophobic or hydrophilic amino acids were exchanged for amino acids of the same character.

Each of these mutants was expressed in HEK 293 cells and formed functional homomeric Ca^{2+}-activated K^+ channels. The apamin sensitivity of the mutants was tested by applying 3 nM apamin. Apamin was used at 3nM because this concentration corresponds to the IC_{50} measured for hSK1 and, therefore, making it possible to measure even small changes in sensitivity towards the toxin. By performing these measurements, we wanted to test whether any of the mutated amino acids affects apamin sensitivity of rSK2. If this is the case, then the corresponding mutations in hSK1 should result in a higher apamin sensitivity than the one measured for hSK1. Figure 7.4 shows the results that were obtained with all mutants. Substitution of three charged amino acids of hSK1 with the corresponding uncharged amino acid of hSK2 did not change the sensitivity of the channels to apamin. In fact, 3 nM apamin inhibited ~50% of the current generated by hSK1-H204N (Fig. 7.4 B), hSK1-R206T (Fig. 7.4 C) and hSK1-E223T mutants (Fig. 7.4 D). Similarly, hSK1-VA221/222TT (Fig. 7.4 E) and hSK1-VL228/229II (Fig. 7.4 F) mutants did not show any change in the sensitivity to the toxin. However, the hSK1-T216S mutant generated a current that was substantially inhibited (80%) by 3 nM apamin (Fig 7.4 G). The concentration-response curve of hSK1-T216S revealed an IC_{50} value of apamin of 167 pM (A. Nolting personal communication). This indicates that hSK1-T216S is ~20 times more sensitive to apamin than hSK1 (IC_{50} 3.2 mM) and ~5 times less sensitive to apamin then SK2 (IC_{50} 30 pM) (A. Nolting personal communication). All together these results show that we have identified a single amino acid located in the extracellular loop between S3 and S4 that is largely responsible for the difference in apamin sensitivity that is observed between hSK1 and SK2.

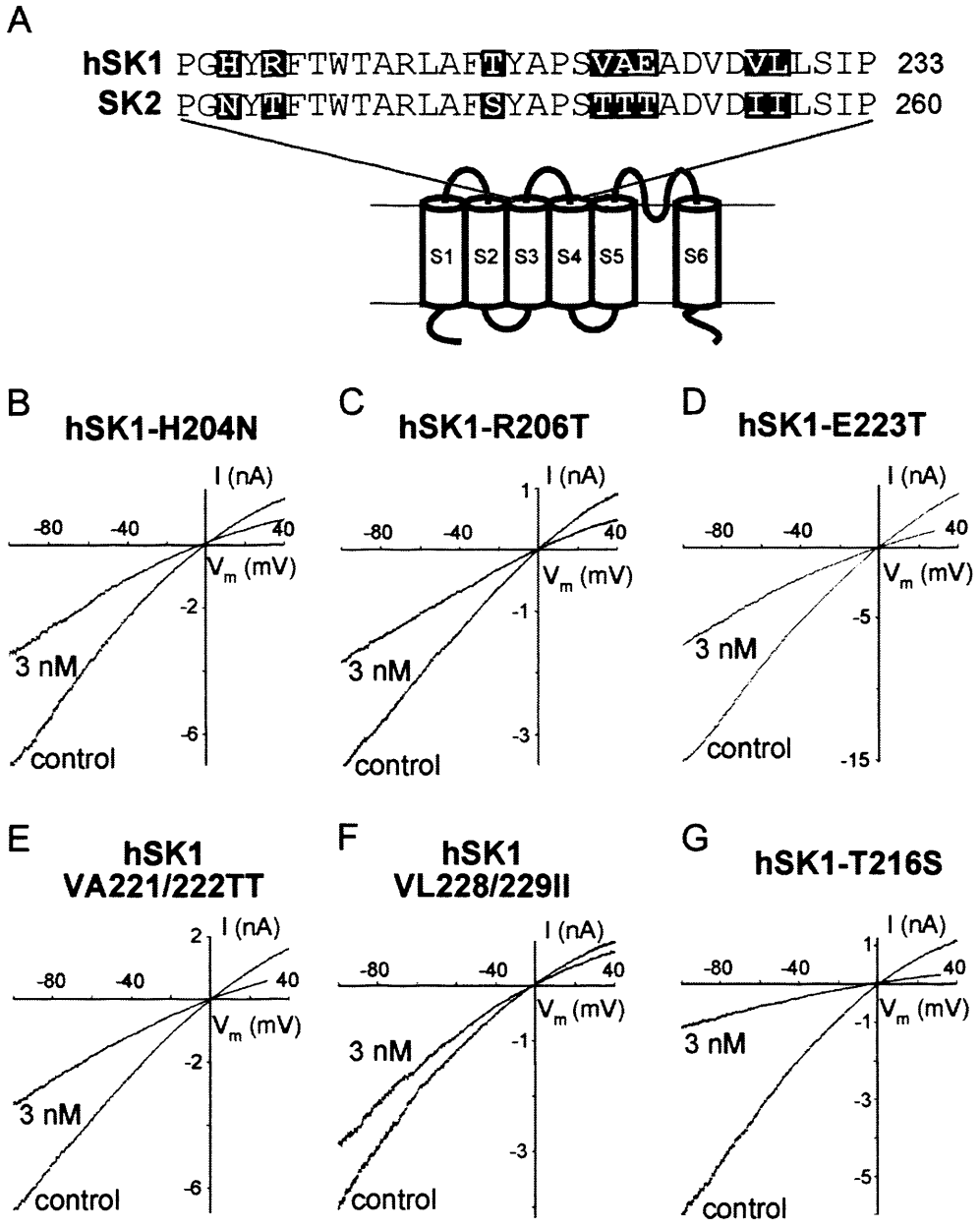

FIGURE 7.4: Identification of a single amino acid in the extracellular loop L3 that affects apamin sensitivity of hSK1. **A**: Sequence alignment in L3 between transmembrane domains S3 and S4 of hSK1 and rSK2. **B-G**: Current traces obtained from HEK 293 cells that express one of the six mutants. The amino acids of hSK1 have been substituted with the corresponding regions of rSK2. The measurements were performed as described in the legend of Figure 7.2. Representative current traces before (control) and after application of 3 nM apamin are shown. In B-F, the application of apamin caused half-maximal inhibition of the currents produced by the mutated hSK1 α subunits. In G, 3 nM apamin inhibited 80% of the current generated by hSK1-T216S mutant.

CHAPTER 8

Discussion

8.1 Characterisation of the anti-NSK2 antibody

Specificity of the anti-NSK2 antibody. The study of the precise subcellular localisation of ion channels is important to understand their specific role in neuronal function. Immunohistochemistry has been extensively used to study the distribution and the subcellular localisation of ion channels in the brain (Trimmer and Rhodes, 2004). The success of the immunohistochemical studies and the quality of the resulting data rely entirely on the specificity of the antibodies used. For this reason, the characterisation of the antibody represents an absolutely critical step. Since one of the aims of this work is the study of the cellular distribution of neuronal SK2 channels, I extensively characterised a fusion protein antibody directed towards amino-terminal domain of the SK2 α subunit. The specificity of this antibody and its ability to recognise the SK2 protein have been demonstrated with different experiments. In order to ensure highest antibody specificity, affinity purification of the anti-NSK2 serum was performed. Following the purification, ELISA assays showed that the purified antibody contained immunoglobulins that recognise the pET-NSK2 fusion protein but not GST. The purified antibody was able to recognise specifically the SK2 protein recombinantly expressed in HEK 293 cells in immunofluorescence assay and in Western blot, where a single immunoreactive band of ~50 kDa was recognised. In rat brain tissue, the affinity purified anti-NSK2 antibody revealed the existence of two SK2 proteins of ~50 kDa and ~80 kDa. In agreement with the data observed in recombinant expression system, the ~50 kDa band represents SK2. The apparent molecular weight of this band is lower than the molecular weight of 63 kDa predicted from the primary sequence of SK2. Anomalous mobility on SDS-PAGE might result from post-translational modifications such as glycosylation or phosphorylation. Glycosylation cannot explain the anomalous running of SK2 because it affects the mobility of proteins on SDS-PAGE resulting, most frequently, in bands with higher molecular weight than the molecular weight calculated from the primary sequence of the protein (e.g. Bennet, 2002). Furthermore, SK channels do not contain extracellular N-linked glycosylation consensus sequences (Kohler et al., 1996). Phosphorylation can also affect the running behaviour of proteins and can result in proteins that migrate faster in SDS gels (Silva-Neto et al., 1996). SK2 channels are directly phosphorylated by PKA (Ren et al., 2006); therefore, one possibility to explain the anomalous running

of SK2 might be that the subunit is phosphorylated. Furthermore, incomplete denaturation might also result in aberrant running behaviour.

The second band, of ~80 kDa, detected in the Western blot, corresponds to a novel SK2 isoform. This variant, called SK2-860, is characterised by an extended amino-terminal domain and, therefore, results in an higher molecular weight protein compared to the originally cloned SK2. A similar variant has been recently reported in mouse brain, where Western analysis demonstrated the existence of two SK2 species of 49 and 78 kDa (Strassmaier et al., 2005), similar to our study in rat. The detection of two SK2 proteins is not in agreement with previous Western analysis with a different anti-SK2 antibody that detects a single band of 67 kDa, in rat, and 64 kDa, in mouse (Sailer et al., 2002; Sailer et al., 2004). The single bands identified might correspond to the high molecular weight SK2 variant. However, a second band corresponding to the ~50 kDa identified in our study (Fig. 3.5 C) and reported by Strassmaier and colleagues was not identified, and the reason for this discrepancy is not known.

In some Western blot experiments, a third band of ~130 kDa was detected by the affinity purified anti-NSK2 antibody (Fig. 3.5 C). Given its molecular weight, the band, most likely, represents SK2 protein aggregates. Surprisingly, although the preadsorption of the antibody resulted in the compete loss of the two SK2 bands, the 130 kDa band was not eliminated. This might be explained by the fact that the aggregates contain a high number of antibody binding sites; therefore, they are detected even in the presence of extremely low amounts of free antibodies, which have not bound to the antigen during the preadsorbtion incubation. However, when we perform immunohistochemistry experiments with the purified anti-NSK2 antibody preadsorbed with the antigen, we detect no signal (Fig. 4.1 B). This observation supports the notion that the antibody is specific and that the 130 kDa band is likely an aggregate of SK2 subunits.

Epitope mapping of the anti-NSK2 antibody. We identified one linear epitope of the the anti-NSK2 antibody. This epitope corresponds to the sequence QPPASVVGG in the amino-terminal part of the NSK2 antigenic determinant. The epitope has been identified by using the peptide scan method and a PepSPOTs membrane which have been extensively used for epitope mapping of polyclonal and monoclonal antibodies (Kobayashi and Jones, 1999; Reineke et al., 2002; Kim et al., 2004).

The identification of this sequence fostered the idea to use the corresponding synthetic peptide (QP-GG peptide) to attempt the purification of the corresponding antibodies from the anti-NSK2 serum. However, the resulting purification had a particularly low IgG concentration, indicating that the antibodies recognising this epitope most likely represent only a small pool of antibodies. The ELISA assay indicates that the purified antibodies detect the QP-GG peptide conjugated to BSA and does not detect GST. Furthermore, the ELISA shows that virtually all the antibodies specific for the peptide have been purified from the anti-NSK2 serum, since the flow through showed only low detection of the QP-GG peptide conjugated to BSA. The purified antibody is able to detect native SK2 subunits expressed in HEK 293 cells, as supported by immunofluorescence and Western blot experiments. Surprisingly, on rat brain membranes, the purified antibody detects only a 90 kDa protein. This unexpected result differs from the bands observed in the previous experiments with the antibody purified by using the pET-NSK2 fusion protein (75 and 50 kDa bands) (Fig. 3.5) and from data obtained in immunoblots of mouse brain membranes with different SK2 antibodies (49 and 78 kDa bands) (Bond et al., 2004; Strassmaier et al., 2005). One likely explanation for this discrepancy might be that the antibody concentration of this purification is too low to detect native SK2 subunits on brain tissue and the antibody probably crossreacts with a different protein highly expressed in brain, that corresponds to the 90 kDa band. On the contrary, the purification that was performed with the pET-NSK2 fusion protein results in the isolation of a mixture of antibody populations directed towards many different epitopes. All together these antibodies recognise different SK2 antigenic determinants and are able to detect the native SK2 proteins both in recombinant expression systems and in brain tissue.

Because of the discrepancies observed in the Western blot on rat brain, and the extremely small amounts of antibody that could be isolated, the antibody purified with the QP-GG peptide was not used for the immunohistochemical studies.

8.2 Distribution of SK2 in the rat brain

Immunohistochemical localisation of SK2 α subunit. The immunohistochemical studies with the anti-NSK2 antibody reveal that the SK2 α subunit is widely distributed in the rat brain. In the regions that were analysed, I found a good

correlation between the signal detected by the anti-NSK2 antibody and the distribution described for the SK2 transcripts (Stocker and Pedarzani, 2000), supporting that both finding describe the SK2 distribution and confirming the specificity of the antibody. Thus, for example, regions such as hippocampus, neocortex, amygdala and thalamus express high levels of SK2 proteins. On the contrary, in the nucleus accumbens, that is one of the few brain areas where SK2 mRNAs were not detected, low SK2 immunoreactivity has been observed.

SK2 distribution in hippocampus and cortex. The strongest SK2 protein expression has been observed in the pyramidal neurones of the neocortical layer V and of the CA1-CA3 regions of the hippocampus. The high levels of expression in these brain regions correlate well with functional data indicating the presence of apamin-sensitive I_{AHP} currents in layer V pyramidal neurones (Schwidt et al., 1992), in CA1 (Stocker et al., 1999) and CA3 (Sailer et al., 2002) hippocampal pyramidal neurones. In agreement with mRNA distribution (Stocker and Pedarzani, 2000; Tacconi et al., 2001), no SK3 immunoreactivity was detected in neocortex and hippocampal CA1-CA3 pyramidal layers (Fig. 6.3). On the contrary, SK1 subunit is expressed in these brain regions, as shown by *in situ* hybridisation (Stocker and Pedarzani, 2000) and immunohistochemical data (Sailer et al., 2002; Sailer et al., 2004). These observations might suggest that SK2 and SK1 subunits form heteromeric channels and contribute to the generation of the I_{AHP} current. Although it is not clear whether such heteromeric assembly occurs in vivo; in heterologous expression systems SK1 and SK2 subunits form heteromeric channels that display reduced apamin sensitivity compared with homomeric SK2 channels (Benton et al., 2003). In CA1 pyramidal neurones, the I_{AHP} current is inhibited by apamin concentrations that are about eight times higher than the apamin concentration necessary to block SK2 homomeric channels in heterologous systems (Stocker et al., 1999), supporting the hypothesis that the apamin-insensitive SK1 subunit, together with SK2, might indeed be a component of the channel that generates the native current. However, a recent study on transgenic mice lacking the SK2 subunit indicate that SK2 channels are necessary and sufficient to generate the I_{AHP} current in CA1 pyramidal neurones, excluding the possibility that SK1 contributes to the current (Bond et al., 2004). Taking this observation into consideration, it is likely that SK2 is the only component of the channel generating the I_{AHP} also in the other neuronal types where SK1 and SK2 are

co-expressed, like, for example, CA3 and neocortical layer V pyramidal neurones. Further electrophysiological experiments on these brain regions on the transgenic mice might confirm this hypothesis.

The analysis of CA1 pyramidal neurones at high resolution indicates that SK2 subunits are localised in the somata and in the proximal portion of the apical dendrites. The SK2 signal in the proximal dendrites is in agreement with other immunohistochemical results (Sailer et al., 2002; Sailer et al., 2004). On the contrary, SK2 expression in the somata does not correlate with the data of Sailer and colleagues that report only a limited somatic SK2 signal. Localisation of SK2 in somata and proximal dendrites of hippocampal pyramidal neurones is also supported by immunocytochemistry on postnatal primary cultures (Fig. 4.9). A recent study proposed the localisation of SK channels in the distal apical dendrites of hippocampal CA1 pyramidal neurones, where they terminate plateau potentials and limit the spread of dendritic calcium spikes (Cai et al., 2004). SK2 is very likely to be the channel subunit that mediate this effect because, as discussed above, SK2 is the only SK subunit underlying the apamin-sensitive I_{AHP} current in CA1 pyramidal neurones (Bond et al, 2004). However, immunohistochemistry on brain sections and on postnatal hippocampal neurones, did not detect SK2 in the distal parts of the dendrites, probably due to detection limitations.

Developmental expression of SK2 in cultured postnatal hippocampal neurones. Interestingly, the expression of SK2 seems to be developmentally regulated *in vitro* as an increase of the SK2 signal intensity in the somata and neurites is observed after two days *in vitro* (DIV), and the highest SK2 signal is reached between 10 and 13 DIV (Fig. 4.9). This observation correlates with electrophysiological studies performed at different stages of the post-natal hippocampal culture, that indicate a progressive increase of the number of neurones expressing apamin-sensitive I_{AHP} currents (R. Tonini personal communication). The maximum number of neurones expressing the current is reached within 10 and 13 DIV, suggesting that the observed increase of SK2 protein expression might explain the progressive increase of the current. However, other mechanisms might also account for the I_{AHP} current increase. For example, in immature hippocampal pyramidal neurons the SK2 channels might be separated from the calcium channels that mediate their activation and, during development, a progressive organisation might lead to an improved functional

coupling. Alternatively, the neurones at the initial stages *in vitro* might have smaller Ca^{2+} currents, resulting in reduced intracellular Ca^{2+} transients in response to membrane depolarization. Another possibility might be that, in young neurons, different mechanisms of calcium buffering and calcium clearance might result in smaller increase of the intracellular calcium concentration compared to mature neurons. Surprisingly, SK2 signal cannot be detected when the immunocytochemistry is performed on cultures prepared from rats at embryonic day 17-18 (E17-E18) (Fig. 4.8). At this developmental stage SK2 transcripts are present, as shown by Northern blot analysis (M. Stocker personal communication). The observed lack of SK2 signal in the cultured neurones might suggest that, although the SK2 transcripts are present, the protein is not expressed. Alternatively, the SK2 subunits might be already expressed at E17, but the isolation procedure and the culture conditions of the neurones may cause changes in the SK2 channel densities that result in the lack of SK2 signal.

SK2 is expressed in hippocampal interneurones. In the postnatal cultures, SK2 protein is also expressed in the somatodendritic compartment of the hippocampal interneurones (Fig. 4.10). This is consistent with the SK2 signal observed in scattered neurones of the stratum oriens and radiatum on brain sections (Fig. 4.2). and with the characterisation of an apamin-sensitive I_{AHP} current that contributes to the mAHP in the CA3 stratum radiatum interneurones (Savic et al., 2001).

SK2 expression in the amygdala. In the amygdala, high expression levels of SK2 have been detected in the basolateral nucleus and, with lower intensity, in the lateral amygdaloid nucleus (Fig. 4.4). In the pyramidal neurones of the lateral amygdaloid nucleus, an apamin-sensitive I_{AHP} has been described (Faber and Sah, 2002). Interestingly, the lateral amygdaloid nucleus, does not express SK3 (Fig. 6.8). These observations, together with the absence of SK1 mRNA (Stocker and Pedarzani, 2000) in the lateral amygdala, indicate that homomeric somatodendritic SK2 channels underlay the I_{AHP} described in this area. In the lateral amygdaloid nucleus, beside the glutamatergic pyramidal-like neurones, a population GABA-ergic interneurones is present. Further experiments based on the use of specific markers might clarify whether the expression of the SK2 protein is limited to the pyramidal cells or if also the GABA-ergic interneurones express the SK2 subunit. Recently, it has been shown that SK channels act as feed-back regulators of synaptic activity at

glutamatergic synapses of the lateral amygdala pyramidal neurones (Faber et al., 2005). In view of these findings, it would be interesting to study the localisation of SK2 subunits at the spines of these neurones. Expression of SK channels at synapses seems to be particularly low and the distribution of SK2 subunits in spines of CA1 pyramidal neurones has been only observed upon overexpression of SK2 channels (Ngo-Anh et al., 2005). The use of antibodies with high affinity might allow the detection of synaptic SK2 channels and their physical colocalisation with NMDA receptors.

SK2 expression in reticular thalamic neurones. In the reticular thalamic neurones, SK2 is abundantly expressed (Fig. 4.5 A), but no SK3 signal has been detected (Fig. 6.5 B). Reticular thalamic neurones are GABA-ergic neurones that modulate and syncronise the thalamic output. An apamin-sensitive mAHP is present in these neurones and is involved in the regulation of the pacemaking properties (Avanzini et al., 1989; Bal-McCormick et al., 1993). The immunohistochemistry data support that somatodendritic SK2 channels are the channels mediating the I_{AHP} in these neurones. However, based on *in situ* hybridisation results (Stocker and Pedarzani, 2000) and on immunohistochemistry data (Sailer et al., 2004) that support the expression of SK1 in these neurones, it cannot be excluded that SK1 subunits contribute to the formation of the channels that underlie the I_{AHP} current. As discussed previously, electrophysiological studies on transgenic animals that lack SK2 indicate that, in CA1 pyramidal neurones, the SK1 subunit does not contribute to the generation of the I_{AHP} current (Bond et al., 2004). Further electrophysiological studies on the SK2 transgenic mice might clarify whether SK2 is the only molecular determinant of the current also in reticular thalamic neurones.

8.3 The rSK2-860 variant

Characterisation of a new rSK2 variant: rSK2-860. We report that a novel SK2 isoform, called SK2-860, is expressed in rat brain along with the originally cloned SK2 subunit. This variant is characterised by an extended amino-terminal domain, compared with the originally cloned SK2 (Kohler et al., 1996). The native expression of the newly identified SK2-860 subunit has been analysed by Western analysis using two antibodies: the anti-NSK2 antibody (Chapter 3), that recognises both SK2 proteins; and the anti-N860, that selectively recognises SK2-860 and is directed to

the extended amino-terminus. Both antibodies recognise a high molecular weight protein of ~80 kDa, corresponding to SK2-860; whereas only the anti-NSK2 antibody detects also the shorter protein corresponding to the originally cloned SK2. Although the relative abundance of the two proteins is difficult to assess, the results obtained with the anti-NSK2 antibody suggest lower expression levels for the SK2 subunit (Fig. 3.5 C). The characterisation of a mouse SK2 isoform comparable to SK2-860 has recently been reported by Strassmaier and colleagues (Strassmaier et al., 2005). Western analysis in the mouse brain revealed the existence of two SK2 species of 49 and 78 kDa (Strassmaier et al., 2005), similar to our study in rat.

The mechanism responsible for the generation of the two proteins is not clear as yet. Given that the predominant SK2 transcript expressed in the rat brain is the SK2-860 mRNA (Kerschensteiner, 2003), it might be possible that the SK2-860 protein is the only protein synthesised and that the generation of the shorter SK2 variant occurs by post-translational processing. For example, the activity of a protease might mediate the specific cleavage of the extended amino-terminus of the SK2-860 protein. If that was the case, a protein fragment of 275 amino acids should be generated. Protein fragments corresponding to that length are not detected in the Western blot and a reason could be that they have a high turnover and are degraded fast.

Immunohistochemical localisation of rSK2-860. The two available antibodies, anti-NSK2 and anti-N860, have been used to analyse the distribution pattern of the SK2 subunits on rat brain sections. Since the only difference between the two variants resides in the extended amino-terminal of SK2-860, it is not possible to generate antibodies that selectively identify the short SK2 subunit; therefore the SK2 distribution cannot be studied in isolation. This limits the possibility to identify brain regions, if they exist, where only the SK2-860 is expressed. In general, the two antibodies revealed a similar distribution profile, indicating that both SK2 subunits might be expressed together in most central neurones. In particular, in the hippocampus, SK2 and SK2-860 are likely coexpressed in the CA2 and CA3 regions. Differently, in the CA1 pyramidal layer and in the subiculum, SK2 is the predominant subunit. Moreover, the two variants are probably co-expressed in hippocampal interneurones of the stratum oriens and radiatum, and in the neocortical layer V. This distribution profile of the SK2-860 subunit was in good agreement with *in situ* hybridisation data that support low expression levels of SK2-860 in the CA1

region and subiculum, but high expression levels in neocortical layer V and CA2-CA3 regions (Kerschensteiner, 2003). At the cellular level, the SK2-860 signal seem to be restricted to the somata and the proximal dendrites of the hippocampal pyramidal neurones and interneurones. However, a more detailed subcellular distribution is difficult to assess because an amplification system, based on the precipitation of TSA species in proximity of the antigen, was used to amplify the SK2-860 immunostaining, and high resolution analysis is limited. Surprisingly, the distribution pattern we have observed with the anti-N860 antibody reveals some differences with the distribution of SK2-L described in mouse (Strassmaier et al., 2005). In fact, in mouse, an intense immunostaining for the SK2-L variant is detected in the CA1 region of the hippocampus, whereas a weaker signal is detected in CA2 and CA3 (Strassmaier et al., 2005). At the cellular level, the SK2-L signal is weak in the pyramidal layer but strong in the stratum oriens and radiatum of the hippocampus, suggesting dendritic localisation of the SK2-L protein; whereas we observe somatodendritic localisation of the SK2-860 variant in rat. Furthermore, no signal has been reported in the neocortical pyramidal neurones layer V (Strassmaier et al., 2005), where, in rat, an intense signal has been observed for the SK2-860 subunit. The reason for these differences is not known but one possible explanation might be the species difference.

The functional role of the newly identified SK2-860 subunit is not clear. The observation that the two variants are likely coexpressed in most neuronal types suggests that that the two subunits might form heteromeric channels, but whether this heteromer has a physiological function has still to be determined. Co-immunoprecipitation studies reported that the SK2-L variant co-assembles with SK2 and with SK3 in mouse brain (Strassmaier et al., 2005). Taking this finding into consideration, it is very likely that also the SK2-860 takes part in the formation of heteromeric channels. The recombinant expression of SK2-860 in HEK 293 (D. D'hoedt personal communication) and SK2-L in CHO cells (Strassmaier et al., 2005) results in functional channels generating calcium-activated potassium currents. The electrophysiological properties and calcium sensitivity of these currents are similar to the properties of the currents generated by the homomeric SK2 subunits (Strassmaier et al., 2005), as expected from the complete identity of the core and of the carboxy-terminal domain which is responsible for calcium gating of SK channels (Xia et al.,

1998; Keen et al., 1999; Schumacher et al., 2001). This might suggest that the subunit might take part to the generation of the I_{AHP} in vivo.

Exogenous expression of SK2-860 in neuronal cells. Although the electrophysiological experiments indicate membrane functional targeting of the SK2-860 subunit, the immunostaining of cells recombinantly expressing the protein revealed a peculiar distribution pattern. In fact, in different cell lines, the SK2-860 subunit localises in clusters distributed throughout the cytoplasm while no immunostaining is associated with the plasma membrane. Co-localisation studies with specific markers for lysosomes, nuclear membrane and Golgi apparatus revealed that the SK2-860 does not localise in any of these intracellular compartments (D'hoedt, 2005). Moreover, although partial overlap was observed with an endoplasmic reticulum (ER) marker (D. D'hoedt personal communication), the appearance of the clusters diverges from the ER morphology and the potential localisation of the SK2-860 subunit in the ER has to be further analysed. Signals present in the extended amino-terminal domain might affect the targeting of the subunit or induce non-specific protein aggregation. However, the SK2-860 protein clusters do not seem to represent aggregates of misfolded protein, as suggested by the lack of co-localisation between the SK2-860 clusters and vimentin or ubiquitin (D'hoedt, 2005), which are markers of misfolded proteins targeted for degradation (Ward et al., 1995; Hicke et al., 1997; Hicke and Dunn, 2003; Johnston et al., 1998). Thus, the nature and the subcellular localisation of the SK2-860 protein clusters have not been understood.

Although many mechanisms for protein targeting are similar in neurones and epithelial cells (Dotti and Simons, 1990), some neuronal proteins have been shown to have unexpected localisation when expressed in epithelial cells (reported in Stowell and Craig, 1999). Therefore, in order to test whether a different localisation pattern was observed in neuronal cells, I characterised the targeting profile of the SK2-860 subunit in different neuronal types. The exogenous expression of SK2-860 either in SCG or in cortical neurons results in the formation of numerous clusters in the cytoplasm and in the proximal dendrites. Additionally, in most neurones, partial membrane localisation of the SK2-860 protein was observed (Fig. 5.6 inset), differently from the non-neuronal cells.

Several hypotheses can be formulated to explain this distribution pattern. One possible explanation relies on the idea that SK2-860 is only a component of a protein complex that forms a complete channel. The interaction with a so far unknown auxiliary subunit or the heteromeric assembly with other SK α subunits might be necessary for the formation of a channel that is efficiently transported to the membrane. For instance, the heterologous expression of the Kv1.2 α subunit results in perinuclear localisation and its surface expression is increased upon co-expression of the Kvβ2 subunit (Shi et al., 1996). It might be possible that the extended amino-terminus contains an unknown retention signal or an aggregation motif responsible for the clustering. The interaction with another channel component might be necessary to mask these signals. Such a mechanism has been recently shown for the assembly of high voltage activated calcium channels: a retention sequence present in the pore forming α1 subunits is shielded by the assembly with the β subunit, which allows the channel complex to reach the membrane (Ma et al., 2002). Kv channel interacting proteins 1-3 (KChIP 1-3) affect the trafficking of Kv4.2 channels (Shibata et al., 2003). The KChIP 1-3 proteins supports the transport to the plasma membrane by masking an amino-terminal hydrophobic domain of Kv4.2 that might otherwise lead to aggregation and degradation of the protein (Shibata et al., 2003).

Taking into consideration that the SK2-860 subunit can interact with the other SK subunits (Strassmaier et al., 2005), it might be possible that the interaction with SK1, SK2 or SK3 might change the subcellular localisation and possibly promote the membrane targeting of SK2-860 subunit. In heterologous expression systems, it has been shown that the co-expression of rSK1 and rSK2 results in larger currents than the ones generated by homomeric SK2 channels (Benton et al., 2003); whereas the coexpression of hSK1 or rSK1 with SK3, diminishes the functional expression of SK3 (Monaghan et al., 2004). These observations suggest that heteromeric assembly can affect the functional expression and the targeting of SK subunits in different ways; therefore it is conceivable to hypothesise that the interaction of the SK2-860 subunit with other SK α subunits might change its subcellular localisation and possibly promote its membrane targeting. As observed in the SCG neurones, when SK2 and SK2-860 subunits are co-expressed their distribution pattern largely overlaps, indicating that the two subunits interact (Fig. 5.9), as reported by Strassmaier and colleagues (Strassmaier et al., 2005). However, no dramatic change

in the levels of the membrane expression of SK2-860 subunit is observed, suggesting that the interaction with the short SK2 subunit is not sufficient to promote the membrane targeting of the SK2-860 subunit and that another factor is necessary. Moreover, the distribution pattern of SK2-860 did not change upon co-expression of rSK1 and SK2-860 (data not shown).

Another mechanism that might influence the membrane targeting of the SK2-860 subunit is the activation of secondary pathways that results in post-translational modifications of the subunit. Some recent evidence has indicated the importance of protein kinases in the regulation of potassium channel targeting (Misonou et al., 2004). Kv2.1 channels are expressed in clusters, in the somata and dendrites of hippocampal pyramidal neurones (Misonou et al., 2004). The channels are inserted into the membrane after glutamate stimulation which increases the intracellular Ca^{2+} concentration. The relocation of the protein from the clusters to the membrane relies on the activation of the phosphatase calcineurin which dephosphorylates the channel and induces its translocation to the membrane surface (Misonou et al., 2004). A similar mechanism could be envisaged for membrane targeting of the SK2-860 subunit. A recent report showed that direct PKA phosphorylation of SK2 decreases membrane expression of SK2 subunits heterologously expressed in COS7 cells, indicating that phosphorylation can modulate SK channel targeting (Ren et al., 2006). Interestingly, inspection of the extended amino-terminus of the SK2-860 subunit indicates the presence of several consensus sequences for protein kinase A, protein kinase C and casein kinases. Further studies might investigate the involvement of these sites in the regulation of the membrane expression of the SK2-860 subunit.

8.4 Immunohistochemical distribution of SK3 α subunits in the rat brain

Anti-CSK3 antibody characterisation. The SK3 channel distribution in the rat brain was analysed using an anti-CSK3 antibody. The specificity of this antibody was demonstrated in Western analysis on rat brain synaptosmal membranes, where the antibody recognised a single band of ~75 kDa, in good agreement with the predicted molecular weight for the SK3 protein of 81.5 kDa. This observation is comparable to the results obtained in Western blots of mouse (Sailer et al., 2004; Bond et al., 2004) and rat (Sailer et al., 2002) brain membranes, with different anti-NSK3 antibodies.

Furthermore, the specificity of the anti-CSK3 antibody is supported by the good correlation between the immunohistochemical data and the distribution of SK3 transcripts described by *in situ* hybridisation studies (Stocker and Pedarzani, 2000; Tacconi et al., 2001; Sarpel et al., 2004; Bosch et al., 2002). For most of the brain regions, the expression profile obtained with the anti-CSK3 antibody is also in agreement with other immnunohistochemical studies recently reported (Tacconi et al., 2001; Sailer et al., 2002; Sailer et al., 2004).

SK3 distribution in the rat brain. Interestingly, at the subcellular level, the SK3 subunit exhibits a differential localisation in different neuronal types, suggesting that the channel might have distinct functions depending on the compartment where it is targeted.

As discussed previously (8.2), the hippocampus showed limited expression of the SK3 α subunit (Fig. 6.3). However a moderate neuropil immunoreactivity was observed in the stratum lacunosum moleculare and in the molecular layer of the dentate gyrus. These regions represent the areas where the axons of the perforant path pathway terminate. In particular, in the molecular layer of the dentate gyrus the axons of the entorhinal cortex form connections with the dendrites of the dentate gyrus granular cells; whereas in the stratum lacinosum moleculare the entorhinal terminals make excitatory synapses with the dendrites of hippocampal pyramidal neurones. Although SK3 transcripts are present in the entorhinal cortex (Stocker and Pedarzani, 2000; Tacconi et al., 2001), the immunohistochemical data indicate limited SK3 immunoreactivity in this area (Table 6.1). However, the presence of the immunostaining in the stratum lacunosum moleculare and in the molecular layer of the dentate gyrus suggests localisation of SK3 channels in the axon terminals of the entorhinal cortex neurones.

Within the thalamus, the SK3 channel is widely expressed. High SK3 expression is detected in most of the principal "relay" thalamic nuclei associated with sensory functions. These comprehend the dorsal lateral geniculate nucleus (DLG) involved in the transmission of visual information from the retina to the cerebral cortex; the medial geniculate complex (MGD and MGV) which represents the main thalamic relay to the primary auditory cortex; and the posterior nuclei (Po) which is predominantly involved in somatosensory signals transmission. Moreover, intense expression is observed in the anterior and lateral nuclei, where also the SK2 α

subunit is highly expressed. However, at the subcellular level, the two subunits exhibit a different localisation. In fact, SK2 expression is restricted to the somata and the proximal portions of the dendrites, whereas SK3 is associated to the neuropil and, in some cases, to fiber-like structures. This observation suggests that the two channels might not form heteromers and might contribute instead to different aspects of neuronal function. Despite the high expression of SK3 and, to less extent, SK2 in most thalamic nuclei, no correlation with physiological studies on the role of the AHP is available. Future studies might assess the contribution of the SK channels on thalamic function.

Differently from the thalamic regions, in the habenula, the subcellular localisation of the two SK subunits partially overlaps. For example, in the medial habenular neurones, both SK2 and SK3 subunits are expressed in the somata (Fig. 4.6 B and 6.7 B), whereas only the SK3 protein is present in the neurites of these neurones (Fig. 6.7 B). This suggests the possibility that the two subunits might form heteromers only in special cellular compartments. Furthermore, in the lateral habenula, SK2 is expressed and exhibits somatic localisation (Fig. 4.6 A), whereas SK3 immunoreactivity is not detected (Fig. 6.7 A). To date, no physiological correlate on the role of the SK channels in the habenular neurons is known; therefore further studies are needed to understand the role of the SK channels in this brain area.

An interesting segregation of the expression of SK2 and SK3 subunits is observed in the amygdala, where SK2 expression is high to moderate in the lateral (LA) and basolateral (BLA) amygdaloid nuclei (Fig. 4.4). On the contrary, the SK3 signal is restricted to the central amygdaloid nucleus (Fig. 6.8). While SK2 might be the channel responsible for the apamin sensitive AHP in the lateral amygdala pyramidal neurones (8.2), the I_{AHP} present in the central amygdala neurones might be generated by the SK3 α subunit (Schiess et al., 1999). However, the molecular determinant of this current have so far not been analysed using the available pharmacological tools that would allow an unequivocal correlation between the current and the expressed subunit.

In the neurosecretory neurones of the supraoptic nucleus (SO), SK3 channels are expressed in the somatodendritic compartment. In these neurones, an apamin-sensitive I_{AHP} regulates the phasic firing and ultimately influences the secretion of the hormones oxytocin and vasopressin (Kirkpatrick and Bourque, 1996). SK3 channels

localised in the somata and proximal dendrites are most likely the main molecular determinants of the I_{AHP}, as supported by pharmacological data (Bourque and Brown, 1987) and by the selective detection of SK3 transcripts and protein (Stocker and Pedarzani, 2000; Tacconi et al., 2000; Sailer at al., 2004). Moreover, within the supraoptic nucleus, the SK3 immunoreactivity is very strong at the base of the supraoptic nucleus, in the ventral glial/dendritic lamina, which is a region that contains a high density of glia cells and dendrites of the SO neurones. However, the fact that the signal is associated with thick filamentous structures and that the SK3 signal colocalises with GFAP immunostaining (Fig. 6.10), indicates that SO glial cells express the SK3 protein. A comparable distribution was recently shown with a different SK3 antibody (Alomone) in SO (Amstrong et al., 2005). This finding does not represent the first observation of the expression of SK channels in glial cells. In fact, Fujita and colleagues recently reported that SK3 is present in the glia cells that enfold the bundles of olfactory nerve axons in the olfactory bulb (Fujita et al., 2003). Moreover, electrophysiological studies have indicated the presence of apamin-sensitive potassium currents, along with other potassium conductances, in cultured cortical (Jalonen et al., 1997), striatal (Bychkov et al., 2001); and hippocampal glial cells (Burnard et al., 1990). It has been proposed that a possible role of calcium activated potassium channels, and of others potassium channels, in glia consists in the potassium buffering action during periods of intense neuronal activity (Sontheimer, 1994). In particular, in the SO neurones, the mechanisms of potassium clearance are particularly effective during intense activity (Coles and Poulain, 1991). It is therefore interesting to hypothesise a role for SK3 channels in such a mechanisms.

In the DVN and in the hypoglossal nuclei a particularly interesting distribution of SK3 was observed. Both the DVN and the hypoglossal neurones revealed a somatic immunotaining (Fig. 6.11 A, C). Somatic expression of the channel might correlate with the apamin sensitive I_{AHP} that has been shown to control the firing behaviour in both cell types (Pedarzani et al., 2000; Viana et al., 1993; Powers et al, 1999; Bayliss et al., 1995). Moreover, we observed SK3 immunolocalisation in fibers resembling axonal profiles. In the DVN, the location of the fibers is consistent with the sites where the axons of the DVN converge to form the vagus nerve (Fig. 6.11 A, B). In

the hypoglossal nucleus, some of the labelled fibers might represent the axons ventrally exiting the nucleus to form the hypoglossal nerve. (Fig. 6.11 D).

An interesting aspect of the study of SK3 subunit localisation emerges from the analysis of brain stem monoaminergic systems such as the substantia nigra, locus coeruleus and dorsal raphe. Monoaminergic neurones of these regions express high to moderate levels of SK3 channels. Given the complexity of the monoaminergic neurones efferent projections that innervate the whole forebrain, these brain regions influence in different ways the general functional state of the brain. Therefore, the understanding of the localisation and of the function of SK3 in these neurones is of particular interest. Intense SK3 signal was present in the substantia nigra pars compacta that contains an homogeneus population of dopaminergic neurones. SK3, which is expressed in the somatodendritic compartment of these neurones, has been shown to be the principal molecular determinant of the apamin-sensitive I_{AHP} involved in setting the regular spiking activity (Wolfart et al, 2001). Interestingly, in the substantia nigra pars reticulata the SK3 antibody reveals somatodendritic immunostaining on scattered neurones. This expression profile might correspond to the scattered pattern of dopaminergic neurones present in this area and would suggest a selective expression of SK3 in the dopaminergic neurones of the substantia nigra. Such a correlation has been indicated by an in situ hybridisation study that showed a comparable distribution of SK3 and TH mRNA-containing neurones in subtantia nigra compacta and reticulata (Sarpal et al., 2004). However, this hypothesis needs to be supported by further experimental evidence. A possible approach would be the concomitant use of SK3 antibody and a specific dopaminergic marker, like a tyrosine hydroxylase (TH) specific antibody which detects the rate limiting enzyme in catecholamine synthesis. Intense SK3 immunostaining is also observed in the somata of the adrenergic neurones in locus coeruleus. Somatic channels might underlie the apamin-sensitive mAHP involved in regulating the interspike interval during fast firing rates in these neurones (Osmanovich et al., 1990; Osmanovich et al., 1992). Interestingly, the immunostaining in the locus coeruleus reveals also a high number of fibers labelled with SK3 immunoreactivity. These fibers, which likely indicate axonal expression of the SK3 channel, suggest that SK3 channels might influence neurotransmitter release. Moderate somatodendritic SK3 expression was observed in the serotoninergic neurones of the dorsal raphe. Also in these neurones, the

expression of SK3 correlates with an apamin-sensitive mAHP (Freedman and Aghajanian, 1987).

Developmental regulation of SK3 in monoaminergic neurones. Given the interesting and possibly selective expression of SK3 in the monoaminergic neurones we have analysed whether any developmental regulation of the expression of this channel occurs during the first stages of postnatal life. We found that in the substantia nigra-VTA system and in locus coeruleus, SK3 is already expressed at day one (P1) and three (P3) after birth. Northern analysis of mRNA from juvenile brains (P1) indicate such an early expression of SK3 mRNA (M. Stocker personal communication). Several lines of evidence indicate that the release of monoamines during perinatal periods has a crucial role on cellular differentiation and on neuronal networks development (Herlenius and Lagercrantz, 2004). It might be possible that SK3, expressed in the early postnatal phases, is involved in these processes by regulating the firing pattern of the developing dopaminergic and noradrenergic neurorones and, ultimately, affecting the release of monoamines. Future studies would be interesting to understand the particular functional role of SK3 channels during the development in these subset of neurones.

Furthermore, in several systems it has been shown that calcium transients have an important role during different stages of neuronal development (Spitzer et al.,1995; O'Donovan, 1999). In Purkinjie neurones, developmental downregulation of the expression of SK2 channels has been shown after the first two weeks of post-natal life. The channel influences the firing properties of developing Pukinjie neurones (Cingolani et al., 2002) and, as a consequence, it might contribute to the regulation of Ca^{2+} transients and oscillations. This suggests that SK channels might be functionally involved in the complex events that result in the maturation of the neuronal network.

The analysis of the SK3 distribution in dorsal raphe revealed a weak SK3 immunoassaying in postnatal brains (P1 and P3). This might suggest that up-regulation of the SK3 signal in dorsal rape neurones might occur during development. However, electrophysiological studies will be needed to determine the functional significance of this difference in protein expression.

8.5 Determinants of apamin sensitivity in SK channels.

The results presented in Chapter seven provide new information concerning the differences in apamin sensitivity of the three SK channels. By using chimeras of SK subunits that have different sensitivity to the toxin, we could demonstrate that the extracellular loop that connects transmembrane segment S3 and S4 (L3) significantly contributes to apamin sensitivity of SK channels.

Previous studies on oocyte expression systems indicated that the molecular determinants of apamin binding reside in the outer pore region of SK channels (Ishii et al., 1997). Besides apamin, a number of other toxins have been shown to be potent inhibitors of SK channels, including scyllatoxin (Chicchi et al, 1988), PO5 (Zerrouuk et al, 1993), tamapin (Pedarzani et al., 2002) and the highly SK2 selective Lei-Dab, which was obtained by replacing the residue M7 of scyllatoxin with the non-natural amino acid di-aminobutanoic acid (Dab) (Shakkottai et al., 2001). Similar to apamin, the sensitivity to scyllatoxin is mediated by amino acids in the outer pore region (Jager and Grissmer, 2004). Mutant cycle analysis suggests that in Lei-Dab, the Dab at position seven directly interacts with an amino acid in the outer vestibule of SK2 (Shakkottai et al., 2001). Furthermore, several pore mutants that have been designed to characterize the pore region of SK channels have indicated that the general architecture of the outer vestibule of SK channels is similar to that of voltage-gated K^+ channels (Ishi et al., 1997; Jager and Grissmer, 2004). A single amino acid mutation in the outer pore of the SK2 subunit rendered the channel sensitive to the Kv channels blockers CTX and KTX (Jager and Grissmer, 2004). Taken together, these observations suggest that apamin and other toxins bind directly to the pore region of SK subunits and inhibit the channels.

In our study, the involvement of regions outside the pore in apamin sensitivity emerged by the puzzling difference that was observed in apamin sensitivity between hSK1 and $rSK1_{NSK2\text{-}CSK2}$ (D'oehdt et al., 2004), despite the identity of their pore. The hypothesis that regions beyond the pore influence the sensitivity to the toxin was confirmed by experimental evidence. In particular, substitution of L3 in $rSK1_{NSK2\text{-}CSK2}$ with the corresponding region of hSK1 results in a channel that is inhibited by apamin. In contrast, substitution of L1 between transmembrane segments S1 and S2 does not produce the same effect, indicating that molecular determinants that influence the sensitivity to the toxin are present only in L3. Interestingly, substitution

of L3 results in a similar apamin sensitivity between chimeric $rSK1_{NSK2\text{-}CSK2}$ and hSK1. This indicates that L3 is largely responsible for the difference of apamin sensitivity between the two channels.

The influence on apamin sensitivity of regions other than the pore is not a peculiarity of $rSK1_{NSK2\text{-}CSK2}$. In fact, similar results were observed between hSK1, which is the least apamin-sensitive SK channel, and rSK2, which is the most apamin-sensitive SK channel. We first observed that the simultaneous substitution of L1 and L3 of hSK1 with the corresponding regions of rSK2 resulted in a substantial increased sensitivity to apamin. Then, we showed that a singe amino acid located in L3 is responsible for this effect. The hSK1-T216S mutated subunit has an apamin sensitivity that is ~20 fold higher compared to hSK1 and only five fold lower than rSK2, indicating that the mutated residue contributes largely to apamin sensitivity of the channel. Taking into consideration the studies of Ishii and colleagues that reported the importance of two amino acids located in the pore region of rSK2 in apamin binding (D341 and N368) (Ishii et al., 1997), it is possible that those two residues, together with the identified amino acids in L3, are necessary to generate a high-affinity receptor for apamin. Several possibilities could be considered to explain how these two regions of the channel affect the sensitivity of SK subunits towards apamin. One possibility is that the contribution of L3 to apamin sensitivity is mediated by an indirect effect. It might be that the T216S mutation in hSK1 or the L3 substitution in $rSK1_{NSK2\text{-}CSK2}$ result in a conformational change of the pore that favours the binding of apamin. In this model, the amino acids located in L3 would not participate to the formation of the toxin receptor but would rather affect the conformation of the outer vestibule, thereby influencing the pharmacological properties of SK channel α subunits. Electrophysiological experiments using TEA, a classic pore blocker, were performed to test whether T216 mutation introduces changes in the architectural organization of the pore (A. Nolting personal communication). The results indicated that TEA sensitivity of hSK1-T216S did not differ from that of hSK1, supporting the view that the mutation T216S did not alter the channel structure.

Alternatively, L3 might influence the binding of apamin by taking part in the formation of the toxin-binding receptor. In this model, crucial residues of L3 might directly interact with amino acids on the surface of the toxin, thereby stabilizing its binding to the channel pore. This model implies that there should be close proximity

between L3 and the pore region of SK subunits. Studies on voltage-gated K^+ channels have indicated that S4 is positioned close to the pore domain (Laine et al., 2003; Lai et al., 2005). If a similar structural organisation occurs also in SK channel α subunits, L3 might be close to the outer pore and be therefore part of the apamin receptor. However, to date, there is no evidence for this prediction.

Sequence alignment of the different SK L3 loops revealed that the serine that confers increased sensitivity to hSK1 in the mutant hSK1-T216S is conserved in rSK2, rSK3 and rSK1(in bold in Fig. 7.5) but not in hSK1, which has a threonine in the corresponding position (in red in Fig. 7.5). Although the lack of apamin sensitivity exhibited by rSK1 cannot be explained on the basis of this single residue, it might be possible that other amino acids located in the same region account for the differences. Close inspection of the sequences indicated that four amino acids differ between hSK1 and rSK1 (Fig. 7.5). Among these four residues, the observation that the tyrosine (Y217 in hSK1) is conserved in all the apamin sensitive channels, hSK1, rSK2 and rSK3, is of particular interest. Further mutations might clarify this aspect.

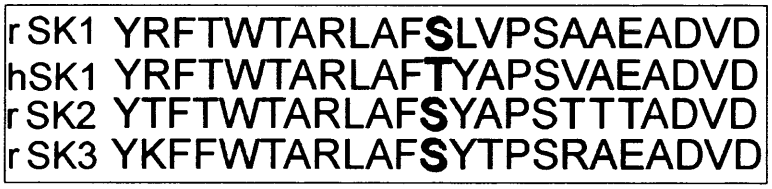

FIGURE 8.1: Sequence alignment in the L3 region of hSK1, rSK1, rSK2 and rSK3.

In conclusion, the results reported in this chapter represent the first indication that a region outside the pore of SK channel subunits contributes to apamin sensitivity. In particular, we found that the L3 extracellular loop connecting transmembrane segments S3 and S4 largely accounts for the difference in apamin sensitivity between different SK channel subunits. Further studies are necessary to elucidate the mechanism by which L3 affects the sensitivity to the toxin.

References

Adelman JP, Shen KZ, Kavanaugh MP, Warren RA, Wu YN, Lagrutta A, Bond CT, North RA (1992) Calcium-activated potassium channels expressed from cloned complementary DNAs. Neuron 9:209-216.

Alexander SP, Mathie A, Peters JA (2004) Guide to receptors and channels, 1st edition. Br J Pharmacol 141:S1-126.

Armstrong WE, Rubrum A, Teruyama R, Bond CT, Adelman JP (2005) Immunocytochemical localization of small-conductance, calcium-dependent potassium channels in astrocytes of the rat supraoptic nucleus. J Comp Neurol 491:175-185.

Ashcroft F (2000). Ion channels and disease. University of Oxford, U.K.

Atkinson NS, Robertson GA, Ganetzky B (1991) A Component of calcium-activated potassium channels encoded by the Drosophila slo locus. Science 253:551-555.

Avanzini G, de Curtis M, Panzica F, Spreafico R (1989) Intrinsic properties of nucleus reticularis thalami neurones of the rat studied in vitro. J Physiol 416:111-122.

Bal T, McCormick DA (1993) Mechanisms of oscillatory activity in guinea-pig nucleus reticularis thalami in vitro: a mammalian pacemaker. J Physiol 468:669-691.

Bayliss DA, Umemiya M, Berger AJ (1995) Inhibition of N- and P-type calcium currents and the after-hyperpolarization in rat motoneurones by serotonin. J Physiol 485:635-647.

Bennett ES (2002) Isoform-specific effects of sialic acid on voltage-dependent Na^+ channel gating: functional sialic acids are localized to the S5-S6 loop of domain I. J Physiol 538:675-690.

Benton DC, Monaghan AS, Hosseini R, Bahia PK, Haylett DG, Moss GW (2003) Small conductance Ca^{2+}-activated K^+ channels formed by the expression of rat SK1 and SK2 genes in HEK 293 cells. J Physiol 553:13-19.

Bichet D, Haass FA, Jan LY (2003) Merging functional studies with structures of inward-rectifier K^+ channels. Nat Rev Neurosci 4:957-967.

Bildl W, Strassmaier T, Thurm H, Andersen J, Eble S, Oliver D, Knipper M, Mann M, Schulte U, Adelman JP, Fakler B (2004) Protein kinase CK2 is coassembled with small conductance Ca^{2+}-activated K^+ channels and regulates channel gating. Neuron 43:847-858.

Bond CT, Herson PS, Strassmaier T, Hammond R, Stackman R, Maylie J, Adelman JP (2004) Small conductance Ca^{2+}-activated K^+ channel knock-out mice reveal the identity of calcium-dependent afterhyperpolarization currents. J Neurosci 24:5301-5306.

Bond CT, Sprengel R, Bissonnette JM, Kaufmann WA, Pribnow D, Neelands T, Storck T, Baetscher M, Jerecic J, Maylie J, Knaus HG, Seeburg PH, Adelman JP (2000) Respiration and parturition affected by conditional overexpression of the Ca^{2+}-activated K^+ channel subunit, SK3. Science 289:1942-1946.

Bosch MA, Kelly MJ, Ronnekleiv OK (2002) Distribution, neuronal colocalization, and 17beta-E2 modulation of small conductance calcium-activated K^+ channel SK3 mRNA in the guinea pig brain. Endocrinology 143:1097-1107.

Bourque CW, Brown DA (1987) Apamin and d-tubocurarine block the afterhyperpolarization of rat supraoptic neurosecretory neurons. Neurosci Lett 82:185-190.

Bowden SE, Fletcher S, Loane DJ, Marrion NV (2001) Somatic colocalization of rat SK1 and D class (Cav1.2) L-type calcium channels in rat CA1 hippocampal pyramidal neurons. J Neurosci 21:RC175.

Brenner R, Jegla TJ, Wickenden A, Liu Y, Aldrich RW (2000) Cloning and functional characterization of novel large conductance calcium-activated

potassium channel beta subunits, hKCNMB3 and hKCNMB4. J Biol Chem 275:6453-6461.

Brewer GJ (1997) Isolation and culture of adult rat hippocampal neurons. J Neurosci Methods 71:143-155.

Burnard DM, Crichton SA, MacVicar BA (1990) Electrophysiological properties of reactive glial cells in the kainate-lesioned hippocampal slice. Brain Res 510:43-52.

Butler A, Tsunoda S, McCobb DP, Wei A, Salkoff L (1993) mSlo, a complex mouse gene encoding "Maxi" calcium acitvated potassium channels. Science 261:221-224.

Bychkov R, Glowinski J, Giaume C (2001) Sequential and opposite regulation of two outward K^+ currents by ET-1 in cultured striatal astrocytes. Am J Physiol Cell Physiol 281:C1373-1384.

Cai X, Liang CW, Muralidharan S, Kao JP, Tang CM, Thompson SM (2004) Unique roles of SK and Kv4.2 potassium channels in dendritic integration. Neuron 44:351-364.

Castle NA, London DO, Creech C, Fajloun Z, Stocker JW, Sabatier JM (2003) Maurotoxin: a potent inhibitor of intermediate conductance Ca^{2+}-activated potassium channels. Mol Pharmacol 63:409-418.

Castellino RC, Morales MJ, Strauss HC, Rasmusson RL (1995) Time-dependent and voltage-dependent modulation of a Kv1.4 channel by a beta-subunit (Kv-beta-3) cloned from ferret ventricle. American Journal of Physiology-Heart and Circulatory 38:H 385-391.

Chandy KG, Fantino E, Wittekindt O, Kalman K, Tong LL, Ho TH, Gutman GA, Crocq MA, Ganguli R, Nimgaonkar V, Morris-Rosendahl DJ, Gargus JJ (1998) Isolation of a novel potassium channel gene hSKCa3 containing a polymorphic CAG repeat: a candidate for schizophrenia and bipolar disorder? Mol Psychiatry 3:32-37.

Chavis P, Ango F, Michel JM, Bockaert J, Fagni L (1998) Modulation of big K^+ channel activity by ryanodine receptors and L-type Ca^{2+} channels in neurons. Eur J Neurosci 10:2322-2327.

Chicchi GG, Gimenez-Gallego G, Ber E, Garcia ML, Winquist R, Cascieri MA (1988) Purification and characterization of a unique, potent inhibitor of apamin binding from Leiurus quinquestriatus hebraeus venom. J Biol Chem 263:10192-10197.

Cingolani LA, Gymnopoulos M, Boccaccio A, Stocker M, Pedarzani P (2002) Developmental regulation of small-conductance Ca^{2+}-activated K^+ channel expression and function in rat Purkinje neurons. J Neurosci 22:4456-4467.

Coetzee WA, Amarillo Y, Chiu J, Chow A, Lau D, McCormack T, Moreno H, Nadal MS, Ozaita A, Pountney D, Saganich M, Vega-Saenz de Miera E, Rudy B (1999) Molecular diversity of K^+ channels. Ann N Y Acad Sci 868:233-285.

Coles JA, Poulain DA (1991) Extracellular K^+ in the supraoptic nucleus of the rat during reflex bursting activity by oxytocin neurones. J Physiol 439:383-409.

Cui J, Cox DH, Aldrich RW (1997) Intrinsic voltage dependence and Ca^{2+} regulation of mslo large conductance Ca^{2+}-activated K^+ channels. J Gen Physiol 109:647-673.

Dale TJ, Cryan JE, Chen MX, Trezise DJ (2002) Partial apamin sensitivity of human small conductance Ca^{2+}-activated K^+ channels stably expressed in Chinese hamster ovary cells. Naunyn Schmiedebergs Arch Pharmacol 366:470-477.

Deutsch C (2002) Potassium channel ontogeny. Annu Rev Physiol 64:19-46.

D'Hoedt D, Dissertation, München (2004) Structure-function analyses of small-conductance, calcium-activated potassium channels.

D'Hoedt D, Hirzel K, Pedarzani P, Stocker M (2004) Domain analysis of the calcium-activated potassium channel SK1 from rat brain. Functional expression and toxin sensitivity. J Biol Chem 279:12088-12092.

Devor DC, Singh AK, Bridges RJ, Frizzell RA (1996) Modulation of Cl^- secretion by benzimidazolones. II. Coordinate regulation of apical GCl and basolateral GK. Am J Physiol 271:L785-795.

Dodd PR, Hardy JA, Oakley AE, Edwardson JA, Perry EK, Delaunoy JP (1981) A rapid method for preparing synaptosomes: comparison, with alternative procedures. Brain Res 226:107-118.

Dotti CG, Simons K (1990) Polarized sorting of viral glycoproteins to the axon and dendrites of hippocampal neurons in culture. Cell 62:63-72.

Doyle DA, Cabral JM, Pfuetzner RA, Kuo AL, Gulbis JM, Cohen SL, Chait BT, MacKinnon R (1998) The structure of the potassium channel - molecular basis of K^+ conduction and selectivity. Science 280:69-77.

Dworetzky SI, Boissard CG, Lumragan JT, McKay MC, Postmunson DJ, Trojnacki JT, Chang CP, Gribkoff VK (1996) Phenotypic alteration of a human BK (hslo) channel by hslo-beta subunit coexpression - changes in blocker sensitivity, activation/relaxation and inactivation kinetics, and protein kinase a modulation. J Neurosci 16:4543-4550.

Edgerton JR, Reinhart PH (2003) Distinct contributions of small and large conductance Ca^{2+}-activated K^+ channels to rat Purkinje neuron function. J Physiol 548:53-69.

Faber ES, Sah P (2002) Physiological role of calcium-activated potassium currents in the rat lateral amygdala. J Neurosci 22:1618-1628.

Faber ES, Delaney AJ, Sah P (2005) SK channels regulate excitatory synaptic transmission and plasticity in the lateral amygdala. Nat Neurosci 8:635-641.

Fink M, Duprat F, Lesage F, Heurteaux C, Romey G, Barhanin J, Lazdunski M (1996) A new K^+ channel beta subunit to specifically enhance Kv2.2 (cdrk) expression. J of Biol Chem 271:26341-26348.

Freedman JE, Aghajanian GK (1987) Role of phosphoinositide metabolites in the prolongation of afterhyperpolarizations by alpha 1-adrenoceptors in rat dorsal raphe neurons. J Neurosci 7:3897-3906.

Fujita A, Takeuchi T, Hanai J, Hata F (2003) Expression of the small conductance Ca^{2+}-activated K^+ channel, SK3, in the olfactory ensheathing glial cells of rat brain. Cell Tissue Res 313:187-193.

Galvez A, Gimenez-Gallego G, Reuben JP, Roy-Contancin L, Feigenbaum P, Kaczorowski GJ, Garcia ML (1990) Purification and characterization of a unique, potent, peptidyl probe for the high conductance calcium-activated potassium channel from venom of the scorpion Buthus tamulus. J Biol Chem 265:11083-11090.

Gargus JJ, Fantino E, Gutman GA (1998) A piece in the puzzle: an ion channel candidate gene for schizophrenia. Mol Med Today 4:518-524.

Goldstein SA, Bayliss DA, Kim D, Lesage F, Plant LD, Rajan S (2005) International Union of Pharmacology. LV. Nomenclature and molecular relationships of two-P potassium channels. Pharmacol Rev 57:527-540.

Goldstein SA, Wang KW, Ilan N, Pausch MH (1998) Sequence and function of the two P domain potassium channels: implications of an emerging superfamily. J Mol Med 76:13-20.

Grunnet M, Jensen BS, Olesen SP, Klaerke DA (2001a) Apamin interacts with all subtypes of cloned small-conductance Ca^{2+}-activated K^+ channels. Pflugers Arch 441:544-550.

Grunnet M, Jespersen T, Angelo K, Frokjaer-Jensen C, Klaerke DA, Olesen SP, Jensen BS (2001b) Pharmacological modulation of SK3 channels. Neuropharmacology 40:879-887.

Gutman GA, Chandy KG, Grissmer S, Lazdunski M, McKinnon D, Pardo LA, Robertson GA, Rudy B, Sanguinetti MC, Stuhmer W, Wang X (2005)

International Union of Pharmacology. LIII. Nomenclature and molecular relationships of voltage-gated potassium channels. Pharmacol Rev 57:473-508.

Habermann E (1972) Bee and wasp venoms. Science 177:314-322.

Habermann E, Fischer K (1979) Bee venom neurotoxin (apamin): iodine labeling and characterization of binding sites. Eur J Biochem 94:355-364.

Heginbotham L, Lu Z, Abramson T, MacKinnon R (1994) Mutations in the K^+ channel signature sequence. Biophys J 66:1061-1067.

Herlenius E, Lagercrantz H (2004) Development of neurotransmitter systems during critical periods. Exp Neurol 190:S8-21.

Hicke L (1997) Ubiquitin-dependent internalization and down-regulation of plasma membrane proteins. Faseb J 11:1215-1226.

Hicke L, Dunn R (2003) Regulation of membrane protein transport by ubiquitin and ubiquitin-binding proteins. Annu Rev Cell Dev Biol 19:141-172.

Hille B (1992) Ionic Channels of Excitable Membranes. Sunderland, MA: Sinauer Associates.

Hirschberg B, Maylie J, Adelman JP, Marrion NV (1998) Gating of recombinant small-conductance Ca-activated K^+ channels by calcium. J Gen Physiol 111:565-581.

Ho SN, Hunt HD, Horton RM, Pullen JK, Pease LR (1989) Site-directed mutagenesis by overlap extension using the polymerase chain reaction. Gene 77:51-59.

Horrigan FT, Aldrich RW (2002) Coupling between voltage sensor activation, Ca^{2+} binding and channel opening in large conductance (BK) potassium channels. J Gen Physiol 120:267-305.

Horrigan FT, Cui J, Aldrich RW (1999) Allosteric voltage gating of potassium channels I. Mslo ionic currents in the absence of Ca^{2+}. J Gen Physiol 114:277-304.

Horton RM, Hunt HD, Ho SN, Pullen JK, Pease LR (1989) Engineering hybrid genes without the use of restriction enzymes: gene splicing by overlap extension. Gene 77:61-68.

Hosseini R, Benton DC, Dunn PM, Jenkinson DH, Moss GW (2001) SK3 is an important component of K^+ channels mediating the afterhyperpolarization in cultured rat SCG neurones. J Physiol 535:323-334.

Hu H, Shao LR, Chavoshy S, Gu N, Trieb M, Behrens R, Laake P, Pongs O, Knaus HG, Ottersen OP, Storm JF (2001) Presynaptic Ca^{2+}-activated K^+ channels in glutamatergic hippocampal terminals and their role in spike repolarization and regulation of transmitter release. J Neurosci 21:9585-9597.

Isaacson JS, Murphy GJ (2001) Glutamate-mediated extrasynaptic inhibition: direct coupling of NMDA receptors to Ca^{2+}-activated K^+ channels. Neuron 31:1027-1034.

Ishii TM, Silvia C, Hirschberg B, Bond CT, Adelman JP, Maylie J (1997a) A human intermediate conductance calcium-activated potassium channel. Proc Natl Acad Sci U S A 94:11651-11656.

Ishii TM, Maylie J, Adelman JP (1997b) Determinants of apamin and d-tubocurarine block in SK potassium channels. J Biol Chem 272:23195-23200.

Lai HC, Grabe M, Jan YN, Jan LY (2005) The S4 voltage sensor packs against the pore domain in the KAT1 voltage-gated potassium channel. Neuron 47:395-406.

Laine M, Lin MC, Bannister JP, Silverman WR, Mock AF, Roux B, Papazian DM (2003) Atomic proximity between S4 segment and pore domain in Shaker potassium channels. Neuron 39:467-481

Jager H, Grissmer S (2004) Characterization of the outer pore region of the apamin-sensitive Ca^{2+}-activated K^+ channel rSK2. Toxicon 43:951-960.

Jalonen TO, Margraf RR, Wielt DB, Charniga CJ, Linne ML, Kimelberg HK (1997) Serotonin induces inward potassium and calcium currents in rat cortical astrocytes. Brain Res 758:69-82.

Jan LY and Jan YN (2004) Molecular properties of ion channels, "Molecules to Networks." Byrne J and Roberts J. Academic Press.

Jenke M, Sanchez A, Monje F, Stuhmer W, Weseloh RM, Pardo LA (2003) C-terminal domains implicated in the functional surface expression of potassium channels. Embo J 22:395-403.

Jensen BS, Strobaek D, Christophersen P, Jorgensen TD, Hansen C, Silahtaroglu A, Olesen SP, Ahring PK (1998) Characterization of the cloned human intermediate-conductance Ca^{2+}-activated K^+ channel. Am J Physiol 275:C848-856.

Johnston JA, Ward CL, Kopito RR (1998) Aggresomes: a cellular response to misfolded proteins. J Cell Biol 143:1883-1898.

Joiner WJ, Wang LY, Tang MD, Kaczmarek LK (1997) hSK4, a member of a novel subfamily of calcium-activated potassium channels. Proc Natl Acad Sci U S A 94:11013-11018.

Jones HM, Hamilton KL, Devor DC (2005) Role of an S4-S5 linker lysine in the trafficking of the Ca^{2+}-activated K^+ channels IK1 and SK3. J Biol Chem 280:37257-37265.

Joober R, Benkelfat C, Brisebois K, Toulouse A, Lafreniere RG, Turecki G, Lal S, Bloom D, Labelle A, Lalonde P, Fortin D, Alda M, Palmour R, Rouleau GA (1999) Lack of association between the hSKCa3 channel gene CAG polymorphism and schizophrenia. Am J Med Genet 88:154-157.

Kaczorowski GJ, Knaus HG, Leonard RJ, McManus OB, Garcia ML (1996) High-conductance calcium-activated potassium channels; structure, pharmacology, and function. J Bioenerg Biomembr 28:255-267.

Kawai T, Watanabe M (1986) Blockade of Ca^{2+}-activated K^+ conductance by apamin in rat sympathetic neurones. Br J Pharmacol 87:225-232.

Keen JE, Khawaled R, Farrens DL, Neelands T, Rivard A, Bond CT, Janowsky A, Fakler B, Adelman JP, Maylie J (1999) Domains responsible for constitutive and Ca^{2+}-dependent interactions between calmodulin and small conductance Ca^{2+}-activated potassium channels. J Neurosci 19:8830-8838.

Kerschensteiner D, Dissertation, Göttingen (2003). Regulation spannungs- und Ca^{2+}-abhängiger Kaliumkanäle durch modulatorische a-Untereinheiten und alternatives Spleißen.

Kim CL, Umetani A, Matsui T, Ishiguro N, Shinagawa M, Horiuchi M (2004) Antigenic characterization of an abnormal isoform of prion protein using a new diverse panel of monoclonal antibodies. Virology 320:40-51.

Kirkpatrick K, Bourque CW (1996) Activity dependence and functional role of the apamin-sensitive K^+ current in rat supraoptic neurones in vitro. J Physiol 494:389-398.

Knaus H-G, Folander K, Garcia-Calvo M, Garcia ML, Kaczorowski GJ, Smith M, Swanson R (1994) Primary Sequence and Immunological Characterization of β-Subunit of High Conductance Ca^{2+}-activated K^+ Channel from Smooth Muscle. J Biol Chem 269:17274-17278.

Kobayashi YM, Jones LR (1999) Identification of triadin 1 as the predominant triadin isoform expressed in mammalian myocardium. J Biol Chem 274:28660-28668.

Kohler M, Hirschberg B, Bond CT, Kinzie JM, Marrion NV, Maylie J, Adelman JP (1996) Small-conductance, calcium-activated potassium channels from mammalian brain. Science 273:1709-1714.

Kolski-Andreaco A, Tomita H, Shakkottai VG, Gutman GA, Cahalan MD, Gargus JJ, Chandy KG (2004) SK3-1C, a dominant-negative suppressor of SKCa and IKCa channels. J Biol Chem 279:6893-6904.

Latorre R, Oberhauser A, Labarca P, Alvarez O (1989) Varieties of calcium-activated potassium channels. Annu Rev Physiol 51:385-399.

Lee WS, Ngo-Anh TJ, Bruening-Wright A, Maylie J, Adelman JP (2003) Small conductance Ca^{2+}-activated K^+ channels and calmodulin: cell surface expression and gating. J Biol Chem 278:25940-25946.

Lesage F, Reyes R, Fink M, Duprat F, Guillemare E, Lazdunski M (1996) Dimerization of TWIK-1 K^+ channel subunits via a disulfide bridge. Embo J 15:6400-6407.

Liman ER, Tytgat J, Hess P (1992) Subunit stoichiometry of a mammalian K^+ channel determined by construction of multimeric cDNAs. Neuron 9:861-871.

Logsdon NJ, Kang J, Togo JA, Christian EP, Aiyar J (1997) A novel gene, hKCa4, encodes the calcium-activated potassium channel in human T lymphocytes. J Biol Chem 272:32723-32726.

Lowry OH, Rosebrough NJ, Farr AL, Randall RJ (1951) Protein measurement with the Folin phenol reagent. J Biol Chem 193:265-275.

Ma D, Jan LY (2002) ER transport signals and trafficking of potassium channels and receptors. Curr Opin Neurobiol 12:287-292.

MacKinnon R (1991) Determination of the subunit stoichiometry of a voltage-activated potassium channel. Nature 350:232-235.

MacKinnon R (2003) Potassium channels. FEBS Lett 555:62-65.

Marty A (1989) The physiological role of calcium-dependent channels. Trends Neurosci 12:420-424.

McManus OB, Helms LM, Pallanck L, Ganetzky B, Swanson R, Leonard RJ (1995) Functional role of the beta subunit of high conductance calcium-activated potassium channels. Neuron 14:645-650.

Meera P, Wallner M, Toro L (2000) A neuronal beta subunit (KCNMB4) makes the large conductance, voltage- and Ca^{2+}-activated K^+ channel resistant to charybdotoxin and iberiotoxin. Proc Natl Acad Sci USA 97:5562-5567.

Meera P, Wallner M, Song M, Toro L (1997) Large conductance voltage- and calcium-dependent K^+ channel, a distinct member of voltage-dependent ion channels with seven N-terminal transmembrane segments (S0-S6), an extracellular N terminus, and an intracellular (S9-S10) C terminus. Proc Natl Acad Sci USA 94:14066-14071.

Miller C (2001) See potassium run. Nature 414:23-24.

Miller MJ, Rauer H, Tomita H, Gargus JJ, Gutman GA, Cahalan MD, Chandy KG (2001) Nuclear localization and dominant-negative suppression by a mutant SKCa3 N-terminal channel fragment identified in a patient with schizophrenia. J Biol Chem 276:27753-27756.

Misonou H, Mohapatra DP, Menegola M, Trimmer JS (2005) Calcium- and metabolic state-dependent modulation of the voltage-dependent Kv2.1 channel regulates neuronal excitability in response to ischemia. J Neurosci 25:11184-11193.

Monaghan AS, Benton DC, Bahia PK, Hosseini R, Shah YA, Haylett DG, Moss GW (2004) The SK3 subunit of small conductance $Ca2^+$-activated K^+ channels interacts with both SK1 and SK2 subunits in a heterologous expression system. J Biol Chem 279:1003-1009.

Morais-Cabral JH, Zhou Y, MacKinnon R (2001) Energetic optimization of ion conduction rate by the K^+ selectivity filter. Nature 414:37-42.

Morales MJ, Castellino RC, Crews AL, Rasmusson RL, Strauss HC (1995) A novel beta-subunit increases rate of inactivation of specific voltage-gated potassium channel alpha-subunits. J Biol Chem 270:6272-6277.

Ngo-Anh TJ, Bloodgood BL, Lin M, Sabatini BL, Maylie J, Adelman JP (2005) SK channels and NMDA receptors form a Ca^{2+}-mediated feedback loop in dendritic spines. Nat Neurosci 8:642-649.

Nimigean CM, Magleby KL (1999) The beta subunit increases the Ca^{2+} sensitivity of large conductance Ca^{2+}-activated potassium channels by retaining the gating in the bursting states. J Gen Physiol 113:425-440.

O'Donovan MJ (1999) The origin of spontaneous activity in developing networks of the vertebrate nervous system. Curr Opin Neurobiol 9:94-104.

Obermair GJ, Kaufmann WA, Knaus HG, Flucher BE (2003) The small conductance Ca^{2+}-activated K^+ channel SK3 is localized in nerve terminals of excitatory synapses of cultured mouse hippocampal neurons. Eur J Neurosci 17:721-731.

Orio P, Rojas P, Ferreira G, Latorre R (2002) New disguises for an old channel: MaxiK channel beta-subunits. News Physiol Sci 17:156-161.

Osmanovic SS, Shefner SA (1993) Calcium-activated hyperpolarizations in rat locus coeruleus neurons in vitro. J Physiol 469:89-109.

Osmanovic SS, Shefner SA, Brodie MS (1990) Functional significance of the apamin-sensitive conductance in rat locus coeruleus neurons. Brain Res 530:283-289.

Papazian DM, Timpe LC, Jan Y-N, Jan L-Y (1991) Alteration of voltage-dependence of Shaker potassium channel by mutations in the S4 sequence. Nature 349:305-310.

Paxinos G and Watson C (1998) The rat brain in stereotaxic coordinates. Fourth edition. Academic Press.

Pedarzani P, Kulik A, Muller M, Ballanyi K, Stocker M (2000) Molecular determinants of Ca^{2+}-dependent K^+ channel function in rat dorsal vagal neurones. J Physiol 527:283-290.

Pedarzani P, Mosbacher J, Rivard A, Cingolani LA, Oliver D, Stocker M, Adelman JP, Fakler B (2001) Control of electrical activity in central neurons by modulating the gating of small conductance Ca^{2+}-activated K^+ channels. J Biol Chem 276:9762-9769.

Pedarzani P, D'Hoedt D, Doorty KB, Wadsworth JD, Joseph JS, Jeyaseelan K, Kini RM, Gadre SV, Sapatnekar SM, Stocker M, Strong PN (2002) Tamapin, a venom peptide from the Indian red scorpion (Mesobuthus tamulus) that targets small conductance Ca^{2+}-activated K^+ channels and afterhyperpolarization currents in central neurons. J Biol Chem 277:46101-46109.

Pedersen KA, Schroder RL, Skaaning-Jensen B, Strobaek D, Olesen SP, Christophersen P (1999) Activation of the human intermediate-conductance Ca^{2+}-activated K^+ channel by 1-ethyl-2-benzimidazolinone is strongly Ca^{2+}-dependent. Biochim Biophys Acta 1420:231-240.

Piskorowski R, Aldrich RW (2002) Calcium activation of BK_{Ca} potassium channels lacking the calcium bowl and RCK domains. Nature 420:499-502.

Pongs O (1992) Molecular biology of voltage-dependent potassium channels. Physiol Rev 72:S69-88.

Powers RK, Sawczuk A, Musick JR, Binder MD (1999) Multiple mechanisms of spike-frequency adaptation in motoneurones. J Physiol Paris 93:101-114.

Rapoport JL, Addington AM, Frangou S, Psych MR (2005) The neurodevelopmental model of schizophrenia: update 2005. Mol Psychiatry 10:434-449.

Reineke U, Ivascu C, Schlief M, Landgraf C, Gericke S, Zahn G, Herzel H, Volkmer-Engert R, Schneider-Mergener J (2002) Identification of distinct antibody epitopes and mimotopes from a peptide array of 5520 randomly generated sequences. J Immunol Methods 267:37-51.

Reinhart PH, Chung S, Levitan IB (1989) A family of calcium-dependent potassium channels from rat brain. Neuron 2:1031-1041.

Ren Y, Barnwell LF, Alexander JC, Lubin FD, Adelman JP, Pfaffinger PJ, Schrader LA, Anderson AE (2006) Regulation of surface localization of the small conductance Ca^{2+}-activated potassium channel, SK2, through direct phosphorylation by cAMP-dependent protein kinase. J Biol Chem 281:11769-11779.

Rettig J, Heinemann SH, Wunder F, Lorra C, Parcej DN, Dolly JO, Pongs O (1994) Inactivation properties of voltage-gated K^+ channels altered by presence of β-subunit. Nature 369:289-294.

Roncarati R, Decimo I, Fumagalli G (2005) Assembly and trafficking of human small conductance Ca^{2+}-activated K^+ channel SK3 are governed by different molecular domains. Mol Cell Neurosci 28:314-325.

Roncarati R, Di Chio M, Sava A, Terstappen GC, Fumagalli G (2001) Presynaptic localization of the small conductance calcium-activated potassium channel SK3 at the neuromuscular junction. Neuroscience 104:253-262.

Sah P (1996) Ca^{2+}-activated K^+ currents in neurones: types, physiological roles and modulation. Trends Neurosci 19:150-154.

Sah P, Davies P (2000) Calcium-activated potassium currents in mammalian neurons. Clin Exp Pharmacol Physiol 27:657-663.

Sah P, Faber ES (2002) Channels underlying neuronal calcium-activated potassium currents. Prog Neurobiol 66:345-353.

Sailer CA, Kaufmann WA, Marksteiner J, Knaus HG (2004) Comparative immunohistochemical distribution of three small-conductance Ca^{2+}-activated potassium channel subunits, SK1, SK2, and SK3 in mouse brain. Mol Cell Neurosci 26:458-469.

Sailer CA, Hu H, Kaufmann WA, Trieb M, Schwarzer C, Storm JF, Knaus HG (2002) Regional differences in distribution and functional expression of small-conductance Ca^{2+}-activated K^+ channels in rat brain. J Neurosci 22:9698-9707.

Sanchez M, McManus OB (1996) Paxilline inhibition of the alpha-subunit of the high-conductance calcium-activated potassium channel. Neuropharmacology 35:963-968.

Sarpal D, Koenig JI, Adelman JP, Brady D, Prendeville LC, Shepard PD (2004) Regional distribution of SK3 mRNA-containing neurons in the adult and adolescent rat ventral midbrain and their relationship to dopamine-containing cells. Synapse 53:104-113.

Savic N, Pedarzani P, Sciancalepore M (2001) Medium afterhyperpolarization and firing pattern modulation in interneurons of stratum radiatum in the CA3 hippocampal region. J Neurophysiol 85:1986-1997.

Schiess MC, Callahan PM, Zheng H (1999) Characterization of the electrophysiological and morphological properties of rat central amygdala neurons in vitro. J Neurosci Res 58:663-673.

Schreiber M, Salkoff L (1997) A novel calcium-sensing domain in the BK channel. Biophys J 73:1355-1363.

Schreiber M, Yuan A, Salkoff L (1999) Transplantable sites confer calcium sensitivity to BK channels. Nat Neurosci 2:416-421.

Schumacher MA, Rivard AF, Bachinger HP, Adelman JP (2001) Structure of the gating domain of a Ca^{2+}-activated K^+ channel complexed with Ca^{2+}/calmodulin. Nature 410:1120-1124.

Schwindt PC, Spain WJ, Crill WE (1992) Calcium-dependent potassium currents in neurons from cat sensorimotor cortex. J Neurophysiol 67:216-226.

Shah M, Haylett DG (2000) The pharmacology of hSK1 Ca^{2+}-activated K^+ channels expressed in mammalian cell lines. Br J Pharmacol 129:627-630.

Shakkottai VG, Chou CH, Oddo S, Sailer CA, Knaus HG, Gutman GA, Barish ME, LaFerla FM, Chandy KG (2004) Enhanced neuronal excitability in the absence of neurodegeneration induces cerebellar ataxia. J Clin Invest 113:582-590.

Shakkottai VG, Regaya I, Wulff H, Fajloun Z, Tomita H, Fathallah M, Cahalan MD, Gargus JJ, Sabatier JM, Chandy KG (2001) Design and characterization of a highly selective peptide inhibitor of the small conductance calcium-activated K^+ channel, SkCa2. J Biol Chem 276:43145-43151.

Shi GY, Nakahira K, Hammond S, Rhodes KJ, Schechter LE, Trimmer JS (1996) Beta subunits promote K^+ channel surface expression through effects early in biosynthesis. Neuron 16:843-852.

Shibata R, Misonou H, Campomanes CR, Anderson AE, Schrader LA, Doliveira LC, Carroll KI, Sweatt JD, Rhodes KJ, Trimmer JS (2003) A fundamental role for KChIPs in determining the molecular properties and trafficking of Kv4.2 potassium channels. J Biol Chem 278:36445-36454.

Shipston MJ (2001) Alternative splicing of potassium channels: a dynamic switch of cellular excitability. Trends Cell Biol 11:353-358.

Shmukler BE, Bond CT, Wilhelm S, Bruening-Wright A, Maylie J, Adelman JP, Alper SL (2001) Structure and complex transcription pattern of the mouse SK1 K_{Ca} channel gene, KCNN1. Biochim Biophys Acta 1518:36-46.

Silva-Neto MA, Atella GC, Fialho E, Paes MC, Zingali RB, Petretski JH, Alves EW, Masuda H (1996) Isolation of a calcium-binding phosphoprotein from the oocytes and hemolymph of the blood-sucking insect Rhodnius prolixus. J Biol Chem 271:30227-30232.

Sontheimer H (1994) Voltage-dependent ion channels in glial cells. Glia 11:156-172.

Spitzer NC, Olson E, Gu X (1995) Spontaneous calcium transients regulate neuronal plasticity in developing neurons. J Neurobiol 26:316-324.

Stocker M, Pedarzani P (2000) Differential distribution of three Ca^{2+}-activated K^+ channel subunits, SK1, SK2, and SK3, in the adult rat central nervous system. Mol Cell Neurosci 15:476-493.

Stocker M, Krause M, Pedarzani P (1999) An apamin-sensitive Ca^{2+}-activated K^+ current in hippocampal pyramidal neurons. Proc Natl Acad Sci U S A 96:4662-4667.

Stocker M, Hirzel K, D'Hoedt D, Pedarzani P (2004a) Matching molecules to function: neuronal Ca^{2+}-activated K^+ channels and afterhyperpolarizations. Toxicon 43:933-949.

Stocker M (2004b) Ca^{2+}-activated K^+ channels: molecular determinants and function of the SK family. Nat Rev Neurosci 5:758-770.

Storm JF (1990) Potassium currents in hippocampal pyramidal cells. Prog Brain Res 83:161-187.

Storm JF (1987) Action potential repolarization and a fast after-hyperpolarization in rat hippocampal pyramidal cells. J Physiol 385:733-759.

Stowell JN, Craig AM (1999) Axon/dendrite targeting of metabotropic glutamate receptors by their cytoplasmic carboxy-terminal domains. Neuron 22:525-536.

Strassmaier T, Bond CT, Sailer CA, Knaus HG, Maylie J, Adelman JP (2005) A novel isoform of SK2 assembles with other SK subunits in mouse brain. J Biol Chem 280:21231-21236.

Strobaek D, Jorgensen TD, Christophersen P, Ahring PK, Olesen SP (2000) Pharmacological characterization of small-conductance Ca^{2+}-activated K^+ channels stably expressed in HEK 293 cells. Br J Pharmacol 129:991-999.

Stuhmer W, Ruppersberg JP, Schroter KH, Sakmann B, Stocker M, Giese KP, Perschke A, Baumann A, Pongs O (1989) Molecular basis of functional diversity of voltage-gated potassium channels in mammalian brain. Embo J 8:3235-3244.

Tacconi S, Carletti R, Bunnemann B, Plumpton C, Merlo Pich E, Terstappen GC (2001) Distribution of the messenger RNA for the small conductance calcium-activated potassium channel SK3 in the adult rat brain and correlation with immunoreactivity. Neuroscience 102:209-215.

Tempel BL, Papazian DM, Schwarz TL, Jan YN, Jan LY (1987) Sequence of a probable potassium channel component encoded at Shaker locus of Drosophila. Science 237:770-775.

Terstappen GC, Pula G, Carignani C, Chen MX, Roncarati R (2001) Pharmacological characterisation of the human small conductance calcium-activated potassium channel hSK3 reveals sensitivity to tricyclic antidepressants and antipsychotic phenothiazines. Neuropharmacology 40:772-783.

Tian L, Duncan RR, Hammond MS, Coghill LS, Wen H, Rusinova R, Clark AG, Levitan IB, Shipston MJ (2001) Alternative splicing switches potassium channel sensitivity to protein phosphorylation. J Biol Chem 276:7717-7720.

Tomita H, Shakkottai VG, Gutman GA, Sun G, Bunney WE, Cahalan MD, Chandy KG, Gargus JJ (2003) Novel truncated isoform of SK3 potassium channel is a potent dominant-negative regulator of SK currents: implications in schizophrenia. Mol Psychiatry 8:524-535, 460.

Trimmer JS (1998) Regulation of ion channel expression by cytoplasmic subunits. Curr Opin Neurobiol 8:370-374.

Trimmer JS, Rhodes KJ (2004) Localization of voltage-gated ion channels in mammalian brain. Annu Rev Physiol 66:477-519.

Tseng-Crank J, Godinot N, Johansen TE, Ahring PK, Strobaek D, Mertz R, Foster CD, Olesen SP, Reinhart PH (1996) Cloning, expression, and distribution of a Ca^{2+}-activated K^+ channel ß-subunit from human brain. Proc Natl Acad Sci USA 93:9200-9205.

Uebele VN, Lagrutta A, Wade T, Figueroa DJ, Liu Y, McKenna E, Austin CP, Bennett PB, Swanson R (2000) Cloning and functional expression of two families of beta-subunits of the large conductance calcium-activated K^+ channel. J Biol Chem 275:23211-23218.

Vergara C, Latorre R, Marrion NV, Adelman JP (1998) Calcium-activated potassium channels. Curr Opin Neurobiol 8:321-329.

Viana F, Bayliss DA, Berger AJ (1993) Multiple potassium conductances and their role in action potential repolarization and repetitive firing behavior of neonatal rat hypoglossal motoneurons. J Neurophysiol 69:2150-2163.

Villalobos C, Shakkottai VG, Chandy KG, Michelhaugh SK, Andrade R (2004) SKCa channels mediate the medium but not the slow calcium-activated afterhyperpolarization in cortical neurons. J Neurosci 24:3537-3542.

Vogalis F, Storm JF, Lancaster B (2003) SK channels and the varieties of slow after-hyperpolarizations in neurons. Eur J Neurosci 18:3155-3166.

Vogalis F, Harvey JR, Furness JB (2002) TEA- and apamin-resistant KCa channels in guinea-pig myenteric neurons: slow AHP channels. J Physiol 538:421-433.

Wallner M, Meera P, Toro L (1999) Molecular basis of fast inactivation in voltage and Ca^{2+}-activated K^+ channels: A transmembrane beta-subunit homolog. Proc Natl Acad Sci USA 96:4137-4142.

Ward CL, Omura S, Kopito RR (1995) Degradation of CFTR by the ubiquitin-proteasome pathway. Cell 83:121-127.

Wei A, Jegla T, Salkoff L (1996) Eight potassium channel families revealed by the C. elegans genome project. Neuropharmacology 35:805-829.

Wei A, Solaro C, Lingle C, Salkoff L (1994) Calcium sensitivity of BK-type K_{Ca} channels determined by a separable domain. Neuron 13:671-681.

Weiger TM, Hermann A, Levitan IB (2002) Modulation of calcium-activated potassium channels. J Comp Physiol A 188:79-87.

Weiger TM, Holmqvist MH, Levitan IB, Clark FT, Sprague S, Huang WJ, Ge P, Wang C, Lawson D, Jurman ME, Glucksmann MA, Silos-Santiago I, DiStefano PS, Curtis R (2000) A novel nervous system beta subunit that downregulates human large conductance calcium-dependent potassium channels. J Neurosci 20:3563-3570.

Wittekindt OH, Visan V, Tomita H, Imtiaz F, Gargus JJ, Lehmann-Horn F, Grissmer S, Morris-Rosendahl DJ (2004) An apamin- and scyllatoxin-insensitive isoform of the human SK3 channel. Mol Pharmacol 65:788-801.

Wolfart J, Roeper J (2002) Selective coupling of T-type calcium channels to SK potassium channels prevents intrinsic bursting in dopaminergic midbrain neurons. J Neurosci 22:3404-3413.

Wolfart J, Neuhoff H, Franz O, Roeper J (2001) Differential expression of the small-conductance, calcium-activated potassium channel SK3 is critical for pacemaker control in dopaminergic midbrain neurons. J Neurosci 21:3443-3456.

Womack MD, Chevez C, Khodakhah K (2004) Calcium-activated potassium channels are selectively coupled to P/Q-type calcium channels in cerebellar Purkinje neurons. J Neurosci 24:8818-8822.

Wu SN (2003) Large-conductance Ca^{2+}-activated K^{+} channels:physiological role and pharmacology. Curr Med Chem 10:649-661.

Xia XM, Zeng X, Lingle CJ (2002) Multiple regulatory sites in large-conductance calcium-activated potassium channels. Nature 418:880-884.

Xia XM, Fakler B, Rivard A, Wayman G, Johnson-Pais T, Keen JE, Ishii T, Hirschberg B, Bond CT, Lutsenko S, Maylie J, Adelman JP (1998) Mechanism of calcium gating in small-conductance calcium-activated potassium channels. Nature 395:503-507.

Xie J, McCobb DP (1998) Control of alternative splicing of potassium channels by stress hormones. Science 280:443-446.

Xu Y, Tuteja D, Zhang Z, Xu D, Zhang Y, Rodriguez J, Nie L, Tuxson HR, Young JN, Glatter KA, Vazquez AE, Yamoah EN, Chiamvimonvat N (2003) Molecular identification and functional roles of a Ca^{2+}-activated K^{+} channel in human and mouse hearts. J Biol Chem 278:49085-49094.

Zerrouk H, Mansuelle P, Benslimane A, Rochat H, Martin-Eauclaire MF (1993) Characterization of a new leiurotoxin I-like scorpion toxin. PO5 from Androctonus mauretanicus mauretanicus. FEBS Lett 320:189-192.

Abbreviations

aa	amino acid
AA/BA	acrylamide/bisacrylamide
ABTS	2, 2'-azinobis (3-ethylbenzothiazoline-6-sulfoicacid)
AP	ammonium persulfate
BLAST	Basic Logical Alignment Search Tool
BSA	bovine serum albumin
cDNA	complementary DNA
°C	degree Celsius
dH_20	deionised H_2O
DAB	3, 3'-diaminobenzidine
ELISA	enzyme-linked immunosorbent assay
DIV	days in vitro
DTT	dithiothreitol
E17	embryonic day 17
FCS	foetal calf serum
GST	glutathione-S-transferase
HEK cells	human embryonic kidney cells
HEPES	N-2-hydroxyethylpiperazine-N'-2-ethanesulfonic acid
HRP	horseradish peroxidase
LB	Luria broth
LDS	lithium dodecylsulfate
min	minute
mg	milligram
µg	microgram
ml	millilitre
µl	microliter
mRNA	messenger RNA
MW	molecular weight
NGS	neonatal goat serum
OD	optical density
P0, P3, P6	postnatal day
PB	phosphate buffer

PBS	phosphate buffered saline
PFA	paraformaldehyde
Pen-Strep	penicillin/streptomycin
s	seconds
SCG	superior cervical ganglion
SDS	sodium dodecylsulfate
TAE	tetraethylammonium
TCEP	Tris(2-carboxyethyl)phosphine hydrochloride
TEMED	N, N, N', N'-Tetramethylenediamine
TBS	Tris buffered saline
Trx	Thioredoxin